



HAL
open science

Gene therapy for autosomal dominant retinitis pigmentosa : repair of rhodopsin mRNA by SMaRT technology

Adeline Berger

► **To cite this version:**

Adeline Berger. Gene therapy for autosomal dominant retinitis pigmentosa : repair of rhodopsin mRNA by SMaRT technology. Genetics. Université Pierre et Marie Curie - Paris VI, 2014. English. NNT : 2014PA066190 . tel-01143555

HAL Id: tel-01143555

<https://theses.hal.science/tel-01143555>

Submitted on 18 Apr 2015

HAL is a multi-disciplinary open access archive for the deposit and dissemination of scientific research documents, whether they are published or not. The documents may come from teaching and research institutions in France or abroad, or from public or private research centers.

L'archive ouverte pluridisciplinaire **HAL**, est destinée au dépôt et à la diffusion de documents scientifiques de niveau recherche, publiés ou non, émanant des établissements d'enseignement et de recherche français ou étrangers, des laboratoires publics ou privés.

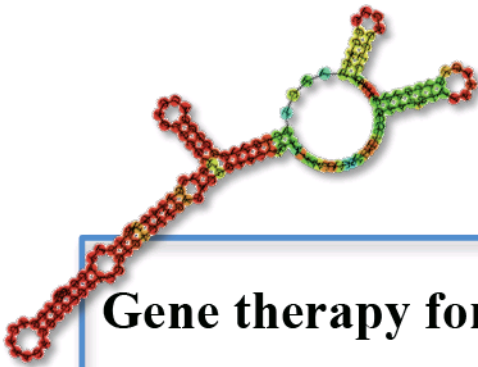
University: Pierre et Marie Curie – Paris VI

Doctoral school: Cerveau, cognition, comportement

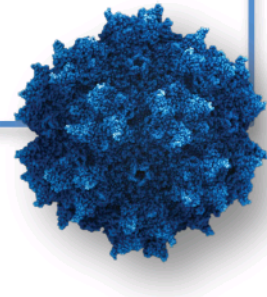
Research center: Institut de la Vision

Adeline Berger

Doctoral thesis in biology



**Gene therapy for autosomal dominant *retinitis pigmentosa*:
repair of rhodopsin mRNA by SMaRT technology**



Publicly presented and defended on September the 16th 2014, in front of the jury composed of:

- Pr. Salima Hacein-Bey-Abina, rapporteur.
- Dr. Bernard Schneider, rapporteur.
- Pr. Alfred Lewin, examiner.
- Pr. Thomas Voit, chairman.
- Pr. José-Alain Sahel, thesis director.
- Dr. Alexis Bemelmans, thesis supervisor.

Acknowledgements/Remerciements

Tout d'abord je tiens à remercier l'ensemble des membres de mon jury pour avoir accepté votre mission, je sais que vous êtes tous débordés, et que votre première pensée n'a sûrement pas été « oh super une thèse ! » mais plutôt « oh non pas encore une thèse...pourvu qu'elle ne me demande pas d'être rapporteur à la fin du mail... ». Merci pour le temps que vous m'avez accordé et pour l'effort que vous faites de jouer le jeu pour nous les thésards qui ne sommes que des petits bleus dans le domaine ! (Particulièrement aux rapporteurs, qui ont en plus eu l'occasion de faire voyager ma thèse au mois d'Août...)

Un grand merci à José, pour avoir dit « oui » quand Alexis a proposé ma candidature, pour avoir accepté d'être mon directeur de thèse (l'officiel, le vrai !), pour avoir pris le temps de m'écouter et de me conseiller, pour être resté disponible à tout moment (malgré cet emploi du temps qui fait peur à tout le monde !) et pour faire de l'Institut ce qu'il est, un endroit plein de richesses scientifiques et personnelles. Merci pour vos encouragements et votre soutien que je n'oublierai pas.

Evidemment, merci à toi Alexis (papa Alexis comme disent les autres du bureau d'à côté ! ☺) pour avoir été mon directeur de thèse (le faux !), pour avoir encadré ma thèse d'une façon juste PARFAITE à mes yeux, c'est-à-dire en m'encadrant (ou me recadrant) comme il le faut, mais en me laissant aussi beaucoup de libertés (merci les 15 Kms qui séparent l'Institut du CEA ! non je plaisante bien sûr). Tu as su m'apprendre la science (et surtout la bio mol) comme elle me plait, me faire confiance (même plus que moi-même je ne me fais confiance) et me conforter sur la pensée qu'il y a des gens droits et honnêtes dans la recherche. Merci d'avoir très largement contribué à faire que ces 4 années de thèse soient très agréables (je dirais même « fingers in the nose » ! ou presque).

Merci aussi pour m'avoir fait découvrir des parfums de Lindt que je ne connaissais pas (et quelle mission !) D'ailleurs à ce propos je tiens à rectifier un fait : le plus gourmand d'entre nous deux, c'est TOI !

En parlant du bureau d'à côté, merci tonton Florian, tonton Xavier, et (j'ose le dire ? bien sûr que j'ose) papy Alvaro (mais un papy jeune !) pour votre bonne humeur, pour vos conseils, pour avoir fait en sorte qu'il y ait toujours quelqu'un pour répondre à nos questions (parfois existentielles) à nous, les jeunes du bureau d'à côté ! Merci pour votre soutien à tous les 3 ! Et un merci particulier à Xavier pour avoir partagé avec moi sa passion pour la bio mol (et même un peu les stats...) et pour avoir gagné le droit d'occuper quelques heures d'avion avec la relecture de cette thèse... ☺

Equipe 6, 10, 14 puis 15+MIRCen... ça représente pas mal de monde tout ça !

Equipe 6 ça sonne comme : Mélissa, merci pour tout ce que tu m'as appris, y compris des mots qui sont uniquement dans le dictionnaire canadien et pour tous les bons moments que l'on a pu partager dans le labo et aussi en dehors ! Peggy, ah...Peggy... ! La plus adorable des filles détestables ! Je me souviendrais toute ma vie de cette phrase : « Bon je ne vais pas descendre avec toi à chaque fois que tu vas devoir tuer une souris et tu ne vas pas remonter en

disant à Alexis que tu n'y arrives pas, alors maintenant ta souris tu la prends et tu la tues !!! » c'était notre première conversation... Même s'il faut gratter assez profond pour te connaître vraiment, je te dis merci Peggy ! Cécile et Valérie, puis Zakia, Laetitia et Elena (les filles d'en bas quoi !) merci pour votre compagnie, nos merveilleux goûters et nos nombreux fou-rires !! Parce qu'il est possible de bien travailler tout en rigolant ! Et bien sûr tous ceux qui sont partis : merci Romain B pour ta joie de vivre quotidienne ! Et merci Sophie C pour ton soutien, ta gentillesse, ton écoute, bref ...ton amitié !

Equipe 10 et 14 c'est aussi à moitié un reste de l'équipe 6 avec la DP71 team ! Alvaro, Ophélie, Brahim, Marie et Hugo, merci à vous tous pour votre gentillesse ! et vive la DP71 ! (mais non je ne veux toujours pas rejoindre votre mafia Alvaro... 😊)

Et c'est aussi à moitié cette nouvelle équipe qui débarque et qui nous envahie ! Florian, Xavier, Elisa, Shulong, Sophie, Olivier, Bertrand, Mike, Fadoua, ainsi que William et Delphine, ça a été un grand plaisir de se faire envahir, et surtout de faire votre connaissance ! Merci à tous pour nos discussions (de science mais surtout de plein d'autres choses !) et pour m'avoir acceptée et intégrée comme si j'étais membre de la zennlab team!

Equipe 15 : Deniz : merci de m'avoir acceptée dans ton équipe avec toute l'autonomie d'un petit électron libre. Hanen, Céline, Arthur, Eleonore : merci pour nos délires au coin de la paillasse dans les moments où j'avais besoin d'oxygéner les deux neurones qui n'étaient pas en pleine rédaction...Bon courage à vous pour la suite !

MIRCen : Chacha, MC, Noëlle, sans oublier Séverine, Gwen et Karine, merci les filles pour votre bonne humeur, votre accueil chez vous (à l'autre bout du monde) et votre aide. Merci particulièrement à toi Chacha, qui en plus d'être une amie, a tout donné pour m'aider à finir ce projet !

Enfin comment ne pas remercier ceux qui m'ont supporté au quotidien à l'Institut : mes colocs de bureau : Ophélie (du début à la fin), merci d'être l'autre blonde du labo (parce que c'est toujours plus facile de se partager les blagues à 2), merci pour nos longues discussions d'après 19h, et merci d'avoir ouvert la voie en étant celle qui soutien en premier ! Ah-Lai, Larissa et Ying, merci les filles pour vos conseils de celles qui sont déjà passées par là, merci pour votre gentillesse et votre bonne humeur. Merci Sophie B pour ta gentillesse et ta sympathie, ainsi que pour tes délicieux cookies (et pour le café aussi...) Puis Célia et Ludo, auxquels je rajouterai Débo et Quentin qui ne font pas partie du bureau mais squattent tellement souvent que c'est comme si... Merci à vous pour m'avoir remonté le moral quand il fallait, pour m'avoir fait rire et pleurer (que de joie bien sûr !) pour tous ces bons moments passés ensemble ! Débo il te revient le rôle de défendre le bureau après mon départ 😊 sauf si on se rejoint de l'autre côté (je t'attends)!!!

Et puis à vous tous, ceux avec qui j'ai discuté un peu, voire beaucoup... qui ont fait que ces 4 années sont passées beaucoup trop vite : Luisa (cytométrie ou vernis...) la petite Céline, Manu (Nunu), Julie, Quénot, Angélique, Amélie, Sacha, Céline (pour nos longues heures partagées au L2), RCaplette, Christophe (l'arnaqueur de pharmacien), Emeline, Georges, Stéphane, Seb et Christophe, Laura, Raph, Katie, Charlotte bien sûr, et tous les autres que j'ai oublié de citer... Merci à vous tous !

Katie et Susannah, un immense merci également pour avoir accepté de relire la langue de Shakespeare que j'ai « essayé » d'utiliser dans cette thèse.

Merci aussi à Marion-Anne et Florent pour m'avoir supportée en prof à la fac, puis en re-prof au labo ! Merci de m'avoir prouvé qu'un(e) stagiaire peut être hyper motivé(e) et hyperagréable ! Bonne route à vous.

Merci à Ronan et Dominique pour avoir fait de moi une monitrice qui achète ses étudiants avec des bonbons ! (je crois que j'ai tout compris, non ?) L'expérience était très enrichissante, et ça a été un plaisir de partager cela avec vous.

Merci à Maud, Michèle, Gilda et Viviane pour avoir été les premiers bonjours et les premiers sourires chaque jour (sans failles !) à mon arrivée à l'Institut. Merci pour votre soutien et votre gentillesse.

Merci évidemment à l'Association Française contre les Myopathies sans qui ce projet n'aurait jamais vu le jour, et qui m'a soutenue jusque dans la réalisation de ma 4^{ième} année à l'Institut. Sans financement la Recherche ne peut rien faire, alors merci à l'AFM et merci à vous qui donnez au Téléthon et à la Recherche en général.

Enfin, ceux sans qui je n'aurai jamais fait cette thèse, ceux qui me soutiennent depuis le début dans tout ce que j'entreprends (même s'ils pensent que je suis un peu folle de faire un truc comme ça !) : ma famille. Merci à mes parents, mon frère et ma belle-sœur et aussi ma belle famille, pour vos encouragements et votre soutien au quotidien ! Merci de me rappeler que oui je peux et je vais y arriver !

Merci également à tous mes amis : les chafouins (Romu, Bastien, Quantin, Jérémie, Emilie, Elisabeth, Alex, Stéph, Damien, Mathilde², Adrien, Noémie, Claire...) merci de m'avoir supportée ! Céline, Fab, François et Mélanie, merci d'avoir partagé cette immense épreuve qu'est la thèse avec moi et en même temps que moi, merci pour nos soirées potins du labo et nos repas à thème pour l'oublier ce labo et surtout cette rédaction ! Merci d'être là !

Et parce que je garde toujours le meilleur pour la fin : merci à toi Julien, pour avoir accepté et assumé avec moi ma décision de faire une thèse, (et le grand départ qui arrive...). Pour m'avoir comprise et soutenue pendant ces 4 années (et aussi avant... et après...et c'est pas fini...). Pour m'aider à avancer tous les jours, en devenant quelqu'un de plus fort. Merci aussi pour le ménage, la vaisselle, les courses...sans oublier la mise en page de ce magnifique « manuscrit » (je n'ai pas dit grimoire non plus). Un immense merci pour tout ça ! Petite rectification pour finir : cette thèse a été rédigée par Madame Adeline HERVE !

Bonne lecture à tous (oui ça c'était la partie marrante, maintenant au boulot !)

Summary

ACKNOWLEDGEMENTS/REMERCIEMENTS	3
RESUME EN FRANÇAIS	8
LIST OF ABBREVIATIONS.....	16
LIST OF FIGURES AND ANNEXES.....	18
PREAMBLE	20
INTRODUCTION.....	22
I. <i>RETINITIS PIGMENTOSA</i> INDUCED BY RHODOPSIN MUTATION	23
I.1. EYE AND VISION.....	23
I.1.a. Generalities	23
I.1.b. The retina.....	23
I.1.c. Human photoreceptors.....	24
I.2. <i>RETINITIS PIGMENTOSA</i>	26
I.2.a. Remodeling of the retina and clinical manifestations.....	26
I.2.b. Genetic involvement.....	27
I.3. RHODOPSIN	28
I.3.a. Rhodopsin synthesis, function and visual cycle	28
I.3.b. Structure of rhodopsin	29
I.3.c. Rhodopsin mutations and consequences	30
I.4. TREATMENTS OF RP	31
I.4.a. General current treatments of RP	31
I.4.b. Treatments of RP in the particular case of RHO mutation.....	33
II. CURRENT STRATEGIES TO PREVENT MUTANT RHODOPSIN EXPRESSION	34
II.1. RHODOPSIN DNA SEQUENCE CORRECTION.....	34
II.1.a. DNA repair by Homologous Recombination (HR).....	34
II.1.b. HR-induced endonucleases	34
II.2. SILENCING OF MUTANT GENE EXPRESSION COUPLED TO EXPRESSION OF A NORMAL COPY	37
II.2.a. Zinc Finger - Artificial Transcription Factors (ZF-ATF).....	37
II.2.b. RNA interference	38
II.2.c. Ribozymes	41
III. <i>TRANS</i>-SPLICING OF RHODOPSIN PRE-MRNA.....	44
III.1. <i>Cis</i> -SPLICING: THE PROTOTYPICAL SPLICE REACTION	44
III.1.a. Splicing is a phase of pre-mRNA maturation	44
III.1.b. Steps of the splicing mechanism.....	45
III.1.c. Regulation of <i>cis</i> -splicing	47
III.2. <i>TRANS</i> -SPLICING BETWEEN TWO RNA MOLECULES	48
III.2.a. Description of the mechanism.....	48
III.2.b. Previous studies led with <i>trans</i> -splicing approaches	48
III.2.c. Strategies of PTM Design	49

III.2.d. Advantages and drawbacks.....	51
IV. VIRAL VECTORS FOR GENE THERAPY OF OCULAR DISEASES	54
IV.1. ADVANTAGES OF THE EYE AS TARGET OF GENE THERAPY WITH VIRAL VECTOR.....	54
IV.2. CHOICE OF THE VIRAL VECTOR FOR OCULAR DISEASES	54
IV.2.a. Classical viral vectors used in gene therapies.....	54
IV.2.b. Previous ocular gene therapies with rAAV	58
V. CELLULAR AND ANIMAL MODELS OF RP LINKED TO RHODOPSIN MUTATIONS.	59
V.1. CELLULAR MODEL OF RHODOPSIN EXPRESSION	59
V.1.a. Primary cultures of photoreceptors	59
V.1.b. Cell lines developed to study rhodopsin mutations	59
V.2. ANIMAL MODELS OF RHODOPSIN-INDUCED <i>RETINITIS PIGMENTOSA</i>	60
V.2.a. Animal models of rhodopsin mutation-induced <i>retinitis pigmentosa</i> and more specifically mouse models	60
V.2.b. Comparison of mouse and human eyes	61
RESULTS.....	64
I. RESULTS OF <i>IN VITRO</i> ANALYSIS OF PTM EFFICIENCY.	65
II. IMPROVEMENT AND CHARACTERIZATION OF AN <i>IN VIVO</i> IMAGING TECHNOLOGY TO MEASURE POTENTIAL EFFECTS OF OUR THERAPEUTIC STRATEGY IN A HUMANIZED MOUSE MODEL.....	95
III. COMPLEMENTARY ONGOING RESULTS.....	108
III.1. DEVELOPMENT OF NEW PTM <i>IN VITRO</i> AND STRATEGIES TO OVERCOME PTM DRAWBACKS.	108
III.1.a. A new PTM that repairs the fifth exon.	108
III.1.b. Production of a truncated protein <i>in vitro</i> after expression of the PTM alone.	108
III.1.c. Strategies to prevent production of truncated protein.	109
III.1.d. Analysis of PTM translation alone <i>in vivo</i>	110
III.2. STUDY OF THE THERAPEUTIC EFFECTS OF <i>TRANS</i> -SPLICING IN A HUMANIZED MOUSE MODEL. ..	111
III.2.a. The humanized Rho ^{+/-} P347S RHO ⁺ mouse model.....	111
III.2.b. Choice of parameters that regulate PTM expression <i>in vivo</i>	111
III.2.c. Effect of AAV2/8 bRho-PTM20 injection in Rho ^{+/-} P347S RHO ⁺ mice.	112
DISCUSSION AND PERSPECTIVES	113
I. THE PTM SEQUENCE: THE KEY TO EFFICIENT SMART TECHNOLOGY.....	114
II. HOW TO ACHIEVE MORE <i>TRANS</i>-SPLICING THAN <i>CIS</i>-SPLICING?	115
III. THE MAIN DRAWBACKS OF PTM.....	117
IV. FOLLOWING-UP POTENTIAL BENEFICIAL EFFECTS IN A HUMANIZED MOUSE MODEL... 	120
V. ENVISAGING A THERAPEUTIC APPLICATION IN HUMANS.....	122
VI. THE FUTURE OF THERAPEUTIC STRATEGIES TO PREVENT MUTANT RHODOPSIN EXPRESSION.....	122
VII. CONSIDERING GENE THERAPIES FOR RETINAL DISEASES OVER THE NEXT FEW DECADES.	123
BIBLIOGRAPHY	125
ANNEXES.....	146

Résumé en français

Thérapie génique pour la rétinite pigmentaire autosomique dominante : réparation de l'ARN de la rhodopsine par la technologie SMaRT.

Lorsque la lumière pénètre dans nos yeux, elle traverse la cornée, la pupille, le cristallin et le vitré avant d'atteindre la rétine qui correspond à une fine membrane de tissu nerveux tapissant le fond de l'œil. Constituée de cellules de maintien (cellules gliales de Müller, astrocytes et microglie), d'un épithélium pigmentaire et de neurones (cellules ganglionnaires, bipolaires, horizontales, amacrines et photorécepteurs), elle est considérée comme la partie neurosensorielle de l'œil. Les photons passent à travers toutes les cellules de la rétine avant d'être captés par les photopigments des photorécepteurs. Ces derniers vont alors transformer le signal lumineux en un signal électrochimique qui va être conduit à travers les neurones rétiniens jusqu'au cerveau où se fait l'interprétation de l'information visuelle. Il existe deux types de photorécepteurs, les cônes et les bâtonnets, qui nous permettent d'avoir une vision correcte dans une large gamme d'intensité de lumière. En effet, alors que les bâtonnets sont capables de détecter la présence d'un photon unique¹, les cônes sont efficaces jusqu'à une intensité lumineuse correspondant à plus de 100 millions de photons/s. Les cônes nous permettent également d'avoir une vision centrale précise et en couleur, alors que les bâtonnets sont impliqués dans la vision périphérique, uniquement en niveaux de gris. Cette différence de perception en couleur ou non est due à la présence de trois opsines dans les cônes, qui sont actives à des longueurs d'ondes différentes, alors que les bâtonnets n'en possèdent qu'une seule. De plus, la forte acuité visuelle obtenue au centre de la rétine s'explique par la présence d'une région particulière appelée macula. Celle-ci possède en son centre une structure appelée fovéa, uniquement composée de cônes, connectés à un nombre beaucoup plus important de cellules bipolaires qu'ailleurs dans la rétine. Il s'agit de l'unique région dépourvue de bâtonnets, qui sont environ 20 fois plus nombreux que les cônes dans le reste de la rétine.

La dégénérescence pathologique des bâtonnets entraîne celle des cônes, générant une perte de vision tout d'abord périphérique évoluant vers la cécité, signes caractéristiques de la rétinite pigmentaire. Plus de 50 gènes des photorécepteurs et de l'épithélium pigmentaire ont été décrits comme pouvant être impliqués dans le développement de cette maladie dégénérative de la rétine, qu'il s'agisse des formes liées à l'X, autosomiques dominantes,

récessives, ou sporadiques. Parmi ceux-ci, le gène codant la rhodopsine² est considéré comme responsable de plus de 30% des formes autosomiques dominantes. La rhodopsine (RHO) est la seule opsine des bâtonnets, qui associée à son chromophore, le 11-*cis* retinal, déclenche l'activation de la cascade de phototransduction en présence de photons. Il s'agit d'un récepteur à 7 domaines transmembranaires, couplé à une protéine G. La structure de la rhodopsine se compose de 3 parties principales : un domaine N-terminal qui se localise entre les disques des segments externes des bâtonnets, une partie intra-membranaire et un domaine C-terminal cytoplasmique³. Plus de 120 mutations, réparties sur l'ensemble de la protéine, ont été décrites comme responsables du développement d'une rétinite pigmentaire (ou dans quelques cas d'une cécité nocturne stationnaire congénitale) (RetNet, <https://sph.uth.edu/retnet/>). Ces mutations sont dominantes, de type gain de fonction ou à effet dominant négatif, ce qui signifie qu'elles apportent à la protéine de nouvelles fonctions qui ont un effet inverse et/ou supérieur à celles des protéines normales. Elles sont regroupées en six classes, en fonction de l'effet de la mutation sur la protéine⁴ (voir tableau ci-dessous). Les rétinites pigmentaires dues à une mutation de la rhodopsine, sont très hétérogènes quant à l'agressivité de la mutation, ainsi que le délai avant l'apparition des premiers symptômes et la vitesse d'évolution de la maladie.

Classification	Comportement
Classe I	Repliement normal mais pas de transport vers le segment externe
Classe II	Rétention dans le réticulum endoplasmique et n'interagit pas facilement avec le 11- <i>cis</i> -retinal
Classe III	Affecte l'endocytose
Classe IV	N'affecte pas forcément le repliement mais perturbe la stabilité et les modifications post-transductionnelles de la protéine
Classe V	Les mutations montrent une augmentation du taux d'activation de la transducine
Classe VI	Activation constitutive de la protéine, en l'absence de chromophore et dans le noir
Non-classées	Aucune observation de défaut cellulaire ou biochimique, ou pas d'étude détaillée

Parmi les stratégies actuellement mises en place pour traiter la rétinite pigmentaire, on trouve :

- des stratégies correctrices de l'ADN ou de l'ARN lorsque le gène impliqué est identifié, telles que :
 - les nucléases, (méganucléases⁵, nucléases avec un domaine en doigt de zinc (ZFN)⁶, nucléases avec un domaine TALE (Transcription Activator Like

Effector)... qui induisent une cassure double brin de l'ADN. La réparation de celle-ci permet d'éliminer la mutation après recombinaison homologue avec une séquence homologue normale, naturellement présente dans la cellule, ou apportée de façon exogène.

- les facteurs de transcription à doigts de zinc (ZF-ATF)⁷, l'ARN interférence⁸⁻¹⁰ et les ribozymes^{11,12}. Ces différentes approches permettent de réduire l'expression du gène muté (ZF-ATF) ou la dégradation des ARN messagers matures qui en résultent (ARNi / ribozymes). Néanmoins, ces stratégies nécessitent l'ajout d'une séquence codant la protéine normale, qui ne sera pas une cible du système.
- des stratégies plus générales, visant à ralentir la dégénérescence des photorécepteurs, telles que l'utilisation de facteurs neurotrophiques^{13,14}, la supplémentation en vitamine A/E... Ils présentent une action pléiotropique, en agissant sur plusieurs types cellulaires de la rétine, et permettent d'élargir la fenêtre thérapeutique en ralentissant la mort des photorécepteurs, mais ne stoppent pas complètement l'évolution de la maladie.
- des stratégies réparatrices, telles que la greffe de cellules¹⁵⁻¹⁸, les approches optogénétiques¹⁹⁻²², ou encore l'implantation de rétines artificielles^{23,24}.

Malgré les efforts mis en œuvre pour l'élaboration de tous ces procédés, il n'existe pas pour le moment de traitement accessible à l'homme qui vienne à bout de la rétinite pigmentaire.

L'objectif de mon projet de thèse était donc de développer une nouvelle approche pour prévenir le développement de la rétinite pigmentaire due à une mutation de la rhodopsine. Nous avons pour cela adapté la technologie SMaRT (*Trans*-épissage de l'ARN généré par le spliceosome) à la réparation de l'ARN de la rhodopsine.

L'épissage des ARN pré-messager est un mécanisme commun aux cellules eucaryotes, qui intervient au cours de la maturation des ARN, et permet l'excision des séquences introniques²⁵. Des séquences spécifiques présentes sur chaque intron à épisser sont reconnues par la machinerie du spliceosome²⁶ (la plus grosse machinerie de la cellule) qui induit à travers deux réactions de transesterification la formation d'une structure en lasso qui porte l'intron excisé, et la séquence épissée reformée par la jonction des deux exons environnants. L'épissage classique se fait en *cis*, c'est-à-dire qu'un seul ARN pré-messager intervient dans la réaction. Le *trans*-épissage quant à lui, correspond à une réaction d'épissage entre deux molécules d'ARN pré-messager. Il existe naturellement chez les eucaryotes, bien que sa fréquence soit très faible. La technologie SMaRT s'inspire de ce mécanisme pour réparer un

ARN pré-messager muté à l'aide d'une molécule appelée PTM pour Pre-ARNm *Trans-splicing Molecule*²⁷. Cette molécule se compose (i) d'un domaine de fixation pour cibler spécifiquement l'ARN pré-messager à réparer, (ii) d'une séquence intronique permettant de générer la réaction d'épissage, (iii) et d'une séquence de remplacement de la séquence mutée. La technologie SMaRT a déjà été utilisée dans le cadre d'approches thérapeutiques ciblant par exemple la mucoviscidose²⁸⁻³¹, l'hémophilie A³², l'amyotrophie spinale³³⁻³⁶, l'immunodéficience liée à l'X³⁷... Ces études montrent des efficacités de *trans*-épissage très variables, allant d'une absence de détection *in vitro* de la protéine issue du *trans*-épissage, à un sauvetage du phénotype *in vivo*.

Tout l'enjeu de la technologie SMaRT repose à la fois sur l'efficacité de *trans*-épissage du PTM développé et sur l'environnement dans lequel il se fait. Par exemple dans le cas de la rhodopsine, la toxicité et l'agressivité des mutations étant variables, le taux de *trans*-épissage requis pour avoir un effet bénéfique sur la dégénérescence des photorécepteurs peut lui aussi également varier.

La première partie de mon projet a donc consisté à créer et tester *in vitro* plusieurs PTM afin de sélectionner celui induisant le plus fort taux de *trans*-épissage. Pour cela, nous avons tout d'abord produit 14 PTM ciblant tous 150 bases du premier intron de la rhodopsine, mais sur des régions différentes. Le fait de cibler le premier intron de l'ARN endogène de la rhodopsine permet de créer un outil capable de remplacer les exons 2, 3, 4 et 5, et donc d'éliminer toutes les mutations de ces exons. Nous avons déterminé l'efficacité de *trans*-épissage de chacun de ces PTM dans des cellules HEK293T qui n'expriment pas la rhodopsine naturellement. Nous avons donc induit l'expression transitoire de la rhodopsine et du PTM par co-transfection de ces cellules avec les deux constructions correspondantes. La quantification du *trans*-épissage au niveau des ARN a montré un taux de 25% obtenu avec le PTM1. Nous avons ensuite montré que l'ajout d'un intron (endogène ou artificiel) entre deux exons de la séquence de remplacement du PTM augmente son efficacité. Le PTM20, qui correspond au PTM1 avec ajout d'un intron artificiel, permet d'obtenir un taux de *trans*-épissage maximal de l'ordre de 40%. Considérant le fait que la co-transfection des deux constructions pourrait favoriser la proximité de l'ARN cible et du PTM et donc augmenter le taux de *trans*-épissage, nous avons créé des lignées cellulaires exprimant de façon stable la rhodopsine. De ce fait, seul le PTM est transfecté, et doit retrouver sa cible dans le noyau avant de pouvoir agir, reproduisant donc davantage les conditions d'une thérapie génique ciblant une cellule pathologique. Nous avons créé 4 lignées de cellules HEK293T par

transduction lentivirale, exprimant la rhodopsine WT (Wild-type), ou portant l'une des mutations P23H, R135W ou P347L. Le choix de ces mutations s'explique par plusieurs arguments : P23H est la plus répandue dans la population caucasienne des Etats-Unis, et également la plus étudiée, mais sa localisation dans l'exon 1 empêche sa réparation par notre système ; elle a donc uniquement servi de contrôle dans nos expériences. Les mutations R135W et P347L, quant à elles, sont assez répandues dans la population européenne et présentes chez des patients de l'hôpital des XV-XX. Une caractéristique intéressante de ces lignées cellulaires est que la rhodopsine va se localiser à la membrane plasmique ou être retenue à l'intérieur des cellules, en fonction de la mutation. Ainsi, la rhodopsine WT et P347L vont rejoindre la membrane plasmique, alors que la rhodopsine P23H et R135W restent séquestrées dans le cytoplasme des cellules. Nous avons tout d'abord quantifié la localisation de ces différentes formes de rhodopsine à l'aide de l'ImageStream^X, un appareil permettant de faire de l'imagerie en flux. Ceci nous a ensuite permis de quantifier la réparation de la rhodopsine par *trans*-épissage au niveau de la protéine, en observant la localisation de la rhodopsine R135W avant et après ajout du PTM. Nous avons donc transfecté les cellules exprimant la rhodopsine R135W avec le PTM20, et observé un retour partiel à la membrane du pool cellulaire de rhodopsine. Ce résultat confirme que le *trans*-épissage intervient dans un modèle d'expression stable de la rhodopsine, et permet la production de protéines normales. L'hypothèse que la rhodopsine mutée soit synthétisée de manière moins efficace, ou dégradée plus rapidement que la protéine normale nous a également conduit à quantifier le taux de protéines avant et après ajout du PTM par western blot. Malheureusement, les conditions requises pour la détection de la protéine n'ont pas permis sa quantification de façon optimale. Cependant, cette approche nous a permis de mettre en évidence la production d'une rhodopsine tronquée à partir du PTM. En effet, des cellules HEK293T transfectées uniquement par le PTM montrent par western blot la présence d'une bande spécifique d'environ 20KDa contre 39KDa pour la protéine entière. Ceci sous-entend que le PTM est assez stable dans la cellule pour être transporté dans le cytoplasme et possède toutes les séquences requises pour sa traduction. Cette propriété du PTM limite son utilisation dans un contexte thérapeutique, nous nous sommes donc attardés à essayer d'empêcher ce phénomène. Etant dépourvu de l'exon1, la traduction du PTM indique la présence, entre les exons 2 et 5, d'un ATG secondaire capable d'initier la traduction. Nous avons donc tout d'abord muté l'ATG suspecté d'être cet ATG secondaire, d'après la taille de la protéine tronquée obtenue, et la présence d'une séquence environnante proche de la séquence KOZAK. Nous avons également induit l'expression du PTM sous contrôle d'un

promoteur dépendant de la polymérase III, afin de limiter l'ajout de la coiffe, et donc d'empêcher la stabilisation du PTM. Néanmoins, aucune de ces deux stratégies n'a permis d'éliminer la production de la protéine tronquée. Nous avons alors voulu tester si ce processus était reproductible *in vivo*. Pour induire la transcription du PTM dans les photorécepteurs de façon spécifique, nous avons transduit les rétines avec un AAV2/8 injecté entre les photorécepteurs et l'épithélium pigmentaire rétinien. L'utilisation de l'AAV2/8 permet une transduction précise des photorécepteurs grâce au tropisme bien défini des AAV, générant une expression stable puisque les photorécepteurs sont des cellules post-mitotiques, sans intégration (pouvant induire une mutagenèse insertionnelle). De plus l'AAV étant un virus non pathogène et peu immunogène, il constitue le vecteur viral de choix pour notre système. L'analyse des protéines issues des rétines de souris invalidées pour la rhodopsine, transduites par l'AAV2/8 *bRho*-PTM20, n'a pas permis d'observer la production de protéine tronquée *in vivo*. Plusieurs hypothèses peuvent expliquer cette différence entre l'étude *in vitro* et l'étude *in vivo*, notamment la possibilité que les cellules HEK293T aient perdu certains mécanismes de surveillance et de dégradation des ARN anormaux, qui sont actifs dans les photorécepteurs. Ce résultat nous a encouragés vers l'étude des effets du *trans*-épissage *in vivo* dans un modèle murin de rétinite pigmentaire.

Mesurer l'effet du *trans*-épissage *in vivo* nécessite la mise en place de techniques permettant de quantifier la dégénérescence des photorécepteurs. Alors que l'histologie informe sur la morphologie et la structure des cellules de la rétine, l'ERG (électrorétinogramme) indique leur fonctionnalité. Bien qu'indispensables, ces deux techniques ne permettent pas de suivre précisément l'évolution de la dégénérescence au cours du temps: l'ERG ne prend pas en compte la possibilité que des cellules non-fonctionnelles perdurent, et l'histologie n'intervient qu'au stade final de l'étude. La tomographie par cohérence optique (SD-OCT, pour spectral domain-optical coherence tomography) est un système d'imagerie non invasif basé sur un principe d'interférométrie qui permet de visualiser chacune des couches de la rétine. Bien que largement utilisée chez l'homme, cette technique génère chez le rongeur des images de qualité moyenne qui ne permettent pas de délimiter avec précision les couches de la rétine externe. Nous avons donc tout d'abord travaillé sur le traitement des images obtenues par SD-OCT, afin d'améliorer leur définition, ce qui nous a permis de délimiter avec précision les couches de la rétine externe. Nous avons montré que cette technique permet un suivi précis et fiable de la dégénérescence des photorécepteurs, en suivant l'évolution de l'épaisseur des couches de la rétine dans un modèle murin invalidé pour la rhodopsine.

Nous avons ensuite utilisé cette technique pour caractériser la dégénérescence des photorécepteurs dans notre modèle murin de rétinite pigmentaire. Les souris *Rho*^{+/-} P347S *RHO*⁺, obtenues après croisement des souris *Rho*^{-/-} avec des souris P347S *RHO*^{+/+}, portent une copie codant pour la rhodopsine normale et l'autre pour la rhodopsine mutée, reproduisant le caractère hétérozygote retrouvé chez l'Homme. L'observation à l'OCT nous a permis de montrer une dégénérescence très rapide des photorécepteurs dans ce modèle, avec une disparition quasi-totale de l'ONL (couche des noyaux des photorécepteurs) à P60 (60 jours après la naissance). Nous avons ensuite co-injecté dans l'espace sous-rétinien de souris *Rho*^{+/-} P347S *RHO*⁺ âgées de 23 jours, l'AAV2/8 *bRho*-PTM20 et l'AAV2/8 *bRho*-GFP dans un ratio 7:1. Une semaine après l'injection, nous avons vérifié l'expression de la GFP, preuve de l'efficacité de transduction, et qui nous laisse supposer que le PTM20 est 7 fois plus exprimé que la GFP dans les cellules transduites. La quantification des ARN *trans*-épissés extraits des rétines transduites a montré que le *trans*-épissage avait bien lieu *in vivo* dans les photorécepteurs. Le taux de *trans*-épissage obtenu, d'environ 10%, correspond au *trans*-épissage observé dans l'ensemble de la rétine, incluant donc les photorécepteurs qui expriment le PTM20, mais également tous ceux qui n'ont pas été transduits. Malgré ce résultat encourageant, le suivi de la dégénérescence des photorécepteurs au cours du temps, dans un second groupe d'animaux injectés, n'a pas permis de mettre en évidence le sauvetage des photorécepteurs. Nous n'avons pas observé de différences entre les animaux injectés avec le PTM20, et ceux injectés avec le PTM0 (contrôle négatif) ou avec la GFP seule, 30 jours après injection. Plusieurs hypothèses peuvent expliquer ce résultat, comme la trop faible efficacité du *trans*-épissage, qui ne permettrait pas de réparer assez de protéines pour avoir un effet sur le phénotype des animaux, ou bien encore la dégénérescence trop rapide du modèle animal utilisé, qui pourrait nécessiter une injection à un stade plus précoce afin d'obtenir un effet. Pour contrecarrer ce dernier point, nous avons testé les injections sous-rétiniennes à P3 et P5 dans les animaux *Rho*^{+/-} P347S *RHO*⁺. L'observation des rétines un mois après injection montre clairement une proportion importante de rétines endommagées, qui présentent des détachements rétiniens non recollés, ou encore une organisation anormale des différentes couches neuronales. Il semble donc que l'injection sous-rétinienne à un âge très précoce ne soit pas la voie d'administration du PTM la plus adaptée pour suivre l'évolution de la dégénérescence des photorécepteurs. Une issue possible que nous pourrions mettre en œuvre dans le futur serait d'injecter par voie intracardiaque au stade précoce un AAV2/9 muté, décrit comme capable de cibler spécifiquement les photorécepteurs quand il est associé à un

promoteur spécifique. De ce fait, l'AAV pourrait conduire l'expression du PTM dans les cellules photoréceptrices encore en développement et de façon uniforme dans toute la rétine.

La réalisation de ce projet nous a permis de montrer que l'utilisation de la technologie SMaRT permet la réparation de l'ARN muté de la rhodopsine, sans modifier le niveau d'expression du gène. Dans un modèle cellulaire par co-transfection transitoire, dans une lignée d'expression stable de la rhodopsine, ou encore *in vivo* dans un modèle murin de rétinite pigmentaire, l'ajout du PTM dans la cellule cible induit un épissage en *trans* capable de remplacer la séquence mutée d'un certain nombre d'ARN pré-messager de la rhodopsine. Le taux de *trans*-épissage nécessaire pour stopper *in vivo* la dégénérescence des photorécepteurs n'est pas défini, et serait très certainement variable en fonction de la toxicité de la mutation impliquée (qui dépend de son mécanisme d'action : voir tableau précédent). L'enjeu de cette approche est donc d'augmenter au maximum le taux de *trans*-épissage, qui peut varier selon plusieurs facteurs comme nous avons pu le voir dans cette étude. L'un des facteurs déterminants pour une utilisation *in vivo* repose bien sûr sur l'apport de cette molécule dans les cellules cibles, à savoir les photorécepteurs. Certaines améliorations sont encore nécessaires de ce point de vue, afin d'apporter la preuve de concept dans notre modèle murin. De plus, une utilisation thérapeutique de cette stratégie, appliquée à l'Homme, requière également de vérifier certains points comme la spécificité du PTM envers la rhodopsine, et sa non-toxicité dans les photorécepteurs en cas d'absence de réaction avec l'ARN cible. Ainsi, bien qu'il reste de nombreux développements à entreprendre avant de pouvoir envisager une application clinique, nous avons démontré avec le présent travail que le *trans*-épissage est une stratégie très prometteuse dans la lutte contre les rétinites pigmentaires dues à une mutation de la rhodopsine, pour lesquelles aucun traitement n'existe à l'heure actuelle.

List of abbreviations

AAV: Adeno-Associated Virus
adRP: autosomal dominant RP
BP: Branch Point
cDNA: complementary DNA
cGMP: cyclic Guanosine MonoPhosphate
CMV: CytoMegaloVirus
CNTF: Ciliary NeuroTrophic Factor
COS: the cells being CV-1 (simian) in Origin, and carrying the SV40 genetic material
CRISPR: Clustered Regulatory Interspaced Short Palindromic Repeats
crRNA: CRISPR RNA
CTD: Carboxy-Terminal Domain
DNA: Deoxyribonucleic Acid
DSB: Double Strand Break
ER: Endoplasmic Reticulum
ERG: ElectroRetinoGrams
ESE: Exonic Splicing Enhancer
ESS: Exonic Splicing Silencer
GTP: Guanosine TriPhosphate
HEK: Human Embryonic Kidney
hnRNP: heterogeneous nuclear RiboNucleoProtein
HR: Homologous Recombination
IS: Inner Segments
ISE: Intronic Splicing Enhancer
ISS: Intronic Splicing Silencer
ITR: Inverted Terminal Repeats
LCA: Leber Congenital Amaurosis
LTR: Long Terminal repeat Regions
MerTK: Mer Tyrosine-protein Kinase
miRNA: microRNA
NHEJ: Non Homologous End Joining

OCT: Optical Coherence Tomography
ONL: Outer Nuclear Layer
OS: Outer Segments
PPT: PolyPyrimidine Tact
PR: PhotoReceptor
pre-mRNA: pre-messenger RNA
PrpF group: Proteins implicated in splicing Function
PTM: Pre-mRNA *Trans*-splicing Molecule
rAAV: recombinant AAV
Rep: proteins required for the AAV life cycle
RHO: human rhodopsin gene
Rho: mouse rhodopsin gene
RHO: rhodopsin protein
RISC: RNAi-Induced Silencing Complex
RNA: RiboNucleic Acid
RNAi: RNA interference
RP: Retinitis Pigmentosa
RPE: Retinal Pigment Epithelium
scDNA: self-complementary DNA
shRNA: short hairpin RNA
siRNA: small interfering RNA
SMaRT: Spliceosome Mediated RNA *Trans*-splicing
snRNA: small nuclear RNA
snRNP: small nuclear RiboNucleoProteins
ssDNA: single stranded DNA
TALEN: Transcription Activator Like Effector nucleases
UPR: Unfolded Protein response
UTR: UnTranslated Region
VP: capsid proteins
VSV-G: Vesicular Stomatitis Virus-Glycoprotein
WT: Wild-Type
ZF-ATF: Zinc Finger Artificial Transcription Factor
ZFN: Zinc Finger Nuclease

List of figures and annexes

Figure 1: Schematic representation of the human eye.	23
Figure 2: The visual information pathway from eyes to visual cortex.	23
Figure 3: Schematic representation of retina layers.	23
Figure 4: Structure of cone and rod photoreceptors.	24
Figure 5: Representation of cones and rods repartition on the human retina.	25
Figure 6: Fundi of a healthy individual (left) and a patient with <i>retinitis pigmentosa</i> (right).	27
Figure 7: ERG responses from a healthy individual and a patient with early autosomal-dominant <i>retinitis pigmentosa</i>	27
Figure 8: Genes associated with autosomal dominant <i>retinitis pigmentosa</i> (adRP).	28
Figure 9: The phototransduction cascade in rod cells.	28
Figure 10: Organization of rhodopsin structure.	29
Figure 11: Steps of double strand break (DSB) repair by homologous recombination (HR).	34
Figure 12: Engineered nucleases developed to induce a DSB in DNA sequence.	35
Figure 13: Human consensus sequences of 5' and 3' splice sites and branch point.	45
Figure 14: Step-wise assembly of the spliceosome and catalytic steps of splicing.	46
Figure 15: Patterns of alternative splicing.	47
Figure 16: Schemes of <i>trans</i> -splicing mechanism.	48
Figure 17: Versatility of mRNA reprogramming by targeted SMaRT.	48
Figure 18: Schematic representation of intravitreal (left) and subretinal (right) injection in a human eye.	54
Figure 19: The lentivirus: an enveloped RNA virus of around 100nm.	55
Figure 20: The adenovirus: a non-enveloped dsDNA virus of 70-90nm.	55
Figure 21: The adeno-associated virus: a non-enveloped ssDNA virus of 25nm.	56
Figure 22: Comparison of a human (left) and a mouse (right) eye.	61

Figure 23: <i>Trans</i> -splicing efficiency of PTM 15.	108
Figure 24: Characterization of RHO by western blot.	108
Figure 25: Strategies developed to avoid translation of the PTM alone.	109
Figure 26: Subretinal co-injection of AAV2/8 <i>bRho</i> -PTM0 or PTM20 and AAV2/8 <i>bRho</i> -GFP in KO <i>RHO</i> mice to study the translation of PTM alone.	110
Figure 27: Characterization of <i>Rho</i> ^{+/-} P347S <i>RHO</i> ⁺ mouse model by SD-OCT.	111
Figure 28: Comparison of <i>bRho</i> and CMV promoters, and test of two viral vector titers <i>in vivo</i>	111
Figure 29: <i>Trans</i> -splicing efficiency determined <i>in vivo</i> after injection of AAV2/8 <i>bRho</i> -PTM20 in <i>Rho</i> ^{+/-} P347S <i>RHO</i> ⁺ mice at P23.	112
Figure 30: Subretinal injections at P3 to P5 in <i>Rho</i> ^{+/-} P347S <i>RHO</i> ⁺ mice.	112
Figure 31: Intracardiac injections of fluorescein in C57Bl6J mice at P4.	121
Figure 32: SMaRT technology for rhodopsin RNA with 5' <i>trans</i> -splicing approach.	122
Figure 33: Stages of retinal degeneration and the forms of gene therapy that can be used in that stage.	123
Table 1: Classification of rhodopsin mutations.	30
Table 2: SMaRT applications.	49
Table 3: Properties of classical viral vectors used in ocular gene therapies.	55
Table 4: Cellular tropism of rAAV serotypes following subretinal injection.	57
Table 5: Comparison of parameters used for the study of the PTM translation <i>in vitro</i> and <i>in vivo</i>	118
Annex 1: mouse versus human sequences of rhodopsin mRNA and proteins.	147
Annex 2: Supplemental materials and methods.	148

Preamble

Retinitis Pigmentosa represent a group of inherited retinal degenerative diseases, which represents one of the most common genetic visual impairments worldwide. To date there is no treatment to prevent development of the disease, meaning that patients are sentenced to progressive vision loss, in some cases resulting in blindness. One gene, coding for rhodopsin and carrying at least one hundred known-point mutations, is alone responsible for more than 30% of the autosomal dominant forms. Consequently several strategies targeting rhodopsin mutations are in progress today, in order to prevent or delay this retinal disorder. While such projects present interesting data, most of them are mutation-dependent and/or present potential off-target and toxicity side effects and/or do not respect the endogenous level of rhodopsin expression that can also be deleterious for the retina.

Having identified these limitations, the purpose of my PhD project was thus to develop a new strategy to repair rhodopsin mutations, with the advantage of being able to target the biggest number of mutations with only one tool and of respecting the physiological expression level of the gene. The technology that I used was based on a rare but natural event in humans, called “*trans*-splicing”.

To place my PhD project in context, I will firstly introduce you some general knowledge about the eye and the vision process paying particular attention to the photoreceptors, as these cells are primarily affected in *retinitis pigmentosa*. Then I will identify characteristics of *retinitis pigmentosa*, in terms of clinical symptoms, treatments and genetic involvement of rhodopsin, whose characteristics will be exposed in details, with a particular emphasis on its function, its structure and the mutations leading to the disease. In the second part, we will address strategies that are currently being developed to cope with rhodopsin mutations. I will then introduce *trans*-splicing in the third part, which is the strategy that we chose to develop in my PhD project. I will first of all cover the more classical *cis*-splicing in a cellular context, discussing the steps and regulation involved in this mechanism, before mentioning natural cases of *trans*-splicing and how researchers have commandeered this process to create SMaRT (Spliceosome Mediated RNA *Trans*-splicing) technology. I will summarize current

approaches using this technique, its characteristics and how to improve this method. The fourth part of my introduction will review viral vectors commonly used in gene therapies for ocular diseases, specifically AAV (Adeno-Associated Virus) vectors, which are the most popular in this field, and that we chose to transport the SMaRT molecule developed in my project. To finish, because each new therapeutic approach needs to be tested in biological models before clinical trials can commence in humans, we will address existing cellular and animal models of rhodopsin expression or mutated rhodopsin-induced RP.

INTRODUCTION

I. Retinitis pigmentosa induced by rhodopsin mutation

I.1. Eye and vision

I.1.a. Generalities

Vision is one of our most important senses, allowing us to move in space, to distinguish faces and objects, and perceive the world around us. Photons constitute the light stimulus that are detected by our eyes, caught by the retina, transformed to an electrochemical signal and transmitted to the brain for its interpretation. From the visible part of the eye to its deepest structure (Figure 1), the light penetrates into the eye through the cornea, a clear and curved layer that protects it from physical damage and bacterial aggression. Then, the amount of light penetrating the eye is modulated by the dilatation or the constriction of the pupil, the central opening of the iris, which depends on the action of the papillary sphincter muscle and dilatator muscle respectively. The iris thus acts as a diaphragm and gives the color to the eye. The light then runs through the lens that acts like a thin biconvex capsule, able to change its shape through the action of the ciliary muscles, to focus the light onto the retina. Behind the lens stands the vitreous, a viscous transparent substance that participates in the maintenance of the intra-ocular pressure. Finally, photons are caught by the retina, the neuro-sensorial part of the eye. After signal transformation and processing by nerve impulses into the retina (described below) visual information is interpreted by the visual cortex, after its transit through the lateral geniculate nucleus (Figure 2). Due to the neuronal nature of most retinal cells and the presence of structures similar to those found in the brain such as the blood brain barrier, the eye is considered an extension of the brain, and a part of the central nervous system.

I.1.b. The retina

The neuroretina, composed of photoreceptors, horizontal cells, bipolar cells, amacrine cells and ganglion cells (Figure 3), is the essential tissue for the capture and transmission of the visual information. When photons enter into the eye, they pass through the retina and are captured by rod and cone photoreceptors, which transform them to an electrochemical signal, itself transmitted to bipolar cells. These last cells extend the signal transmission to ganglion cells, whose fibers form the optic nerve that drives the information into the visual cortex. Amacrine cells and horizontal cells participate in visual information processing by permitting

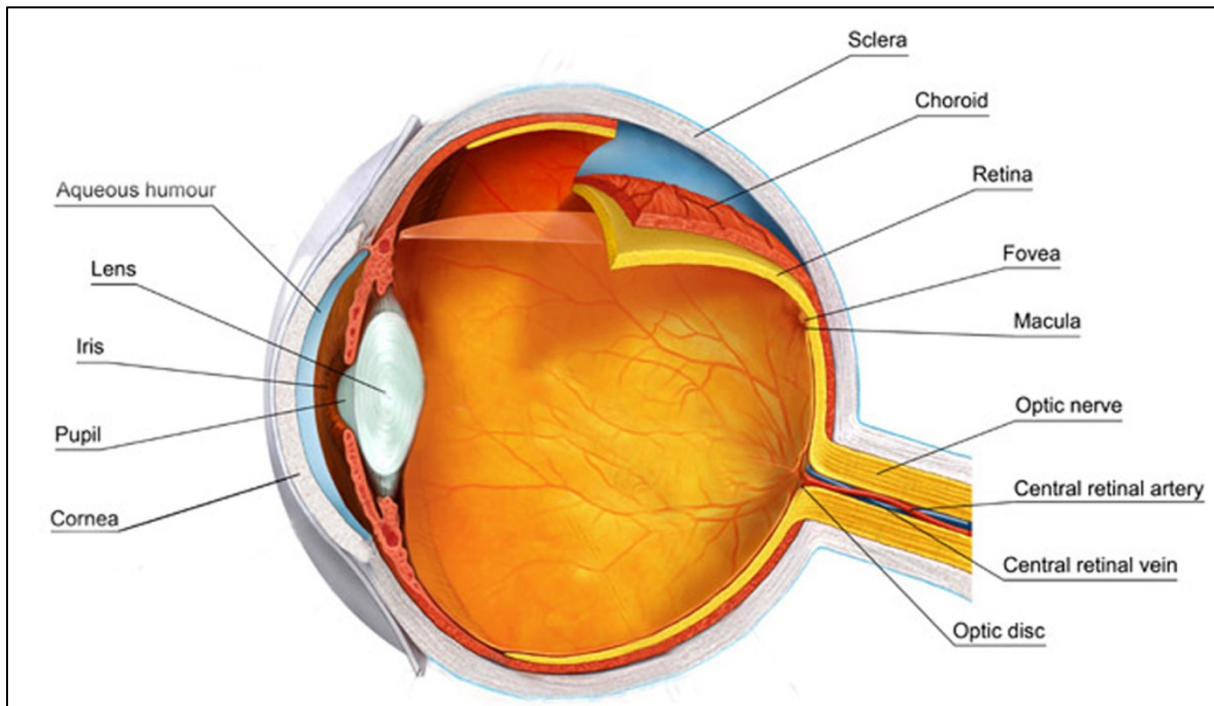


Figure 1: Schematic representation of the human eye.

When a photon enters into the eye, it goes across the cornea, the aqueous humor, the pupil, the lens and the vitreous before reaching the retina. Adapted from *virtualmedicalcentre.com*.

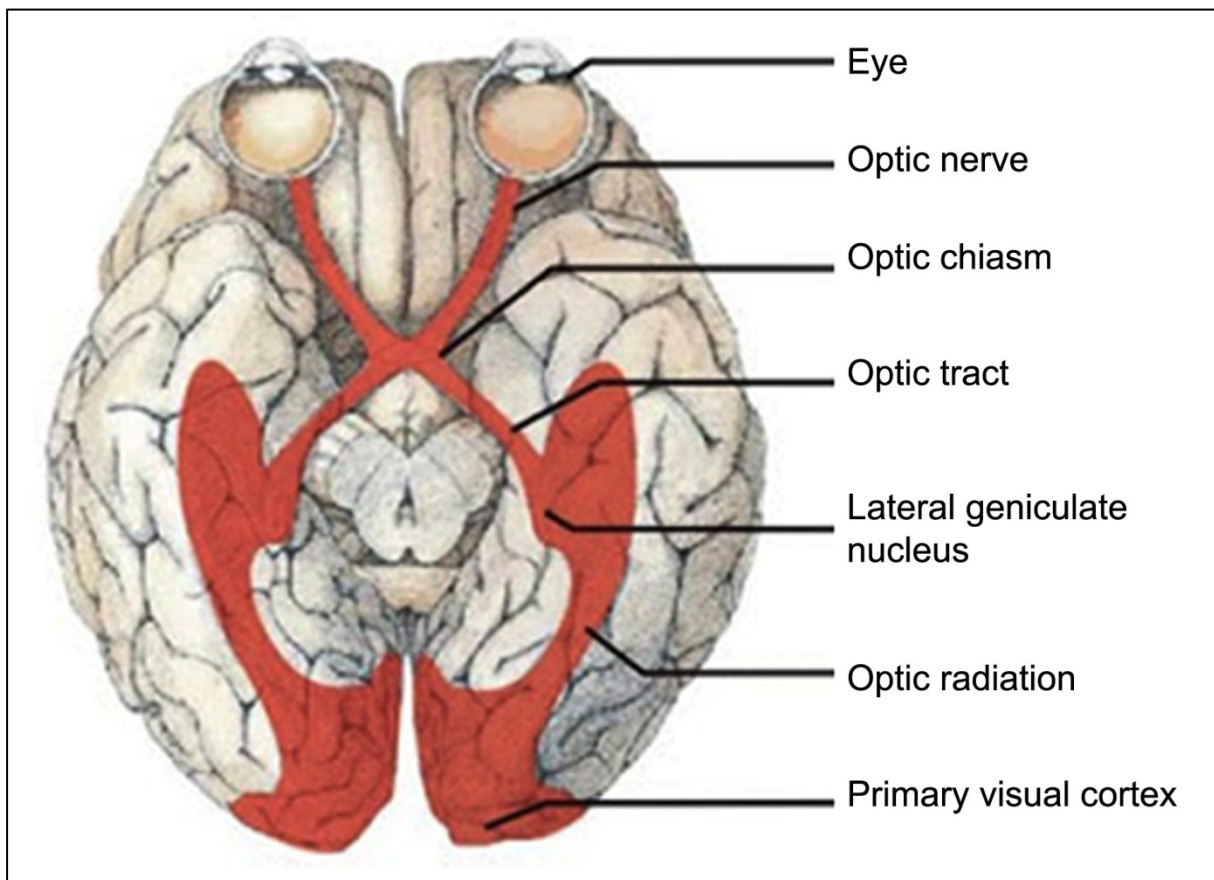


Figure 2: The visual information pathway from eyes to visual cortex.

A visual signal reaches the primary visual cortex from the eye, through the optic nerve, the optic chiasm, the optic tract, the lateral geniculate nucleus and the optic radiation.

a better propagation of the signal and improve contrast and definition of the visual stimuli, for example by lateral inhibition.

The neuroretina would not be efficient without the presence of Müller cells, astrocytes and microglial cells, which represent the glial cells of the retina and contribute to maintaining the structure of this tissue. Last but not least of the retinal cells are those of the retinal pigment epithelium, which have many important functions, including recycling of 11-*cis*-retinal, absorption of scattered light, providing photoreceptors with nutrients and oxygen, and phagocytosis of damaged photoreceptor outer segments.

All these cells are organized in strata, the retina can be divided in 10 layers (Figure 3), from the vitreous to the choroid (i.e. from the inner to the outer retina):

- The inner limiting membrane, a basal membrane composed of proteins from the extracellular matrix and feet of Müller glial cells,
- The optic nerve fiber layer, constituted of the axons of ganglion cells, which gather to form the optic nerve,
- The ganglion cell layer, represented by the cell body of ganglion cells,
- The inner plexiform layer, which is an entanglement of axons and dendrites of ganglion, amacrine and bipolar cells,
- The inner nuclear layer, which contains the cell bodies of bipolar, amacrine, horizontal and Müller cells,
- The outer plexiform layer, composed of axons and dendrites of bipolar and horizontal cells and photoreceptors,
- The outer nuclear layer (ONL), formed by the nuclei of photoreceptors (PR),
- The outer limiting membrane, which is a “zonula adherens”, a region of adherence between two cell types, here between PR and Müller glial cells,
- The segments of the PR, constituted of inner and outer segments (IS-OS),
- The retinal pigment epithelium (RPE) composed of cells of the same name.

I.1.c. Human photoreceptors

Two types of PR are present in the retina: cones and rods, which take their names from their shapes (Figure 4). They are made up of (i) a synaptic terminal connected to bipolar and horizontal cells, (ii) a cell body that contains the nucleus, (iii) an IS where metabolism, biosynthesis and endocytosis take place, explaining the presence of numerous mitochondria at this level, (iv) a connecting cilium, the bridge between segments, which shares morphology and composition of a primary cilia, and (v) an OS, composed of around 1000 flattened,

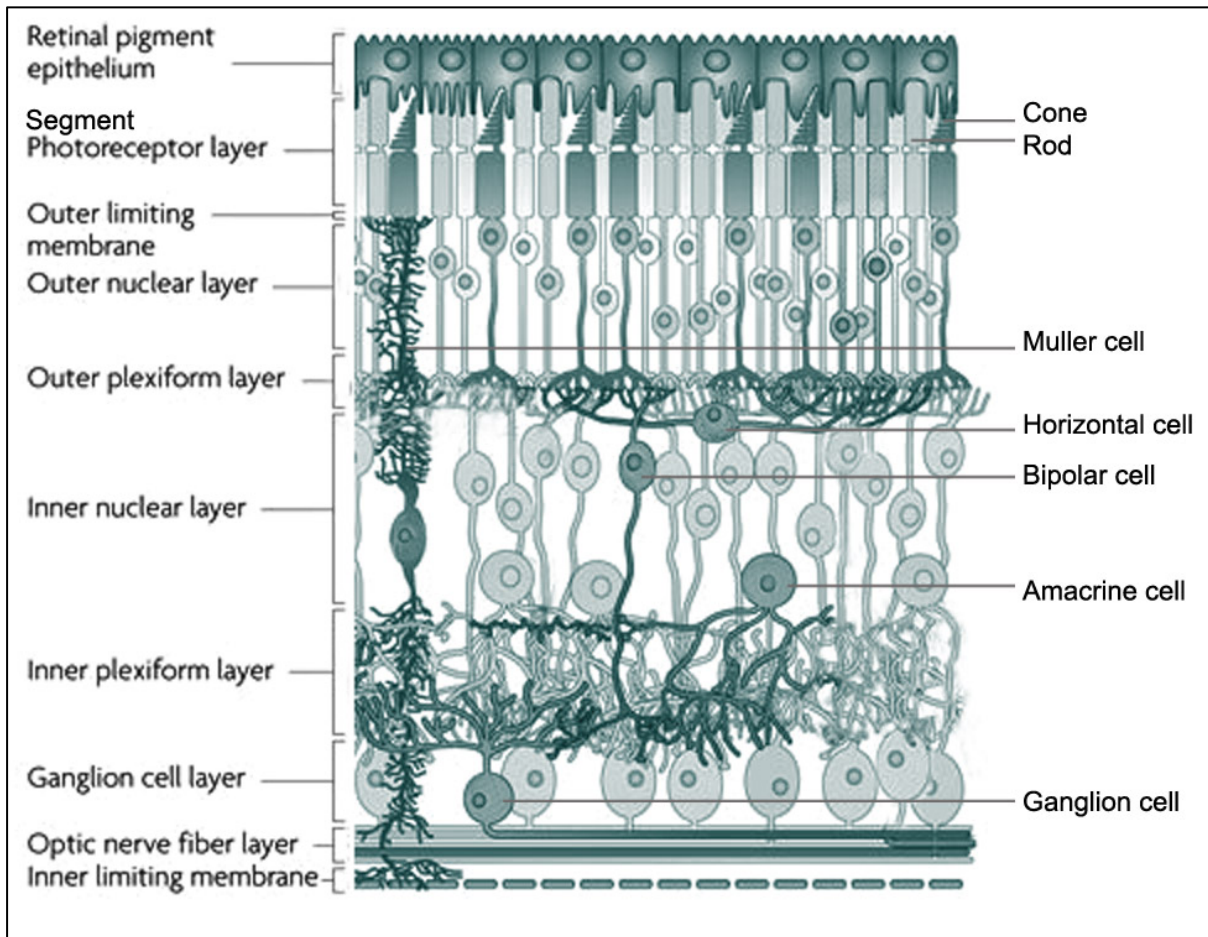


Figure 3: Schematic representation of retina layers.

Name of each retinal cells are indicated on the right, and denomination of retina layers on the left. Adapted from *Swaroop et al., Nature Reviews Neuroscience, 2010.*

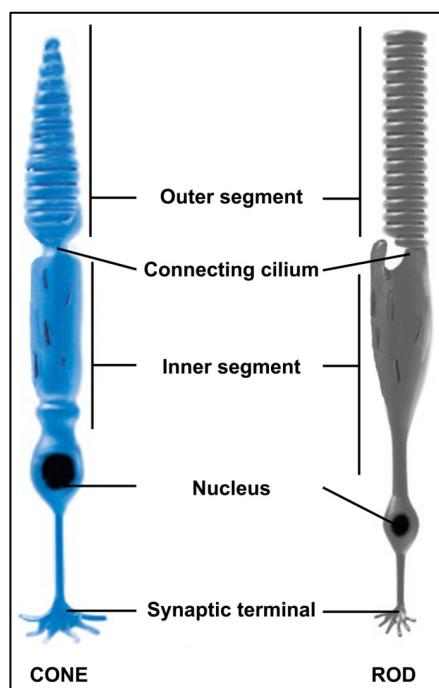


Figure 4: Structure of cone and rod photoreceptors.

Photoreceptors are composed of three main parts: a somato-dendritic compartment, an inner and an outer segment. Adapted from *visualdictionaryonline.com*

lamellar-shaped membrane discs³⁸, which considerably increase the total membrane surface of the cell. These very specific structures mainly contain opsins, light-sensitive molecules that are involved in the first step of the phototransduction cascade that transforms the light stimulus in an electrochemical signal.

Cones and rods are both distributed quite uniformly on the surface of the retina, except in one particular region specific to humans and other higher primates, the macula. The macula is localized in the central retina, where cones are the majority PR. The central part of the macula is the fovea and is exclusively composed of cones (Figure 5), it represents the region where the acuity is maximal. Cones are thus essential to visual acuity, but require normal or high-light conditions. In humans and some primates, each cone synthesizes one of the three cone opsins that possess maximal absorption at different wavelengths of light: (i) long wavelength sensitive opsin (OPN1LW) detects photons in the red region of the visible light spectrum, (ii) middle wavelength sensitive opsin (OPN1MW) for the green region of the spectrum, (iii) and short wavelength sensitive opsin (OPN1SW) for the blue region of the spectrum. These three kinds of proteins allow color vision, which is totally created by the brain, after combinatorial analysis of the input sent by these cells.

In the other hand, rods are implicated in dim-light, and peripheral vision. They are the most numerous cells in our retina, counting for around 60 million per retina, nearly twenty times more represented than cones³⁹. Rods contain only one kind of opsin, called rhodopsin, which represent more than 90% of rod OS proteins and absorbs light maximally at 495nm. While cones continue to function at more than one hundred million photons per second, rods saturate at several thousand photons, but the high density of rhodopsin combined with its sensitivity allows the retina to detect a single photon¹. This important difference between rods and cones concerning the amount of light required to induce a response, allows to the retina to cover a large range of light intensities. Rods are PR required for dim-light, peripheral and high-sensibility vision, while cones are involved in normal or high light, acute, central and color vision.

PR present a hazardous environment, resulting from a high exposure to light and a strong presence of free radicals due to their high oxygen consumption, but because these cells are post-mitotic neurons, they have developed a unique mechanism, to avoid damage. Indeed, PR and more precisely OS are continuously regenerated. Around 10% of OS disks are phagocytosed in a circadian manner every day by the RPE, and immediately replaced by new components produced at the base of the OS⁴⁰, which necessitates the synthesis of up to 10^7 new molecules of rhodopsin/OS/day.

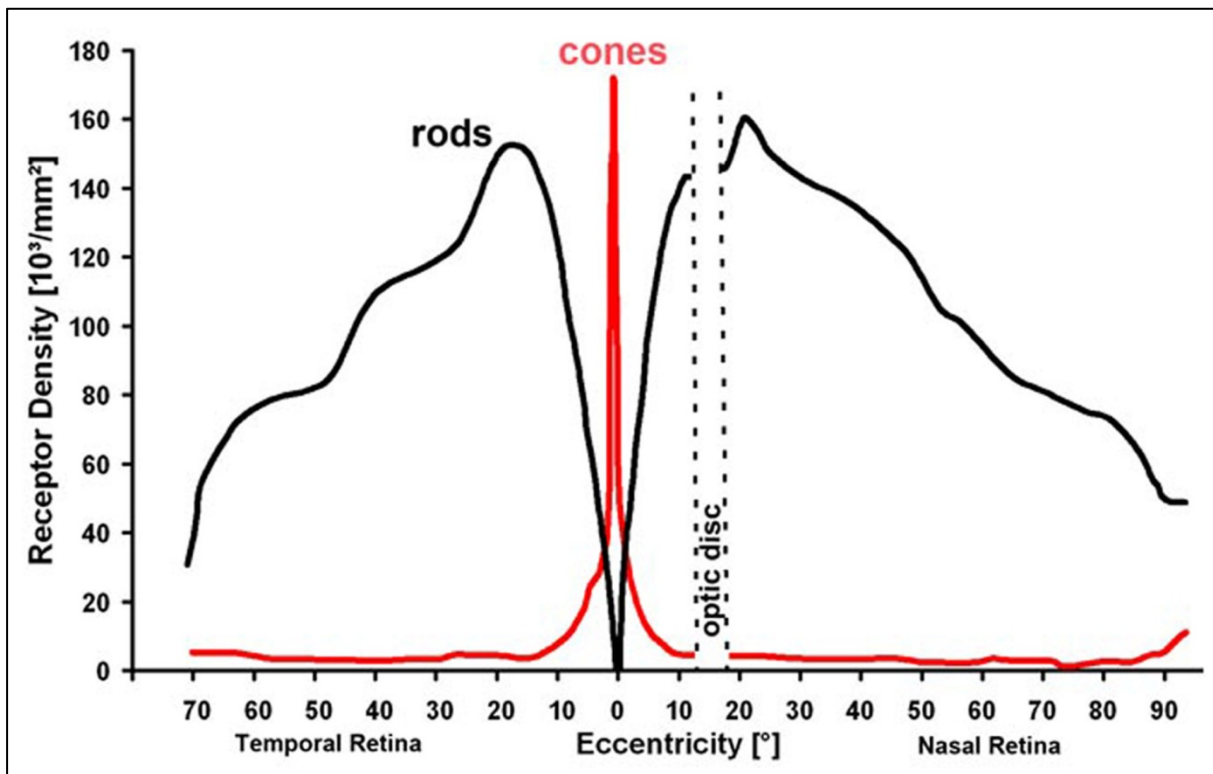


Figure 5: Representation of cones and rods repartition on the human retina.

Rods represent the majority of retinal photoreceptors. They are absent from only two distinct regions: the fovea where cones are the only photoreceptors, and the optic disc, the blind point of the eye, which corresponds to the head of the optic nerve.

I.2. Retinitis pigmentosa

Retinitis pigmentosa (RP) make up a heterogeneous group of inherited retinal degenerative disorders, firstly characterized by a loss of scotopic vision associated to a mid peripheral visual field failure and usually followed by a central vision loss, leading to blindness. A particularity of this disease is its very important heterogeneity in terms of severity, evolution speed, age of onset and gene mutation, which makes of it a complex disease to study. Although considered as a rare disease due to the small number of patients for each gene, the overall prevalence of RP is around 1 in 4000, making it one of the most common causes of visual impairment in all age groups, and the most prevalent among the working population in developed countries⁴¹.

I.2.a. Remodeling of the retina and clinical manifestations

The retinal degeneration observed in RP is primarily due to the death of rod PR, which is then followed by the death of cone PR. The first observation is the shortening of the rod OS, often associated to connecting cilium dysfunction and sprouting of rod neurites, which appears before the apoptotic death of the cell. Cones then follow the same fate, but this is not the only cell lineage to be affected; the subretinal space disappears, due to the migration of RPE cells toward the inner side of the retina, the choriocapillaris (the vascular network located under the retina and responsible for providing oxygen and nutrients to the RPE/PR layers) degenerates and Müller cells enter in an active gliosis phase⁴². The culmination of all these phenomena lead to the outer retinal degeneration that causes the vision loss.

Patients with RP firstly present a defective dark adaptation, accompanied by mid-peripheral vision loss. These two symptoms are due to the death of rods and constitute the firsts manifestations of the disease that are often hardly noticeable by the affected individuals. The course of the disease leads more or less rapidly to constriction of the visual field, which occurs when most of rods have degenerated. Central visual acuity is often preserved until later stages of the disease, even if cones are also partly damaged.

RP is mainly diagnosed by observation of the fundus appearance, and functional testing of the retina. Some changes are often observed in the fundus, but are not specific to RP, like arteriolar narrowing, retinal vessel attenuation, waxy pallor of the optic nerve, posterior subcapsular cataracts, dust-like particles in the vitreous, white dots deep in the retina...⁴³ The most famous and typical modification observed in RP, giving its name to the disease, is the loss of pigment from the RPE, which form intraretinal clumps of melanin that appear like

black spots on the retina (Figure 6). Optical Coherence Tomography (OCT) can also be used to measure retinal thickness and thus follow the degeneration course. It consists in an interferometric technique, typically employing near-infrared light, to penetrate deeply into tissues. It captures micrometer-resolution images, which allow identification of each layer of the retina with RP patients presenting a reduction in thickness of ONL and PR segments layers.

In addition to these purely descriptive aspects, functional criteria also participate to RP diagnosis. Testing of the visual field is used to determine presence of scotomas (blind spots) corresponding to regions where PR have degenerated. Electroretinograms (ERG) are also very informative regarding the functional state of PR. After dark-adaptation, electrical potentials in response to light are recorded by electrodes placed in contact with the cornea. Dim-light stimulation allows measurement of the rod efficiency, and cone function is measured in normal light conditions. Electrical signals are representative of the general state of the retina (focal ERG) or a particular region of this one (multifocal ERG). Patients with RP present rod and cone delayed responses with reduced amplitudes (Figure 7).

1.2.b. Genetic involvement

RP can be syndromic⁴⁴ (affecting other neurosensory systems or even systemic, affecting multiple tissues), or non-syndromic (affecting only vision). About 20-30% of RP patients present syndromic RP, listed in more than 30 syndromes, which associate non-ocular disorders, including:

- Usher syndrome, which represents 10-20% of RP, and is characterized by hearing loss⁴⁵,
- Bardet-Biedl syndrome^{46,47}, in which RP is variably associated with obesity, cognitive impairment, polydactyly, hypogenitalism and retinal disease, accounts for 5-6% of RP cases.
- And many other rare syndromes including:
 - Refsum's disease⁴⁸, in which RP is systematically associated with anosmia and often other variable symptoms,
 - Bassen-Kornzweig syndrome, caused by abetalipoproteinaemia⁴⁹, inducing among other symptoms: balance and coordination difficulties, developmental delay, muscle weakness...
 - α -tocopherol transport protein deficiency⁵⁰, causing ataxia with vitamin E deficiency.

In non-syndromic forms, RP is genetically heterogeneous, including autosomal dominant,



Figure 6: Fundi of a healthy individual (left) and a patient with *retinitis pigmentosa* (right). In the image of the diseased eye, optic-disc pallor, attenuated retinal arterioles, and peripheral intraretinal pigment deposits in a bone-spicule configuration are seen. Extracted from *Hartong et al., The Lancet, 2006.*

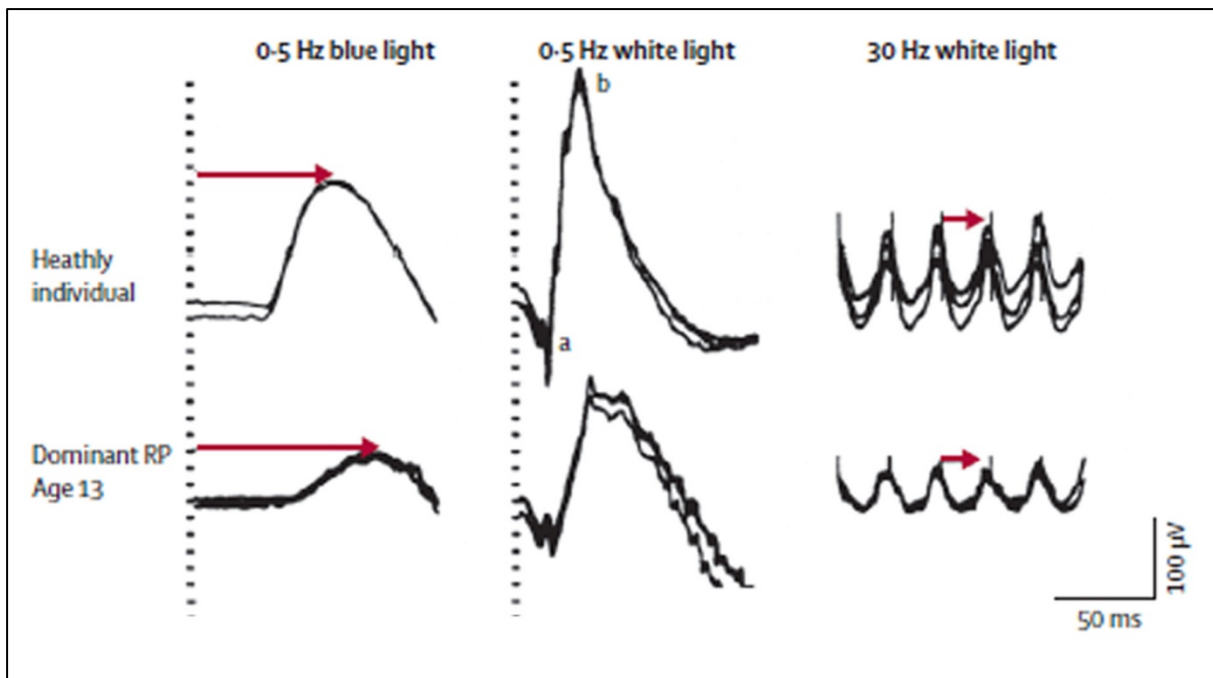


Figure 7: ERG responses from a healthy individual and a patient with early autosomal-dominant *retinitis pigmentosa*.

RP=retinitis pigmentosa. a=a wave. b=b wave. Vertical dotted lines (left and centre columns) and vertical shock artifacts (right column) represent stimuli. Arrows indicate response times (called implicit times). Extracted from *Hartong et al., The Lancet, 2006.*

autosomal recessive, X-linked, sporadic and very rare digenic forms. Autosomal dominant RP (adRP) is the most common form of the disease with a prevalence of around 20% as documented in the literature. There is great heterogeneity regarding the degeneration speed and impact on the retina depending on the gene and the mutation implicated, knowing that 25 genes have been associated to adRP⁴³ to date (RetNet, <https://sph.uth.edu/retnet/>) (Figure 8) with environmental factors also affecting outcomes. Genes already characterized in adRP mainly encode for proteins involved in phototransduction, visual cycle, PR structure or gene expression, but more surprisingly, there is also an important group of genes that encode for proteins implicated in splicing function (PrpF group) and there is no real evidence to date explaining precisely why a mutation on a ubiquitous protein, induces damages only in the eye. Moreover, the involved gene remains unknown in more than 40% of cases. In 1989, the rhodopsin gene (*RHO*)² was for the first time found to be linked to adRP by MacWilliam and co-workers⁵¹. To date, *RHO* has been the gene most frequently implicated in adRP with a proportion of 30 to 40% of total adRP occurrences. More than one hundred point mutations of *RHO* directly associated to adRP have been described, each one being sufficient to develop the disease.

I.3. Rhodopsin

I.3.a. Rhodopsin synthesis, function and visual cycle

While there are three different opsins in cone cells, the *RHO* gene encodes the only opsin of rod cells. It is firstly synthesized and post-translationally modified by N-Glycosylation into the rough endoplasmic reticulum. After its transport to the Golgi apparatus, proteins are assembled into vesicles, to be exported from the IS through the connecting cilium to attain the OS, where rhodopsin proteins (RHO) are directly integrated into newly synthesized disc membranes. RHO is a G protein-coupled receptor, with 7 trans-membrane domains, which must be associated to the 11-*cis*-retinal chromophore, a derivative of vitamin A, to be functional. This molecule is covalently bound via a protonated Schiff base to the polypeptide chain of RHO, creating the photopigment of the rods. When the light enters into the retina, photons are absorbed by the 11-*cis*-retinal, driving to its isomerization to all-*trans*-retinal isomer. This reaction is the first step of the activation of phototransduction cascade (Figure 9), which transforms the light stimulus caught by the retina into an electrochemical signal that will be transmitted toward the brain. Firstly, some modifications on RHO structure appear, leading to core opening, which permit identification of metarhodopsin I then II⁵². As an

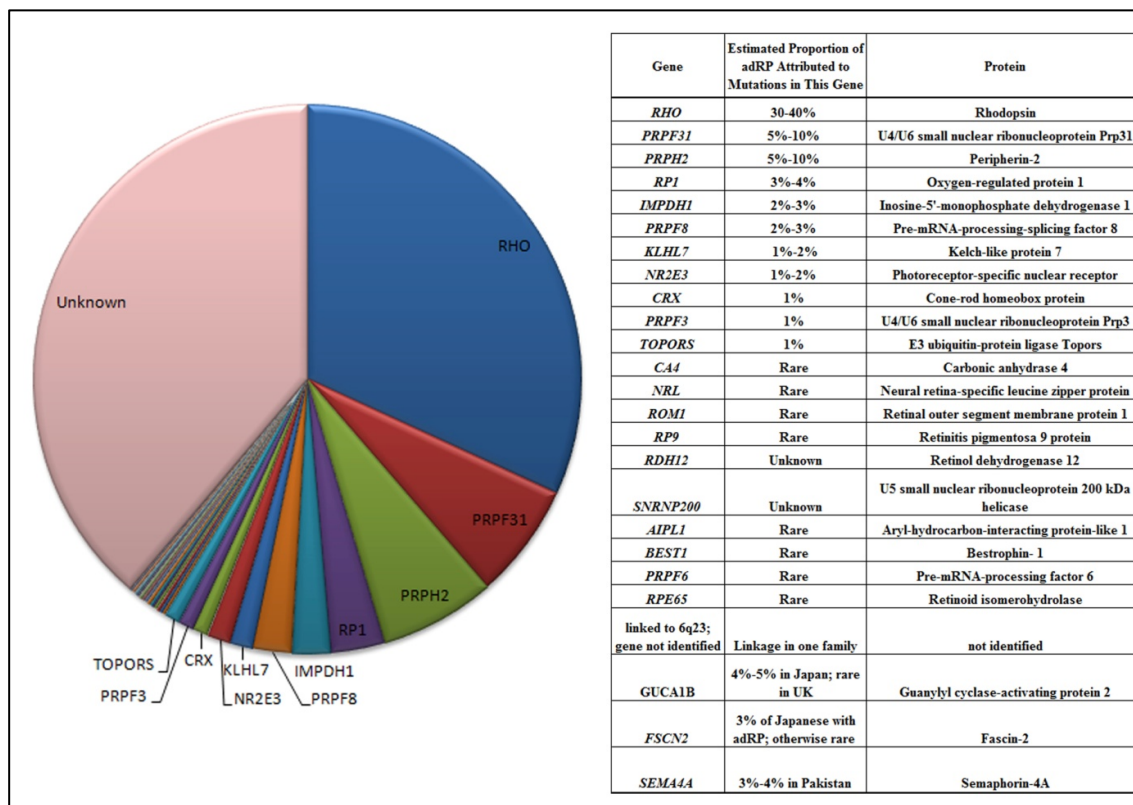


Figure 8: Genes associated with autosomal dominant retinitis pigmentosa (adRP).

Adapted from sph.uth.edu/retnet/ and Fahim et al., *GeneReviews*, 1993.

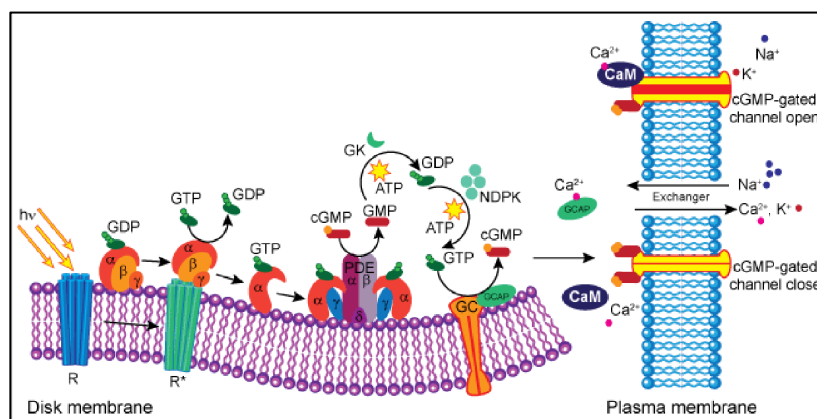


Figure 9: The phototransduction cascade in rod cells.

In the dark, opsin is bound to 11-*cis*-retinal to form inactive rhodopsin (R) in the disc membranes. Basal activity of the guanylyl cyclase (GC) keeps cGMP levels high. The binding of Ca²⁺-bound calmodulin (CaM) confers high affinity for cGMP to cGMP-gated channels in the plasma membrane, allowing these channels to remain open. Both Na⁺ and Ca²⁺ enter the channels resulting in high Ca²⁺ levels and Ca²⁺-bound guanylate cyclase-activating protein (GCAP). Light (hv) results in photoisomerization of 11-*cis*-retinal to all-*trans*-retinal, forming activated rhodopsin (R*), which binds and activates the heterotrimeric G protein, transducin (αβγ). The GTP-bound transducin α subunit activates cGMP phosphodiesterase (PDE), which hydrolyzes cGMP to GMP, reducing the cGMP concentration and the binding of cGMP to the cGMP-gated channel. The probability of channel closing increases proportional to light intensity, reducing Ca²⁺ influx. Intracellular Ca²⁺ is further depleted by activity of the Na⁺-Ca²⁺, K⁺ exchanger. Low intracellular Ca²⁺ leads to active GCAP, which in turn activates GC to synthesize cGMP from GTP supplied by the guanine nucleotide cycle. This comprises guanylate kinase (GK) and nucleoside diphosphate kinase (NDPK). Release of Ca²⁺ from CaM leads to its dissociation from the cGMP-gated channels conferring a lower affinity for cGMP and further closure of the channels. Extracted from mutagenetix.utsouthwestern.edu

activated G-protein coupled receptor, metarhodopsin II then activates transducin, a trimeric G protein, composed of α , β and γ subunits. The activation of transducin induces the exchange of a guanosine diphosphate for a guanosine triphosphate (GTP) and the subsequent dissociation of transducin α -subunit-GTP from the rest of the complex. Transducin α -subunit-GTP in turn allows the activation of the phosphodiesterase. This last step transforms the cyclic guanosine monophosphate (cGMP) present in rods into GMP, leading to closure of cGMP-gated $\text{Na}^+/\text{Ca}^{2+}$ membrane channels. Finally, this disruption in exchanges across the membrane promotes its hyperpolarization stopping glutamate release. Indeed, in a basal state, i.e. without light stimulus, glutamate is released and PR are depolarized; while light stimuli induce an hyperpolarization. Once activated, RHO also becomes the target of the kinase arrestin, which initiates and completes its inhibition. After a period of time, this complex dissociates, and RHO is dephosphorylated by a phosphatase. RHO is thus available again to bind 11-*cis*-retinal and to react to light-exposure after about 400s⁵³. On its side, all-*trans*-retinal is regenerated to be available again for binding to opsin by a series of reactions taking place both in the PR and the RPE cells, and which bear the name of "visual or retinoid cycle"⁵⁴.

I.3.b. Structure of rhodopsin

As in all G protein-coupled receptors, RHO possesses a seven α -helical trans-membrane architecture, which varies in length from 20 to 33 residues. The trans-membrane region represents about 65% of the protein, while the rest of the amino acids are quite equally distributed in the N-terminal region located inside the discs, and the cytoplasmic C-terminal region (Figure 10).³

RHO presents a highly conserved sequence between mammalian species, with around 95% of amino acid sequence that is common from human to mouse, rabbit and rat (NCBI).

The 37 first amino acids constitute the amino terminal domain, which is co-translationally acetylated and glycosylated in the endoplasmic reticulum at two asparagine residues (Asn2 and Asn15). These modifications seems to be essential to folding and/or insertion of the protein to the membrane⁵². Amino acids 38 to 311 form the seven trans-membrane helices and intra or extra-cellular loops between each of them. This sequence includes a disulfide bond necessary for the correct formation of the tertiary structure of the protein at the level of the retinal chromophore binding site (Lys 296) and transducin binding regions. The last part of RHO is the cytoplasmic carboxyl-terminus domain including two

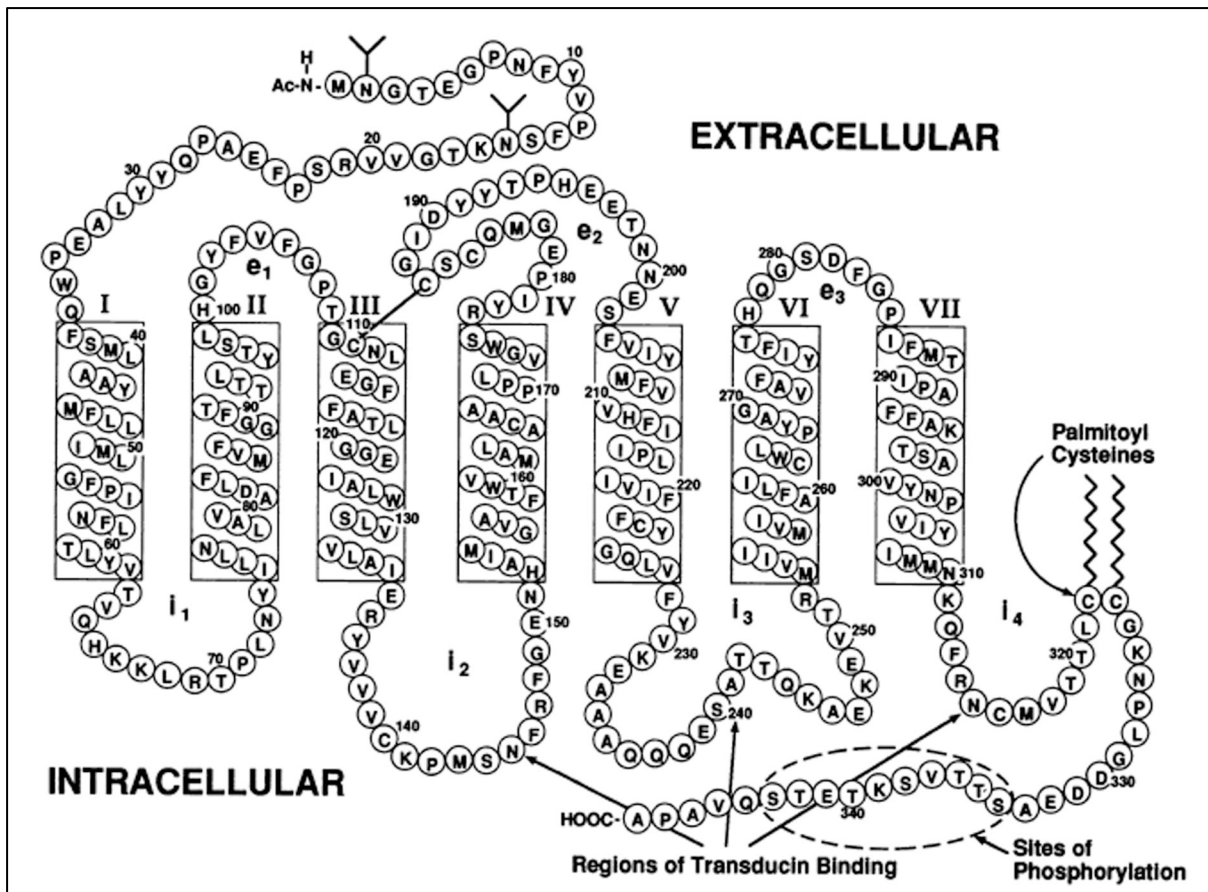


Figure 10: Organization of rhodopsin structure.

Rhodopsin is a 7 α -helical trans-membrane G protein-coupled receptor, with a cytoplasmic C-terminal domain and a N-terminal domain located between discs of rod photoreceptor outer segments. Extracted from *Hargrave, FASEB, 1992.*

palmitoyl cysteine residues and a sequence of nine amino acids comprising several serine and threonine, which can be phosphorylated, creating a binding domain of arrestin⁵². The fifth last amino acids constitute the QVAPA domain, which is the autonomous OS-targeting signal, and is therefore essential to the transport of RHO to the OS⁵⁵.

I.3.c. Rhodopsin mutations and consequences

More than 120 point-mutations have been described in *RHO*, each one leading to retinal degeneration, most of the time adRP, but also sometimes autosomal recessive RP or congenital stationary night blindness. These mutations are quite homogeneously distributed on *RHO*. The P23H mutation is the most frequent mutation in US Caucasians with a prevalence of about 10% of adRP patients (RetNet, <https://sph.uth.edu/retnet/>), while P347L and R135W are frequent mutations in European population⁵⁶.

Among numerous existing classifications that ordered RHO mutations, I choose to follow those of Mendes et al.⁴. This classification divides RHO mutations in 6 classes based on the cellular dysfunction and described in Table 1.

Concerning the properties of these mutations, the fact that homozygous *RHO*-knockout mice present an almost complete loss of PR after 90 post-natal days while heterozygous ones showed only a mild PR degeneration⁵⁷, suggests that RHO mutations should be dominant-negative or gain-of-function mutations. Added to this is the wide description of gain-of-function mechanisms that have been observed to date, one can in particular mention:

- The unfolded protein response (UPR) activation. The UPR or ER stress is partially mediated by accumulation of mis-folded proteins. In RP cases, class II RHO mutations (including P23H) have been described to be retained in the ER in cellular models^{58,59}, inducing the UPR activation^{60,61}, which can lead to cell death by apoptosis. This could be an explanation for PR degeneration, but this observation is still under debate in the *in vivo* context^{62,63}.
- The aggresome formation. Several studies show in cellular models that class II RHO mutants (including P23H) develop a capacity to aggregate as a gain-of-function^{64,65}. Aggresomes are pericentriolar inclusion bodies into which aggregated proteins are sequestered by active retrograde transport on microtubules. By creating aggresomes, RHO mutants could lead to a generalized impairment of the ubiquitin proteasome system and suggests a mechanism by which PR death might be induced.
- Disruption of the post-Golgi traffic and OS targeting. Class I RHO mutants (including Q344Ter and P347L/S) present a defective or absent QVAPA domain, which is essential for a

Classification	Behaviour	Site of point mutation	Misfolds
Class I	Fold normally but are not transported to the outer segment	L328, T342, Q344, V345, A346, P347	No
Class II	Are retained in the ER and cannot easily reconstitute with 11- <i>cis</i> -retinal	T17, P23, G51, T58, V87, G89, G106, C110, L125, A164, C167, P171, Y178, E181, G182, C187, G188, D190, H211, C222, P267, S270, K296	Yes
Class III	Affect endocytosis	R135	No
Class IV	Do not necessarily affect folding but affect rod-opsin stability and posttranslational modification	T4	No
Class V	Mutations show increased activation rate for transducin	M44, V137	No
Class VI	Show constitutive activation of opsin in the absence of chromophore and in the dark	G90, T94, A292,	No
Unclassified	No observed biochemical or cellular defect or not studied in detail	N15, Q28, L40, F45, L46, P53, G109, G114, S127, L131, Y136, C140, E150, P170, G174, P180, Q184, S186, T193, M207, V209, P215, M216, F220, E249, G284, T289, S297, E341	

Table 1: Classification of rhodopsin mutations.
Adapted from *Mendes et al., TRENDS in Molecular Medicine, 2005.*

properly targeting to the PR-OS. These mutants are thus retained into others compartments of the cell^{55,66}, and by this way should induce PR death by interfering with cellular processes or submerging the normal vesicular traffic machinery.

- Abnormal arrestin binding and impaired endocytic activity. Mutations at the R135 residue that constitutes the class III mutants, recruit arrestin in the absence of 11-*cis*-retinal, and the complex formed by the two proteins might alter the morphology of endosomal compartments and damage receptor-mediated endocytic functions⁶⁷.

- Constitutive or dys-regulated activation. Several mutations have been described to generate a constitutively active RHO, for example a mutation on lysine 296 (class II) that is the chromophore binding site. These mutants are suspected to be more or less directly linked to PR degeneration^{68,69}.

- Structural instability within the OS. As discussed previously, a lot of RHO mutations are not correctly folded and/or addressed to PR-OS, creating instability of the protein in the cell, and instability of the OS structure. Indeed, because RHO is essential to OS formation and maintenance^{57,70}, mutations can lead to default in OS formation or degradation of OS, which can induced PR death.

Some of these studies suggest that RHO mutants (including P23H) can also have a dominant-negative effect on WT proteins by disturbing its post-translational maturation, by retaining it in aggresomes, by amplifying its proteasome-mediated degradation and steady-state ubiquitination. Dominant-negative and gain-of-function effects are not exclusive and can also act in concert leading to PR death.

This heterogeneity in RHO mutations, concerning their localization on the gene sequence and their potential mechanism of action highlights the obvious difficulty in finding a global treatment effective for all these mutations, except in the case of developing a single tool able to replace the mutated rhodopsin gene in all the affected cells.

I.4. Treatments of RP

I.4.a. General current treatments of RP

All approaches that are currently developed to avoid progression of RP can be classified in three groups depending on the progress of the disease:

- Before the degeneration of PR and in the case of identification of the responsible genetic factor, strategies of gene replacement or nucleic acid correction can be promoted, to

prevent establishment of the disease. The most accomplished therapy by gene replacement developed for an eye-disease to date has been done in RPE cells, and is for Leber Congenital Amaurosis, a severe form of RP affecting children (exposed in details in part IV.2.b). Gene replacement is efficient for recessive diseases, for which it is sufficient to restore the expression of the normal gene, but this is usually not the case in the context of a dominant mutation. In this case, nucleic acid corrections are required (these strategies will be developed in part II).

- If only few rods have degenerated, the other cells may be saved by neuroprotective treatments:

- Neurotrophic factors. Numerous proof-of-concept of therapeutic efficiency of neurotrophic factors have been demonstrated in *in vivo* models of RP^{13,71,72}, but they delay degeneration more than they prevent the disease. Nonetheless, they can be used to enlarge the therapeutic window. One of the advantages of this type of treatment is its non-specificity with regards to the disease-responsible gene. An intraocular implant secreting ciliary neurotrophic factor (CNTF)¹⁴ is currently in Phase II/III clinical trials for RP and Age-related Macular Degeneration⁷³. Nevertheless, the results of these clinical trials do not support a beneficial effect on PR function. Moreover, neurotrophic factors are often pleiotropic and might have other effects on the retina that could question their long-term use.

- Vitamin A and/or vitamin E supplementation. Oral vitamin A and/or E supplements can have beneficial effects on the natural course of RP (observation of slower declines of ERG amplitudes compared to untreated patients). However, clinical measures such as visual acuity and visual field appear unaffected by supplementation. Vitamin E seems to present a significant negative effect at higher doses⁷⁴ and vitamin A had potentially dangerous side effects for older and pregnant patients⁷⁵⁻⁷⁷. These treatments both require a regular monitoring of patients.

- Docosahexaenoic acid. This omega-3 fatty acid is highly enriched in PR membranes and it thus suspected to be important for PR function. Even if relationship exists between concentration of docosahexaenoic acid in red-blood cells and RP course, a benefit of its supplementation has not been demonstrated⁷⁸.

- Lutein. A phase I/II clinical study showed a significant effect on visual field, and might improve visual acuity, but have no effect on contrast sensitivity⁷⁹. Associated with vitamin A, Lutein supplementation showed a slower loss of mid-peripheral visual field on average among nonsmoking adults with RP.

▪ When all rods have degenerated, several more general therapeutic strategies are currently being developed:

- Cell therapy, by transplantation of stem cells, for replacement of lost PR¹⁵⁻¹⁸ and/or RPE⁸⁰.

- Treatment of remaining cones with Rod-derived Cone Viability Factors (RdCVFs) to prevent cone degeneration^{81,82}.

- Optogenetic approaches that aim at rendering non PR-retinal neurons light-sensitive. One can thus envision to transform bipolar^{19,20} or ganglion cells into PR, or even to re-sensitize cones to light after degeneration of their segments²¹,

- Artificial retinal implants, that can electrically stimulate the remaining part of the retina^{23,24}.

Despite promising results, none of these approaches are able to definitively cure RP.

I.4.b. Treatments of RP in the particular case of RHO mutation

Because RHO mutations have either gain-of-function properties or dominant-negative effect (see part I.3.c), it is very difficult to prevent disease progression only by re-introduction of WT proteins. Nevertheless, it has been found to be surprisingly efficient in case of P23H mutation⁸³, however this strategy is not applicable to the majority of RP-induced RHO mutations.

Several groups have tried to prevent RP by targeting rhodopsin gene or RNA. At DNA level, Zinc Finger Artificial Transcription Factor (ZF-ATF) reduce WT and mutant *RHO* expression, and Zinc Finger Nuclease (ZFN) can partially induce the repair of DNA sequences.

At RNA level, RNA interference coupled or not to a "silencing-resistant" wild type *RHO* sequence has shown efficiency on *RHO* knock-down and interesting results on disease course. In the same objective, the use of ribozymes has given proof of therapeutic efficiency in *in vitro* and *in vivo* models. All these techniques, adapted to RHO mutations will be discussed in details in the following section.

In the particular case of class II RHO mutants, such as P23H, which present mis-folding and seem to be involved in UPR and ER stress, some studies have demonstrated a potential therapeutic value of retinoid and chaperone expression on reducing these cellular mechanisms and RP slow down⁸⁴⁻⁸⁷, certainly by reducing PR apoptosis. Because these mechanisms are not all specific to RHO, it is necessary to take into account that modifying these pathways could have unwanted side effects on the cell.

II. Current strategies to prevent mutant rhodopsin expression

II.1. Rhodopsin DNA sequence correction

II.1.a. DNA repair by Homologous Recombination (HR)

To date a lot of strategies are used to silence or modify the expression of a target gene, but those that are developed in order to repair the mutated sequence are relatively rare. DNA corrective strategies are all based on the use of HR.

DNA is permanently exposed to endogenous and exogenous factors that can create Double Strand Break (DSB), including for example: nucleases and metabolic products such as reactive oxygen species, ionizing radiation, ultraviolet light, chemical agents used in anti-cancer therapy. Even physical stress during mitosis is suspected to be involved in DSB. DSB are also induced more “willingly” by the cell, for example for genetic mixing and proper chromosome segregation during meiosis^{88,89}. To repair these DSB, the cell machinery uses two main mechanisms: HR and Non Homologous End Joining (NHEJ). NHEJ naturally ligates two broken ends together. It has frequently been considered as the error-prone DSB-repair pathway that generates small insertions or deletions. However, the error rate is only about 10^{-3} per joining event between fully compatible DSB ends⁹⁰. Unlike NHEJ, HR provides a modified homologue sequence that facilitates recombination at the broken site, and allow the replacement of the mutated sequence by the normal one (or vice versa)^{91,92} (Figure 11). HR occurs in three steps: (i) the resection of the DNA 5' end, (ii) strand invasion into a homologous DNA duplex and strand exchange, and (iii) resolution of recombination intermediates.

II.1.b. HR-induced endonucleases

HR naturally only occurs at a rate of 10^{-6} , as a result different kinds of endonucleases have been developed and engineered to stimulate this mechanism by creating DSB and to bring a more important specificity to the reaction^{93,94}. Among them, Meganucleases, Zinc Finger nucleases (ZFN), Transcription Activator Like Effector nucleases (TALEN), and Clustered Regulatory Interspaced Short Palindromic Repeats (CRISPR) systems will be described, due to their involvement in past or ongoing studies in *RHO* repair strategies.

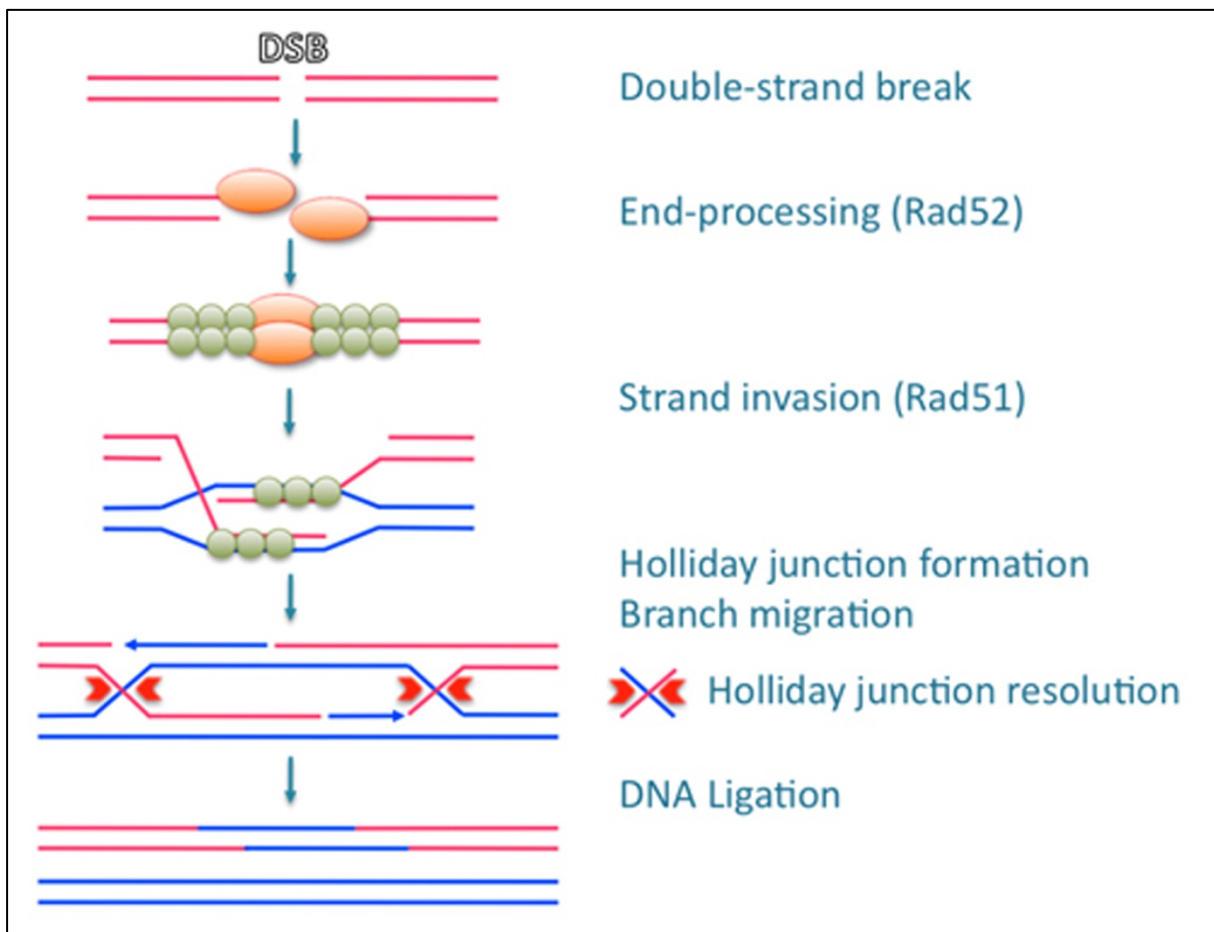


Figure 11: Steps of double strand break (DSB) repair by homologous recombination (HR).
 Extracted from *Christian Biertümpfel illustration at Max Planck institute of biochemistry.*

- Meganucleases, also called homing endonucleases. The Meganuclease family gathers 5 classes based on structures and sequences: LAGLIDADG, GIY-YIG, HNH, His-Cys box and PD-(D/E)XK⁹⁵. The first one is the most common and the most described in the literature, generally encoded in introns or inteins. These proteins, naturally present in all kingdoms of life, cut double strand DNA with a great specificity due to a large recognition site ranging from 12 to 40 bp. The obvious drawback of natural Meganucleases is the requirement to have a cleavage site near the region of interest, which is naturally extremely rare because of the great specificity of their recognition site and the small natural repertoire of Meganucleases which is around 300 proteins, most of them being still uncharacterized⁹⁶. Nevertheless, it is possible to create artificial Meganucleases by, for instance, fusing domains of several proteins (also called domain swapping) or mutating specific residues⁹⁵, but efforts are still required to obtain an artificial Meganuclease for each target site, that also conserves the specificity and efficiency of the natural ones.

Concerning *RHO*, Collectis has filed a patent on a batch of Meganuclease variants cleaving a DNA target sequence from *RHO* (number of patent: WO2011141825 A1). Moreover, Chan *et al.*⁵ have already demonstrated the efficiency of Meganuclease cleavage in PR *in vivo*, after transduction with a recombinant AAV encoding the Meganuclease. Unfortunately there is no natural Meganuclease cleavage site in the rhodopsin gene and they had to introduce one in their model. Nevertheless, they highlight the potential of HR repair in post-mitotic cells, even without introducing a DNA sequence to correct the DSB. They therefore suggested engineering a Zinc-Finger Nuclease, in order to cleave specifically *RHO* and to promote DSB repair by HR with the help of a non mutated *RHO* sequence also brought into the cell by gene transfer.

- Zinc Finger Nucleases (Figure 12). ZFN represent the first group of engineered nucleases composed of a sequence-specific DNA-binding domain fused to a nonspecific DNA cleavage module. The first one is usually composed of several zinc-finger units, each one containing about 30 amino acids, in a $\beta\beta\alpha$ configuration, with some amino acids in contact with 3-4 bases of the target DNA sequence. It is possible to obtain a more specific molecule by gathering several zinc finger motifs, usually at least six are used to recognize a sequence of 18 bp. The DNA cleavage module is usually that of a FokI endonuclease. ZFN are active as a dimer, with two zinc finger binding sites separated by a 5-7bp sequence, containing the cleavage site of FokI⁹⁷.

In 2010, Greenwald *et al.* established the first use of a ZFN for a retinal disease gene, by engineering a ZFN designed to bind and cleave a sequence of the human *RHO*, associated to

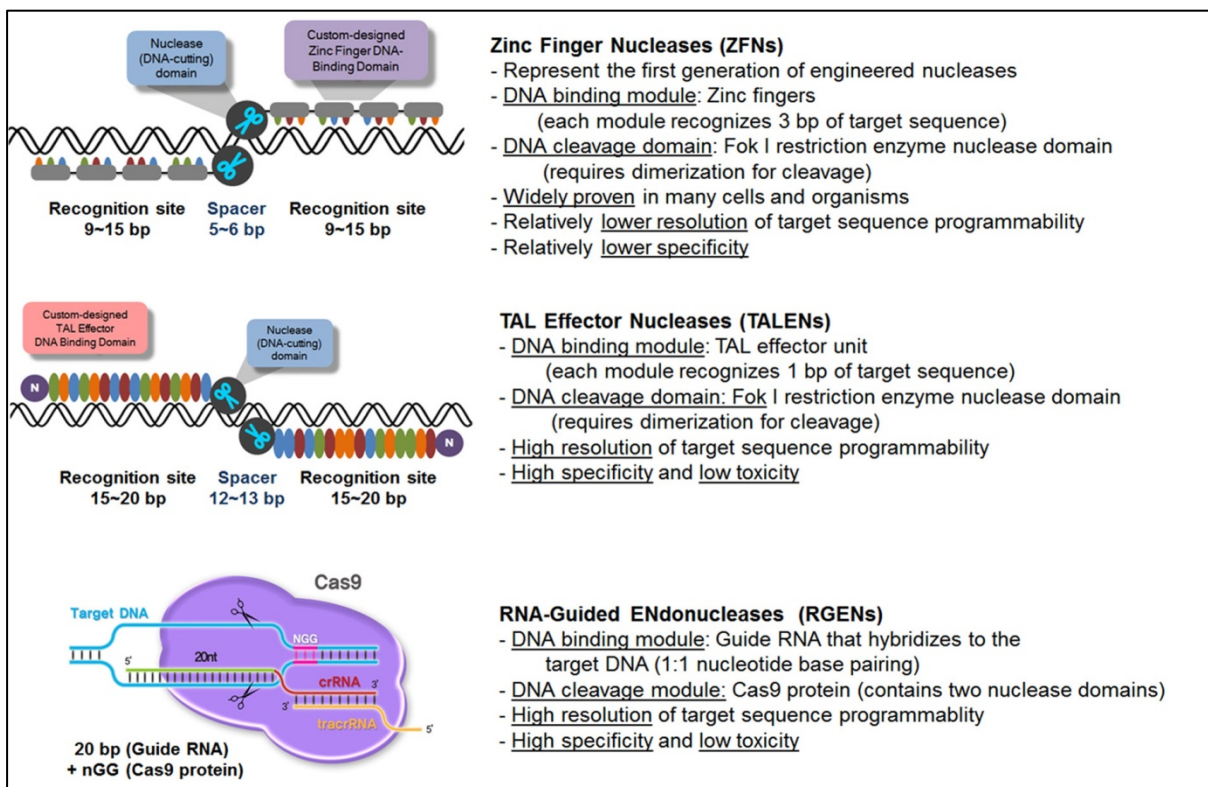


Figure 12: Engineered nucleases developed to induce a DSB in DNA sequence.

The first generation of engineered nucleases--zinc finger nucleases (ZFNs)--have successfully implemented the power of genome engineering in various cells and organisms. Recently, new generations of engineered nucleases--TAL effector nucleases (TALENs) and RNA-Guided ENdonucleases (RGENs)/Cas9 nucleases--have been developed, leading to the expansion of applications in research and industry. Extracted from <http://www.toolgen.com>.

an ectopic donor DNA fragment homologous to the human *RHO* sequence, and modified to be insensitive to the ZFN⁶. They showed in P23H HEK cell lines that the ZFN correctly cleaved *RHO*, and induced an increase of 11.7 fold of HR. ZFN could thus be a good strategy to repair mutations on *RHO*, taking into account that more than 120 mutations have been described to date. Only one *RHO*-specific ZFN may be sufficient, but only if the frequency of the induced HR does not dramatically decrease with the increase in distance from the DSB.

Moreover, these approaches usually still induce off-target effects, such as unspecific cleavage sites, that can be toxic for the cell. Another drawback is the fact that conventional DNA or RNA-based methods for delivering ZFN into the cell (using viral vectors) are restricted to certain cell types, and can induce side effect like insertional mutagenesis, toxicity, and low efficiency⁹⁷. Direct delivery of ZFN into the cell can be a solution but requires a good control of the cell targeting.

- Transcription Activator Like Effector Nucleases (Figure 12). TALE proteins have been discovered more recently, and are naturally expressed by *Xanthomonas* bacteria. TALE proteins possess DNA-binding domains composed of a series of about 30 repeat domains of 33-35 amino-acid-sequence-motifs, each one containing 2 hypervariable residues that recognize a single base pair. Like ZF domains, TALE proteins can be associated to endonucleases, recombinases, transposases, to name a few in the same way. TALEN are active as dimers, and often coupled with a FokI endonuclease domain, to promote cleavage of the DNA targeted at the spacer sequence between the two TALE DNA binding domains⁹⁷.

Despite the fact that TALEN opens the door to an alternative platform for engineering DNA-binding proteins more easily, this technology presents two other new drawbacks, firstly the necessity to start the binding site with a T base, and secondly the difficulty inherent in cloning TALE repeated sequences. Moreover, TALEN possess too many repeated sequences to be delivered by lentiviral transduction, being subject of rearrangements, and their large size preclude their delivery by AAV vectors.

- Clustered Regulatory Interspaced Short Palindromic Repeats system (also called RNA-Guided Endonucleases) (Figure 12). CRISPR systems arose in bacteria as a kind of immunity against foreign DNA from phages and plasmids⁹⁸. Indeed, short sequences of foreign DNA called spacers, are introduced into the host genome at the CRISPR loci, before being transcribed and processed into short CRISPR RNA (crRNA). These last ones enable the silencing of foreign DNA, by its cleavage after the recruitment of CRISPR associated (Cas) proteins⁹⁹. This is thus a programmable RNA-guided DNA endonuclease that requires co-delivery of plasmid encoding a Cas endonuclease (Cas9 is the simplest system often used),

and the crRNA components⁹⁷. While this technology presents an interesting potential method to manipulate expression^{100,101}, numerous studies are ongoing to evaluate the utility of this system, including potential off-target effects.

One of the major drawbacks of all these strategies based on HR, is the necessity to bring into the cell the modified enzyme able to induce the DSB, also in addition to the correct homologous sequence to repair the targeted gene. The fact that two elements have to be introduced into the cell can represent a brake in term of the delivery method. Furthermore, in order to reduce possible off-target effects, it will be interesting to limit the duration of meganuclease expression in targeted cells, but while it is easily conceivable in mitotic cells, systems for transient expression in post-mitotic cells *in vivo* still need to be improved.

Because nucleases can induce potentially toxic DNA double-strand breaks in the cell, and because this methodology requires the proper functioning of HR in the target cell, which is variable upon cell cycle, recombinases and transposases have been fused to ZF or TALE domains, allowing site-specific DNA integration, excision and inversion. Nonetheless, these new technologies require improvement in performance and flexibility of these enzymes^{102,103}.

II.2. Silencing of mutant gene expression coupled to expression of a normal copy

II.2.a. Zinc Finger - Artificial Transcription Factors (ZF-ATF)

As described previously, Zinc Finger DNA binding domains can be linked to enzymatic proteins such as nucleases, recombinases, transposases and so forth (See part II.1.b) but these binding motifs can also be used to specifically repress or activate gene transcription by coupling with a transcription factor. Indeed, the Zinc Finger DNA binding domain allows binding to a target promoter, and the transcription factor can then modify its activity, and thus repress or increase the expression of a specific gene. Several activator and repressor domains have already been described and are routinely used in ZF-ATF¹⁰⁴.

Mussolino *et al.*⁷ engineered a Zinc finger based mutation-independent approach to repress human *RHO* expression in a P347S^{+/-} humanized mouse model. They simulated a two-step repression replacement method, with the silencing of *RHO* expression by an AAV vector on one hand and gene replacement on the other. In their study, they considered that the gene replacement function, which is to produce expression equivalent to a normal gene copy, is done by the endogenous mouse rhodopsin genes (*Rho*). They demonstrated the efficiency of ZF-transcriptional repressor on human *RHO*, with a decrease of *RHO* expression, and a

slowdown of PR degeneration. Nevertheless, the method has now to be tested in a heterozygous context, with a normal human allele and a mutant one, in a mouse knockout background model. Moreover, they only evaluated potential toxicity by histology and ERG, but they did not verify the absence of off-target by analyzing gene expression on DNA chips for example.

Generally, a particular difficulty of this strategy is to correctly design Zing Finger binding domains, to allow their binding on a promoter, meaning that accessibility of the sequence and chromatin state have to be taking into account (by *in silico* studies or nucleases tests conducted prior, for example).

II.2.b. RNA interference

RNA interference (RNAi) is a well-conserved gene-defense mechanism across model organisms, already observed in plants^{105,106}, but firstly described as RNAi by Andrew Fire and Creg Mello, in *C. elegans* in 1988¹⁰⁷. It is based on the repression of gene expression by a short antisense RNA involved in transcriptional gene silencing at least in yeast¹⁰⁸, but has been described in all organisms including mammals, to induce degradation of a targeted endogenous RNA, or to inhibit its translation by post-transcriptional gene silencing¹⁰⁹.

Among the expansive world of non-coding regulatory RNA, two pathways are to date widely described in animals: short interfering RNA (siRNA) and micro RNA (miRNA). The first ones are derived from viral infection or transcription of transposable elements and are formed from long double-stranded RNA molecules, while the second ones are triggered by long, single-stranded RNA sequences that fold into hairpin structures¹¹⁰. Following the transcription of the dsRNA and its export to the cytoplasm, the siRNA pathway includes support by an enzyme called Dicer, which cut the RNA into a small molecule of around 21 to 23 nucleotides with a 3' overhangs of 2 nucleotides (this molecule corresponds to the siRNA). This step induces the formation of the RNAi-induced silencing complex (RISC) by recruiting, among others, Argonaute proteins. RISC separates the two strands of the siRNA, and uses it to scan mRNA. After identification of a perfect matching between the siRNA-mRNA duplex, the targeted mRNA is cleaved inducing its degradation. The miRNA pathway shares some steps and factors with the siRNA one, however it requires that firstly the long miRNA precursor is cut by the Drosha enzyme into miRNA before its export from the nucleus. RISC also differs a little from that of the siRNA pathway by its composition particularly in Argonaute proteins. The biggest difference between the two pathways is due to the non-perfect homology between the targeted mRNA and the miRNA. This pathway can also induce

significant degradation of mRNA targets despite imperfect mRNA-miRNA base-pairing, but mostly, it leads to repression of translation by inhibition of translation initiation, elongation, premature termination or cotranslational protein degradation¹¹¹.

Faced with this new natural way of gene silencing, RNAi strategy has totally exploded in the past two decades and has become an indispensable tool in gene function analysis. RNAi protocols now used in therapeutic strategies gather 3 types of molecules:

- miRNA under the control of a polymerase II promoter.
- chemically synthesized siRNA. These are usually administrated via cell transfection, meaning that they are transiently efficient.
- short hairpin RNA (shRNA), mimic pre-miRNA, and can be stably expressed after stable transfection, or transduction with a gene transfer vector. Nevertheless, shRNA are expressed under the control of a polymerase III promoter, and skip the first steps of the RNAi pathway. The solution will thus to deliver shRNA into an endogenous miRNA backbone¹¹².

The most important drawback of RNAi is certainly the potential off-target effects, which can be due to (i) sequence-based homology with non-target RNA, (ii) aberrant processing of small RNA (iii) general cell perturbations owing to the copious presence of RNA species. This strong expression of small RNA can also induce cell toxicity by saturation of the endogenous RNAi machinery^{113,114}. Another difficulty met in the use of RNAi is the incomplete understanding of the mechanism involved in this RNA-induced silencing, often leading to unpredictable and disappointing efficiency¹¹⁵⁻¹¹⁷, which vary between experiments and laboratories.

In the particular case of rhodopsin, the first RNAi was developed to silence mouse *Rho* in a mutation-independent way: after validation of shRNA efficiency to induce more stable silencing compared to siRNA, mutated gene replacement was designed to maintain a natural rhodopsin expression level¹¹⁸. The same group then engineered shRNA targeting human *RHO* and tested it in humanized mouse models. They demonstrated an efficiency of at least 85% silencing of human *RHO* in cells transduced by an AAV2/5 encoding the shRNA, and a decrease of PR degeneration by histological analysis when the shRNA was coupled in the AAV vector to a shRNA-insensitive codon-modified human *RHO* replacement cDNA, in a P23H *RHO*^{+/-} *Rho*^{+/-} mouse model¹¹⁹. In order to evaluate the maximal beneficial effect of RNAi silencing/gene replacement strategy in rhodopsin context, they also studied the effect of mutated *RHO* silencing by AAV-shRNA injection in the *RHO* P347S^{+/-} *Rho*^{+/+} mouse model. By this way, they suppressed mutated *RHO* expression, and considered that mouse *Rho*,

which is not targeted by the shRNA, acts as replacement gene. They obtained a significant retardation of the disease, observed by histology and ERG⁸.

In parallel, to avoid the necessity of providing two molecules, an allele-dependent RNAi approach to specifically silence the P23H *RHO* allele in a rat model was also developed¹²⁰. Nevertheless, this study did not bring convincing results, certainly due to an insufficient silencing rate, unable to slow PR degeneration.

Among all these studies, the most impressive one conducted with RNAi on RHO mutations was certainly the report of Mao *et al.*⁹, that showed a long-term rescue (until 9 months post-injection) of retinal structure and function by a single injection of AAV2/5 expressing both siRNA and rhodopsin replacement gene in a P23H transgenic mouse model. They obtained a real beneficial effect with an ERG response at 9 months post-treatment reaching 80% of the a-wave and 95% of the b-wave amplitudes compared to WT mice.

Nonetheless, it is important to take into account that the *RHO* expression level necessary to conserve healthy PR can be dramatically dependent on the RHO mutation. Indeed, delivery of WT *RHO* is sufficient to preserve retinal function in the context of a P23H mutation⁸³, which is not the case for a P347S mutation. This strategy needs to be tested in other animal models in the hope of extending its application to all RHO mutations. Moreover, due to the potential off-target effects of siRNA/shRNA, and even if the choice in AAV vector serotype allows us to restrict targeting to a specific cell type, it should be preferable to use a specific pol II promoter over an ubiquitous pol III promoter as is the case here, to increase specificity and limit RNAi-expressing cells. This can be done for example by using a miRNA encoded in the 3'UTR of the replacement gene sequence. By the same way, it will be possible to keep a single AAV vector expressing both molecules.

In this objective, miRNA was also tested recently to silence *RHO* expression *in vivo*, in a P347S *RHO* context, on a *Rho*^{-/-} background¹⁰. By co-injection of two AAV2/9 in a ratio 1:2, respectively containing the miRNA sequence and the codon-modified replacement gene, they observed a rescue in AAV-miRNA-injected eyes, but without significant improvement when co-injected with the AAV-replacement gene. Moreover, they only observed a short-term rescue, probably due to the choice of the AAV vector.

Among all these approaches, some points remain under debate, such as:

- mutation-independent or mutation-dependent strategy. If the first one allows generalizing the tool to all RHO mutations, there is also a requirement to be associated to the replacement gene expression unlike the second strategy, because *RHO* haplo-insufficiency presents a less severe phenotype than most other RHO mutations.

- the use of one or two AAV vectors to vehicle RNAi and replacement gene^{119,121}. The use of two distinct vectors allows manipulation of the ratio between the two molecules, but including the whole system in a single vector ensures that both mechanisms are co-activated in each targeted cell.

II.2.c. Ribozymes

Ribozymes gather all RNA molecules that possess a catalytic activity, highlighting the fact that not only proteins possess an enzymatic function (or considered as) in cells. Several groups have engineered new self-cleaving ribozymes from natural ribozymes present in different model organisms, such as self-splicing group I introns, RNase P and small RNA associated with plant viruses¹²². They are based on hairpin and hammerhead ribozymes, which are today the most used to specifically inhibit gene expression, due to their small size and their great specificity. These two groups of ribozymes require a specific folding to promote site-specific cleavage of a target RNA phosphodiester bond, by a transesterification reaction. This particular secondary structure is induced by conformational changes in the presence of metal ions. Indeed, the hairpin ribozyme undergoes site-specific self-cleavage in the presence of magnesium ions, while hammerhead ribozyme require magnesium or other bivalent ions (including manganese, calcium and cobalt) to promote folding and act as co-factors^{123,124}. Hammerhead ribozyme requires a NUX sequence in the target RNA - where N is any nucleotide, U an uracil and X any nucleotide except a guanine - and a catalytic hammerhead sequence of 21 nucleotides, while hairpin ribozyme possesses a larger catalytic core with 34 nucleotides, and requires more specificity, with the following recognition sequence: NNYNGUCNNNNNN, where N is any nucleotide, and Y is a pyrimidine¹²⁵.

In a mutation-dependent approach, Drenser *et al.* firstly designed hairpin and hammerhead ribozymes against RHO P23H mutation, and a hammerhead one against the S334Ter mutation¹²⁶. They showed that ribozymes can actively and specifically cleave synthetic or full length transgenic mRNA. Nevertheless, they also demonstrated that some parameters can dramatically influence the cleavage potential, such as magnesium concentrations and of course the nature of the NUX sequence¹²⁷. Then the same group¹²⁸ also demonstrated the efficiency of their ribozyme in a P23H rat model, after AAV injection. They obtained a specific decrease of P23H mRNA leading to prolonged survival of PR and ERG responses on long-term and even with late-stage gene transfer¹¹. Nevertheless, they also observed a partial rescue with inactive ribozyme that they suggested to attribute to anti-sense effect¹²⁵. Moreover, they demonstrated that efficiency of cleavage on NUX sequences is

extremely variable¹²⁶, whereas a selective degradation of the mutant mRNA requires the cleavage site at less than 4 residues away from the mutated base. This last information brings the proof that not all possible target sites will result in optimal cleavage, depending on the NUX sequence because most mutations do not create NUX target motifs and are often not localized in an accessible region of the RNA. The mutation-dependent approach can thus be used only for some cases of RHO mutations.

In parallel, mutation-independent ribozymes were also developed to cleave rhodopsin mRNA *in vitro*, such as monomeric or multimeric hammerhead ribozymes, designed to target accessible regions as predicted by computer program^{129–131}. Gorbatuyk *et al.*¹³¹ firstly obtained a clear reduction of rhodopsin mRNA and reduction of b-wave amplitudes after injection of the ribozyme by AAV transduction in a *Rho+/-* mouse model at P6. However, no impact on ERG was observed in the same animal model injected at one month, or on WT mice, even if the RHO amount was reduced. After this first proof of mutation-independent ribozyme efficiency *in vivo*, it is now necessary to combine this molecule with an untargeted replacement gene. To date, the only *in vivo* work has been done by the same team, which tested another more efficient ribozyme, in a P23H rat model, expressing one transgenic copy of a mouse mutant allele, and one copy of WT rat allele. This ribozyme targets dog, mouse and human rhodopsin mRNA but not the rat one. In this experiment, the untargeted normal rat copy simulates the effect of the replacement gene. They demonstrated a significant preservation (around 50%) of scotopic ERG a- and b-wave amplitudes in injected eyes, one month after injection¹². Nevertheless, ERG response continues to decline in injected eyes at a parallel rate than in control eyes.

Ribozymes have the advantage of being more specific to one mutation, because of their short recognition sequence. This characteristic allows easier design of a ribozyme specific to a mutated allele than a RNAi, with only one base difference, but also brings the drawback of the off-target effects. Indeed, the recognition sequence of a ribozyme is more highly represented in the genome than those of a RNAi.

These three last strategies allow silencing of the rhodopsin gene (mutated and normal copies or only the mutated one), but most of the time, require the insertion of a normal *RHO* allele, rendered insensitive to silencing by modification of its nucleic acid sequence, to promote the expression of this essential protein for PR survival. This suggests introducing a silencing molecule and gene replacement in the same time, in the same cells and inducing both mechanisms in a relative equivalent proportion. To do that, it would be necessary to

express both molecules into the same AAV vector. Nevertheless, the size of both sequences, together with the regulatory elements is too big to be packaged in only one AAV, and the delivery will be a crucial point to take into account for these strategies.

III. *Trans*-splicing of rhodopsin pre-mRNA

The approach that we have used to correct rhodopsin mutations on RNA sequence is based on artificially induced *trans*-splicing reaction. This strategy allows reducing mutant rhodopsin expression while restoring normal rhodopsin one, in only one reaction and with only one molecular tool. It is widely inspired by natural *trans*-splicing events that occur in the cell, a rarely used alternative to *cis*-splicing. This is therefore a strategy that deflects *cis*-splicing, a process occurring in eukaryotic cells, and discovered concomitantly to the existence of introns (INTRagenic RegiON¹³²) in 1976 in the transcripts of adenovirus firstly^{133,134}, and then in eukaryotic coding genes^{135,136}.

III.1. *Cis*-splicing: the prototypical splice reaction

III.1.a. Splicing is a phase of pre-mRNA maturation

Each protein of the cell is the result of the expression of a gene, which has required three major steps:

- The transcription of the gene to produce a pre-mRNA,
- The maturation of the pre-mRNA into a mature mRNA,
- The translation of the mature mRNA in a functional protein.

While transcription and translation have always been considered as the two major steps in gene expression, maturation of pre-mRNA is also an essential process necessary for the transition from the first to the second. It includes 3 crucial phases:

- Capping of the 5' end: a cap is formed by the addition of a guanine to the terminal base of the transcript, via a 5'-5' link. This action is done by a guanylyl-transferase, shortly after transcription initiation, when the polymerase is doing a pause around 30 nucleotides after the initiation site. This guanine is then most of the time monomethylated at its 7 position, by a guanine-7-methyltransferase. The capping influences mRNA stability by protecting its 5' extremity from exonucleases, its splicing, export and translation.

- Splicing: while RNA splicing was first considered only as an intermediate in protein synthesis, we know today that this step is also subject to very strict regulations and permits to create diversity in gene expression, which will be exposed in part III.1.c. Splicing consists to excise intronic sequences of the pre-mRNA, conserving only exonic sequences, which are the

support of the genetic information that must be translated. Because a classical pre-mRNA includes, on average, seven or eight exons at around 100 to 200bp, spread out over 15 to 20 kb, we can easily imagine that a very complex process is implicated in splicing to avoid mistakes; this one will be exposed in the following part.

- Polyadenylation of the 3' end: 2 sequences are essential for polyadenylation: an AAUAAA motif, followed by a U-rich or GU-rich element. Several complexes are associated with a polyadenylation mechanism, which induces the cleavage of the pre-mRNA by an endonuclease, then the addition of around 200 adenosine by a poly(A) polymerase. This poly(A) tail controls also mRNA stability, and influences translation.

III.1.b. Steps of the splicing mechanism

To initiate a splicing reaction, several elements are required on the pre-mRNA:

- The 5' donor and 3' acceptor splice sites that constitute the two exon-intron boundaries. Even if there exists consensus sequences around these two sites (Figure 13), surprisingly, the only nucleotides that are mandatory are GU on the 5' site (the first two nucleotides of the intron) and AG on the 3' site (the last two nucleotides of the intron), meaning that the cell machinery is able to recognize these two pairs of nucleotides sometimes separated by hundreds or even thousands of bases. Because the two sites have different sequences, this gives the orientation of the splice reaction. These sites are generic and not tissue-specific. Splice signals are read in pairs and in a relatively linear order.

- The A branch site. This is an adenosine in the RNA intron, 18 to 40 nucleotides upstream of the 3' splice site. This adenosine is surrounded by a consensus sequence quite variable in eukaryotes, except in yeast with the following consensus sequence: UACUAAC where A is the branch point (BP).

- A polypyrimidine rich sequence (PPT for PolyPyrimidine Tact), just before the 3' splice site, often composed of uracil repetition.

Splicing is realized by the biggest ribonucleic enzymatic complex of the cell, called a spliceosome²⁶. Like the ribosome, the spliceosome depends on RNA-RNA interactions as well as protein-RNA and protein-protein interactions. It is composed of more than 40 proteins in small nuclear ribonucleoproteins (snRNP), 5 small nuclear RNA (snRNA), 70 splicing factors and at least 30 other proteins, forming a complex of about 12 megadaltons. Each snRNP possesses a single snRNA (that gives its name to the snRNP) and several proteins,

including a common structural core of eight Sm proteins. “Pre-splicing complexes” are sequentially assembled on the pre-mRNA to form the active final spliceosome.

The first step of RNA splicing is the binding of U1 snRNP onto the 5' splice site, by base pairing. In parallel, the branch point binding protein SF1 interacts with the branch point sequence, and the protein U2AF binds to the polypyrimidine tract. SR proteins, which constitute a group of splicing factors that possess RNA-recognition motifs, act in strengthening these links. This is the formation of the “commitment complex” also called the E complex. This step leads to the folding of the RNA, allowing interaction between all these factors. The following step is the addition of U2 snRNP by base pairing between U2 snRNA and the branch point sequence. This constitutes the A complex. The binding of a trimer composed of U5 and U4/U6 snRNPs (usually found as a di-snRNP) forms the B complex, converting to the B* complex after U1 and U4 release. This last one allows restructuring in some snRNP and particularly in U6 that was sequestered by U4, and leads by this way to the activated state of the spliceosome, called C1 complex. The two *trans*-esterification reactions can then occur. To begin, a nucleophilic attack of the A at the branch site on the 5' donor splice site creates a branched structure called the lariat, in which the 5' end *trans*-esterifies to be linked by a 2'-5' bond to the adenosine of the branch point. Next, under the action of the C2 complex, the free 3'-OH extremity, created by the first reaction, reacts with the 3' splice site, leading to another *trans*-esterification. The two exons are thus joined and the intron contained into the lariat is “de-branched” before being rapidly degraded^{25,137}. A lot of splicing factors play a role in the successful completion of these steps. Finally RNA helicases recycle snRNPs for the next spliceosome assembly (Figure 14).

While more than 98% of splice sites follow the GU-AG rule (corresponding to 5' and 3' site sequence respectively), few introns possess AU-AC sites, and are spliced by an alternative spliceosome, the U12 spliceosome. This minor class of introns exists in a variety of genomes and is often found in the same gene as major introns. The vast majority of steps and factors involved in splice reaction are conserved, but some differences appear: (i) compared to the machinery described above, the processing machinery of minor spliceosomes are composed of U11, U12 (which respectively replace U1 and U2), U5 (the same as in the major spliceosome) and U4_{atac} and U6_{atac}, (ii) minor introns contain a highly conserved branch point: UCCUUPuAPy that pairs with U12, (iii) while in major spliceosomes U1 and U2 independently bind its paired sequences, U11 and U12 form a complex before interacting with the RNA sequence to splice.

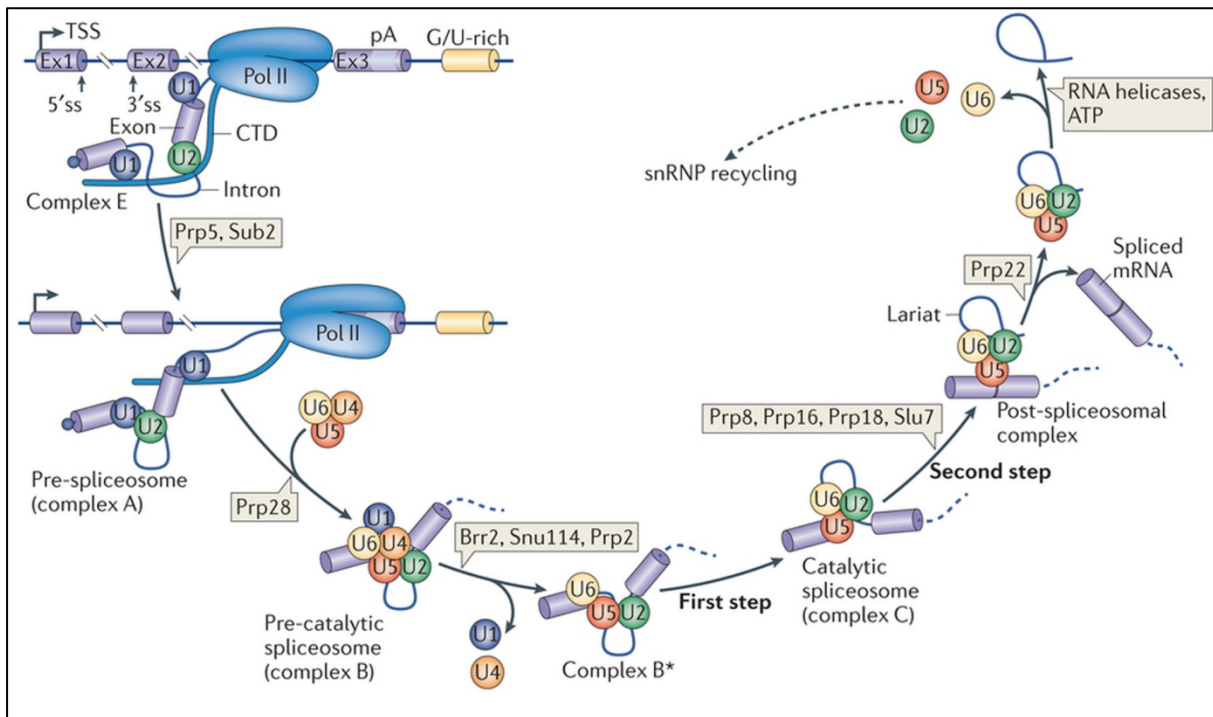


Figure 14: Step-wise assembly of the spliceosome and catalytic steps of splicing.

Spliceosome assembly takes place at sites of transcription. The U1 and U2 small nuclear ribonucleoproteins (snRNPs) assemble onto the pre-mRNA in a co-transcriptional manner through recognition of the 5' splice site (5'ss) and 3'ss, which is mediated by the carboxy-terminal domain (CTD) of polymerase II (Pol II). The U1 and U2 snRNPs interact with each other to form the pre-spliceosome (complex A). This process is dependent on DExD/H helicases pre-mRNA-processing 5 (Prp5) and Sub2. In a subsequent reaction catalysed by Prp28, the preassembled tri-snRNP U4-U6-U5 is recruited to form complex B. The resulting complex B undergoes a series of rearrangements to form a catalytically active complex B (complex B*), which requires multiple RNA helicases (Brr2, 114 kDa U5 small nuclear ribonucleoprotein component (Snu114) and Prp2) and results in the release of U4 and U1 snRNPs. Complex B* then carries out the first catalytic step of splicing, generating complex C, which contains free exon 1 (Ex1) and the intron-exon 2 lariat intermediate. Complex C undergoes additional rearrangements and then carries out the second catalytic step, resulting in a post-spliceosomal complex that contains the lariat intron and spliced exons. Finally, the U2, U5 and U6 snRNPs are released from the mRNP particle and recycled for additional rounds of splicing (dashed arrow). Release of the spliced product from the spliceosome is catalysed by the DExD/H helicase Prp22. Extracted from *Matera and Wang, Nature Reviews Molecular Cell Biology, 2014*.

III.1.c. Regulation of *cis*-splicing

RNA splicing was firstly described though a simple step in RNA maturation allowing the excision of all introns. With more than 90% of genes alternatively spliced in mammals it is now obvious that splicing is used to generate gene expression diversity^{138,139}. Because splicing sites are conserved across mammalian genomes, it seems likely that alternative splicing exists to preserve the regulation of gene expression at the level of RNA processing, and is not just a splicing mistake with exon skipping. Alternative splicing is generally tissue-specific and can lead to intron retention, exon skipping, alternative polyadenylation... by alternative 5' and 3' splice sites, mutually exclusive exons or combinatorial mechanisms (Figure 15)²⁵. This idea highlights the fact that one gene does not give only one mRNA, but a combination, including possible modifications in (i) mRNA stability and protein synthesis by adding stop codons, which can activate the nonsense-mediated mRNA decay, (ii) protein function by changing a part of its amino acid sequence, (iii) protein location by adding or deleting some localization site to name a few.

Alternative splicing is mainly influenced by the effect of splicing regulators. It thus exists in all eukaryotic cells proteins that are able to recognize elements of exons or introns of the pre-mRNA, near the alternative splice site, and to influence positively or negatively the splice reaction. The binding sequences of these proteins on the pre-mRNA are called ESE (Exonic Splicing Enhancer), ISE (Intronic Splicing Enhancer), ESS (Exonic Splicing Silencer) or ISS (Intronic Splicing Silencer)¹⁴⁰. SR proteins are among the best-characterized regulators: these proteins bind ESE, stabilizing by this way U1 on the 5' splice site, and U2AF near the 3' one. SR proteins are thus classified by essential splicing factors as described in part III.1.b, and alternative splicing regulators. Conversely, hnRNP A and B proteins binds ESS to suppress splice site selection and thus inhibit the reaction.

Moreover, many other splicing regulators act with a positional effect, like proteins of the Nova and Fox families, which are RNA-binding splicing regulators that can promote or suppress splice site selection depending on their localization. For example, binding of these proteins upstream to the splice site generally results in suppression of the exon. Because all these factors are usually submitted to a tissue-specific expression, this can be another way to regulate splicing in a tissue-specific manner.

Then, even if splicing and transcription are two distinct mechanisms that can take place independently *in vitro*, many splicing events are completed before the end of the transcription, meaning that these processes are temporally coupled. Indeed, it has been demonstrated that

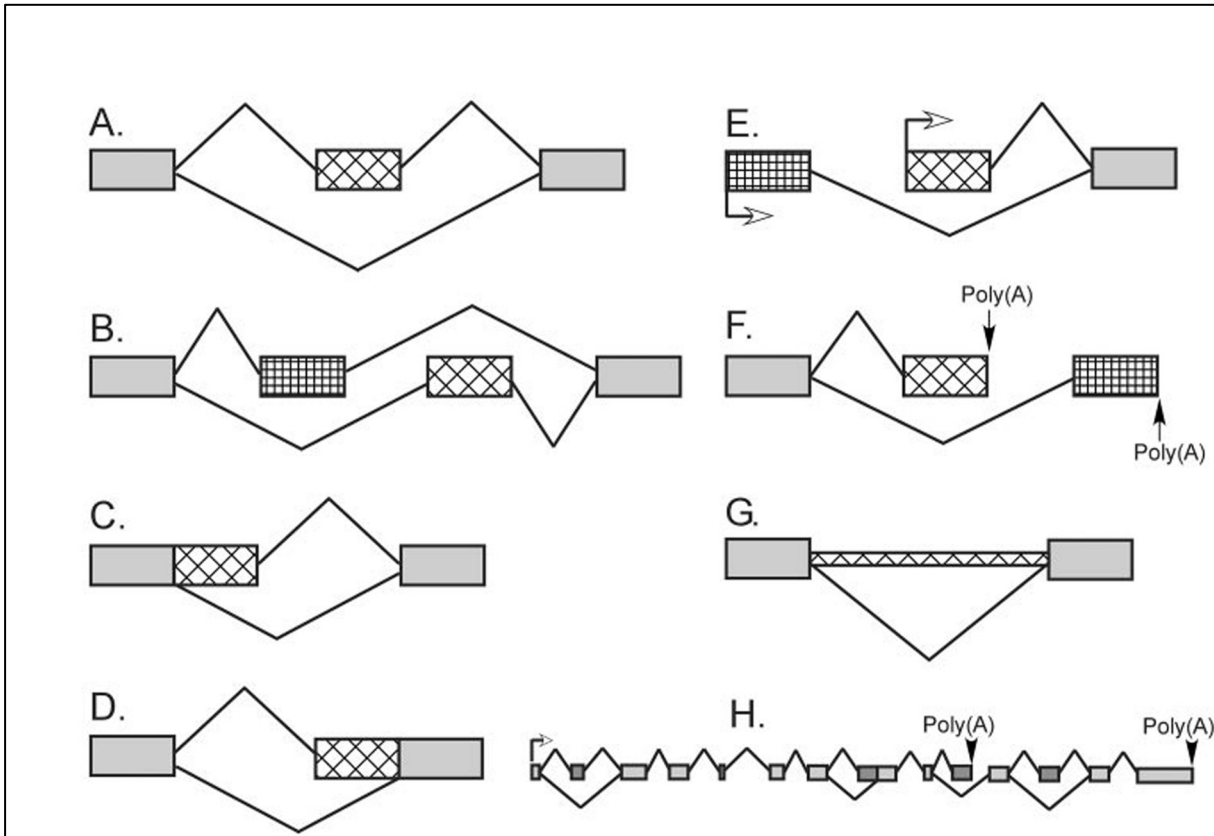


Figure 15: Patterns of alternative splicing.

Constitutive sequences present in all final mRNAs are gray boxes. Alternative RNA segments that may or may not be included in the mRNA are hatched boxes. (A) A cassette exon can be either included in the mRNA or excluded. (B) Mutually exclusive exons occur when two or more adjacent cassette exons are spliced such that only one exon in the group is included at a time. (C, D) Alternative 5' and 3' splice sites allow the lengthening or shortening of a particular exon. (E, F) Alternative promoters and alternative poly (A) sites switch the 5'- or 3'-most exons of a transcript. (G) A retained intron can be excised from the pre-mRNA or can be retained in the translated mRNA. (H) A single pre-mRNA can exhibit multiple sites of alternative splicing using different patterns of inclusion. These are often used in a combinatorial manner to produce many different final mRNAs. Extracted from Black, *Annual Review of Biochemistry*, 2003.

the C-terminal domain of the largest subunit of polymerase II (CTD for Carboxy-terminal domain) interacts with elements of the splicing machinery¹⁴¹. This idea emphasizes a potential influence of transcription on alternative splicing. Indeed, the transcription speed during the elongation phase could play a role on the choice of the subsequent splice sites. For example, slow transcription enables a splice reaction to occur when there is a weak splice site, before the transcription of a downstream splice site, which might be stronger and promote exon skipping.

III.2. *Trans*-splicing between two RNA molecules

III.2.a. Description of the mechanism

Unlike *cis*-splicing, *trans*-splicing occurs between two different pre-mRNA. The molecular process is exactly the same, but the final mRNA is composed of the first exon(s) of one pre-mRNA and the following(s) of the other, creating a chimeric molecule. Based on the same principle, ribozyme-mediated *trans*-splicing requires the action of an exogenous ribozyme¹⁴².

This phenomenon was firstly discovered in tripanosoma^{143,144}(Figure 16), and is now described in mammals¹⁴⁵, even in humans^{146–150}, and a databank screen suggests that many other examples of *trans*-spliced human RNA should be discovered¹⁵¹.

Trans-splicing is another way to create diversity in protein production, but is also for molecular biologists a real tool to influence gene expression. In the SMaRT (Spliceosome-Mediated RNA *Trans*-splicing) technology²⁷, engineered PTM (Pre mRNA *Trans*-splicing Molecule) which targets a mutated pre-mRNA, allows *trans*-splicing based replacement of the mutated sequence. PTM must specifically bind the targeted pre-mRNA, and stimulate splicing in *trans* more efficiently than in *cis*, to induce the replacement of downstream exons by PTM.

Firstly engineered for 3' exon replacement, SMaRT technology has then been extended to 5' exon replacement^{28,152,153} and internal exon replacement¹⁵⁴ as described on Figure 17. Nevertheless, efficiency of 5' and internal exon replacement remains to be improved.

III.2.b. Previous studies led with *trans*-splicing approaches

After an initial study leading to the proof of concept that artificially-induced *trans*-splicing can efficiently promote a functional protein *in vitro*²⁷, *trans*-splicing has been developed in different strategies, which can be classified in two groups:

- The first one, and the most common, concerns the RNA repair strategy, which has been widely used: cystic fibrosis^{28–31}, hemophilia A³², dysferlinopathies and titinopathies¹⁵⁵,

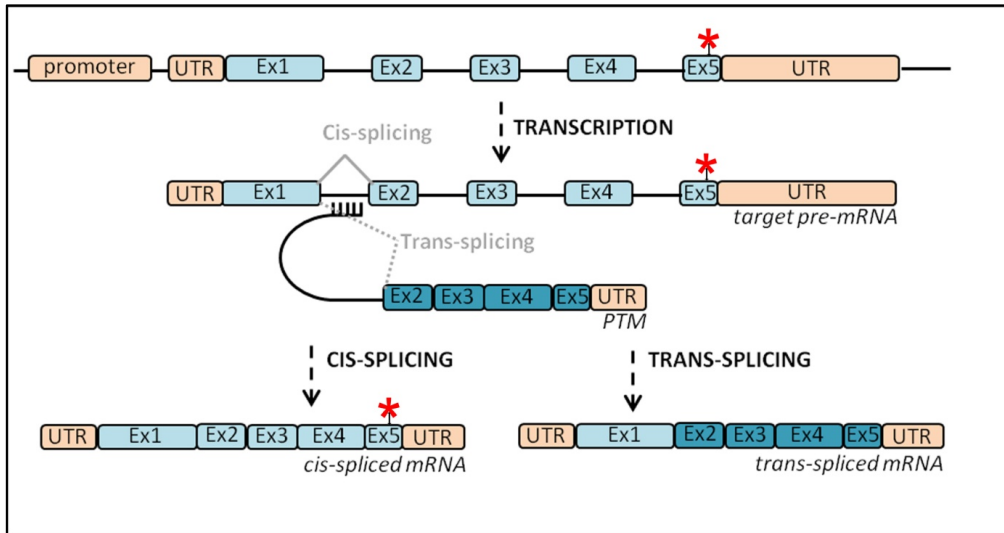


Figure 16: Schemes of *trans*-splicing mechanism.

After transcription of the rhodopsin gene, the PTM binding domain recognized a sequence of the rhodopsin pre-mRNA first intron, which allowed promoting a splicing in *trans* instead of *cis*, leading to the production of a chimeric mRNA devoid of any mutation in exons 2 to 5. * represents a potential mutation.

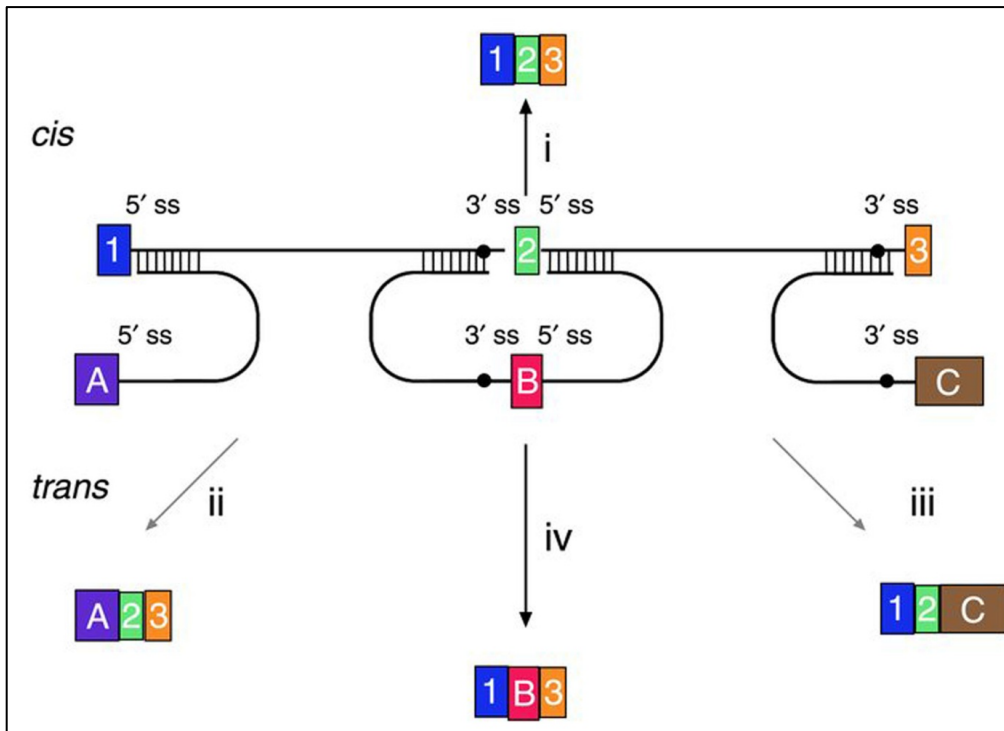


Figure 17: Versatility of mRNA reprogramming by targeted SMaRT.

The figure shows a schematic of splicing reactions involving a three-exon pre-mRNA and PTMs. A conventional constitutive *cis*-splicing reaction leading to the production of the expected 1•2•3 mRNA is shown (i). Three targeted SMaRT reactions are shown. PTM[A] contains a functional 5' splice site that can *trans*-splice to the 3' splice site adjacent to exon 2 in the pre-mRNA target (ii). This *trans*-splicing produces a chimeric A•2•3 mRNA by 5' exon replacement. PTM[C] contains a functional 3' splice site that can *trans*-splice to the 5' splice site adjacent to exon 2 in the pre-mRNA target (iii). This *trans*-splicing produces a chimeric 1•2•C mRNA by 5' exon replacement. Finally, PTM[B] contains both 3' and 5' splice sites bordering an exon, and these splice sites can *trans*-splice with the 5' splice site adjacent to exon 1 and the 5' splice site adjacent to exon 3, respectively (iv). These two *trans*-splicing reactions lead to internal exon replacement and produce the chimeric 1•B•3 mRNA. Extracted from Garcia-Blanco, *JCI*, 2003.

X-linked immunodeficiency with hyper-IgM³⁷, medullary thyroid carcinomas¹⁵⁶, tauopathies^{157,158}, sickle cell anemia and β -thalassemia¹⁵⁹, spinal muscular atrophy³³⁻³⁶, severe combined immune deficiency¹⁶⁰, dystrophin myotonia type 1¹⁶¹, Duchenne muscular dystrophy^{162,163}, epidermolysis bullosa^{153,154,164-166}, Huntington's disease¹⁵², mucopolysaccharidosis type VII¹⁶⁷. *In vitro* and *in vivo* results obtained in these studies are synthesized in Table 2. In these cases, the aim is to replace the sequence of the mRNA transcript that contains the disease-causing mutation, or to correct the disorder linked to aberrant splicing.

- The second one has been developed to deflect endogenous mRNA production to synthesize a therapeutic protein *in vivo*, suicide gene therapy or molecular imaging. For example, Wang *et al.* have demonstrated that it is possible to produce *in vivo* functional proteins using a small amount of albumin mRNA¹⁶⁸. As albumin is a highly abundant protein of mammalian cells, a *trans*-splicing rate of 3-6% as was observed, has no direct consequences on albumin level, but allows a significant amount of therapeutic proteins to be obtained. By the same approach, it has been shown that *trans*-splicing can be used to induce the production of a suicide protein, particularly used in cancer therapy¹⁶⁹⁻¹⁷¹, or a reporter protein for *in vivo* imaging^{172,173}. In contrast to mRNA repair approaches, the *trans*-splicing rate should be kept here to a minimum. Advantages, drawbacks and strategies of PTM design exposed below, are more applicable to strategies of mRNA repair, where *trans*-splicing rate need to be maximal.

III.2.c. Strategies of PTM Design

Trans-splicing might be considered as a kind of alternative splicing, where the splice machinery can make the choice between two potential acceptor splice sites, one in *cis* and the other in *trans*. The challenge is based on the efficiency of the PTM, and thus the ratio between *trans*-splicing and *cis*-splicing. Because it is often not possible to predict the *trans*-splicing rate necessary to prevent the disease development, the main objective is to promote a maximum of splicing in *trans*. In order to unbalance the splice event in favor of *trans*-splicing, the design of the PTM can be modified following several strategies:

- Exactly as for *cis*-splicing, Puttaraju *et al.*²⁷ have demonstrated that *trans*-splicing induced by PTM requires the presence of several structures into the PTM molecule, such as a functional BP, a PPT and AG at the 3' splice site. Moreover, to stabilize the PTM and because

Disease	Gene	Trans-splicing	Authors	Year	vitro/vivo
Dystrophic Epidermolysis Bullosa	COL7A1	3'	Murauer <i>et al.</i>	2013	vitro
recessive dystrophic Epidermolysis Bullosa	COL7A1	3'	Murauer <i>et al.</i>	2010	vitro
Cystic Fibrosis	CFTR	3'	Liu <i>et al.</i>	2002	vitro
Cystic Fibrosis	CFTR	3'	Liu <i>et al.</i>	2005	vitro
Cystic Fibrosis	CFTR	3'	Mansfield <i>et al.</i>	2000	vitro
Frontotemporal dementia with parkinsonism linked to chromosome 17	MAPT	3'	Rodriguez-Martin <i>et al.</i>	2005	vitro
Frontotemporal dementia with parkinsonism linked to chromosome 17	MAPT	3'	Rodriguez-Martin <i>et al.</i>	2009	vitro
Severe combined immune deficiency	DNA-PKcs	3'	Zayed <i>et al.</i>	2007	vitro
Dystrophia myotonica type 1	DMPK	3'	Chen <i>et al.</i>	2009	vitro
Medullary thyroid carcinomas	RET	3'	Kikumori <i>et al.</i>	2001	vitro
Hemophilia A	FVIII	3'	Chao <i>et al.</i>	2003	vitro+vivo
Spinal muscular atrophy	SMN2	3'	Coady <i>et al.</i>	2007	vitro
Spinal muscular atrophy	SMN2	3'	Coady <i>et al.</i>	2008	vitro+vivo
Spinal muscular atrophy	SMN2	3'	Coady <i>et al.</i>	2010	vivo
Spinal muscular atrophy	SMN2	3'	Shababi <i>et al.</i>	2011	vitro+vivo
Dysferlinopathies/ Titinopathies	Dysferlin/ Titin	3'	Monjaret <i>et al.</i>	2014	vitro+vivo
Duchenne muscular dystrophy	mdx	3'	Lorain <i>et al.</i>	2013	vitro+vivo
X-linked immunodeficiency with hyper-IgM	CD40L	3'	Tahara <i>et al.</i>	2004	vivo
Epidermolysis Bullosa	COL17A1	internal	Koller <i>et al.</i>	2011	vitro
Duchenne muscular dystrophy	mdx	internal	Lorain <i>et al.</i>	2010	vitro
Cystic Fibrosis	CFTR	5'	Mansfield <i>et al.</i>	2003	vitro
Epidermolysis Bullosa Simplex	PLEC1	5'	Wally <i>et al.</i>	2007	vitro
Epidermolysis Bullosa Simplex	K14	5'	Wally <i>et al.</i>	2010	vitro
Huntington's disease	HTT	5'	Rindt <i>et al.</i>	2012	vitro
Sickle cell anemia and β -thalassemia	β -globin	5'	Kierlin-Duncan <i>et al.</i>	2007	vitro
Mucopolysaccharidosis type VII	GUSB	5'-3'-internal	Sachot <i>et al.</i>	2009	vitro

Table 2: SMaRT applications.

In vitro and *in vivo* studies using SMaRT technology to repair pre-mRNA in different diseases contexts.

it seems to slightly enhance *trans*-splicing efficiency²⁸, a poly(A) tail is usually added into the PTM sequence.

- Engineering of binding sequence that differ in size and location. An obvious clue in PTM design is that a great part of the success remains in the binding domain. Indeed, most of the groups working on *trans*-splicing have tried to modify the size and the location of this sequence, and observed direct consequences on *trans*-splicing efficiency and specificity^{28,156,164,174}. Several screening systems have thus been implemented^{154,164,165} and are still in development today to select the most effective binding domain.

- Designing the binding domain against a sequence included in a long intron. Indeed, it seems that *trans*-splicing efficiency increases with time of synthesis of the sequence between endogenous 5'ss and 3'ss of the target intron¹⁷⁵. This is certainly due to the competition between *cis*-splicing that needs availability of both natural splice sites, and *trans*-splicing that is only possible after the binding of the PTM.

- Addition of a stem-loop structure on the PTM, encompassing its splice site, to prevent nonspecific splicing. While in the hands of Puttaraju et al.²⁷ this strategy seems to work, it is not always the case^{156,174}, casting doubts about utility of this sequence.

- Insertion of an intron in the replacement cDNA. Mansfield *et al.* and Lorain *et al.* have shown that the presence of an intron in the PTM can increase *trans*-splicing efficiency^{28,162}.

- Addition of ISE in the intronic sequence of the PTM. Consideration should be given to this point, due to the observation that ISE can promote splicing event (see part III.1.c). Even if it is still difficult to predict the effect of an ISE, depending on its sequence, its location regarding which exon to include and its potential to recruit splicing enhancer factors, some data are now available¹⁷⁶ and should be useful to increase PTM efficiency.

- Targeting of sequences implicated in *cis*-splicing. *Murauer et al.*¹⁶⁵ tried to block *cis*-splicing by designing a binding domain complementary to the acceptor site present just downstream of the targeted intron. They described that blocking of the endogenous 3'ss led to an increase of *trans*-splicing efficiency.

- Combination of PTM with splice-site blocking antisense oligonucleotide. Coady et al.³⁵ and Shababi *et al.*³³ have demonstrated the capacity of this last one in increasing the *trans*-splicing rate by its binding on the endogenous 3'ss. They have developed a single vector for antisense and PTM delivery and shown its efficiency *in vivo*³⁴. These results highlight a great potential in *trans*-splicing improvement, but require caution concerning the potential exon skipping that could also be induced by the binding of the antisense oligonucleotide.

- The adjuvant effect of U7snRNA. U7snRNA is naturally a part of the U7 small nuclear ribonucleoproteins complex involved in the maturation of histone pre-mRNA and should be used to improve splicing manipulation. Antisense U7 snRNA has been applied when masking *cis*-acting sequences, to promote exon skipping^{177,178} or *trans*-splicing. An optimized U7snRNA seems to enhance 5' *trans*-splicing but has no effect on 3' *trans*-splicing or internal replacement^{36,167}.

In the case of RHO mutations, it is important to keep in mind that:

- By targeting the first intron, only one PTM should be able to repair around 70-80% of all known RHO mutations. The cases concerned by the remaining 20-30% being widely represented by P23H mutation, for which a mutation dependent strategy can be developed.

- The first intron extends on 1781 bp and is the longest one of *RHO*, giving some choice concerning the 150b binding sequence, and allowing us to take advantage of the delay between 5'ss and 3'ss synthesis.

- The size of the *RHO* cDNA coding sequence from exon 2 to 5, to incorporate in the PTM, is only of 686 bp, which is a real advantage allowing supplementation of the basal molecule with elements that might increase *trans*-splicing rate while conserving a size compatible with AAV encapsidation.

- The *trans*-splicing rate necessary to prevent the disease cannot be predicted, because it is totally depending on the RHO mutation, and its severity, meaning that a partial *trans*-splicing rate might be sufficient to bring a therapeutic benefit.

- Integrity of each rod PR cell is not absolutely required to conserve vision, meaning that even if the PTM transduction is not pan-retinal, it may be sufficient to stop the general degenerative process and maintain the vision in a steady state.

Independently of the PTM design, another way to influence *trans*-splicing rate is to modify the ratio between the pre-mRNA target and the PTM²⁷. Even if there is some limitation to this approach, due in part to the delivery of the PTM, it can play an important role on *trans*-splicing rate. Following the same idea, the way of delivery of the PTM is crucial to improve its specificity and efficiency. This parameter is discussed in the following part.

III.2.d. Advantages and drawbacks

Like all molecular mechanisms used to modify gene expression, SMaRT technology presents some drawbacks:

- The specificity of the PTM: it is essential to avoid off-target binding of the PTM and the production of aberrant proteins. Increasing the size of the binding site might limit off target binding. By lengthening the binding sequence to 150b, the probability of finding the corresponding sequence in a human genome is approximately 1.6×10^{-81} , meaning that the designed sequence is highly specific. However long binding sequence can only partially bind to the targeted mRNA and promote *trans*-splicing in spite of low homology. It is thus necessary to limit the delivery of the PTM to the targeted cells, and to control off-target effects as well as possible, even if these hybrid mRNA should be processed by as nonsense mediated decay or nonstop decay¹⁷⁹. This point also highlights the importance of the 3' splice site and its potency, which can induced more or less off-target¹⁵⁶. Always in this objective, it is also important to take into account the expression level of the targeted mRNA, and to adapt PTM expression consequently, in order to avoid the presence of useless PTM into the cell.

- Accessibility of RNA targeted sequence: despite several tools developed to predict the secondary structures of pre-mRNA (<http://www.tbi.univie.ac.at/RNA/> - <http://nhjy.hzau.edu.cn/kech/swxxx/jakj/dianzi/Bioinf4/miRNA/miRNA1.htm> - [http://mfold.rna.albany.edu/?q=mfold/RNA-Folding-Form ...](http://mfold.rna.albany.edu/?q=mfold/RNA-Folding-Form...)), it remains quite difficult to estimate the final shape of RNA and thus to design binding sequences based on this information.

- Production of truncated proteins due to the translation of the PTM alone. Because the PTM possesses all elements that are required to promote its translation, except the first exon, the possibility to obtain a truncated protein should be taken into account. Indeed, even if the PTM do not possess the first exon, because its transcription is induced by a RNA polymerase II, it seems that it can be naturally capped and thus stabilized¹⁸⁰. Moreover, while the great majority of transcripts are translated from the first AUG included into the KOZAK sequence, secondary ATG can also be used to initiate the translation.

- A common drawback of most nucleic acids modification approaches is that the continuous transcription of PTM is necessary to correct all new-targeted pre-mRNA. This is an important point in dividing cells, which can be solved by the PTM delivery as for example the integration of PTM DNA sequence into the cell genome after lentiviral transduction or by imaging to target tissue stem cells³⁰.

On the other hand, among advantages offered by SMaRT technology, there are:

- Firstly, by targeting the first intron of the targeted pre-mRNA, and hence replacing all the subsequent sequence (depending of course of the cDNA size), only one PTM should be necessary to repair numerous mutations.

- The preservation in time, space and quantity, of the endogenous regulation of the target mRNA expression, because the PTM is in theory inert in the cell without the presence of its pre-mRNA target. The regulation of expression of the “chimeric” RNA is thus totally dependent on the natural regulation of the targeted pre-mRNA. This information is crucial in gene therapy, where the expression of a gene has to be constrained to a strict spatio-temporal pattern, and in the case of dominant diseases kept at a physiologic level.

- The dual capacity of the PTM to reduce mutated protein synthesis and to promote the normal one in a single reaction. In contrast to all other approaches that require the delivery of two molecules, *trans*-splicing only requires the delivery of the engineered PTM, the two others component of the reaction (targeted pre-mRNA and spliceosome) being naturally produces by the cells.

- As PTM includes only a part of the cDNA sequence needed for repair, SMaRT technology relies on a small size restorative molecule while all other gene therapy systems required a full-length cDNA. This facilitates the choice in viral vectors for PTM delivery in targeted cells. Indeed, the size of transgenic cassette is usually a major limitation in viral vector choice leading thus, for example, to the inability to use AAV vectors. Using SMaRT technology could therefore enlarge viral vector choice for diseases implicating genes that are usually considered too large to be included in an AAV vector.

IV. Viral vectors for gene therapy of ocular diseases

IV.1. Advantages of the eye as target of gene therapy with viral vector

The fact that the retina is part of this small closed organ, which is the eye, brings really interesting advantages in the context of gene therapy using viral vectors:

- Firstly, because of its transparency and accessibility, viral injections are quite simple to realize. Moreover, thanks to technologies developed for *in vivo* imaging, outcomes can be easily and precisely followed-up.
- Secondly, the size of the eye allows the use of high viral concentrations with a low injection volume. Furthermore, because this organ is a closed compartment, in which the neural retina is isolated from the general circulation by blood-retinal barriers, this avoids uncontrolled dissemination, particularly in the blood.
- Thirdly, another property, made possible by the action of these barriers among others, is the immune privilege existing for the neural retina, meaning that there is a local inhibition of immune responses¹⁸¹.
- Then, because the eye is compartmentalized, several injection routes are available: in the anterior chamber, in the vitreous and in the subretinal space (Figure 18). The choice of the injection route is of course dependent on the targeted cells, but the absence of direct communication between these different compartments allows concentrating the viral particles into a given location and to be more specific regarding targeted cells.
- Finally, in the case of the retina particularly, most of the cells are post-mitotic neurons, meaning that non-integrative viruses can be used without the concern of transgene dilution through divisions, and the risk of insertional mutagenesis.

IV.2. Choice of the viral vector for ocular diseases

IV.2.a. Classical viral vectors used in gene therapies

Transduction of cells is the adaptation of a natural process that has been diverted to create viral vectors applicable in a therapeutic context. To do that, all viral vectors developed have certain viral genes replaced by a gene of interest; consequently, the viral vector is still able to

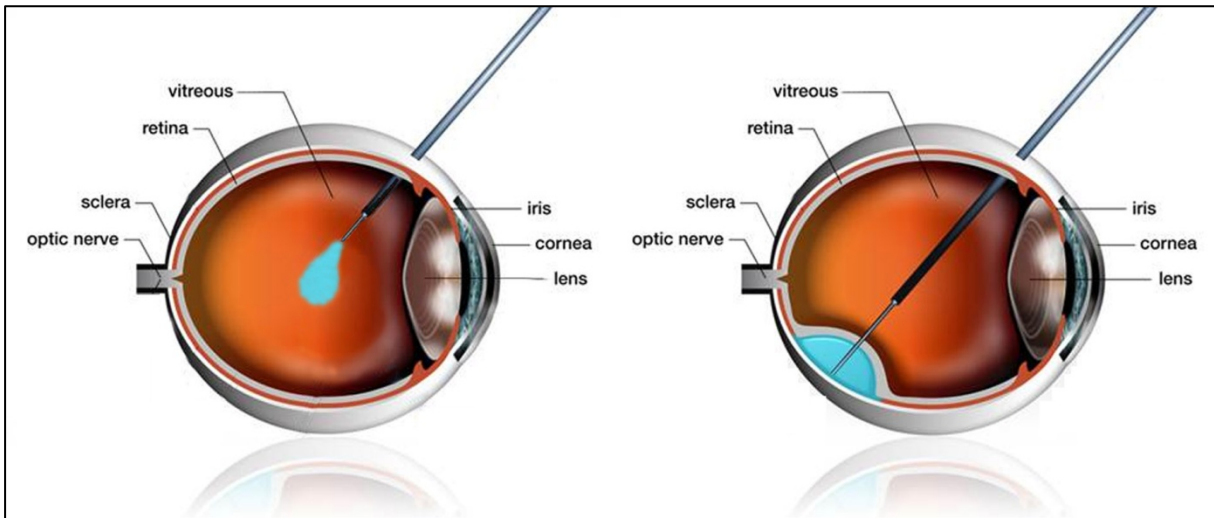


Figure 18: Schematic representation of intravitreal (left) and subretinal (right) injection in a human eye.

Adapted from an image of Moorfields Eye Hospital and University College London.

transfer its genetic material into the target cell, but is now non-replicative. Proteins required for all processes linked to viral infection are thus encoded by viral genes brought independently of the recombinant viral genome. Building a viral vector for safe gene delivery in a specific cell type requires taking into account five main parameters: (i) the packaging capacity, i.e. the size of the transgene cassette that can be incorporated into the viral genome, (ii) the specific targeting to given cells, (iii) the stability of transgene expression over time, (iv) the potential immune reaction that may damage tissues, and (v) the potential oncogenic capacity occurring through vector genome integration. Properties of lentiviral, adenoviral and AAV (Adeno-Associated Virus) vectors, which have given proof of efficiency for ocular gene therapy, are summarized in Table 3.

- Lentiviruses are enveloped RNA viruses, with a viral genome of around 10 kb (Figure 19). The lentiviruses group includes the infamous human immunodeficiency virus, the etiologic agent of acquired immunodeficiency syndrome. Lentivirus vectors are usually produced by a co-transfection of several plasmids into the productive host cells: the first one encoding the envelope proteins, the second one all proteins required for reverse transcription and packaging of the viral genome, and the third encodes the vector genome, with the transgene cassette included between the two LTR (Long Terminal repeat Regions). Lentiviral vectors integrate into the host cell genome, allowing a sustainable expression over time, even in divided cells. Thanks to these properties, lentiviral vectors were used in the first true success story concerning gene therapy: the successful treatment of severe combined immunodeficiencies^{182,183}. Unfortunately, transactivation of neighboring genes of the integration site by a native LTR sequence present in the first generation of this vector was also at the origin of side effects, leading to the development of leukemia-like conditions for several patients¹⁸⁴. Since that, modifications have been done to improve their safety, such as the development of self-inactivating vectors¹⁸⁵ or non-integrating vectors¹⁸⁶. Nevertheless, concerning retinal cells transduction, while lentiviruses efficiently deliver genes to the RPE, their efficiency to transduce PR is more limited¹⁸⁶⁻¹⁹⁰, even with the VSV-G (Vesicular Stomatitis Virus-Glycoprotein) pseudotype, which is the most efficient when targeting the neural retina¹⁹¹.

- Human adenoviruses are non-enveloped dsDNA viruses of 70-90nm that cause significant numbers of respiratory, ocular and gastrointestinal diseases (Figure 20). First generation of recombinant adenoviral vectors retained a significant portion of viral coding sequence in their genome and were described to elicit robust cytotoxic T lymphocyte-mediated immune response¹⁹². Since this first generation of adenoviral vectors, many changes

	Lentivirus	Adenovirus	AAV
Viral genome	RNA	dsDNA	ssDNA or scDNA
Packaging capacity	10 Kb	36 Kb	4,7 or 2,3 Kb
Targeting (subretinal injection)	RPE and PR (low efficiency)	RPE and PR (low efficiency)	RPE and PR
Expression stability	Long time expression thanks to integration	Short expression due to immune reaction. Longer with gutless adenoviruses	As long as studied in post mitotic cells
Side effects	Potential oncogenic properties due to insertional mutagenesis	Strong immune reaction, reduced with gutless adenoviruses Helper viruses required for production could be an issue	No known side effect

Table 3: Properties of classical viral vectors used in ocular gene therapies.

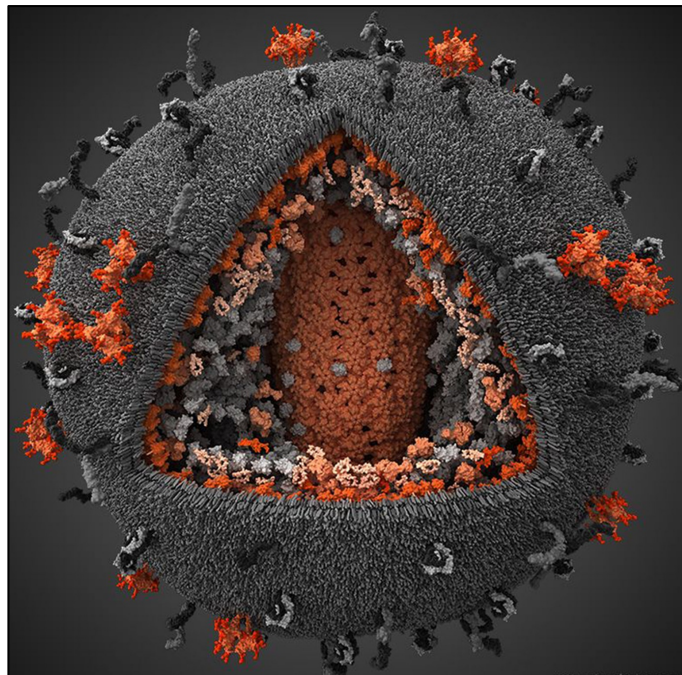


Figure 19: The lentivirus: an enveloped RNA virus of around 100nm.
Image from *Visual Science Company*.

have been done to improve their capacities and reduce their drawbacks, leading to the new group of adenoviral vectors called gutless, gutted or high capacity adenoviral vectors. Totally devoid of viral genes, they have a high capacity of packaging compared to other viruses (about 36kb), but they need a complex system involving a helper virus for the production of the viral particles. In turn, this absence of viral gene expression in the transduced cells leads to a decreased immune reaction. These helper-dependent adenoviral vectors have been tested to transduce cells in the retina, and they allow long-term transgene expression in RPE¹⁹³, unlike previous ones that were implicated in a time-limited expression, probably due to immune or toxicity-related mechanisms. Nevertheless, they have shown a questionable transduction efficiency of PR (depending on the dose)¹⁹⁴, limiting their utility for treating adRP.

- AAV was firstly described in 1965 by Atchison *et al.*¹⁹⁵ as DNA-containing particles present in adenovirus preparation. AAV are small ssDNA viruses of the *Parvoviridae* family, *Parvovirinae* subfamily and *Dependovirus* genus. AAV are still unassociated to disease in humans, which is a considerable advantage for therapeutic application compared to all other viral vectors. AAV infection of a cell in the absence of a helper virus results in the onset of the latent cycle in which the virus may integrate into human chromosome 19 or persist in an episomal form¹⁹⁶. Indeed, AAV require a helper virus to replicate, such as the adenovirus or herpes virus. AAV are non-enveloped viruses, composed of a capsid surrounding a 4,7kb DNA viral genome (Figure 21). This last one carries several viral genes between the two palindromic inverted terminal repeats (ITR) including those of non-structural proteins (Rep) and capsid ones (VP). Rep proteins regulate every phase of the AAV life cycle such as encapsidation of mature DNA, while VP proteins constitute the 60-subunits of the 25nm icosahedral virion particle. More than 100 different natural serotypes of AAV have been isolated, and among them 10 have been more extensively characterized and classified. They differ on the composition of their capsids, and consequently, their affinity for cell surface receptors is modified, determining their tropism. The most studied serotype, AAV2, utilizes membrane associated heparan sulfate proteoglycan as its primary receptor, associated to co-receptors, while other serotypes such as AAV1 and AAV5 seem to bind cells through sialic acids¹⁹⁷.

Recombinant AAV (rAAV) vectors have now been widely engineered to use this virus as a therapeutic vehicle. Most of rAAV are based on the AAV2 genome by replacing the entire viral genome with the expression cassette of the transgene of interest, and conserving only the two ITR. The nomenclature usually used indicates two numbers as followed: rAAV2/5, where

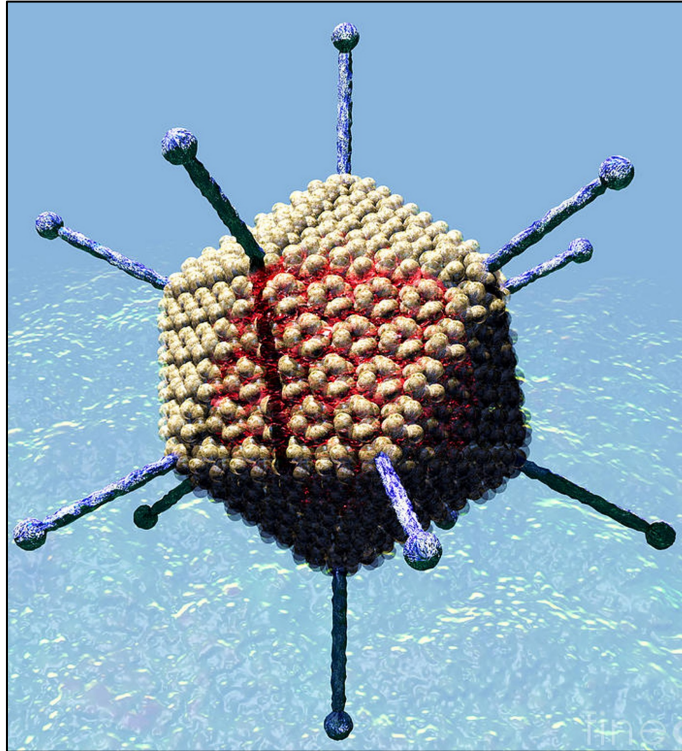


Figure 20: The adenovirus: a non-enveloped dsDNA virus of 70-90nm.
Image from *Russell Kightley Science Images*.

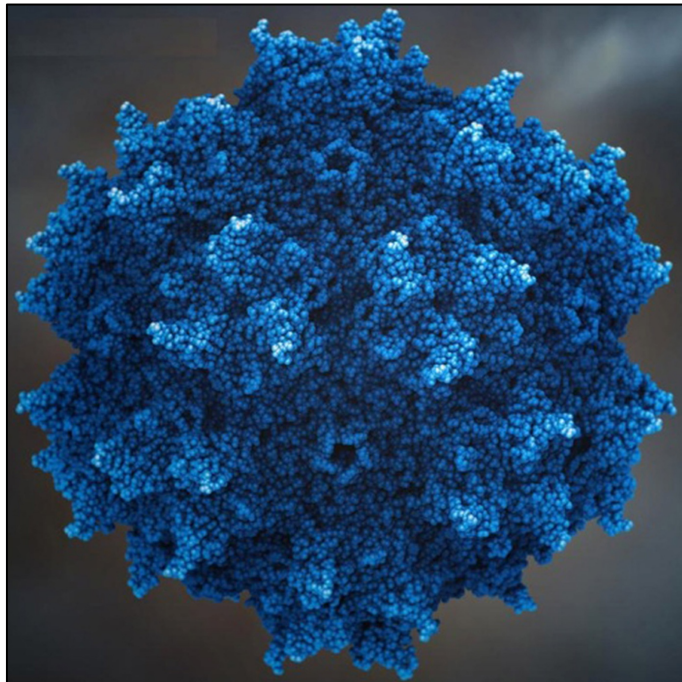


Figure 21: The adeno-associated virus: a non-enveloped ssDNA virus of 25nm.
Image from *genetics-genomics.wikia.com*.

the first one refers to the origin of the ITR of the recombinant genome, and the second one to the capsid. In addition to all natural serotypes, rational mutagenesis is now used to select more and more efficient rAAV to transduce a given cell type¹⁹⁸.

The efficiency of transgene expression by transduction of a rAAV is thus depending on three parameters: (i) the capsid serotype, (ii) the promoter used to control the transgene expression and (iii) the mode of administration.

First studies directed to induce gene expression in the retina were done with rAAV2/2, and showed transduction of a large cell population of the retina, including ganglion cells, Müller cells, PR and RPE cells, which persists at least 80 days post-injection, without any sign of inflammatory response or toxicity, after subretinal injection in adult mice^{199,200}. The gene expression can be restricted to PR, by using a rod-specific promoter such as the rhodopsin²⁰¹. From these first results a wide diversity of combinations of natural AAV variant capsids associated to the genome of rAAV2, have been tested to transduce the retina (Table 4 extracted from Stieger *et al.*²⁰²). Among them, several have demonstrated a great potential to transduce PR, depending on the promoter used and the delivery route: rAAV2/5 serotype transduces specifically RPE and PR, but more efficiently than rAAV2/2¹⁸⁸. Moreover, the more recently developed rAAV2/7, rAAV2/8 and rAAV2/9 also very efficiently transduce RPE and PR in mice. Associated with a CMV promoter, these last ones present a distribution and an expression level apparently similar to those of rAAV2/5, except that rAAV2/9 also transduces Müller cells²⁰³. The same group provided the proof that when associated to a specific rhodopsin promoter and injected subretinally, rAAV2/7 and rAAV2/8 induce six- to eightfold greater transgene expression, making them the most efficient rAAVs to transduce PR cells of the mouse retina²⁰³. The use of rAAV2/8 to efficiently transduce PR has then been demonstrated in pigs²⁰⁴, dogs²⁰⁵ and non-human primates²⁰⁶. The group of R. Ali has also shown that modifying the single strand rAAV2/8 to a self-complementary one introduced to the viral vector provided a faster onset and higher level of transgene expression²⁰⁷. This modification consists in mutating one of the ITR of the recombinant genome, so avoiding its recognition by the virus endonuclease. This leads to encapsidation of double-stranded genome that bypasses the limiting step of second-strand synthesis occurring in the target cell. As a corollary, self-complementary AAVs have half the packaging capacity of conventional AAV.

Certainly the main drawback of AAV is its packaging capacity and thus the size limitation of the transgene cassette.

To overcome this issue, several groups^{208,209} have demonstrated that it is possible to drive the expression of a large gene after intermolecular concatamerization, transcription and

rAAV serotype	Mouse	Rat	Dog	Primate
rAAV 2/1	RPE	-	-	-
rAAV 2/2	RPE, PR	RPE, PR	RPE, PR	RPE, PR
rAAV 2/3	-	-	n.d.	n.d.
rAAV 2/4	-	RPE	RPE	RPE
rAAV 2/5	RPE, PR	RPE, PR	RPE, PR	RPE, PR
rAAV 5/5	RPE, PR	n.d.	n.d.	RPE, PR
rAAV 2/6	RPE	n.d.	n.d.	n.d.
rAAV 2/7	RPE, PR	n.d.	n.d.	n.d.
rAAV 2/8	RPE, PR	RPE, PR, INL, GC	RPE, PR, INL, GC	n.d.
rAAV 2/9	RPE, PR, MC, INL	n.d.	n.d.	n.d.

Table 4: Cellular tropism of rAAV serotypes following subretinal injection.

RPE= retinal pigmented epithelium, PR= photoreceptors, MC= Müller cells, INL= inner nuclear layer, GC= ganglion cells, n.d.= not determined. Extracted from *Stieger et al., Methods in Molecular Biology, 2011.*

splicing of 2 RNA produced from sequences of 2 independent AAV vectors, each one carrying a part of the expression cassette. As a result it is now possible to induce stable expression of a long gene by transduction of recombinant AAV.

rAAV are thus viral vectors (i) able to specifically transduce a given cell type, including PR, thanks to serotypes diversity and tropism associated to each one, (ii) that allow a high expression level of the transgene, particularly when combined to a specific promoter, (iii) that induce only a low immunogenicity linked to their non-pathogenic nature, (iv) that present a persistent transgene expression in non-dividing cells (v) that are unable to produce insertional mutagenesis (no integration or only at a very low frequency). All these characteristics make of rAAV one of the most employed viral vector in gene therapy and the first one in the context ocular diseases.

IV.2.b. Previous ocular gene therapies with rAAV

The pioneering and the most famous ocular gene therapy, which paved the way, is the RPE65 gene replacement for Leber Congenital Amaurosis (LCA). LCA is the most severe retinal dystrophy, which appears during childhood. This disease can be induced by mutations in any one of at least 17 genes^{210,211}, encoding various proteins implicated in retinal functions, including RPE65, the retinoid isomerase that converts all-*trans*-retinoids to 11-*cis*-retinal during pigment regeneration. Several groups have firstly demonstrated the proof-of-principle of RPE65 gene replacement therapy in Briard dogs²¹² and its efficiency on long-term restoration²¹³ after subretinal injection of rAAV2/2. A lot of studies (summarized here²¹⁴) have thus been leading before to begin phase I clinical trials in humans²¹⁵⁻²¹⁷ that are a success and provide stable clinical benefits²¹⁸⁻²²¹. Despite differences in promoter, dose, etc... all studies employed a rAAV2/2 vector carrying a normal human RPE65 cDNA, delivered subretinally, and showed significant beneficial effects on vision. These clinical trials have been shown to be safe, free of serious complications and efficient regarding progress in vision, which justify the beginning of a phase III clinical trial (NCT00999609). Other clinical trials of retinal gene therapy are today ongoing, based on AAV vector; such as a phase I clinical trials for MERTK-associated autosomal recessive *retinitis pigmentosa*, choroideremia and exudative age-related macular degeneration²¹⁴.

V. Cellular and animal models of RP linked to rhodopsin mutations.

V.1. Cellular model of rhodopsin expression

V.1.a. Primary cultures of photoreceptors

Unlike cone PR, from which a cell culture line, the 661W cell line²²², has been derived, so far no one has managed to create a cell line featuring cellular and biochemical characteristics of rod PR cells, except for the Y-79 retinoblastoma cell line, which only expresses a subset of the rod-specific genes²²³. To study rod PR properties *in vitro*, methods have thus been developed to keep them in primary cultures. Nevertheless, these primary cell cultures can survive only 2 weeks, and remain heterogeneous cell cultures, in which rods are mixed with all other retinal cell types²²⁴; even in PR-enriched primary culture, cones are very numerous²²⁵. The advantage of working with primary PR cell cultures is to observe and study RHO in cells that express the protein physiologically; however, rods kept in primary culture lose their OS quite rapidly. This is an important drawback considering the fact that RHO is physiologically localized in disc membranes of rod OS. The only way to preserve PR properties *in vitro* is to make organotypic cultures of the entire retina, but these too can only be maintained for two weeks *in vitro*²²⁶. To study PR *in vitro*, it is also now possible to generate retinal PR or progenitor cells from embryonic stem cells²²⁷ or induced pluripotent stem cells²²⁸, and to select ES-derived or iPS-derived PR²²⁹. Nevertheless generating these kinds of cells and keeping them in culture requires technically complex and laborious protocols.

V.1.b. Cell lines developed to study rhodopsin mutations

Due to the limitations of PR primary cultures mentioned above, most of the research groups are using classical cultures of immortalized cell lines transfected or transduced to express *RHO*. Among them, Sung *et al.*^{55,58} have tested, in two distinct studies, 34 mutations of RHO associated with adRP in HEK293S cells, by transient transfection. The authors demonstrated that WT RHO is correctly synthesized and folded in HEK293S cells by measuring the spectrophotometric absorbance of the photopigment after incubation with 11-*cis*-retinal. In these cells, WT RHO is localized to the plasma membrane, showing that it is correctly transported. Moreover, they revealed that mutated RHO could differ from the WT

protein in its capacity to bind the 11-*cis*-retinal, as well as in its cellular localization, depending on the mutation. Other groups also demonstrated in HEK293 or COS cells that the P23H mutation seems to induce the retention of proteins in intra-cytoplasmic inclusions called aggresomes^{64,230}. A few years later, classical cell lines transfected with mutated forms of RHO were also used to prove the involvement of some RHO mutations in the Unfold Protein Response pathway.^{231–233}

All these studies thus helped to determine a classification for RHO mutations, detailed in part I.3.c., to define role and properties of each part of the protein²³⁴ and determine potential mechanisms involved in PR cell death due to mutated RHO.

These findings establish the fact that classical cell lines commonly used in cell culture such as HEK293 or COS cells can be useful to study and characterize RHO mutations. These cell lines present the advantage of being easily kept in culture, and easy-to-transfect and transduce. Nevertheless, it is important to keep in mind that HEK293 and COS cells differ greatly relative to rod PRs in their cellular structure, morphology and lineage, which can account for differences in terms of protein localization, interactions and signaling, as can be exemplified by localization of Q344Ter RHO that is similar to those of WT RHO in HEK293 and different in rod PR⁵⁵.

V.2. Animal models of rhodopsin-induced *retinitis pigmentosa*

V.2.a. Animal models of rhodopsin mutation-induced *retinitis pigmentosa* and more specifically mouse models

Mouse models have been created to study the impact on rod PR of the lack of one or two alleles of *RHO*. Humphries *et al.*⁷⁰ and Lem *et al.*⁵⁷ showed that retinas without *Rho* initially develop normally, with the exception that the rod OS never forms. As the retina matures over the course of the following months, PR cells degenerate completely. The same evolution occurred in mice with only one allele of *Rho*, but happened with a slower time course, suggesting that RHO is essential in the development and maintenance of rod PR⁵⁷. Conversely, another group also demonstrated that overexpression of *Rho* also leads to PR degeneration⁶³. These studies highlighted the importance of RHO in rod homeostasis and brought first pieces of evidence that RHO modification dramatically influences the retinal state.

In addition to a natural RP dog model induced by a RHO mutation²³⁵, many animal models expressing a mutated form of RHO have been generated to date, including in

drosophila^{236,237}, zebrafish²³⁸, rat^{128,239}, rabbit²⁴⁰, pig^{241,242} and most frequently, mouse^{55,62,63,66,68,243–245}. These models encompass mutations present in all domains of the protein, from the N-terminal part (P23H mutation) to the C-terminal part involved in transport of the protein (Q344Ter, P347S mutation) through the intermediate part (E150K, D190N, K296E mutations). Most of the models reproduce RP symptoms such as rod PR degeneration. P23H, P347S and Q344Ter mutations all lead to rod degeneration, even if the P23H and P347S mutated RHO are mainly localized near the rod OS^{62,66} while the Q344Ter mutation induces abnormal RHO accumulation in the plasma membrane of the rod cell body⁵⁵. All these mouse models that accurately reproduce some of the RP symptoms observed in humans are thus essential to study the effect *in vivo* of mutations affecting the structure, transport, degradation and functionality of RHO, and to understand the mechanisms that can lead to rod degeneration. They are also an indispensable step in the development of tools and strategies to prevent retinal degeneration in RHO-induced RP patients.

Among the mouse models described above, some express one or two mouse *Rho* mutated alleles^{55,62,243,245}, while others present the mutated human allele(s). The former strategy employing mouse *Rho* can represent an obstacle for projects that aim to develop therapeutic tools adaptable for humans, particularly if these target nucleic acids, either at the gene or at the transcript level, due to a few differences that exist between human and mouse rhodopsin genes (Annex 1), particularly in the intron sequences.

V.2.b. Comparison of mouse and human eyes

The mouse is the organism in which most human disease models are generated, including ocular diseases, as previously mentioned. Despite the fact that the eye's main properties are conserved between the human and the mouse, there are notable discrepancies that should be taken into account when using a mouse model to simulate a human ocular disease. The most important differences are listed below.

- Firstly, the size of the organ: while the human eye measures ~24mm in diameter, that of the mouse is more than 7-fold smaller (3.4mm), which must be taken into account at the moment of the injection.
- Relative to the eye size, the lens is bigger in the mouse compared to the human eye. The vitreous cavity volume in the mouse eye (~5µL) is thus 1000-fold less than in the human (~5.2 mL). This implies a highly limited volume that can be injected in the mouse eye (Figure 22).

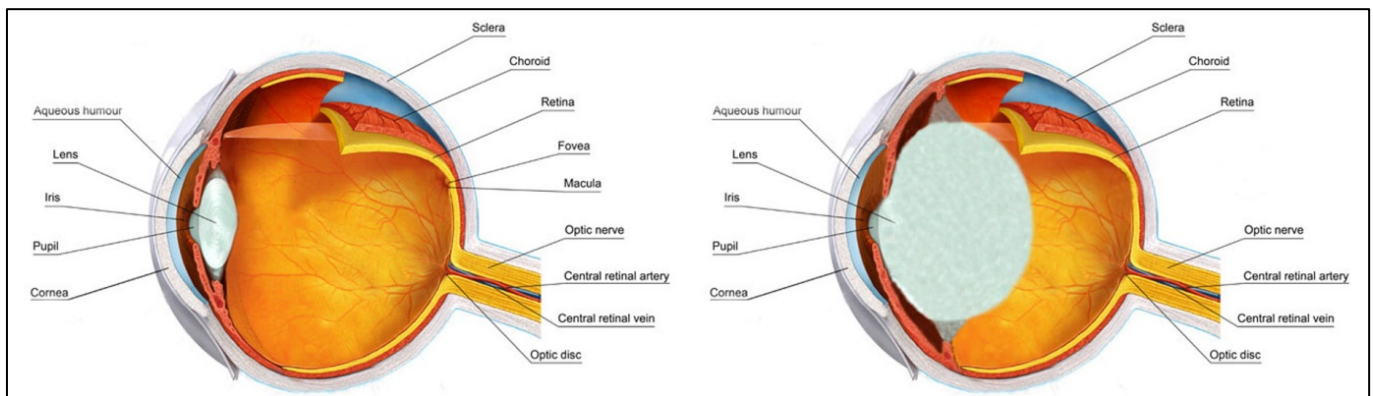


Figure 22: Comparison of a human (left) and a mouse (right) eye.

Adapted from virtualmedicalcentre.com.

- The composition of the retina, and more precisely at the level of PR, differs between humans and mice. While rods and cones are present in both species, with rods highly outnumbering cones, the imbalance between rods and cones is even more significant in the mouse eye due to the absence of the macula. Indeed, the human macula is densely packed with cones (see part I.1.c for more details on the macula).

- The cone opsins are different between the two species: while humans have three different opsins defining three types of cone PR (see part I.1.c for details), mice display dichromatic vision with only two kinds of cone opsins, lacking the long wavelength sensitive opsin (OPN1LW), which catches photons in the red region of the visible light spectrum.

- The maturation of the retina is much later in mice than in humans, with regards to embryonic development. This is particularly true for rods, which are generated around fetal week 10 in humans, while they are generated from embryonic day 12 to postnatal day 10 in mice²⁴⁶. This means that during the first post-natal days, mouse retinal cells are not completely formed and mature, unlike in humans.

Despite these few differences between the human and mouse eye, mice present a very similar organ to that of humans, in terms of structure and function. The mouse eye thus represents a powerful model to reproduce human ocular diseases in order to characterize them and establish proofs-of-concept for new treatments. Moreover, among all animal models available in biology, mice present the advantages of being easy to reproduce and manipulate, and less expensive than others. A lot of methods and apparatuses have now been adapted to perform experiments on these animals. This explains why the mouse is the most broadly used animal model, with a wide variety of human disease mouse models, including ocular ones. Before translating from mouse models to human clinical applications, however, new treatments must be tested in bigger animals, such as dogs, pigs or often non-human primates. It follows that relevant models of the studied diseases have been developed in these species as well, although no such model has been established in our case. Indeed, no big animal model has been developed to date, expressing the whole human rhodopsin gene. Large animal models can thus be used only to implement biodistribution and toxicity tests, making the rodent models the most powerful ones established so far for the assessment of the therapeutic efficiency of our therapeutic strategy.

As noted above, there being no treatment to date to prevent mutated autosomal dominant RP due to rhodopsin mutations, and the current strategies presenting several important drawbacks, SMaRT technology based on *trans*-splicing is a promising approach for dominant diseases. We thus decided to apply SMaRT technology to the rhodopsin case.

The following part of this thesis will summarize all the results obtained on that topic during my PhD project. It will be presented in three chapters described below, the first corresponding to a manuscript that is currently under review for publication in *Molecular Therapy*, the second to an article that has been published in the May 2014 issue of *PLoS One*, and the third one corresponding to additional results, some of which should give rise to a third publication.

The first chapter will expose the results of the design, screen and optimization of *trans*-splicing molecules in *in vitro* models. We characterized the effects of *trans*-splicing by quantification at RNA and protein levels.

Before testing the *in vivo* effect of the best molecule selected by *in vitro* experiments, we provided some improvements on an *in vivo* imaging technology used to probe for and monitor degeneration in mouse models.

Finally, the third chapter will develop two groups of results that are still ongoing: the first concerns supplemental strategies to optimize the *trans*-splicing molecule *in vitro*, and the second is about first results of effect of *trans*-splicing on retinal degeneration in a humanized mouse model of rhodopsin mutation.

RESULTS

I. Results of *in vitro* analysis of PTM efficiency.

Repair of rhodopsin mRNA by spliceosome-mediated RNA *trans*-splicing: a new approach for autosomal dominant *retinitis pigmentosa*.

Adeline Berger, Stéphanie Lorain, Charlène Joséphine, Melissa Desrosiers, Cécile Peccate, Thomas Voit, Luis Garcia, José-Alain Sahel, Alexis-Pierre Bemelmans.

In order to correct rhodopsin mutations involved in RP, we used a therapeutic strategy called SMaRT (Spliceosome-Mediated RNA *Trans*-splicing). The idea was to induce a splice reaction in *trans* between the endogenous mutated rhodopsin pre-mRNA, and an exogenous PTM (Pre-mRNA *Trans*-splicing Molecule). The first challenge of this project was to select a PTM able to favor splicing in *trans* of the endogenous rhodopsin pre-mRNA at a maximal rate. The sequence of our PTM was expressed by a plasmid composed of a binding sequence to specifically recognize the target pre-mRNA, an artificial intronic sequence to accept the splice reaction, and the cDNA sequence to replace that of the mutated pre-mRNA. To select the best molecule, we designed and screened 14 different PTM that differed only by their binding sequence, which we tested by transient co-transfection with a *RHO* expression construct in HEK293T cells. With the best PTM, we obtained a maximal *trans*-splicing rate of 25% after quantification at the RNA level. We then improved this molecule by modifying the replacement sequence and reached a *trans*-splicing rate of 40%. We thus demonstrated that the target sequence of the PTM on the endogenous pre-mRNA was critical for PTM efficiency, as well as the replacement sequence of the PTM. Then, we created wild-type and mutated RHO cell lines by lentiviral transduction, to measure the PTM efficiency in a cellular model that stably expressed the target mRNA, a paradigm closer to physiological conditions. Because several RHO mutations including R135W induced a mislocalization phenotype in HEK293T cells, we quantified the efficiency of the best PTM at the protein level by studying the rescue of the phenotype after transfection of the PTM expression construct. We established that enough *trans*-splicing reactions occurred in these stable expression models to promote a partial rescue of the phenotype, which prompted us to study the PTM effect *in vivo*. This work represents the first application of SMaRT technology for an ocular disease, and the first study that presents a high-enough *trans*-splicing rate to expect a therapeutic effect in case of a dominant disease.

Repair of rhodopsin mRNA by spliceosome-mediated RNA *trans*-splicing: a new approach for autosomal dominant *retinitis pigmentosa*.

Adeline Berger¹, Stéphanie Lorain², Charlène Joséphine^{3,4}, Melissa Desrosiers¹, Cécile Peccate², Thomas Voit², Luis Garcia⁵, José-Alain Sahel^{1,6,7,8}, Alexis-Pierre Bemelmans^{1,3,4}.

¹Centre de recherche Institut de la Vision, Sorbonne Universités, Université Pierre et Marie Curie UM80, INSERM U968, and CNRS UMR 7210, Paris, France;

²Centre de recherche en Myologie, Sorbonne Universités, Université Pierre et Marie Curie, UM76, INSERM U974 and CNRS FRE 3617, Paris, France;

³CEA, DSV, I²BM, Molecular Imaging Research Center (MIRCen), Fontenay-aux-Roses, F-92265, France;

⁴CNRS, CEA URA 2210, Fontenay-aux-Roses, F-92265, France;

⁵UFR des sciences de la santé Simone Veil, Université Versailles Saint-Quentin, Montigny-le-Bretonneux, France;

⁶Centre Hospitalier National d'Ophtalmologie des Quinze-Vingts, INSERM-DHOS CIC 503, Paris, F-75012, France;

⁷Fondation Ophtalmologique Adolphe de Rothschild, Paris, France;

⁸Institute of Ophthalmology, University College of London, London EC1V 9EL, UK.

Correspondence should be addressed to A-PB, MIRCen/CEA, 18 route du Panorama, BP6, F-92265 Fontenay-aux-Roses, France. Tel: +33 146 54 96 29, Email: alexis.bemelmans@cea.fr

Short Title: *trans*-splicing therapy for retinal degeneration

Abstract

Promising clinical results achieved in recent years in the field of ocular gene therapy pave the way for gene supplementation in case of recessively inherited retinal degenerations. The situation is more complex for dominant mutations involving removal of mutated gene toxic product. To overcome this hurdle, we applied spliceosome-mediated RNA *trans*-splicing, a strategy of transcript repair, to rhodopsin, the most frequently mutated gene in autosomal dominant *retinitis pigmentosa*. We tested twenty different molecules to target pre-mRNA intron 1 by transient transfection of HEK-293T cells and subsequent *trans*-splicing quantification at the transcript level. This showed that some parts of the intron are more favorable than others to promote efficient *trans*-splicing, and that *trans*-splicing rate may be increased by modifying the replacement sequence. Then, we developed cell-lines showing stable expression of rhodopsin to assess relevant phenotypic criteria in relation to the pathological process of *retinitis pigmentosa*. Using this model, we have shown that *trans*-splicing can partially restore proper localization of the protein to the plasma membrane of the cells. This work paves the way for *in vivo* application of *trans*-splicing in the case of *retinitis pigmentosa* caused by a rhodopsin mutation and in a broader framework for genetic diseases with dominant transmission.

Introduction

Retinitis pigmentosa (RP) is a group of inherited retinal degenerative diseases, which represents one of the most common visual impairment worldwide and for which there is no treatment to date. RP is characterized by a progressive degeneration of rod photoreceptors leading to night-blindness and constriction of the visual field, followed by degeneration of cone photoreceptors inducing total vision loss. RP is genetically heterogeneous, including autosomal dominant, autosomal recessive, X-linked and sporadic forms involving mutations in more than 60 different genes that are expressed either in rod photoreceptors or in the retinal pigment epithelium (RetNet™, <https://sph.uth.edu/retnet/>). The rhodopsin gene (*RHO*) is alone responsible for 30 to 40% of autosomal dominant form of RP (adRP), with at least one hundred known-point mutations, and is thus the most frequently mutated gene in this disease (RetNet™). Rhodopsin (*RHO*) is the only photopigment of rod photoreceptor cells, in which it converts the light stimuli into electrochemical signals. These cells are necessary for dim light and peripheral vision, and essential for long-term maintenance of a functional retina¹⁻². The degeneration of rod photoreceptor cells induced by *RHO* mutations, is more or less rapid, depending on the aggressiveness of the mutation³. Different strategies are under investigation to prevent or slow down the disease progression, before or after beginning of the degeneration, mainly including gene replacement and neuroprotection through trophic factors. The first strategy consists usually to silence the mutant gene using for example RNA interference, in combination or not to supplementation with a silencing-insensitive *RHO* allele⁴⁻⁶, but this involves mastering the *RHO* expression level, and has the drawbacks to present some “off-target effects” and to potentially be toxic⁷. The second one has already shown its efficiency on photoreceptor protection in therapeutic trials⁸⁻¹⁰, but present major side effects like the disadvantage of not being specific to photoreceptor cells¹¹, and toxic depending of the dose¹².

To design the ideal approach to prevent retinal degeneration due to *RHO* mutation, it is necessary to take into account that (i) most of *RHO* mutations are gain-of-function or dominant negative effect mutations, requiring not only to provide the normal protein synthesis, but also to reduce the mutant protein one, (ii) it is essential to keep *RHO* expression level close to the endogenous one to avoid deleterious effect on the retina¹³⁻¹⁴, and (iii) because more than one hundred known-point mutations have been found in *RHO*, a generic therapeutic tool is required, to target a wide array of *RHO* mutations.

Spliceosome-Mediated RNA *Trans*-splicing (SMaRT) technology allows respecting these major constraints¹⁵. *Trans*-splicing is a natural splicing mechanism firstly discovered in tripanosoma¹⁶⁻¹⁷ but also later found in rats¹⁸ and humans¹⁹⁻²². Poorly represented compared to *cis*-splicing, *trans*-splicing occurs between two distinct pre-mRNA and leads to a final mRNA composed of the 5' part of the first pre-mRNA and the 3' part of the second one. SMaRT technology uses this natural phenomenon to develop a powerful tool for RNA repair strategies by engineering molecules that are able to *trans*-splice a specific endogenous pre-mRNA (target mRNA), replacing by this way the sequence located before (3'-replacement) or after (5'-replacement) the *trans*-splicing site. Unlike ribozyme *trans*-splicing, SMaRT implicates the endogenous cell spliceosome machinery and only requires the introduction of an exogenous RNA termed PTM for pre-mRNA *trans*-splicing molecule. This PTM is composed of (i) a binding domain to specifically target the endogenous pre-mRNA, (ii) an artificial intronic sequence comprising all the necessary elements for splicing and (iii) the cDNA replacement sequence. 3' replacement *trans*-splicing has indeed already been used *in vitro* and *in vivo*, in a therapeutic context, for several genetic diseases, such as cystic fibrosis²³⁻²⁵, spinal muscular atrophy²⁶⁻²⁸, hemophilia A²⁹, tauopathies³⁰⁻³¹, *epidermolysis bullosa simplex*³², X-linked immunodeficiency with hyper-IgM³³, severe combined immune deficiency³⁴, *dystrophia myotonica* type 1³⁵, frontotemporal dementia with parkinsonism linked to chromosome 17³⁰, Duchenne muscular dystrophy³⁶, dysferlinopathy³⁷. Recently, *trans*-splicing has also been considered for developing therapeutic strategies for cancer therapies³⁸⁻³⁹, production of therapeutic proteins⁴⁰ and molecular imaging⁴¹.

Among advantages offered by SMaRT technology, there is the preservation in time, space and quantity, of the endogenous regulation of the target mRNA expression, because the PTM is in theory inert in the cell without the presence of its pre-mRNA target. Moreover, the replacement of the mutated sequence allows, in only one reaction, to reduce mutated protein synthesis and to promote the normal one, which is an important point, particularly in case of dominant disease. Because PTM includes only a part of the gene sequence to repair, another main advantage of SMaRT technology is the small size of the restorative molecule compared to all others gene therapy systems. Finally, by targeting the first intron of rhodopsin pre-mRNA, and thus replacing exons 2 through 5, only one PTM should be able to repair around 70-80% of all known RHO mutations.

The present study reports the use of SMaRT technology as a therapeutic tool for mutations of RHO, and shows for the first time a level of efficiency that opens the door to its possible use

in a dominant disease context. Using an *in vitro* cellular assay, we screened fourteen PTM differing only by the target of their binding domain on rhodopsin pre-mRNA intron 1. We quantified the *trans*-splicing rate at the RNA level and showed that the best PTM reached a rate of 25%. Furthermore, we increased the efficiency up to 41% by adding additional intronic sequence into the partial replacement cDNA of the PTM. Finally, after developing HEK293T cells-derived lines expressing mutant RHO stably, we demonstrated that *trans*-splicing repair of rhodopsin mRNA led to synthesis of a correct protein, which is characterized by a relocation of RHO to the plasma membrane of the cells as assessed by imaging flow cytometry.

Results

PTM engineering and screening: influence of binding domain and replacement sequence.

The PTM sequence encodes for (i) a binding domain, complementary of 150 nucleotides of rhodopsin pre-mRNA first intron, (ii) an intronic sequence constituted of all the necessary elements for spliceosome recruitment: a branch point, a polypyrimidine tract and a 3' acceptor splice site, and (iii) the replacement exons 2 to 5 of rhodopsin cDNA, devoid of any mutation (Fig. 1a). All the challenge of this technology is to induce the PTM binding on rhodopsin pre-mRNA, to promote splicing in *trans* instead of *cis*, leading to the repair of any mutation that could be present in exons 2 to 5 (Fig. 1b).

Among the different strategies that can be developed in order to tip the balance in favor of *trans*-splicing, previous studies showed that length and position of the binding domain are essential points to engineer efficient PTM^{33-35,42}. At first, we designed and tested 14 different PTM targeting *RHO* intron 1, differing only in their binding domain, all with a length of 150 b but at different location on the intron. To evaluate *trans*-splicing efficiency we co-transfected HEK-293T (293T) cells with the PTM-expressing constructs and a plasmid encoding the whole rhodopsin gene. We then quantified the *trans*-splicing rate by amplification of rhodopsin mRNA and specific restriction cutting allowing discrimination of the *cis*- and *trans*-spliced transcripts, thanks to a silent mutation introduced by site-directed mutagenesis in the replacement cDNA of the PTM construct (Fig. 2). This methodology was used throughout our study to quantify *trans*-splicing efficiency at the RNA level.

The first three PTM (1-2-3) that we tested targeted respectively the 5'-, the middle-, and the 3'-part of intron 1 (Fig. 3a). Our results provided evidence that the binding sequence is crucial for *trans*-splicing events, showing efficiency ranging from near to zero% (PTM0: negative control devoid of binding domain, PTM2, PTM3) to 25% (PTM1, $p < 0.0001$ assessed by Dunn's multiple comparisons test vs PTM0; Fig. 3b). To increase further *trans*-splicing efficiency, we next engineered new PTM targeting specific sequences of rhodopsin pre-mRNA, surrounding PTM1 target site (PTM4-5-6-7-8-9-10, Fig. 3a) or directed against the 3' acceptor splice site of *RHO* exon 2 (PTM14, Fig. 3a). *Trans*-splicing quantifications showed that PTM1 was still the most efficient PTM, but PTM7 and 8, whose binding domain sequence overlaps with that of PTM1, also showed a significant level of *trans*-splicing ($p < 0.05$ and 0.01 respectively assessed by Dunn's multiple comparisons test vs PTM0; Fig. 3b). This suggests that there is at least one region more favorable for *trans*-splicing on intron 1 of *RHO*.

Next, we wanted to assess that the *trans*-splicing reaction led to the correct mRNA sequence. To that aim, we sequenced the PCR product obtained from mRNA reverse transcription and amplification. This showed that correct sequence of the mRNA was respected at the *trans*-splicing site, i.e. at the junction between exons 1 and 2. In addition, the electrophoregram of the Sanger sequence reaction demonstrated a mixture of *cis*- and *trans*-spliced transcripts at the site where the silent mutation was inserted (Fig. S1).

Another group reported that modifications on PTM cDNA replacement sequence could also greatly influence the efficiency of *trans*-splicing⁴³. We thus tried to improve *trans*-splicing rates obtained with the two most efficient molecules (PTM1 and 8) by adding natural or artificial intronic sequence in this part of the molecule. We reintroduced *RHO* intron 3 at its original place to create PTM19 and 22 respectively, or added an artificial intronic sequence between *RHO* exon 2 and 3 (PTM20 and PTM23) or inside exon 3 (PTM21 and PTM24) (Fig. S2a). *Trans*-splicing quantification showed that efficiency of PTM1 and 8 can actually be modulated positively or negatively, depending on the sequence and the localization of the added intron (endogenous intron 3, significant increase $p < 0.001$, artificial intron between exons 2 and 3, significant increase $p < 0.0001$, artificial intron inside exon 3, significant decrease $p < 0.01$, assessed by Dunnett's multiple comparisons test vs PTM1 and 8 without additional sequence; Fig. 3c and Fig. S2b). These results showed that the cDNA replacement part of the PTM is also determinant for *trans*-splicing efficiency. The most efficient PTM obtained to date was thus the PTM20, which contains an artificial intron between *RHO* exon 2

and 3, with a *trans*-splicing efficiency greater than 40%, as assessed by transient co-transfection of 293T cells with plasmids expressing respectively the *RHO* gene and the PTM. Finally, we wanted to check whether *trans*-splicing was dependent upon PTM expression level. To test this hypothesis, we transfected 293T cells with different ratio of the *RHO* expressing plasmid and the PTM1 expressing plasmid. As expected, this experiment demonstrated that *trans*-splicing rate was correlated to PTM expression level (Fig. 3d).

Development of rhodopsin stable expression cell lines: *trans*-splicing in physiological conditions and quantification at protein level.

To make the first PTM screen easier and faster, experiments reported above have been done in transient co-transfection conditions. However, this methodology might not be fully indicative of the *in vivo* situation. One can for instance speculate that using co-transfection could bring closer the PTM and the *RHO* constructs, thus promoting the *trans*-splice event easier. We thus created cell lines derived from 293T cells and expressing stably wild type (WT) or different mutant alleles of *RHO*. To that aim we took advantage of lentiviral vectors encoding the full gene. This small-size gene (5 Kb including 5' and 3'UTR) is indeed compatible with the packaging capacity of lentiviral vector, which integrates into genome of the host cells leading to stable expression of the transgene.

It is well described that WT *RHO* is localized in plasma membrane in HEK-293S cells or COS-7 cells, while mutated *RHO* can be retained into the cell in different kinds of aggresomes, depending on the mutation⁴⁴⁻⁴⁶.

We generated four different cell lines expressing respectively WT, P23H, R135W or P347L mutated *RHO*. These alleles were selected according to the following criteria. P23H mutation is the most studied and the most representative mutation in North American patients⁴⁷⁻⁴⁹, known to induce retention of the protein into the cell. However, by its location in exon1, it cannot be repaired by our PTM, and we used it as a control for a mutation leading to a strong phenotype. P347L mutation is certainly the second most prevalent mutation worldwide⁴⁷⁻⁴⁸, and the first in european patients⁵⁰. Nevertheless this mutation does not induce *RHO* mislocalization in 293T cells. The third mutation studied, R135W, is also a frequent cause of RP in european patients⁵⁰. It is localized in *RHO* exon2, thus amenable with our 3' replacement strategy and slightly modifies the export of *RHO*, which is described to be both localized to the plasma membrane and into the cell.

Following transduction of 293T cells with RHO-expressing lentiviral vector, we firstly observed that more than 95% of the cells expressed RHO (data not shown). Then, we studied RHO sub-cellular localization using immunocytofluorescence. As expected, WT and P347L RHO were present at the plasma membrane while P23H RHO was retained into the cell. Unexpectedly, R135W RHO was also very clearly retained inside the cell in our hands and we did not observe R135W protein at the plasma membrane (Fig. 4a). Moreover, to plainly establish RHO sub-cellular localization, we performed additional immunocytofluorescence labeling before and after cell permeabilization. This confirmed that P23H and R135W mutations led to retention of the protein in the cytoplasm (Fig. 4b).

To objectively quantify the RHO phenotype, we used a flow imaging technique based on the ImageStream^X set-up, which can measure various cytological parameters on a large population of cells. Digital masks were applied to the cells to discriminate membrane and cytoplasmic RHO and compute an internalization score, determined automatically by the ImageStream^X device (Fig. 5a). Whereas WT and P347L RHO presented an internalization score of 0.41 and 0.34 respectively, those of P23H and R135W RHO were greater than 1, meaning that proteins were mainly intracellular (scores: 2.26 and 2.25 respectively) ($p < 0.0001$ assessed by Dunnett's multiple comparisons test vs WT RHO; Figs. 5 b-c, S3). To quantify the effect of *trans*-splicing on RHO sub-cellular localization in these cell lines, we determined the internalization score in co-transfected cells with the PTM1- or PTM20-expressing plasmid and a Cerulean-expressing plasmid, which allowed selection of transfected cells only. In the WT RHO cell line, the internalization score was unchanged irrespective of the PTM with which the cells were transfected while in the R135W RHO cell line, the internalization score showed a tendency toward reduction after transfection with PTM1, an effect that was even more pronounced with PTM20 (Fig. 5d). Considering that maximal expected variation of internalization score should be obtained between R135W RHO and WT RHO cells, we observed that, compared to PTM0, PTM20 did not change internalization score in WT RHO cells (2.18% decrease), whereas it led to 22.32% decrease in R135W RHO cells ($p < 0.05$ assessed by T-test; Fig. 5e). This demonstrated that *trans*-splicing also occurs when the cells expressed the target pre-mRNA stably. Moreover, it showed that *trans*-splicing of the mRNA is accompanied by a synthesis of repaired protein, which presents a correct localization.

Discussion

In this study, we demonstrated that dominant mutations of *RHO* can be repaired by RNA *trans*-splicing. Using two different cellular models of *RHO* expression we showed that a significant proportion - up to 40 % - of the mRNA can be repaired, leading to an improvement of the phenotype, characterized by sub-cellular localization of *RHO*.

We started by engineering different PTM and screened them by transient co-transfection of 293T cells. A significant advantage of our system is that the size of the *RHO* expression cassette (5375bp from the transcription start site to the end of the 3' untranslated region) allows us to easily produce an expression plasmid with the entire gene. We were thus able to test the PTM efficiency by co-transfection with a construct expressing the full *RHO*, instead of an artificial minigene, as usually used in *trans*-splicing studies. This procedure allows testing the effectiveness of PTM on their real target, i.e. the entire rhodospin pre-mRNA, which helps to ensure that the results obtained from the screen will be replicated *in vivo*, first in the animal model of the pathology, then in patients. The screen of 14 different binding domains showed that this part of the PTM is decisive for *trans*-splicing efficiency. Indeed, localization of the binding domain plays a crucial role and our results revealed a hotspot sequence for *trans*-splicing efficiency in the target intron. This hotspot may be directly linked to the sequence of the binding domain, or to the secondary structure of the PTM, but also to that of the target pre-mRNA that can be more accessible in that location. Interestingly, PTM14 that targets the endogenous 3' acceptor splice site was not efficient, despite results obtained previously by other groups that used an equivalent strategy^{42,51}. In our case, the small size of the overlapping sequence between PTM14 binding domain and exon 2 (only 5 bp) can be at the origin of this result. Nevertheless, even if masking the endogenous 3' acceptor splice site by the PTM binding might favour *trans*-splicing, it should be kept in mind that it could also induce exon skipping by promoting reaction of exon 1 donor splice site with the acceptor splice site of exon 3 or following. The binding domain is not the only parameter that affects PTM efficiency. We indeed showed that it is possible to play on the replacement cDNA by introducing sequences promoting splicing, such as introns. Depending on sequence and localization of this intron, it can promote or reduce the *trans*-splicing efficiency (Fig. S2). Even if splicing mechanism is more and more suspected to occur sequentially from the first to the last intron because of its coupling with transcription⁵², *in vivo* splicing products have already shown that the first intron is not inevitably the first to be removed⁵³. We thus hypothesized that adding a supplementary intron in the PTM sequence

recruits the spliceosome and thus by proximity, favors its binding on the PTM 3' acceptor splice site relative to the endogenous pre-mRNA one. Binding domain localization and supplementary intron are two examples of PTM modifications that can significantly improve *trans*-splicing efficiency, but other strategies could be implemented. One can for example imagine to play on the length of the binding domain, or to introduce intronic splicing enhancer (ISE) just after the binding domain. Facing with this complexity, different systems have been developed to facilitate the screening work^{32,51,54}, but it is still clearly difficult to precisely predict a PTM effect *in vivo*, above all because these screening system have been tested on artificial mini-genes which might not reflect faithfully the physiological context.

Another crucial point for *trans*-splicing efficiency is the ratio between the quantities of PTM and its target pre-mRNA. Intuitively, one might speculate that the higher the proportion of PTM is, the more the *trans*-splicing is favoured. To assess this hypothesis, we transfected 293T cells with different ratios of the PTM-expressing plasmid and the *RHO* construct. This demonstrated that the *trans*-splicing rate is directly correlated with the quantity of PTM. These results confirm those obtained by Puttaraju and colleagues in a different system¹⁵. This has very important implication for the *in vivo* application, especially in the case of rhodopsin that is expressed at very high levels in rod photoreceptors⁵⁵. To expect a therapeutic benefit in animal models, it will thus be mandatory to express high levels of PTM in the target cells. Hopefully, latest vector developments have shown that AAV can transduce rod photoreceptors very efficiently and safely⁵⁶. In combination with a strong tissue specific promoter such as the rhodopsin one, it will most probably allow to reach therapeutic level of expression of the PTM *in vivo*.

Next, we wanted to ensure that *trans*-splicing repair of mutant mRNA led to at least partial restoration of wild-type protein levels in cells based on a phenotypic index. To study RHO sub-cellular localization in a more physiological context than transient transfection, we created cell lines expressing the protein stably, thanks to integrating properties of lentiviral vectors. Transduced 293T cells proved to be a functional system, with almost all of the cells expressing RHO. Even if the localization phenotype observed in 293T cells was different from that described in rods photoreceptors⁵⁷, this can be explained by the differential structure between these two cell types. Rods present indeed a very particular structure in which RHO is contained: phospholipid bilayers arranged in stacks of discs in the outer segment that have no equivalent in 293T cells. Nonetheless, the ImageStream^X set-up allowed us to quantify this phenotype and to show that the R135W RHO cell line can be partially rescued by *trans*-

splicing. Two important points have been highlighted by the results: (i) the proof that *trans*-splicing is efficient and quantifiable in conditions close to physiological ones, where PTM has to enter into the nucleus, be transcribed, bind and react with the endogenous pre-mRNA before its prospective *cis*-splicing, (ii) the demonstration of a *trans*-splicing repair at the protein level, leading to its re-localization in a physiological way.

Our results bring the proof, for the first time, that *trans*-splicing can reach a significant enough rate to expect a therapeutic benefit in the context of a dominant disease. Indeed, considering the fact that patients suffering from dominant diseases are in most cases heterozygous, converting 40% of mutated mRNA back to normal will get the ration of mutant against normal protein to almost 1/4 vs 3/4. This ratio could even lean more in favor of the normal protein if it appears that the mutant is less stable. In conclusion, this work highlights that SMaRT can be a powerful tool, not only for recessive disease cases, but also for dominant ones, and shows that a lot of different tricks can be applied to increase *trans*-splicing rate. Future evaluation will focus on *in vivo* evaluation using AAV vectors and humanized mouse models expressing a mutant allele of the complete human *RHO*.

Material and methods

Plasmid construction

Plasmids' backbone used for *RHO* expression contained a self-inactivating lentiviral genome and were previously described⁵⁸. Human Wild Type (WT) *RHO* was amplified from HEK-293T cells genomic DNA using the following primers: 5'-CACCAGAGTCATCCAGCTGGAGCC-3' and 5'-GTCCTAGGCAGGTCTTAGGC-3'. The PCR product was subsequently sub-cloned in pENTR/D-TOPO plasmid according to the manufacturer's instructions (Life Technologies, Saint-Aubin, France), and sequence of the whole insert was verified. P23H, R135W and P347L mutations were inserted by site-directed mutagenesis (QuickChange kit, Agilent). Wild-type or mutant alleles of the human *RHO* were then introduced in the lentiviral shuttle plasmid by Gateway recombination (Life Technologies, Saint-Aubin, France) under the transcriptional control of the short form of the ubiquitous promoter elongation factor 1 alpha (EF1alpha) promoter. The transgene expression cassette was inserted in reverse orientation of the lentiviral genome to avoid rhodopsin intron splicing during vector production.

PTM were cloned into a shuttle plasmid for self-complementary AAV vector production that was previously described⁵⁹. PTM expression was under the control of the ubiquitous cytomegalovirus (CMV) immediate early promoter, and terminated by the BGH (Bovine Growth Hormone) poly-adenylation signal. 14 different binding sequences targeting rhodopsin intron 1 were synthesized by Eurofins MWG Operon (Les Ulis, France) and cloned into the AAV-PTM expression plasmid using HindIII/SacII restriction sites. The final PTM (PTM 1 to 14) were composed of a binding sequence, followed by an artificial intronic sequence and the rhodopsin partial cDNA. The rhodopsin partial cDNA of PTM1 and PTM8 were modified by addition of the endogenous rhodopsin intron 3 (PTM19, 22) or another artificial intronic sequence, inserted at nucleic acid position 172 (PTM20, 23) or 296 (PTM21, 24) after the beginning of exon 2. The artificial intronic sequence³⁶ was composed of several elements important for splicing: a branch point, a poly-pyrimidine tract and a 3' acceptor splice site.

Cell culture and transfection

Human Embryonic Kidney cells (HEK-293T) were grown in Dulbecco's modified Eagle's medium (Gibco, Life Technologies, Saint-Aubin, France) supplemented with 10% heat-inactivated fetal bovine serum (Gibco, Life Technologies, Saint-Aubin, France), 100 U/mL penicillin and 100µg/mL streptomycin (Gibco, Life Technologies, Saint-Aubin, France). HEK-293T cells were incubated at 37°C with 5% CO₂. For transfection, HEK-293T cells were plated in 6-well plate at a density of 500,000 cells/well, transfected by 2.5µg plasmid DNA using the CaCl₂ precipitate method the following day, and analysed 48 hours after transfection.

Virus production and cell transduction

Recombinant lentiviral particles were produced by transient transfection of HEK-293T cells as previously described⁵⁸. Viral supernatants were concentrated by ultracentrifugation at 70,000 g for 90 min at 4 °C. Finally, viral pellets were resuspended in a minimal volume of PBS to achieve a 1,000-fold concentration of the initial supernatant. Aliquots of 5–10 µl were then stored at –80 °C until further use. Total particle concentration of the viral stocks was estimated by quantification of the p24 capsid protein using RETRO-TEK HIV-1 p24 Antigen ELISA kit (ZeptoMetrix, Buffalo, New York, United States) according to the manufacturer's instructions. HEK-293T cells were transduced with a quantity of lentivirus corresponding to 2 pg of p24 protein per cell.

Quantification of *trans*-splicing rate at RNA level

A silent point mutation was introduced by site-directed mutagenesis (QuickChange kit, Agilent) in the partial rhodopsin cDNA of the PTM. This mutation was designed to change a BglII restriction site into NheI. For *trans*-splicing quantification, HEK-293T cells were lysed, mRNA were collected (Nucleospin RNA II extraction kit, Macherey-Nagel, Düren, Germany) and reverse-transcribed into cDNA (superscript II and OligodT, Life Technologies) before amplification of rhodopsin cDNA by end-point PCR. Primers used were: 5'-GCACGCCTCTCAACTAC-3' and 5'-TCTTGCCGCAGCAGATG-3'. PCR product was separated into two equal batches for restriction cutting using respectively BglII and NheI. Partial digestion was then quantified on a Bioanalyzer (2100 Bioanalyzer, Agilent Technologies, Les Ulis, France).

Immunocytochemistry

Single labelling protocol: Cells were plated in twenty-four-well plates on a glass coverslip and fixed in PFA 4% for 10 minutes twenty-four hours later. Cells were permeabilized 15 minutes in PBS-1% NGS-0.2% triton before 1 hour incubation with rhodopsin primary antibody (Rho4D2 antibody MABN15, Merck-Millipore, 1/500 dilution in PBS-1% NGS) and then 45 minutes with Alexa-488 secondary antibody (Alexa Fluor A11001, Life Technologies, 1/1,000 dilution in PBS-1% NGS) followed by a 5 minutes incubation in PBS-dapi (1/5,000 dilution).

Double labelling protocol (before and after permeabilization): Cells were plated in twenty-four-well plates on a glass coverslip and fixed in PFA 2% for 10 minutes twenty-four hours later. Coverslips were incubated for 1 hour with rhodopsin primary antibody (Rho4D2 antibody MABN15, Merck-Millipore, 1/500 dilution in PBS-1% NGS) and then for 45 minutes with Alexa-594 secondary antibody (Alexa Fluor A11005, Life Technologies, 1/1,000 dilution in PBS-1% NGS). Cells were thus fixed again in PFA 2% 10 minutes, then permeabilized 15 minutes in PBS-1% NGS-0.2% triton. Coverslips were once again incubated 1 hour with rhodopsin primary antibody, followed by an 45 minutes with Alexa-488 secondary antibody (Alexa Fluor A11001, Life Technologies, 1/1,000 dilution in PBS-1% NGS), before a 5 minutes incubation in PBS-dapi (1/5,000 dilution).

After mounting on a glass slide, cells were observed on an Olympus FV1000 laser-scanning confocal microscope.

ImageStream X imaging

HEK-293T cells were transfected as described above. A reporter plasmid expressing a cyan fluorescent protein⁶⁰ was used to label transfected cells. Cells were then pelleted and fixed for 10 minutes in 4% PFA, followed by 15 minutes permeabilization in PBS-1% NGS-0.05% triton. After labelling with rhodopsin primary antibody (Rho4D2 antibody MABN15, 1/500 dilution, Merck-Millipore) and Alexa-647 secondary antibody (Alexa Fluor A31571, 1/1,000, Life Technologies), cells were analysed on an ImageStream^X technology (AMNIS). Parameters used were: Cerulean detection: excitation by 488 laser (100mW), emission in Channel 02; Alexa-647 detection: excitation by 658 laser (120mW), emission in Channel 11; Magnification: x40; Core diameter: 8 µm; No compensation was necessary.

The minimal number of events that was considered to be statistically representative was 500 cells. All experiments were done with at least 500 cells.

Statistics

GraphPad Prism 6 (GraphPad Software, San Diego, USA) was used for data analysis and graphic representation. All values are reported as medians. Details of statistical analysis are given in each figures' legend.

Acknowledgements

The authors wish to thank Nicole Boggetto and Luisa Riancho for their precious advices and technical accompaniment on the use of the ImageStream^X flow cytometer in ImagoSeine Institut Jacques Monod platform (Université Paris 7) and the flow cytometer of the Institut de la Vision (Université Paris 6) respectively. The authors also sincerely thank Dr Christina Zeitz for her help on Rhodopsin labeling.

This work was supported by grant from Association Française contre les Myopathies (AFM grant 14814) and performed in the frame of the LABEX LIFESENSES [reference ANR-10-LABX-65] supported by French state funds managed by the ANR. Adeline Berger is a recipient of a PhD fellowship from Association Française contre les Myopathies.

Figures

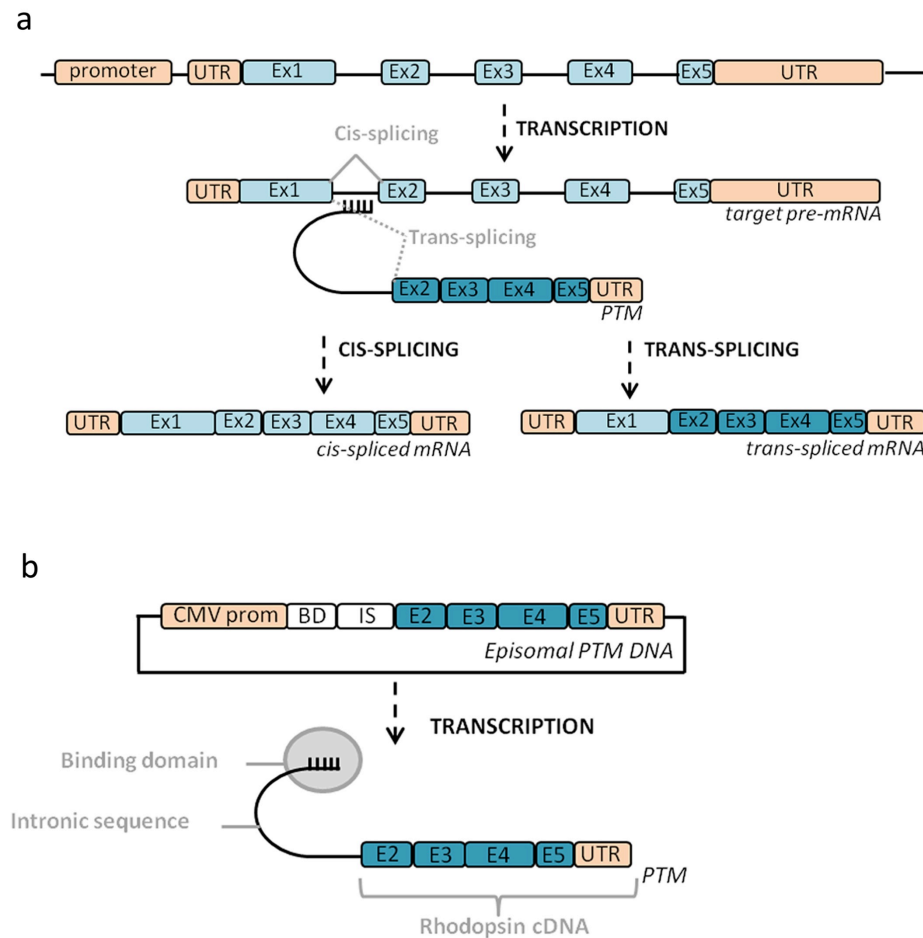


Figure 1: Schemes of a Pre-Trans-splicing Molecule construct and *trans*-splicing mechanism.

(a) After transcription of the rhodopsin gene, the PTM binding domain recognized a sequence of the rhodopsin pre-mRNA first intron, which allowed promoting a splicing *in trans* instead of *cis*, leading to the production of a chimeric mRNA devoid of any mutation in exons 2 to 5. * represents a potential mutation. (b) PTM expression plasmid, in which the coding sequence of the PTM is under the control of a cytomegalovirus promoter (CMV prom), and composed from 5' to 3' of a binding domain (BD), an intronic sequence (IS), the rhodopsin replacement cDNA (ex2 to 5) and the Untranslated Terminal Region (UTR) of the bovine growth hormone gene containing the polyadenylation signal.

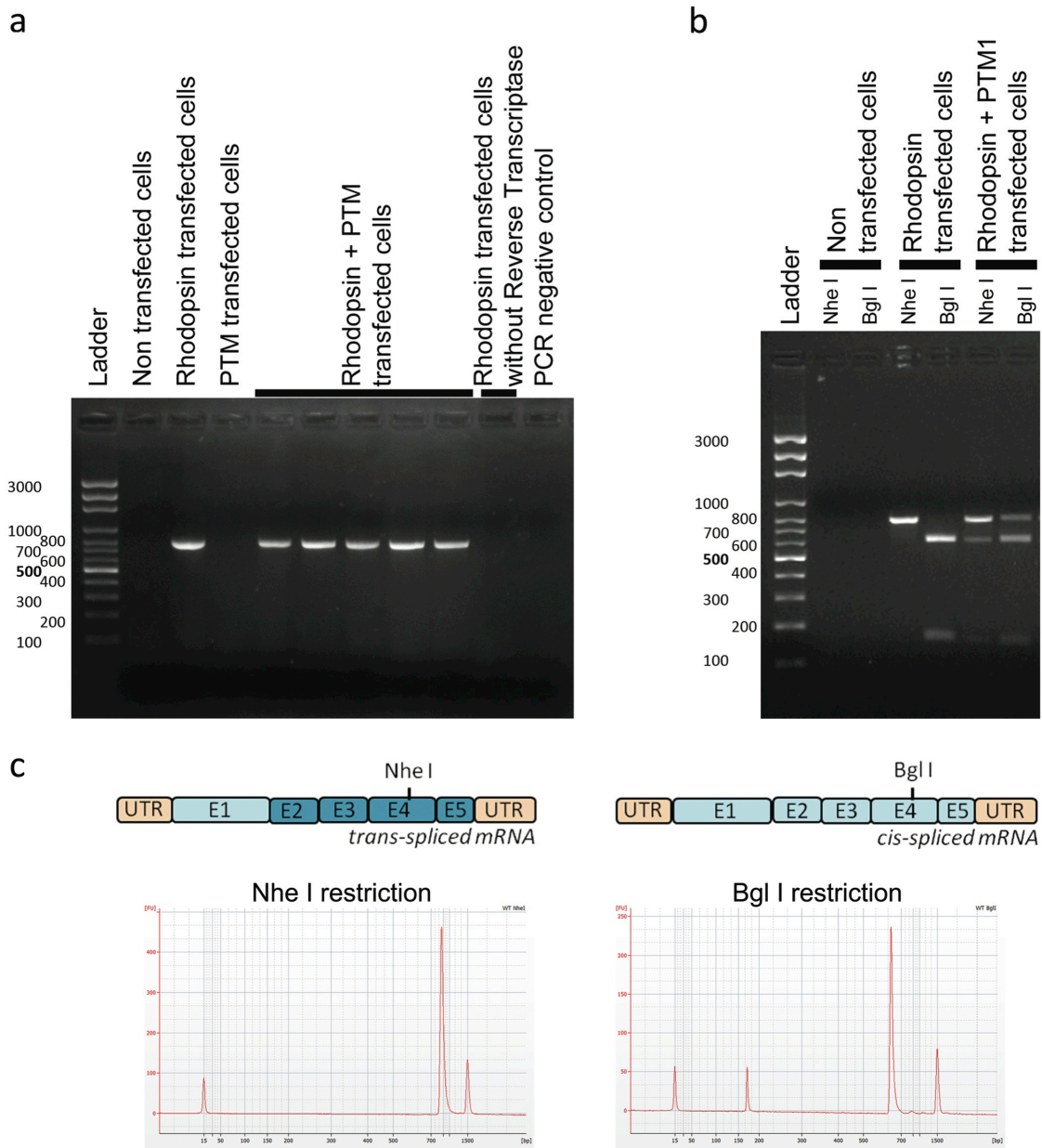


Figure 2: Method for precise quantification of *trans*-splicing rate using end-point PCR.

(a) PCR amplification of cDNA obtained from *cis* and *trans*-spliced rhodopsin mRNA, loaded on a 2% agarose gel. Expected size: 771bp. (b) Restriction cutting of PCR products, by respectively NheI and BglI, loaded on a 2% agarose gel. Expected sizes of restriction fragments: 165bp + 606bp. (c) Schematic representation of *trans*-spliced and *cis*-spliced mature mRNA, with localization of Bgl I and Nhe I restriction sites. Electropherograms of digested products after migration on capillary electrophoresis (corresponding to wells 4 and 5 of panel b). Each peak represents a DNA product, whose quantity is accurately determined by calculating peak area. The two most extreme peaks of each electropherogram are internal controls and are not included in calculation of the peak area.

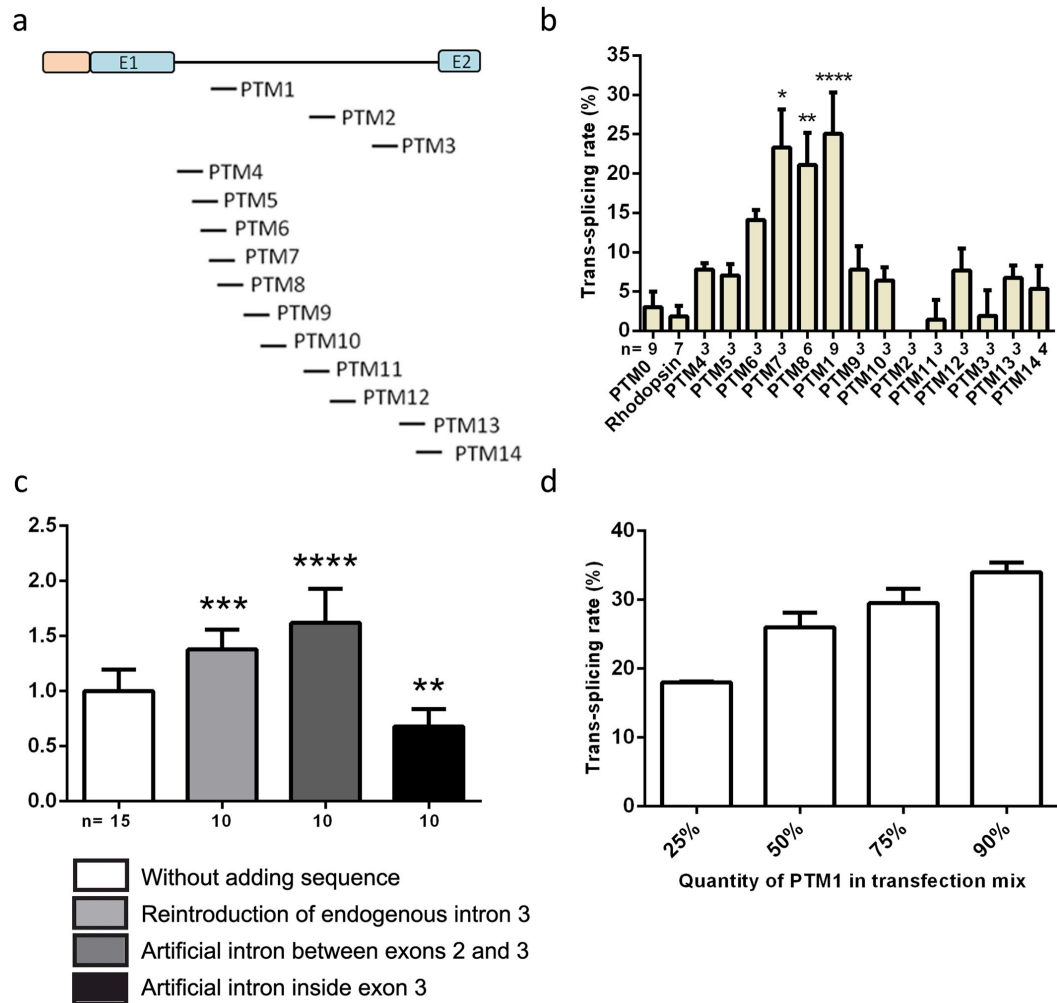


Figure 3: Effect of binding domain and intronic sequence on *trans*-splicing efficiency.

(a) Schematic representation of binding domains localization on intron 1. Each binding domain is represented by a dash indicating its location following a vertical line on the intron diagrammed above. (b) *Trans*-splicing rate of PTM0 to 14. PTM0 that is devoid of binding domain served as a negative control. Each experiment was performed with a minimum of three culture wells and replicated several times. The number of replicates is indicated under the x-axis for each PTM. Statistical analysis was performed by comparison of PTM0 versus all other groups using Dunn's test. (c) Effect of intron addition inside the replacement cDNA sequence. *Trans*-splicing rates were calculated after modification of PTM1 and 8 with each intronic sequence (see Fig. S2). Efficiency of each intron addition was normalized against *trans*-splicing rate obtained for PTM1 and 8 before addition of the intronic sequence. Statistical analysis was performed by comparison of PTM1 and 8 versus all other groups using Dunnett's test. (d) Variations of PTM1 *trans*-splicing rate as a function of its quantity in transfection mix. The cells were transfected with the same amount of total DNA. The proportion of PTM-expressing plasmid with regards to total DNA amount is indicated under the x-axis.

In all these experiments, *trans*-splicing rates were determined at RNA level after transient co-transfection of PTM and *RHO* constructs in HEK-293T cells. All values are presented as medians +/- SD.

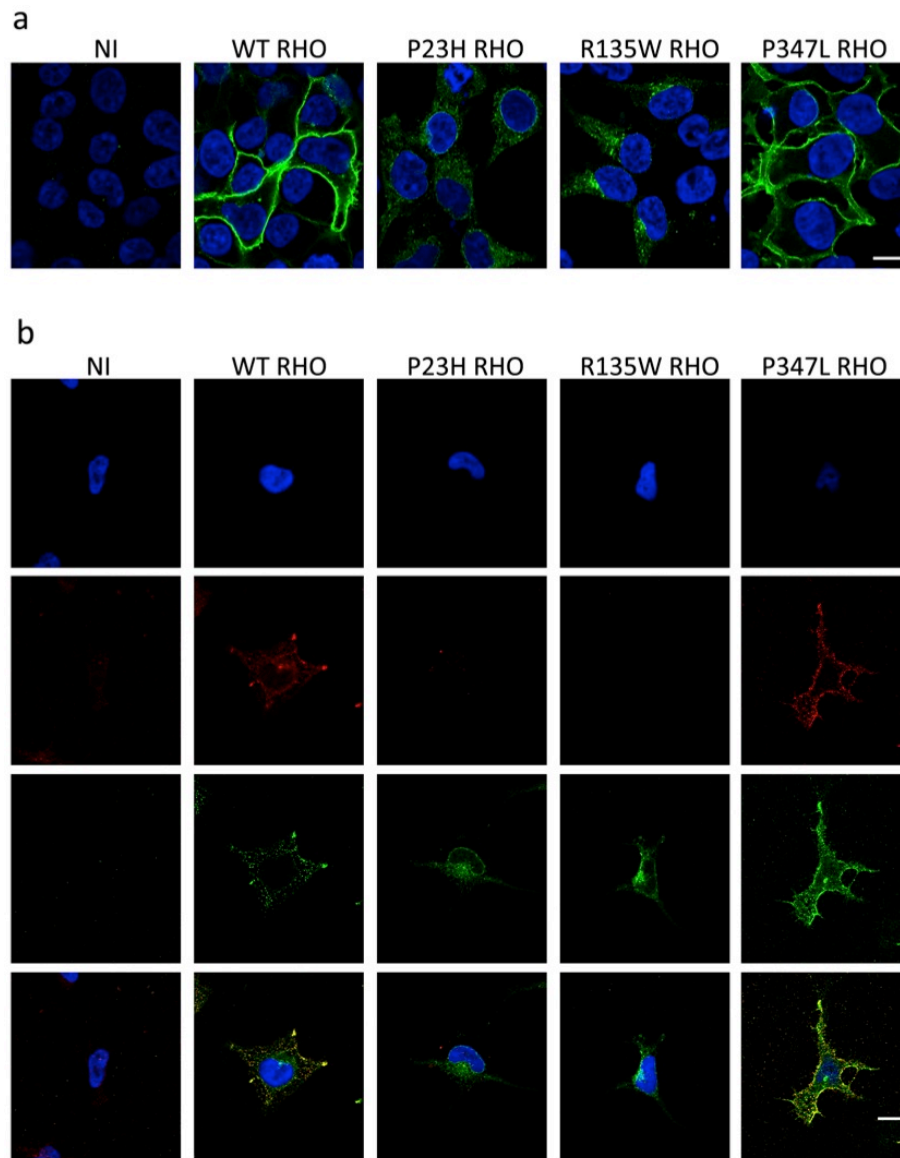


Figure 4: Cellular localization of WT, P23H, R135W or P347L human RHO stably expressed in HEK-293T cells.

HEK-293T cells were transduced with lentiviral vectors to create cell lines expressing stably normal or mutated RHO. (a) Confocal microscope slices of confluent HEK-293T cells following immunofluorescence labelling of rhodopsin (AF488, green) and staining of the nucleus (DAPI; blue). In non-transduced cells (NT) no RHO is detected. In cell lines expressing WT or P347L RHO, the staining is localized at the periphery of the cells and the cytoplasm appears almost devoid of staining. On the contrary, with P23H and R135W mutation, the staining is concentrated in the perinuclear space. (b) Immunolabelling of a representative transduced cell for each cell lines, before and after permeabilization. 1st line: DAPI staining; 2nd line: rhodopsin staining before permeabilization; 3rd line: rhodopsin staining after permeabilization; 4th line: merged views. Scale bar: 10µm.

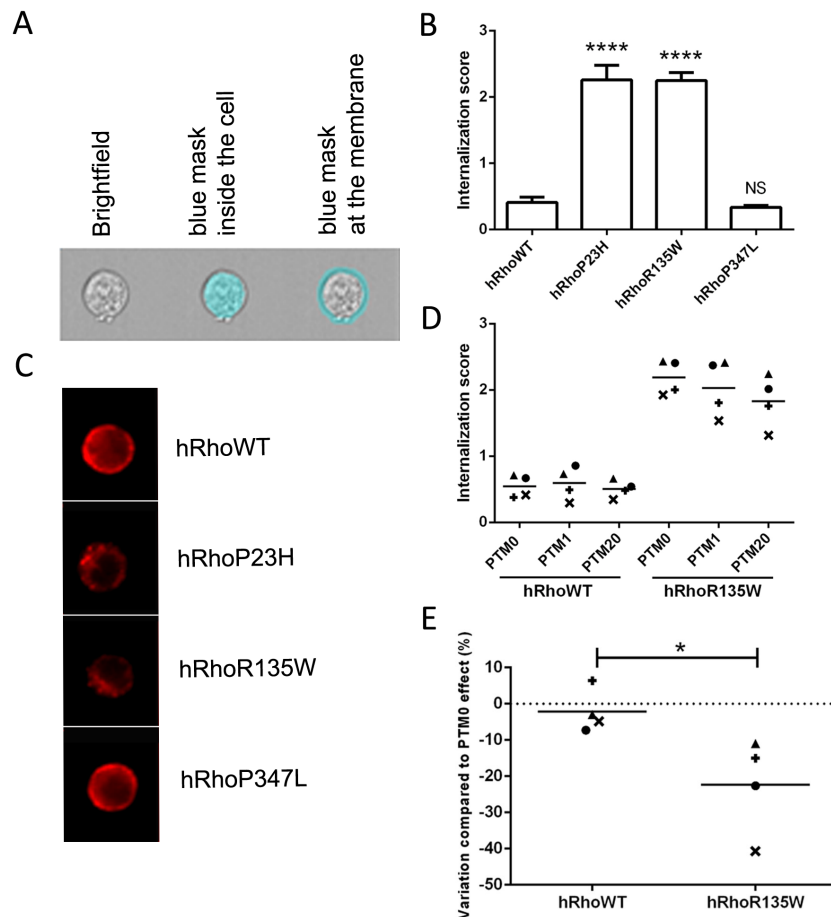


Figure 5: Quantification of RHO localization by ImageStream technology before and after *trans-splicing*.

(a) Representative example of a bright-field image of a cell acquired with the ImageStream^x (left). This image is used to automatically define masks corresponding to the cell cytoplasm (middle) and to the plasma membrane (right). (b) RHO internalization score calculated in each cell line in function of fluorescence quantified in the two masks. An internalization score above 1 means that fluorescence is mainly present inside the cell. Data were collected from 3 independent experiments in which at least 500 cells were analyzed (statistically representative). Statistical analysis was performed by comparison of WT RHO internalization score versus all other groups using Dunnett's test. (c) Representative rhodopsin immunofluorescence staining of the 4 cell lines visualized on the ImageStream^x. (d) WT and R135W RHO cell lines were co-transfected with a PTM construct and a plasmid expressing the cerulean fluorescent plasmid (CFP). Internalization scores were determined after selection of transfected cells using CFP fluorescence. Data were collected from 4 independent experiments (represented by the 4 different symbols) and each point corresponds to observation of at least 500 cells (statistically representative). (e) Effect of PTM20 in WT RHO and R135W RHO cell lines, expressed in percentage of maximal variation obtained with PTM0 in these same cell lines. Statistical analysis was performed by T-test comparison of the two groups.

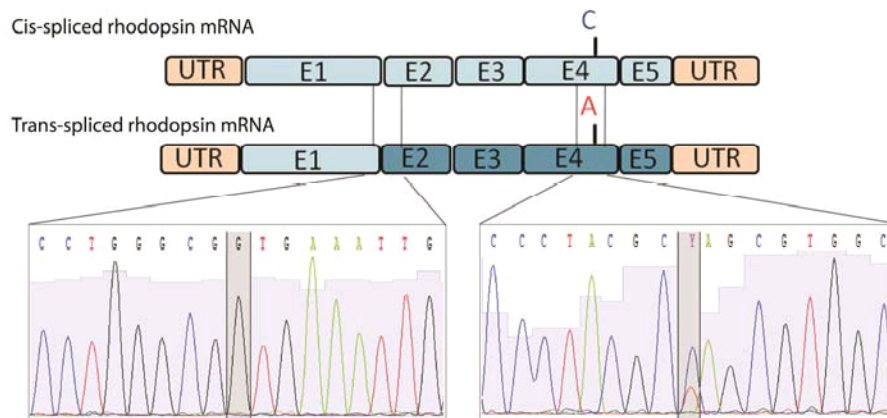


Figure S1: Validation of conformity of the rhodopsin mRNA obtained from cis and trans-spliced.

HEK-293T cells were co-transfected with the RHO construct and the plasmid expressing PTM1. 48 hours after transfection, mature mRNA were extracted and reverse transcribed, then RHO cDNA was PCR amplified and sequenced by Sanger technique using a forward PCR primer located in exon 1 of RHO. The left electrophoregram shows that both cis and trans-spliced mRNA generated the correct transition between RHO exon 1 and 2. The G highlighted by the shaded box is the first nucleic acid of exon 2. Right electrophoregram: the mutation from C to T modifies the Bgl I restriction site (GCCNNNNNCCG) into a Nhe I restriction site (GCTAGC) that we used to quantify trans-splicing rate by restriction analysis of the PCR product. The grey box shows the presence of two peaks at this position, demonstrating that both molecular species were present in the mRNA pool.

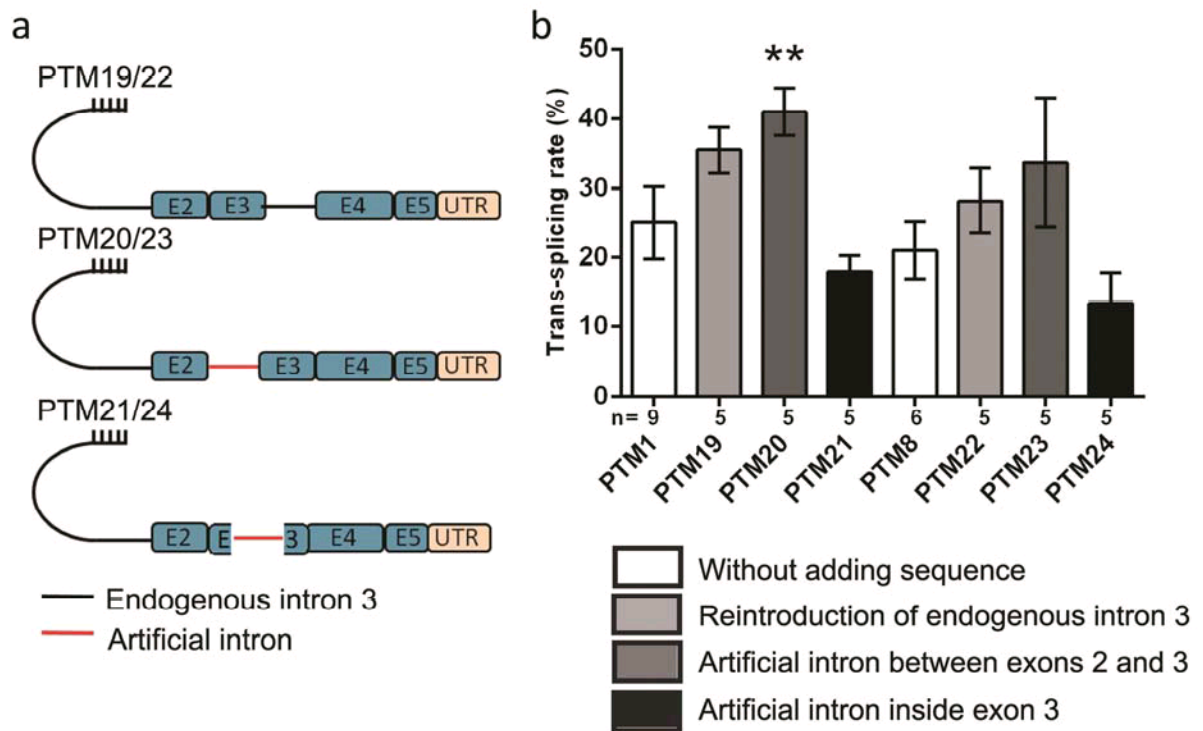


Figure S2: Effect of the addition of an intronic sequence into the replacement cDNA of the PTM.

(a) Schematization of the modification introduced in the replacement cDNA of PTM1 and 8 to generate respectively PTM19 to 21 and PTM22 to 24. (b) Trans-splicing rates obtained after modification of the replacement cDNA of PTM1 (PTM19 to 21) and 8 (PTM22 to 24). Trans-splicing rates were quantified at RNA level, after transient co-transfection in HEK-293T cells. Statistical analysis was performed by comparison of PTM1 versus PTM19, 20 and 21 or PTM8 versus PTM22, 23 and 24 using Dunn's test.

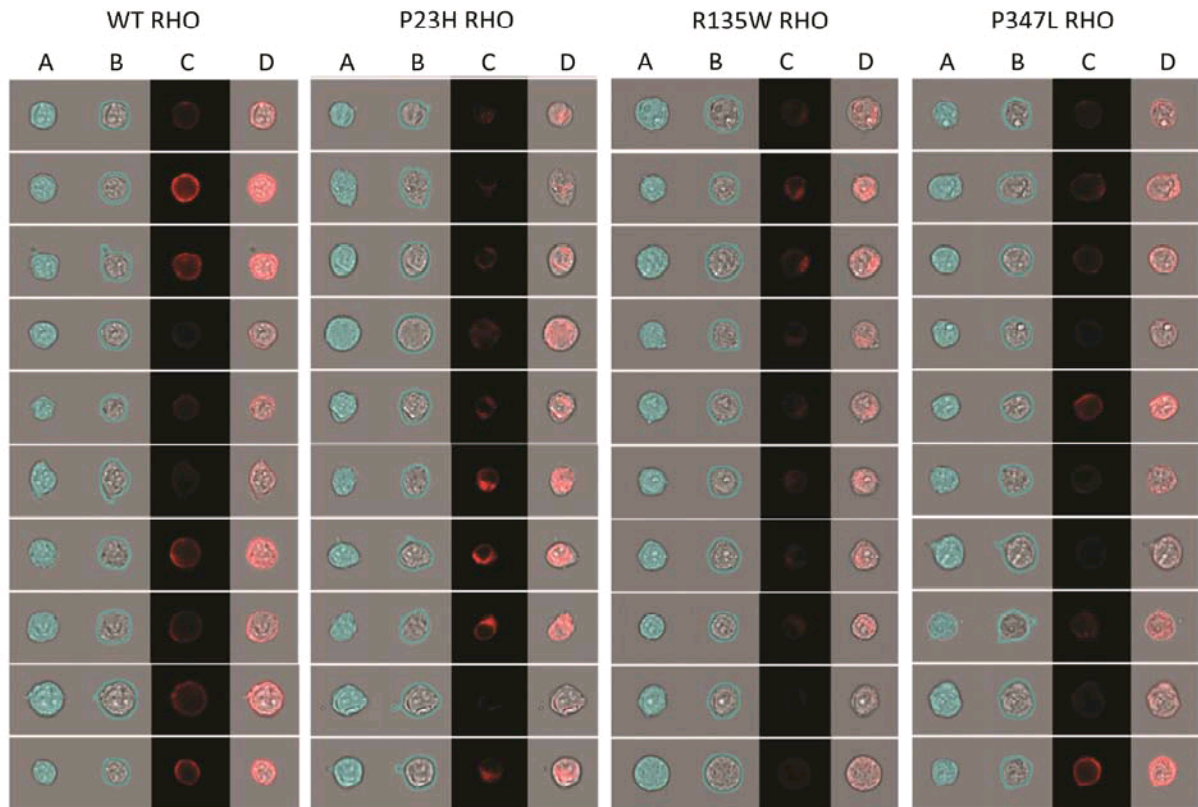


Figure S3: Visualization of RHO cell lines phenotype by imaging flow cytometry.

Representative examples of 10 cells analyzed by imaging flow cytometry with the ImageStreamX for the 4 different cell lines. For each cell line, the cytoplasmic digital mask (blue) overlay on the bright-field view (A), the plasma membrane digital mask (blue) overlay on the bright-field view (B), the rhodospin immunofluorescence labelling (red, C), and the merged view of bright-field and red channel (D), are shown.

References

- 1 Birch, D. G., Anderson, J. L. & Fish, G. E. Yearly rates of rod and cone functional loss in retinitis pigmentosa and cone-rod dystrophy. *Ophthalmology* **106**, 258-268, (1999).
- 2 Hartong, D. T., Berson, E. L. & Dryja, T. P. Retinitis pigmentosa. *Lancet* **368**, 1795-1809, (2006).
- 3 Wilson, J. H. & Wensel, T. G. The nature of dominant mutations of rhodopsin and implications for gene therapy. *Mol Neurobiol* **28**, 149-158, (2003).
- 4 Gorbatyuk, M., Justilien, V., Liu, J., Hauswirth, W. W. & Lewin, A. S. Suppression of mouse rhodopsin expression in vivo by AAV mediated siRNA delivery. *Vision Res* **47**, 1202-1208, (2007).
- 5 O'Reilly, M., Palfi, A., Chadderton, N., Millington-Ward, S., Ader, M., Cronin, T. *et al.* RNA interference-mediated suppression and replacement of human rhodopsin in vivo. *Am J Hum Genet* **81**, 127-135, (2007).
- 6 Mao, H., Gorbatyuk, M. S., Rossmiller, B., Hauswirth, W. W. & Lewin, A. S. Long-term rescue of retinal structure and function by rhodopsin RNA replacement with a single adeno-associated viral vector in P23H RHO transgenic mice. *Hum Gene Ther* **23**, 356-366, (2012).
- 7 Martin, J. N., Wolken, N., Brown, T., Dauer, W. T., Ehrlich, M. E. & Gonzalez-Alegre, P. Lethal toxicity caused by expression of shRNA in the mouse striatum: implications for therapeutic design. *Gene Ther* **18**, 666-673, (2011).
- 8 Li, Y., Tao, W., Luo, L., Huang, D., Kauper, K., Stabila, P. *et al.* CNTF induces regeneration of cone outer segments in a rat model of retinal degeneration. *PLoS One* **5**, e9495, (2010).
- 9 Liang, F. Q., Aleman, T. S., Dejneka, N. S., Dudus, L., Fisher, K. J., Maguire, A. M. *et al.* Long-term protection of retinal structure but not function using RAAV.CNTF in animal models of retinitis pigmentosa. *Mol Ther* **4**, 461-472, (2001).
- 10 McGee Sanftner, L. H., Abel, H., Hauswirth, W. W. & Flannery, J. G. Glial cell line derived neurotrophic factor delays photoreceptor degeneration in a transgenic rat model of retinitis pigmentosa. *Mol Ther* **4**, 622-629, (2001).

- 11 Rodger, J., Drummond, E. S., Hellstrom, M., Robertson, D. & Harvey, A. R. Long-term gene therapy causes transgene-specific changes in the morphology of regenerating retinal ganglion cells. *PloS one* **7**, e31061, (2012).
- 12 Touchard, E., Heiduschka, P., Berdugo, M., Kowalczyk, L., Bigey, P., Chahory, S. *et al.* Non-viral gene therapy for GDNF production in RCS rat: the crucial role of the plasmid dose. *Gene Ther* **19**, 886-898, (2012).
- 13 Lem, J., Krasnoperova, N. V., Calvert, P. D., Kosaras, B., Cameron, D. A., Nicolo, M. *et al.* Morphological, physiological, and biochemical changes in rhodopsin knockout mice. *Proc Natl Acad Sci U S A* **96**, 736-741, (1999).
- 14 Tan, E., Wang, Q., Quiambao, A. B., Xu, X., Qtaishat, N. M., Peachey, N. S. *et al.* The relationship between opsin overexpression and photoreceptor degeneration. *Invest Ophthalmol Vis Sci* **42**, 589-600, (2001).
- 15 Puttaraju, M., Jamison, S. F., Mansfield, S. G., Garcia-Blanco, M. A. & Mitchell, L. G. Spliceosome-mediated RNA trans-splicing as a tool for gene therapy. *Nat Biotechnol* **17**, 246-252, (1999).
- 16 Murphy, W. J., Watkins, K. P. & Agabian, N. Identification of a novel Y branch structure as an intermediate in trypanosome mRNA processing: evidence for trans splicing. *Cell* **47**, 517-525, (1986).
- 17 Sutton, R. E. & Boothroyd, J. C. Evidence for trans splicing in trypanosomes. *Cell* **47**, 527-535, (1986).
- 18 Caudevilla, C., Serra, D., Miliar, A., Codony, C., Asins, G., Bach, M. *et al.* Natural trans-splicing in carnitine octanoyltransferase pre-mRNAs in rat liver. *Proc Natl Acad Sci U S A* **95**, 12185-12190, (1998).
- 19 Finta, C. & Zaphiropoulos, P. G. Intergenic mRNA molecules resulting from trans-splicing. *J Biol Chem* **277**, 5882-5890, (2002).
- 20 Flouriot, G., Brand, H., Seraphin, B. & Gannon, F. Natural trans-spliced mRNAs are generated from the human estrogen receptor-alpha (hER alpha) gene. *J Biol Chem* **277**, 26244-26251, (2002).

- 21 Romani, A., Guerra, E., Trerotola, M. & Alberti, S. Detection and analysis of spliced chimeric mRNAs in sequence databanks. *Nucleic Acids Res* **31**, e17, (2003).
- 22 Wu, C. S., Yu, C. Y., Chuang, C. Y., Hsiao, M., Kao, C. F., Kuo, H. C. *et al.* Integrative transcriptome sequencing identifies trans-splicing events with important roles in human embryonic stem cell pluripotency. *Genome Res* **24**, 25-36, (2014).
- 23 Mansfield, S. G., Kole, J., Puttaraju, M., Yang, C. C., Garcia-Blanco, M. A., Cohn, J. A. *et al.* Repair of CFTR mRNA by spliceosome-mediated RNA trans-splicing. *Gene Ther* **7**, 1885-1895, (2000).
- 24 Liu, X., Jiang, Q., Mansfield, S. G., Puttaraju, M., Zhang, Y., Zhou, W. *et al.* Partial correction of endogenous DeltaF508 CFTR in human cystic fibrosis airway epithelia by spliceosome-mediated RNA trans-splicing. *Nat Biotechnol* **20**, 47-52, (2002).
- 25 Liu, X., Luo, M., Zhang, L. N., Yan, Z., Zak, R., Ding, W. *et al.* Spliceosome-mediated RNA trans-splicing with recombinant adeno-associated virus partially restores cystic fibrosis transmembrane conductance regulator function to polarized human cystic fibrosis airway epithelial cells. *Hum Gene Ther* **16**, 1116-1123, (2005).
- 26 Coady, T. H., Baughan, T. D., Shababi, M., Passini, M. A. & Lorson, C. L. Development of a single vector system that enhances trans-splicing of SMN2 transcripts. *PLoS One* **3**, e3468, (2008).
- 27 Coady, T. H., Shababi, M., Tullis, G. E. & Lorson, C. L. Restoration of SMN function: delivery of a trans-splicing RNA re-directs SMN2 pre-mRNA splicing. *Mol Ther* **15**, 1471-1478, (2007).
- 28 Coady, T. H. & Lorson, C. L. Trans-splicing-mediated improvement in a severe mouse model of spinal muscular atrophy. *J Neurosci* **30**, 126-130, (2010).
- 29 Chao, H., Mansfield, S. G., Bartel, R. C., Hiriyanna, S., Mitchell, L. G., Garcia-Blanco, M. A. *et al.* Phenotype correction of hemophilia A mice by spliceosome-mediated RNA trans-splicing. *Nat Med* **9**, 1015-1019, (2003).
- 30 Rodriguez-Martin, T., Anthony, K., Garcia-Blanco, M. A., Mansfield, S. G., Anderton, B. H. & Gallo, J. M. Correction of tau mis-splicing caused by FTDP-17 MAPT

mutations by spliceosome-mediated RNA trans-splicing. *Hum Mol Genet* **18**, 3266-3273, (2009).

31 Rodriguez-Martin, T., Garcia-Blanco, M. A., Mansfield, S. G., Grover, A. C., Hutton, M., Yu, Q. *et al.* Reprogramming of tau alternative splicing by spliceosome-mediated RNA trans-splicing: implications for tauopathies. *Proc Natl Acad Sci U S A* **102**, 15659-15664, (2005).

32 Wally, V., Brunner, M., Lettner, T., Wagner, M., Koller, U., Trost, A. *et al.* K14 mRNA reprogramming for dominant epidermolysis bullosa simplex. *Hum Mol Genet* **19**, 4715-4725, (2010).

33 Tahara, M., Pergolizzi, R. G., Kobayashi, H., Krause, A., Luetlich, K., Lesser, M. L. *et al.* Trans-splicing repair of CD40 ligand deficiency results in naturally regulated correction of a mouse model of hyper-IgM X-linked immunodeficiency. *Nat Med* **10**, 835-841, (2004).

34 Zayed, H., Xia, L., Yerich, A., Yant, S. R., Kay, M. A., Puttaraju, M. *et al.* Correction of DNA protein kinase deficiency by spliceosome-mediated RNA trans-splicing and sleeping beauty transposon delivery. *Mol Ther* **15**, 1273-1279, (2007).

35 Chen, H. Y., Kathirvel, P., Yee, W. C. & Lai, P. S. Correction of dystrophin myotonia type 1 pre-mRNA transcripts by artificial trans-splicing. *Gene Ther* **16**, 211-217, (2009).

36 Lorain, S., Peccate, C., Le Hir, M., Griffith, G., Philippi, S., Precigout, G. *et al.* Dystrophin rescue by trans-splicing: a strategy for DMD genotypes not eligible for exon skipping approaches. *Nucleic Acids Res* **41**, 8391-8402, (2013).

37 Monjaret, F., Bourg, N., Suel, L., Roudaut, C., Le Roy, F., Richard, I. *et al.* Cis-splicing and Translation of the Pre-Trans-splicing Molecule Combine With Efficiency in Spliceosome-mediated RNA Trans-splicing. *Mol Ther* **22**, 1176-1187, (2014).

38 Gruber, C., Koller, U., Murauer, E. M., Hainzl, S., Huttner, C., Kocher, T. *et al.* The design and optimization of RNA trans-splicing molecules for skin cancer therapy. *Mol Oncol* **7**, 1056-1068, (2013).

- 39 Nakayama, K., Pergolizzi, R. G. & Crystal, R. G. Gene transfer-mediated pre-mRNA segmental trans-splicing as a strategy to deliver intracellular toxins for cancer therapy. *Cancer Res* **65**, 254-263, (2005).
- 40 Wang, J., Mansfield, S. G., Cote, C. A., Jiang, P. D., Weng, K., Amar, M. J. *et al.* Trans-splicing into highly abundant albumin transcripts for production of therapeutic proteins in vivo. *Mol Ther* **17**, 343-351, (2009).
- 41 Wally, V., Murauer, E. M. & Bauer, J. W. Spliceosome-mediated trans-splicing: the therapeutic cut and paste. *J Invest Dermatol* **132**, 1959-1966, (2012).
- 42 Puttaraju, M., DiPasquale, J., Baker, C. C., Mitchell, L. G. & Garcia-Blanco, M. A. Messenger RNA repair and restoration of protein function by spliceosome-mediated RNA trans-splicing. *Mol Ther* **4**, 105-114, (2001).
- 43 Mansfield, S. G., Clark, R. H., Puttaraju, M., Kole, J., Cohn, J. A., Mitchell, L. G. *et al.* 5' exon replacement and repair by spliceosome-mediated RNA trans-splicing. *RNA* **9**, 1290-1297, (2003).
- 44 Saliba, R. S., Munro, P. M., Luthert, P. J. & Cheetham, M. E. The cellular fate of mutant rhodopsin: quality control, degradation and aggresome formation. *J Cell Sci* **115**, 2907-2918, (2002).
- 45 Sung, C. H., Davenport, C. M. & Nathans, J. Rhodopsin mutations responsible for autosomal dominant retinitis pigmentosa. Clustering of functional classes along the polypeptide chain. *J Biol Chem* **268**, 26645-26649, (1993).
- 46 Sung, C. H., Schneider, B. G., Agarwal, N., Papermaster, D. S. & Nathans, J. Functional heterogeneity of mutant rhodopsins responsible for autosomal dominant retinitis pigmentosa. *Proc Natl Acad Sci U S A* **88**, 8840-8844, (1991).
- 47 Berson, E. L., Rosner, B., Weigel-DiFranco, C., Dryja, T. P. & Sandberg, M. A. Disease progression in patients with dominant retinitis pigmentosa and rhodopsin mutations. *Invest Ophthalmol Vis Sci* **43**, 3027-3036, (2002).
- 48 Dryja, T. P., Hahn, L. B., Cowley, G. S., McGee, T. L. & Berson, E. L. Mutation spectrum of the rhodopsin gene among patients with autosomal dominant retinitis pigmentosa. *Proc Natl Acad Sci U S A* **88**, 9370-9374, (1991).

- 49 Dryja, T. P., McGee, T. L., Reichel, E., Hahn, L. B., Cowley, G. S., Yandell, D. W. *et al.* A point mutation of the rhodopsin gene in one form of retinitis pigmentosa. *Nature* **343**, 364-366, (1990).
- 50 Audo, I., Manes, G., Mohand-Said, S., Friedrich, A., Lancelot, M. E., Antonio, A. *et al.* Spectrum of rhodopsin mutations in French autosomal dominant rod-cone dystrophy patients. *Invest Ophthalmol Vis Sci* **51**, 3687-3700, (2010).
- 51 Murauer, E. M., Koller, U., Hainzl, S., Wally, V. & Bauer, J. W. A reporter-based screen to identify potent 3' trans-splicing molecules for endogenous RNA repair. *Hum Gene Ther Methods* **24**, 19-27, (2013).
- 52 Bentley, D. L. Coupling mRNA processing with transcription in time and space. *Nat Rev Genet* **15**, 163-175, (2014).
- 53 Zeitlin, S. & Efstratiadis, A. In vivo splicing products of the rabbit beta-globin pre-mRNA. *Cell* **39**, 589-602, (1984).
- 54 Koller, U., Wally, V., Mitchell, L. G., Klausegger, A., Murauer, E. M., Mayr, E. *et al.* A novel screening system improves genetic correction by internal exon replacement. *Nucleic Acids Res* **39**, e108, (2011).
- 55 Sung, C. H. & Chuang, J. Z. The cell biology of vision. *J Cell Biol* **190**, 953-963, (2010).
- 56 Allocca, M., Mussolino, C., Garcia-Hoyos, M., Sanges, D., Iodice, C., Petrillo, M. *et al.* Novel adeno-associated virus serotypes efficiently transduce murine photoreceptors. *J Virol* **81**, 11372-11380, (2007).
- 57 Mendes, H. F., van der Spuy, J., Chapple, J. P. & Cheetham, M. E. Mechanisms of cell death in rhodopsin retinitis pigmentosa: implications for therapy. *Trends Mol Med* **11**, 177-185, (2005).
- 58 Bemelmans, A. P., Bonnel, S., Houhou, L., Dufour, N., Nandrot, E., Helmlinger, D. *et al.* Retinal cell type expression specificity of HIV-1-derived gene transfer vectors upon subretinal injection in the adult rat: influence of pseudotyping and promoter. *J Gene Med* **7**, 1367-1374, (2005).

- 59 McCarty, D. M., Monahan, P. E. & Samulski, R. J. Self-complementary recombinant adeno-associated virus (scAAV) vectors promote efficient transduction independently of DNA synthesis. *Gene therapy* **8**, 1248-1254, (2001).
- 60 Goedhart, J., von Stetten, D., Noirclerc-Savoye, M., Lelimosin, M., Joosen, L., Hink, M. A. *et al.* Structure-guided evolution of cyan fluorescent proteins towards a quantum yield of 93%. *Nat Commun* **3**, 751, (2012).

II. Improvement and characterization of an *in vivo* imaging technology to measure potential effects of our therapeutic strategy in a humanized mouse model.

Spectral-domain optical coherence tomography of the rodent eye: highlighting layers of the outer retina using signal averaging and comparison with histology.

Adeline Berger, Sophie Cavallero, Elisa Dominguez, Peggy Barbe, Manuel Simonutti, José-Alain Sahel, Florian Sennlaub, William Raoul, Michel Paques, Alexis-Pierre Bemelmans.

Concomitantly to the *in vitro* screening to select the most efficient PTM, we started to characterize different mouse models of rhodopsin deficiency that subsequently could be useful to assess the therapeutic efficacy of our *trans*-splicing strategy *in vivo*. Following order to monitor the evolution of a degenerative retinal disease *in vivo*, and measure potential beneficial effects of a therapeutic approach, powerful imaging technologies are required. To that aim, we were interested in Spectral-Domain Optical Coherence Tomography (SD-OCT) that gave a cross-sectional visualization of the retina. This non-invasive technology allows one to observe and measure the evolution of each retina cell layer over time. Despite an increasingly widespread use in rodents, SD-OCT images were often of medium quality that increased difficulties in their interpretation. Notably, layers of the inner retina were quite well defined, while images of the outer part were trickier to interpret. We first developed a tool to process the images as to improve their quality. Thanks to this approach, we were able to clearly identify each outer retina layer after comparison between pigmented and albino mice, and with histological sections. We also clearly established that SD-OCT is a very accurate technology, at least as histology, and moreover avoids variations due to sampling and treatment of the sections. By following retinal degeneration in a RHO knockout mouse model, we demonstrated that SD-OCT is a powerful technology to study the evolution of a retinal disease over time in the same animal. This approach may require some complementation with other techniques, such as histology and ERG to obtain information concerning cellular details and functionality. Yet the work presented here brings the proof that SD-OCT is a potent *in vivo* imaging technology for the visualization of retinal cellular layers, particularly adapted to the follow-up of degenerative diseases and can be now used to follow with higher confidence the evolution of the outer layers of the rodent retina.



Spectral-Domain Optical Coherence Tomography of the Rodent Eye: Highlighting Layers of the Outer Retina Using Signal Averaging and Comparison with Histology

Adeline Berger^{1,2,9}, Sophie Cavallero^{1,2,9}, Elisa Dominguez^{1,2}, Peggy Barbe^{1,2}, Manuel Simonutti^{1,2}, José-Alain Sahel^{1,2,3}, Florian Sennlaub^{1,2}, William Raoul^{1,2}, Michel Paques^{1,2,3}, Alexis-Pierre Bemelmans^{1,2,4,5*}

1 Inserm, U 968, Paris, France, 2 UPMC Univ Paris 06, UMR_S 968, Institut de la Vision, Paris, France, 3 Centre Hospitalier National d'Ophthalmologie des Quinze-Vingts, INSERM-DHOS CIC 503, Paris, France, 4 CEA, DSV, I²BM, Molecular Imaging Research Center (MIRcen), Fontenay-aux-Roses, France, 5 CNRS, CEA URA 2210, Fontenay-aux-Roses, France

Abstract

Spectral-Domain Optical Coherence Tomography (SD-OCT) is a widely used method to observe retinal layers and follow pathological events in human. Recently, this technique has been adapted for animal imaging. This non-invasive technology brings a cross-sectional visualization of the retina, which permits to observe precisely each layer. There is a clear expansion of the use of this imaging modality in rodents, thus, a precise characterization of the different outer retinal layers observed by SD-OCT is now necessary to make the most of this technology. The identification of the inner strata until the outer nuclear layer has already been clearly established, while the attribution of the layers observed by SD-OCT to the structures corresponding to photoreceptors segments and retinal pigment epithelium is much more questionable. To progress in the understanding of experimental SD-OCT imaging, we developed a method for averaging SD-OCT data to generate a mean image allowing to better delineate layers in the retina of pigmented and albino strains of mice and rats. It allowed us to locate precisely the interface between photoreceptors and retinal pigment epithelium and to identify unambiguously four layers corresponding to the inner and outer parts of photoreceptors segments. We show that the thickness of the various layers can be measured as accurately *in vivo* on SD-OCT images, than post-mortem by a morphometric analysis of histological sections. We applied SD-OCT to different models and demonstrated that it allows analysis of focal or diffuse retinal pathological processes such as mutation-dependant damages or light-driven modification of photoreceptors. Moreover, we report a new method of combined use of SD-OCT and integration to quantify laser-induced choroidal neovascularization. In conclusion, we clearly demonstrated that SD-OCT represents a valuable tool for imaging the rodent retina that is at least as accurate as histology, non-invasive and allows longitudinal follow-up of the same animal.

Citation: Berger A, Cavallero S, Dominguez E, Barbe P, Simonutti M, et al. (2014) Spectral-Domain Optical Coherence Tomography of the Rodent Eye: Highlighting Layers of the Outer Retina Using Signal Averaging and Comparison with Histology. PLoS ONE 9(5): e96494. doi:10.1371/journal.pone.0096494

Editor: Alan Stitt, Queen's University Belfast, United Kingdom

Received: November 22, 2013; **Accepted:** April 8, 2014; **Published:** May 2, 2014

Copyright: © 2014 Berger et al. This is an open-access article distributed under the terms of the Creative Commons Attribution License, which permits unrestricted use, distribution, and reproduction in any medium, provided the original author and source are credited.

Funding: This work was supported by grants from Association Française contre les Myopathies (AFM grant 14814) INSERM ANR Geno 2009 (R09099DS), ANR Programme Emergence 2012 (ANR-EMMA-050), and ERC starting Grant (ERC-2007 St.G. 210345). Adeline Berger is a recipient of a PhD fellowship from Association Française contre les Myopathies and Florian Sennlaub is a recipient of contract « Interface » from Assistance Publique-Hopitaux de Paris. The funders had no role in study design, data collection and analysis, decision to publish, or preparation of the manuscript.

Competing Interests: The authors have declared that no competing interests exist.

* E-mail: alexis.bemelmans@cea.fr

These authors contributed equally to this work.

Introduction

Rodents are widely used animal models for the study of the retina, both physiologically and during degenerative diseases. The mouse and rat retinal anatomy is indeed similar in many aspects to that of humans. In addition there is a wide variety of mouse strains that reproduce many inherited retinal degeneration observed in humans. *In vivo*, retinal function is usually evaluated by electroretinography [1]. This technique, although providing a reliable functional index, does not allow assessing the actual degeneration of the different neuronal layers in the retina. The most widely used morphological approach in animal experimentation is histology on transverse sections of the retina, on which it is possible to achieve different quantifications and especially the thickness of retinal layers. However, this technique has several drawbacks. First, it is a rather tedious technique. Second, the fixation process can induce

artifacts causing contractions and/or expansions of tissue, which then lead to significant measurement variability [2,3]. Third, this technique is terminal by its nature, so it does not allow longitudinal monitoring of animals. Transparency of ocular tissues has made possible to develop alternative techniques, to directly visualize the retina and longitudinally monitor the degeneration, such as funduscopy, confocal scanning laser ophthalmoscopy (cSLO) and angiography [4,5]. Although these techniques allow visualizing the posterior pole of the eye and identifying morphological abnormalities, they do not provide similar data to those obtained by histology on cross-sections of the retina. The only technique that can provide very similar images to transverse histological sections of the retina is spectral-domain optical coherence tomography (SD-OCT) [6]. This method is non-invasive, fast and produces high-resolution cross-sectional images, which are generated by the interference between a reference optical path and another one that

is reflected back from the eye [7,8]. In humans, this technique is currently the gold standard for longitudinal monitoring of retinal degeneration in a large number of pathologies such as age-related macular degeneration [9,10] and diabetic retinopathy [9,11] among others. This technique has logically been applied to animal species used in ophthalmic research, and equipments suitable for the rodents' eye examination have been developed. The BiopTigen 840 nm HHP is one of the most used. It provides "en face" views of the posterior segment of the eye and scans of transverse sections [12]. These scans are used to measure the various nuclear layers of the retina: inner nuclear layer (INL), outer nuclear layer (ONL) and ganglion cell layer (GCL). However, there are still uncertainties about the histological correspondence of the outermost layers of the retina, i.e. the inner and outer segments of the photoreceptors (PR), the retinal pigment epithelium (RPE) and the choriocapillaris.

In this report, we describe a method for averaging SD-OCT images of the rodent retina that allows a better analysis of fine structures in the outer layers. The higher signal-to-noise ratio of these images allowed us to define in rats and mice interfaces generated by the outer limiting membrane (OLM), the inner segment, the outer segment, the RPE and Bruch's membrane, the choriocapillaris and the large choroidal vessels. In addition, the comparison of pigmented and albino animals underlined the effect of melanin pigment on SD-OCT imaging. The comparison of these results with histological data demonstrates that averaging of SD-OCT images allows thickness quantification of the various retinal layers with greater precision. Finally, we show that the SD-OCT acquisition method we have developed allows to identify discrete events or retinal lesions induced by different types of light insults.

Material and Methods

Animals

Six to 12 weeks-old C57BL/6JRj or C57BL/6NRj (with *rd8* mutation) or BALB/cJ mice were purchased from Janvier SA (Le Genest-Saint-Isle, France). *Rhodopsin*^{-/-} (*rho*^{-/-}) mice were provided by Dr Janis Lem (Tufts University, Boston, MA, USA). Mice were maintained at the Institut de la Vision animal facility under pathogen-free conditions. All animals were housed in a 12 h/12 h light/dark cycle with food and water available *ad libitum*.

Ethics statement

All manipulations were performed in accordance with the association for research in vision and ophthalmology (ARVO) Statement for the Use of Animals in Ophthalmic and Vision Research. In addition, all the experimental procedures were permitted by the Institutional Animal Care and Use Committee, "Comité d'éthique pour l'expérimentation animale Charles Darwin" (ID Ce5/2010/044), which also specifically approved the study reported in the present manuscript.

SD-OCT imaging

Pupils were dilated with tropicamide (Mydriaticum, Théa, France) and phenylephrine (Néosynéphrine, Europhtha, France). Animals were then anesthetized by inhalation of Isoflurane (Axiencia, France) and placed in front of the SD-OCT imaging device (BiopTigen 840 nm HHP; BiopTigen, North Carolina, USA). Eyes were kept moisturized with 9% NaCl during the whole procedure. Image acquisitions were performed using the following parameters: Rectangular scan/1000 A-scan per B-scan/100B-scan 1 frame or 4B-scans 16 frames. Acquired images were

saved as .avi files and processed with Fiji software (available at <http://fiji.sc/Fiji>). Firstly, image artifacts due to breathing movements were eliminated by using the StackReg Plugin. Then, using "Z project" function set to "Sum Slices", each movie was converted into a single image by compiling a Z-projection of all images of the movie. Thus, the final image results from the maximum projection of sixteen or one hundred images sampled every micron, which means 16 or 100 microns retinal width depending on the selected parameter. This manipulation eliminates most of the noise observed on individual images, which helped to show very clearly the reflectance differences present at the level of the outer retina (Fig. S1, Supporting Information S1 and S2). Thickness of retinal layers were manually measured on this maximum projection image in an axis perpendicular to the individual layers and 500 μm from the centre of the optic nerve using Fiji software [13].

Subretinal injections. Animals were anesthetized by intraperitoneal injection of ketamine (50 mg/kg, Virbac, France) and xylazine (10 mg/kg, Bayer HealthCare, Germany), and their pupils were dilated as described previously. Subretinal injections were performed with a 33-gauge blunt needle mounted on a 10 μl syringe (Hamilton, USA). Briefly, a hole was created through the sclera/choroid/retina layers using the sharp tip of a 32-gauge needle, and the blunt needle of the Hamilton syringe was then gently inserted into the vitreous through this hole. The needle was then pushed further into the vitreous until crossing the retina to the opposite side of its entry site into the eye. After injection, the needle was left in place for an additional 10 seconds to prevent leakage of the injected fluid. A successful subretinal injection was checked by visualization of subretinal bleb. Mineral oil (Sigma-Aldrich, France) was injected in the subretinal space to visualize boundary between PR and RPE.

Light-challenge model

This protocol was adapted from our previous study [14]. Briefly, 3-month-old C57BL/6JRj mice were adapted to complete darkness for 12 hours and pupils were daily dilated with 1% Atropin (Novartis, France). Animals were then exposed to green LED light (4500 Lux, JP Vezon équipements, France) for 4 days and subsequently kept in cyclic 12 h/12 h normal animal facility conditions. SD-OCT was performed 3, 7, 14 and 21 days after light exposure.

Laser-photocoagulation and choroidal neovascularization (CNV) scar quantification

Three-month-old male C57BL/6JRj mice were anesthetized by intraperitoneal injection of ketamine (50 mg/kg) and xylazine (10 mg/kg). Pupils were fully dilated with 1% tropicamide. Coverslips positioned on the mouse cornea were used as a contact lens. Laser-photocoagulations (400 mW, 50 ms, 100 μm spot size) were performed 1 to 2 disc diameters away from the papillae with a Laser Yag 532 Eyelite (Alcon, USA) mounted on a slit lamp (BQ 900, Hagg-Streitt, France). Laser photocoagulation and rupture of Bruch's membrane were confirmed by immediate observation of a bubble. Choroidal neovascularization (CNV) was quantified 7 days after Laser impact and reported as volume units (μm³). Volumetric data obtained from SD-OCT sequences, viewed and analyzed with Imaris software (Bitplane, CT, USA) were compared to data obtained by direct measures of oblate spheroid CNV from the same SD-OCT sequences treated by FIJI software as described before. Extrapolated volume was calculated with the following formula $(4/3\pi*a*b^2)/2$ (in which a is the polar radius and corresponds to the measure along the vertical axis and b is the equator radius and corresponds to the horizontal axis). To

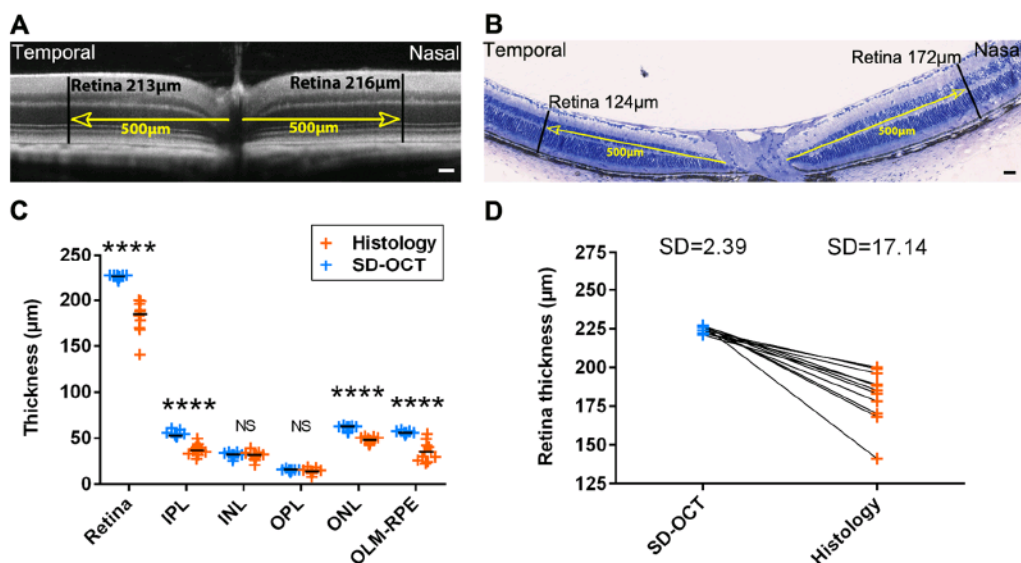


Figure 1. Retinal layer thickness measures in C57BL/6JRj wild-type mice by SD-OCT and histology. Retinal thickness in nasal and temporal sides in SD-OCT image (A) and in corresponding histological section (B). (C) Measures of retinal layers thickness by SD-OCT and histology in C57BL/6JRj mice, $n=11$, Mann Whitney test. (D) Retinal thickness evaluated by SD-OCT and histology in C57BL/6JRj mice. Each pair of point represents the whole retina thickness of the same eye measured with SD-OCT (blue dots) and histology (orange dots). IPL: inner plexiform layer, INL: inner nuclear layer, OPL: outer plexiform layer, ONL: outer nuclear layer, OLM: outer limiting membrane, RPE: retinal pigmented epithelium. SD: Standard Deviation. Scale bars: 50 μm . doi:10.1371/journal.pone.0096494.g001

determine the power of the extrapolation method compared to 3D rendering method, a linear regression was performed with GraphPad software (San Diego, USA).

Histology. Animals were euthanized by CO_2 inhalation. Before enucleation, a mark with an ophthalmic cautery was made at the nasal quadrant of the cornea, so as to subsequently differentiate upper, lower, nasal and temporal quadrants. For Histo-resin-sections processing, eyes were fixed by immersion in 0.5% glutaraldehyde and 4% paraformaldehyde in PBS for 2 hours, dehydrated by successive ethanol baths, and included in Histo-resin (Leica Microsystems, Germany). Oriented sections (5 μm thickness) were cut with a microtome (Microm HM 355S, ThermoScientific, USA) and stained with toluidin blue. Slides were scanned with a Nanozoomer 2.0 HT (Hamamatsu, Japan). Each retinal layer was measured manually. For cryostat-sections processing, eyes were fixed in 4% paraformaldehyde in PBS overnight, cryoprotected at 4°C in successive solutions of PBS containing 10, 20 and 30% of sucrose and embedded in a 10% gelatine/30% sucrose solution, before rapid freezing in an isopentane bath cooled to -40°C . Retinal sections (16 μm thickness) were cut with a cryostat (Microm HM560, Thermo Scientific, USA) and stored at -20°C until further use. For nuclear labelling, sections were incubated 5 min with 4,6-diamidino-2-phenylindole (DAPI, Sigma-Aldrich, France), rinsed and mounted under coverslips with Mowiol reagent. ONL thickness was then automatically quantified by a program specially developed on Metamorph software package (Roper Scientific, France), coupled to Nikon Eclipse Ti inverted microscope.

Statistics

GraphPad Prism 5 (GraphPad Software, San Diego, USA) was used for data analysis and graphic representation. All values are reported as medians. Statistical analysis is described in legend of each figure. All statistic tests have been implemented with an

α -risk of 0.05. Parametric tests have been used after assessment of normal data distribution with the d'Agostino and Pearson omnibus normality test. Statistical significance has been indicated in each figure as following: * = p-value < 0.05, ** = p-value < 0.01, *** = p-value < 0.001, **** = p-value < 0.0001.

Results

Accuracy and reliability of SD-OCT imaging

At first, we wanted to verify that the averaging technique that we used to remove most of the noise from SD-OCT images allowed us to obtain a data quantification that was at least as informative as the one obtained through histological sections. We compared SD-OCT and histological morphometric measures obtained pre- and post-mortem in the same animals. All measures were done at identical locations in SD-OCT images and in corresponding histological sections. As illustrated in Fig. 1A and B, while SD-OCT data showed very similar thicknesses in temporal and nasal sides, more important variations could be observed in histology for the same sample. Moreover, significant differences have been observed between SD-OCT measures and histological ones for the entire retina and some individual layers (Fig. 1C). This could be explained by the treatment of samples for histology. Indeed, we tried to keep our histological samples in good conditions, but it is clear that the extraction and treatments of samples can be responsible of a variation that cannot be excluded in histology and which is preventable with SD-OCT. This phenomenon could also be responsible of the lower reproducibility observed here by histology compared to SD-OCT (Fig. 1D). This highlights that SD-OCT allows a great confidence in data reproducibility simply because *in vivo* measurements avoid potential variations due to sample treatments necessary for *ex vivo* measurements.

Retinal outer layers characterization in rodents

Although SD-OCT allows observation of all retina layers, the outer part of the sensory retina remains less precisely described than the inner one. In order to delimit these outer layers, we compared SD-OCT images to histological sections in pigmented and albino animals. Firstly, we improved the quality of images generated by SD-OCT (Fig. S1) to align layers detected on SD-OCT images and histological sections of the retina (Fig. 2A–D). Comparison of histology and SD-OCT images in pigmented and albino mice revealed the localization of the RPE and showed also notable differences in the SD-OCT imaging of the choriocapillaris (Fig. 2A–D). While in pigmented mice RPE and Bruch's membrane resulted in a white line and a black one from the inner to the outer part of the retina, we observed the opposite in albino mice (Fig. 2B and D), indicating that melanin is a major factor of RPE reflectivity. Also, choroid and sclera appeared clearly defined in albino mice, mainly because of a better light penetration than in pigmented animals in which most of the light is arrested by choroidal pigmentation. To confirm RPE localization, we induced a retinal detachment by subretinal injection of 0.5 μ L of oil just before SD-OCT imaging. As expected, detachment occurred immediately internal of these above-mentioned retinal layers in pigmented and albino mice (Fig. 2E and F). This line of fractionation induced by the retinal detachment allowed us to precisely define the outer boundary of the PR segments layer, while the inner boundary was itself clearly defined by the outer limiting membrane (OLM), which appeared as a thin hyper-reflective line on the outer edge of the ONL. This allowed us to conclude that the segments of the PR appear as four successive bands of different reflectivity. The first two layers immediately below the OLM presumably correspond to the PR inner segments and the following two layers to the PR outer segments. As expected, no difference could be evidenced at this level between pigmented and albino mice. Based on these results, we can therefore precisely locate the interface between the PR layer and the RPE, and the bands corresponding to the inner and outer portions of the segments (Fig. 2G–J). Analysis of pigmented and albino strains of rats showed similar results (Fig. S2).

In vivo follow-up in the retina

After having established reliability of SD-OCT for imaging of healthy retina, we wanted to show the usefulness of this technology to characterize the occurrence of physiological or pathological events in the rodent retina. Firstly, we studied degeneration of PR in a *retinitis pigmentosa* mouse model. *Rho*^{-/-} mice are a retinal degeneration model [15] that presents a loss of almost all photoreceptors at post-natal day 90 (P90). We followed this degeneration by SD-OCT from P21 to P180, and compared quantification of INL and ONL thickness to those of C57BL/6Jrj control mice (Fig. 3A–D). While INL thickness variation was equivalent between *rho*^{-/-} and control mice (Fig. 3E), ONL thickness dramatically decreased until complete vanishing at P180 in *rho*^{-/-} mice (Fig. 3F). As expected, the same observation was done by histology after DAPI labeling and automated measurements (Fig. 3G). Nevertheless, values' dispersion was far more important with histological measures than with SD-OCT imaging. This highlights that SD-OCT is a valuable tool for *in vivo* monitoring of retinal degeneration in the same animal.

After improving SD-OCT image quality, and following *in vivo* processes, we then questioned whether SD-OCT imaging might also be useful to visualize discrete physiological or pathological events. For example, we wondered if "rosettes" described in C57BL/6NRj carrying the *rd8* mutation in the *arb1* gene [16], were observable by SD-OCT imaging. As shown on Fig. 4A, we

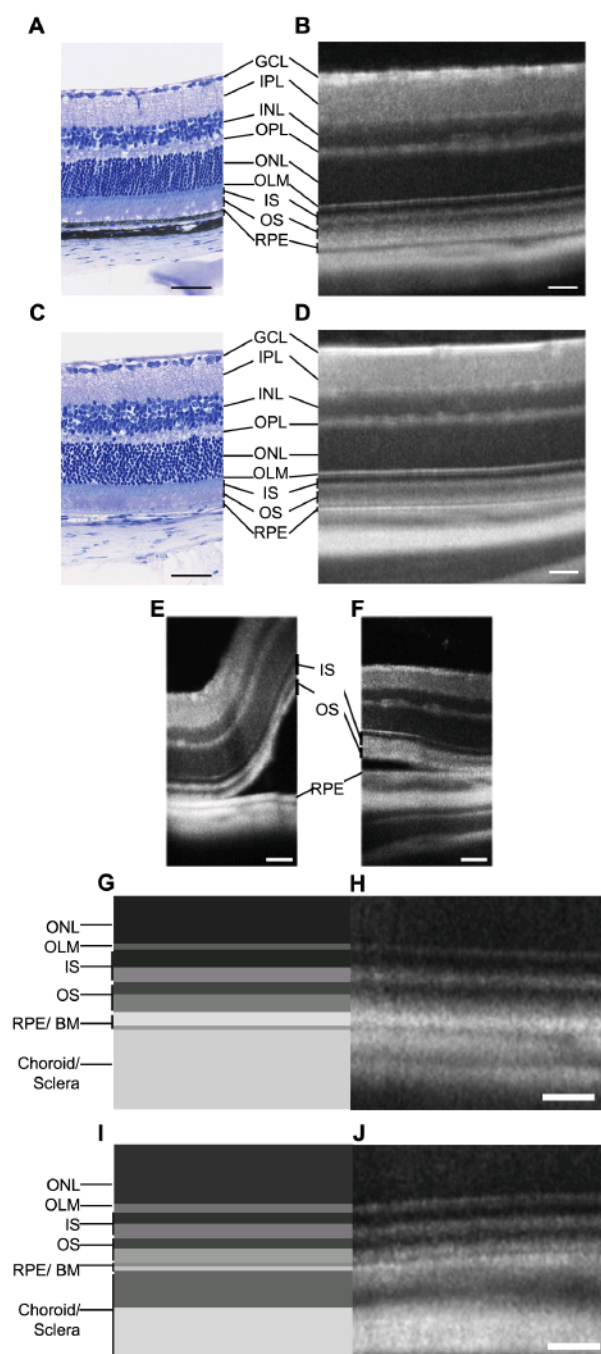


Figure 2. Characterization of pigmented and albino retina layers by SD-OCT. Histological sections of C57BL/6Jrj pigmented mouse retina (A) and BALB/cj albino mouse retina (C). SD-OCT images of pigmented mouse retina (B) and albino mouse retina (D). Retinal detachment induced by subretinal oil injection in C57BL/6Jrj pigmented mouse (E) and BALB/cj albino mouse (F). Schematic representations of pigmented mouse outer retina (G) and albino mouse outer retina (I). Zoom on pigmented mouse outer retina (H) and albino mouse outer retina (J). GCL: ganglion cell layer, IPL: inner plexiform layer, INL: inner nuclear layer, OPL: outer plexiform layer, ONL: outer nuclear layer, OLM: outer limiting membrane, IS: inner segments, OS: outer segments, RPE: retinal pigmented epithelium, BM: Bruch's membrane. Scale bar: 50 μ m. doi:10.1371/journal.pone.0096494.g002

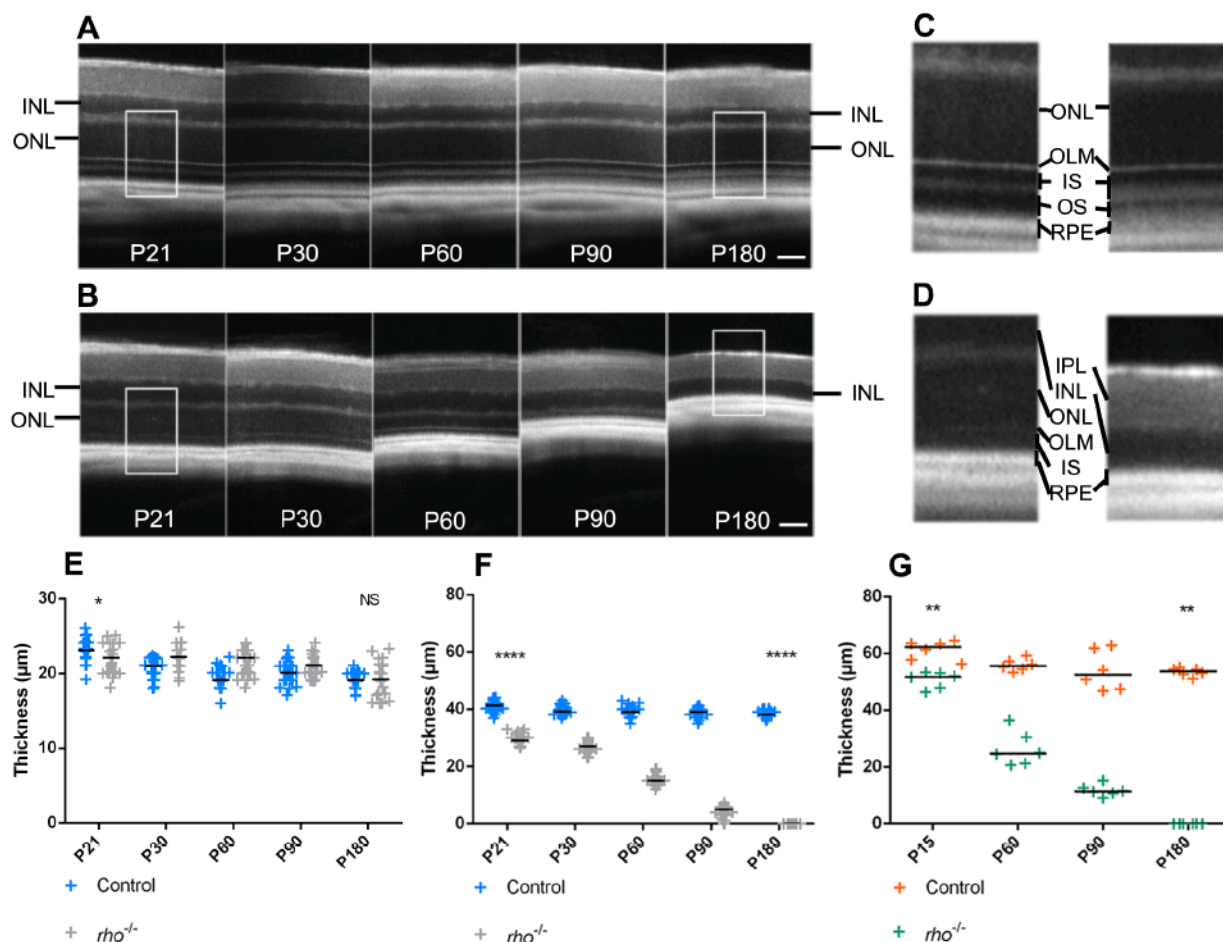


Figure 3. Characterization of a retinal degeneration mouse model by SD-OCT. SD-OCT images of control mice retina (A) and *rho*^{-/-} mice retina (B) from post-natal day 21 (P21) to 180 (P180). Magnification (X2.4) of P21 and P180 control mice outer retina (C) and *rho*^{-/-} mice (D). (E) Measures of INL thickness obtained from SD-OCT data in control and *rho*^{-/-} mice (P21: $p=0.0123$; P180: $p=0.7125$). (F) Measures of ONL thickness obtained from SD-OCT data in control and *rho*^{-/-} mice (P21 and P180: $p<0.0001$). (G) Measures of ONL thickness obtained from morphometric measurements on cryostat sections in control and *rho*^{-/-} mice (P15 and P180: $p=0.0022$). Statistical significance of the difference between groups was analyzed at the initial time-point (P15 or P21) and the latest time-point (P180) studied by Student's T-test for E and F ($n=23$ per group) and by Mann Whitney test for G ($n=6$ per group). IPL: inner plexiform layer, INL: inner nuclear layer, ONL: outer nuclear layer, OLM: outer limiting membrane, RPE: retinal pigmented epithelium. SD: Standard Deviation. Scale bars: 50 μm . doi:10.1371/journal.pone.0096494.g003

indeed easily evidenced these features on *rd8* genotyped mice. Another example is the light-challenge model, a type of light exposition that we developed to study the relationship between oxidative stress, neuroinflammation and photoreceptor apoptosis in different mouse strains [14]. We thus monitored the changes occurring in outer retinal structures during and after exposition to toxic levels of light for 4 days, performed on C57BL/6Rj animals. In albino animals, this type of exposition leads to a massive death of the photoreceptors occurring through an apoptotic mechanism [17]. However, this light regimen, which we call “light-challenge” instead of “light-damage”, does not lead to such PR degeneration in the pigmented animals used here. After 3 days of continuous illumination (Fig. 4C panel D3), SD-OCT imaging showed layers very similar to those of the control non-illuminated (Fig. 4B) even if the white layer of outer segments seemed to disappear. At day 7 (i.e. 3 days after stopping continuous illumination) the two different layers defining the outer segments were no longer distinguishable (Fig. 4C panel D7 and Fig. S3). This phenomenon

was just temporary, because at D14 and D21, inner and outer segments had regained their original appearance. One of the hypotheses to explain this variation is a possible link with inflammatory processes already described [14]. This observation further confirmed the usefulness of SD-OCT imaging to monitor *in vivo* the occurrence of discrete events in the rodent retina.

Finally, SD-OCT imaging can also provide detailed structure of choroidal neovascularization (CNV) occurring above the RPE (Fig. 5A) after laser photocoagulation. Laser-induced CNV indeed mimics some major aspects of wet age-related macular degeneration [18]. We wondered whether extrapolated CNV volumes obtained by direct quantification of SD-OCT images (after signal integration as described in the methods section) were comparable with volumetric data obtained from the same SD-OCT sequences viewed and analyzed with Imaris software (Fig. 5C–F). Here we showed that direct measures on SD-OCT sequences represented a faster and reliable alternative to CNV analysis using a dedicated 3D rendering software (Fig. 5B). We sought here to provide a new

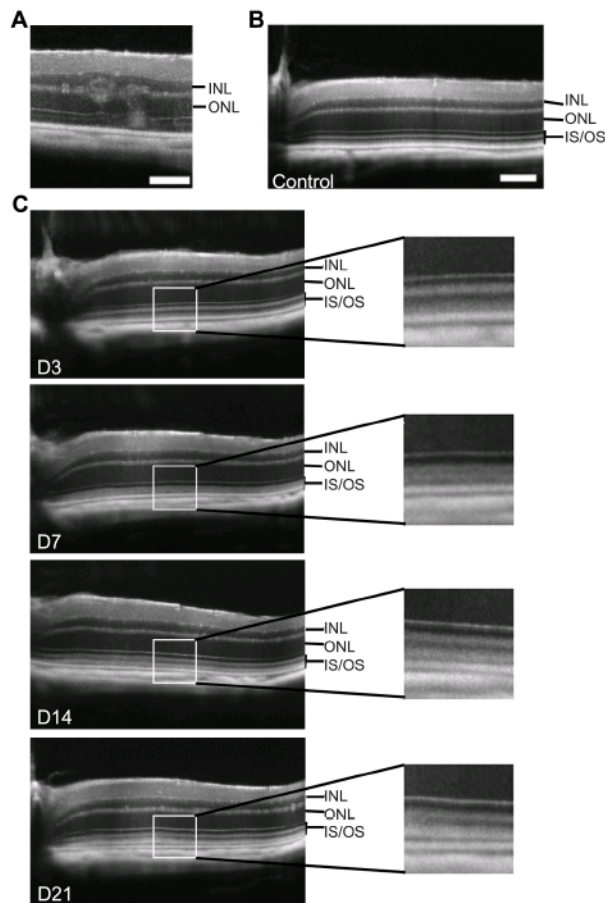


Figure 4. SD-OCT imaging in other pathological models: *rd8* mutation and light-challenge. (A) Typical ocular lesions of *rd8* mutation in *crb1* gene (C57BL/6NRj mice in which presence of the *rd8* mutation was confirmed by genotyping). (B–C) SD-OCT follow-up of the outer retina during a light-challenge in C57BL/6JRj mice. Control unexposed three month-old mouse has a normal appearance with 4 bands of different reflectance corresponding to the PR segments (B). Mice were then exposed to light during 4 days as described in the “methods” section and the retina was imaged by SD-OCT at day 3 (D3), 7, 14 and 21 after starting the illumination (C). The light-challenge leads to a temporary abolition of the distinction between the two bands forming the outer segment, with a peak at D7 (right panels: enlargement of the area enclosed by a white box on the left view). INL: Inner Nuclear Layer, ONL: Outer Nuclear Layer, IS: Inner Segments, OS: Outer Segments. Scale bars: 50 μ m. doi:10.1371/journal.pone.0096494.g004

procedure to optimize SD-OCT imaging and CNV quantification. All together these data show that SD-OCT imaging is a powerful tool to describe different phenomena affecting the retina and not only reduction of layers thickness.

Discussion

During the last decade, SD-OCT imaging has taken a prominent place in the clinic for the follow-up of patients with retinal degeneration [19]. Application of this technology to rodents has been developed more recently, in part probably because in first intention histological tissue analysis seems more informative and versatile. In this study, we aimed at investigating the specific interest of SD-OCT for the study of rodent models of retinal

degeneration. We first developed a method for acquisition and averaging of images that allowed to increase the signal to noise ratio. With this method we could analyze on SD-OCT images the nature of the different reflectance layers of the outer retina of pigmented and albino strains of rodents. Comparison of the results obtained after histological analysis or quantification of SD-OCT imaging finally clearly demonstrated the accuracy and reproducibility of the latter for the quantification of retinal degeneration in rodents. This was certainly due to tissue shrinkage or expansion occurring during histological processing that was not consistent from one sample to another or even within a given sample. Fixation itself is the source of artifacts [3]. Thus, in our study, we observed a tendency to tissue retraction with Histoiresin embedding and microtome sectioning (Fig. 1), and rather a trend to dilation following gelatin/sucrose embedding and cryostat sectioning (Fig. 3). Similarly, Jiao and colleagues showed in a recent study on rats that retinas processed by paraffin embedding displayed a significant tissue retraction compared with those treated by cryostat sectioning [20]. This clearly highlights one of the advantages of SD-OCT imaging, which is to collect *in vivo* data, allowing to monitor over time the same animal, and avoiding potential variations due to sample treatments.

Interpretation of reflectance variations of the outermost retinal and choroidal layers remains debated [21,22]. This is due to the uncertainty that exists as to the exact boundary between the RPE and PR and also the relatively noisy appearance of SD-OCT images in rodents. In addition, the number of layers detected between OLM and RPE through SD-OCT imaging (4 according to our interpretation described below) do not match the number of layers observed in histology (2, corresponding to the inner and outer part of PR segments). We circumvented the first hurdle by implementing an averaging of the acquisitions, which significantly increased the signal-to-noise ratio compared to conventional rodent SD-OCT images obtained with the BiopTigen 840 nm HHP [23,24]. We then used an experimental artifice consisting in detaching the neuroretina from the RPE by subretinal injection of oil, to precisely locate the interface between the RPE and PR. This allowed us to confirm the location of the inner segment and outer segment (Fig. 2G and H) each corresponding to two bands of different reflectance. This interpretation is consistent with that recently proposed by Spaide and Curcio for the human peripheral retina, obtained after comparison of histological findings from dozens of publications with SD-OCT data [25]. For the inner segment, the two bands most likely match to myeloid and ellipsoid [26]. For the outer segment, the presence of two bands can be explained by the microvilli of the RPE ensheathing only the most peripheral part of the outer segment of the PR. In humans, these microvilli can indeed extend for as long as half of the outer segment [27]. The RPE and the PR layers are thus entangled into one another, which may explain at least partly the poor contrast observed by SD-OCT between these two layers. In contrast, the basal pole of the RPE and the Bruch’s membrane appear perfectly delineated. External to this structure, the presence of three layers of different reflectance most likely corresponds to the choriocapillaris, choroid and sclera layers (Fig. 2G–J), although there is no definitive clue allowing to clearly establish the boundaries of these structures. Finally, the comparison between albino and pigmented animals shows as expected that no reflectance difference is observed in these two genetic backgrounds for the non-pigmented cells layers. However, peripheral from the RPE, we observed a greater light penetration and less defined boundaries in albino animals (Fig. 2 and Fig. S2). In particular, the OCT imaging of the choroid showed notable variations linked to the presence of melanin: while whole choroidal thickness was better imaged in

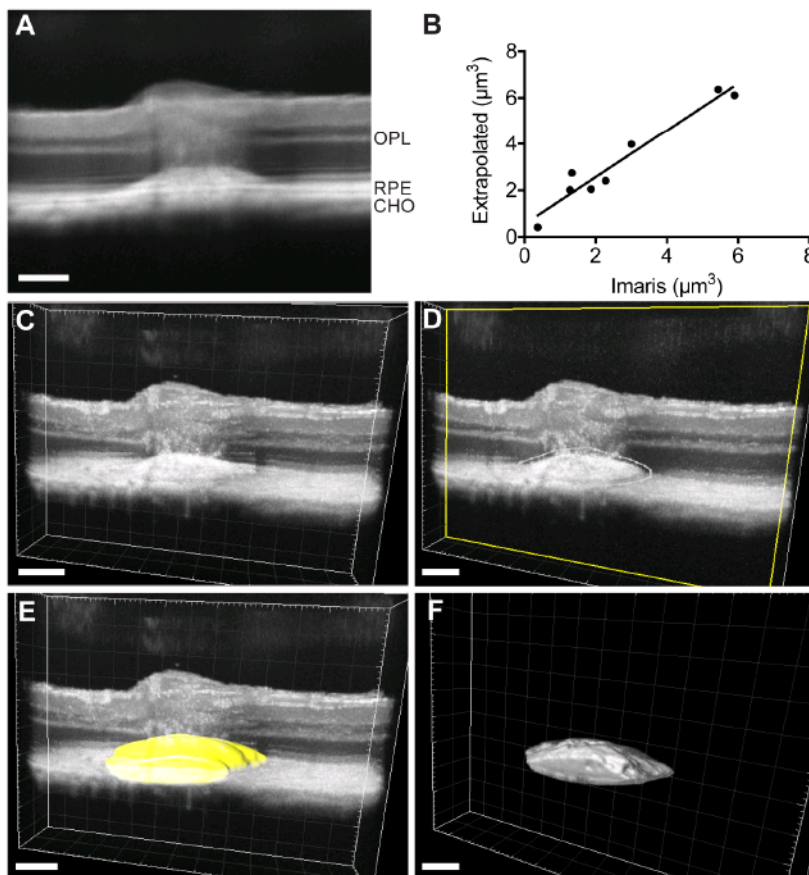


Figure 5. Quantification of laser-induced choroidal neovascularization (CNV) in C57BL6/JRj. (A) Laser-induced CNV (Yag 532 Eyelite parameters: 100 μm, 50 ms, 400 mW) was visualized immediately after laser impact using SD-OCT imaging as described in the “materials and methods” section. Based on this image, a CNV volume is extrapolated using the following formula $(4/3\pi \cdot a \cdot b^2)/2$, in which a is the polar radius and corresponds to the measure along the vertical axis and b is the equator radius and corresponds to the horizontal axis. (B) Linear regression showing that data obtained from extrapolation or Imaris 3D reconstruction (described step by step hereafter) are statistically equivalent ($r^2 = 0,94$, $n = 8$). (C) Imaris software allows a 3D rendering of SD-OCT imaging. Data shown here arise from the same SD-OCT sequence than shown in panel A. (D) The neovascularization volume, just above the RPE cell layer, was delimitating manually (representative white dotted line in one slice) in about 20 slices (over 100) along z-axis to create a 3D mask. Based on this manual delimitation the Imaris software computed a 3D mask shown in yellow (E). The final visualization, that allowed CNV volume quantification, was obtained after automated mask thresholding (F). OPL: Outer Plexiform Layer, RPE: Retinal Pigmented Epithelium, CHO: Choroid. Scale bar: 50 μm.
doi:10.1371/journal.pone.0096494.g005

albino eyes, the choroicapillaris was distinguishable only in pigmented eyes.

Finally, a significant advantage of SD-OCT imaging compared to conventional histological techniques when considering ethical issues, is the ability to perform more easily longitudinal follow-up of animal models. For example, for the study of the time-course of retinal degeneration in *rho*^{-/-} mice, a total of only 12 animals is in theory necessary for acquisition of SD-OCT data ($n = 6$ per group), whereas 48 animals are needed for histology data ($n = 6$ per group). Thus, the use of SD-OCT imaging allows a very significant gain in the amount of work needed to achieve a more reliable result. Moreover, this technique is applicable to a large number of pathological situations. It allows not only to detect subtle variations in retinal layers thickness, reflecting a possible degeneration, but also to highlight other phenomena, such as the change in reflectance of the segments layers observed after exposure of the animals to light-challenge, even with moderate levels of light. Presumably an acceleration of phagocytosis of photoreceptors discs and/or a phenomenon of photostasis

associated with inflammatory processes are causing these changes in reflectance. In the CNV model, our goal was not to compare benefits obtained from histological findings or SD-OCT images, which have been previously discussed. Previous studies [20,28,29] showed that CNV size or thickness follow-up using SD-OCT was comparable with data obtained from histological sections. Here we sought to provide a non-invasive and optimized tool to quantify CNV. Based on integrated SD-OCT images, we propose a simple method of calculation that allows a fast and reliable CNV quantification comparable with 3D rendering. Thus, SD-OCT imaging can not only accurately quantify retinal layers thickness, but also highlight more subtle phenomena reflecting metabolic changes in the tissue. However, the histology remains an indispensable complement to the study of animal models due to the versatility of the techniques that can be implemented (histochemical staining, immunolabeling, in situ hybridization, etc.) and the fact that histology gives access to a cellular resolution allowing for example to quantify the number of rows of PR's nuclei in the ONL. In addition histology is useful when the

peripheral retina is particularly affected, because this part of the retina is barely accessible to SD-OCT imaging.

In conclusion, signal averaging of SD-OCT scans in rodent increases its capacity to quantify the thickness of retinal layers with a strong reproducibility. Moreover, it allows a better determination of reflectance's correlation with anatomical structures of the outer retina layers. All these features make of SD-OCT an ideal tool for the exploration of various rodent pathological models that can be followed-up longitudinally in the same eye.

Supporting Information

Figure S1 Enhancement of SD-OCT resolution by image averaging. The fundus of a C57BL/6JRj mouse was imaged by SD-OCT using the BiopTigen 840 nm HHP device. Individual scans are relatively noisy and do not allow to precisely delineate the different layers of the outer retina located peripheral to the outer limiting membrane (A). After acquisition and averaging by the ImageJ software of 16 images separated from each other by 1 μm , these layers appear much more clearly (B). Scale bar = 50 μm . (TIF)

Figure S2 Comparison of SD-OCT images and histological sections of pigmented and albino rat retina. Histological sections of Long Evans pigmented rat retina (A) and Wistar albino rat retina (D). SD-OCT images of pigmented rat retina (B) and albino rat retina (C). Zoom on pigmented rat outer retina (E) and albino rat outer retina (F). GCL = Ganglion Cell Layer, IPL = Inner Plexiform Layer, INL = Inner Nuclear Layer, OPL = Outer Plexiform Layer, ONL = Outer Nuclear Layer, OLM = Outer Limiting Membrane, IS = Inner Segments,

References

- Chang B, Hawes NL, Hurd RE, Davisson MT, Nusinowitz S, et al. (2002) Retinal degeneration mutants in the mouse. *Vision Res* 42: 517–525.
- McLean M, Prothero JW (1991) Three-dimensional reconstruction from serial sections. V. Calibration of dimensional changes incurred during tissue preparation and data processing. *Anal Quant Cytol Histol* 13: 269–278.
- Margo CE, Lee A (1995) Fixation of whole eyes: the role of fixative osmolarity in the production of tissue artifact. *Graefes Arch Clin Exp Ophthalmol* 233: 366–370.
- Sharp PF, Manivannan A, Xu H, Forrester JV (2004) The scanning laser ophthalmoscope—a review of its role in bioscience and medicine. *Phys Med Biol* 49: 1085–1096.
- Paques M, Simonutti M, Roux MJ, Picaud S, Levasseur E, et al. (2006) High resolution fundus imaging by confocal scanning laser ophthalmoscopy in the mouse. *Vision Res* 46: 1336–1345.
- Toth CA, Narayan DG, Boppart SA, Hee MR, Fujimoto JG, et al. (1997) A comparison of retinal morphology viewed by optical coherence tomography and by light microscopy. *Arch Ophthalmol* 115: 1425–1428.
- Huang D, Swanson EA, Lin CP, Schuman JS, Stinson WG, et al. (1991) Optical coherence tomography. *Science* 254: 1178–1181.
- Yaqoob Z, Wu J, Yang C (2005) Spectral domain optical coherence tomography: a better OCT imaging strategy. *Biotechniques* 39: S6–13.
- Wolf S, Wolf-Schnurrbusch U (2010) Spectral-domain optical coherence tomography use in macular diseases: a review. *Ophthalmologica* 224: 333–340.
- Regatieri CV, Branchini L, Duker JS (2011) The role of spectral-domain OCT in the diagnosis and management of neovascular age-related macular degeneration. *Ophthalmic Surg Lasers Imaging* 42 Suppl: S56–66.
- Chung H, Park B, Shin HJ, Kim HC (2012) Correlation of fundus autofluorescence with spectral-domain optical coherence tomography and vision in diabetic macular edema. *Ophthalmology* 119: 1056–1065.
- Ferguson LR, Balaiya S, Grover S, Chalam KV (2012) Modified protocol for in vivo imaging of wild-type mouse retina with customized miniature spectral domain optical coherence tomography (SD-OCT) device. *Biol Proced Online* 14: 9.
- Schindelin J, Arganda-Carreras I, Frise E, Kaynig V, Longair M, et al. (2012) Fiji: an open-source platform for biological-image analysis. *Nat Methods* 9: 676–682.
- Sennlaub F, Auvynet C, Calippe B, Lavalette S, Poupel L, et al. (2013) CCR2(+) monocytes infiltrate atrophic lesions in age-related macular disease and mediate photoreceptor degeneration in experimental subretinal inflammation in Cx3cr1 deficient mice. *EMBO Mol Med* 5: 1775–1793.
- Lem J, Krasnoperova NV, Calvert PD, Kosaras B, Cameron DA, et al. (1999) Morphological, physiological, and biochemical changes in rhodopsin knockout mice. *Proc Natl Acad Sci U S A* 96: 736–741.
- Mehalow AK, Kameya S, Smith RS, Hawes NL, Denegre JM, et al. (2003) CRB1 is essential for external limiting membrane integrity and photoreceptor morphogenesis in the mammalian retina. *Hum Mol Genet* 12: 2179–2189.
- Grimm C, Reme CE (2013) Light damage as a model of retinal degeneration. *Methods Mol Biol* 935: 87–97.
- Grossniklaus HE, Kang SJ, Berglin L (2010) Animal models of choroidal and retinal neovascularization. *Prog Retin Eye Res* 29: 500–519.
- Adhi M, Duker JS (2013) Optical coherence tomography—current and future applications. *Curr Opin Ophthalmol* 24: 213–221.
- Jiao J, Mo B, Wei H, Jiang YR (2012) Comparative study of laser-induced choroidal neovascularization in rats by paraffin sections, frozen sections and high-resolution optical coherence tomography. *Graefes Arch Clin Exp Ophthalmol* 251: 301–307.
- Fleckenstein M, Charbel Issa P, Helb HM, Schmitz-Valckenberg S, Finger RP, et al. (2008) High-resolution spectral domain-OCT imaging in geographic atrophy associated with age-related macular degeneration. *Invest Ophthalmol Vis Sci* 49: 4137–4144.
- Huber G, Beck SC, Grimm C, Sahaboglu-Tekgoz A, Paquet-Durand F, et al. (2009) Spectral domain optical coherence tomography in mouse models of retinal degeneration. *Invest Ophthalmol Vis Sci* 50: 5888–5895.
- Ferguson LR, Dominguez Ii JM, Balaiya S, Grover S, Chalam KV (2013) Retinal Thickness Normative Data in Wild-Type Mice Using Customized Miniature SD-OCT. *PLoS One* 8: e67265.
- Wang R, Jiang C, Ma J, Young MJ (2012) Monitoring morphological changes in the retina of rhodopsin^{-/-} mice with spectral domain optical coherence tomography. *Invest Ophthalmol Vis Sci* 53: 3967–3972.
- Spaide RF, Curcio CA (2011) Anatomical correlates to the bands seen in the outer retina by optical coherence tomography: literature review and model. *Retina* 31: 1609–1619.
- Carter-Dawson LD, LaVail MM (1979) Rods and cones in the mouse retina. I. Structural analysis using light and electron microscopy. *J Comp Neurol* 188: 245–262.
- Bonilha VL, Rayborn ME, Bhattacharya SK, Gu X, Crabb JS, et al. (2006) The retinal pigment epithelium apical microvilli and retinal function. *Adv Exp Med Biol* 572: 519–524.

28. Giani A, Thanos A, Roh MI, Connolly E, Trichonas G, et al. (2011) In vivo evaluation of laser-induced choroidal neovascularization using spectral-domain optical coherence tomography. *Invest Ophthalmol Vis Sci* 52: 3880–3887.
29. Liu T, Hui L, Wang YS, Guo JQ, Li R, et al. (2013) In-vivo investigation of laser-induced choroidal neovascularization in rat using spectral-domain optical coherence tomography (SD-OCT). *Graefes Arch Clin Exp Ophthalmol* 251: 1293–1301.

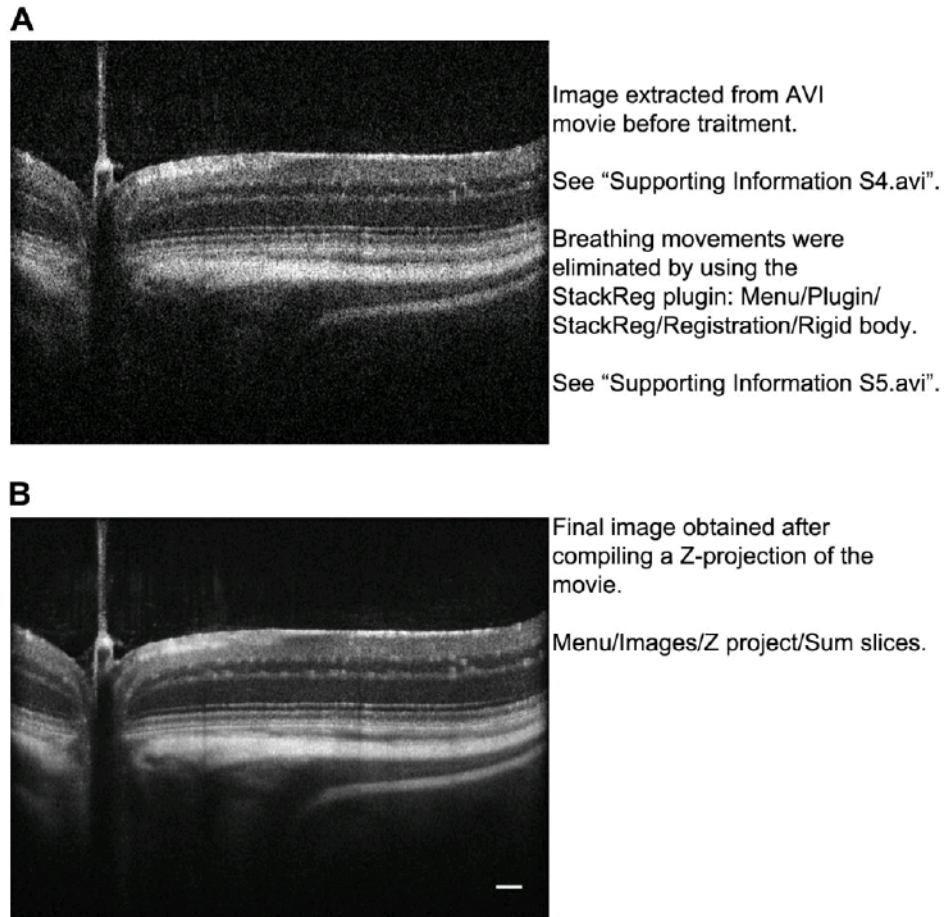


Fig. S1: Enhancement of SD-OCT resolution by image averaging.

The fundus of a C57BL/6JRj mouse was imaged by SD-OCT using the Biotigen 840 nm HHP device. Individual scans are relatively noisy and do not allow to precisely delineate the different layers of the outer retina located peripheral to the outer limiting membrane (A). After acquisition and averaging by the ImageJ software of 16 images separated from each other by 1 μm , these layers appear much more clearly (B). Scale bar = 50 μm .

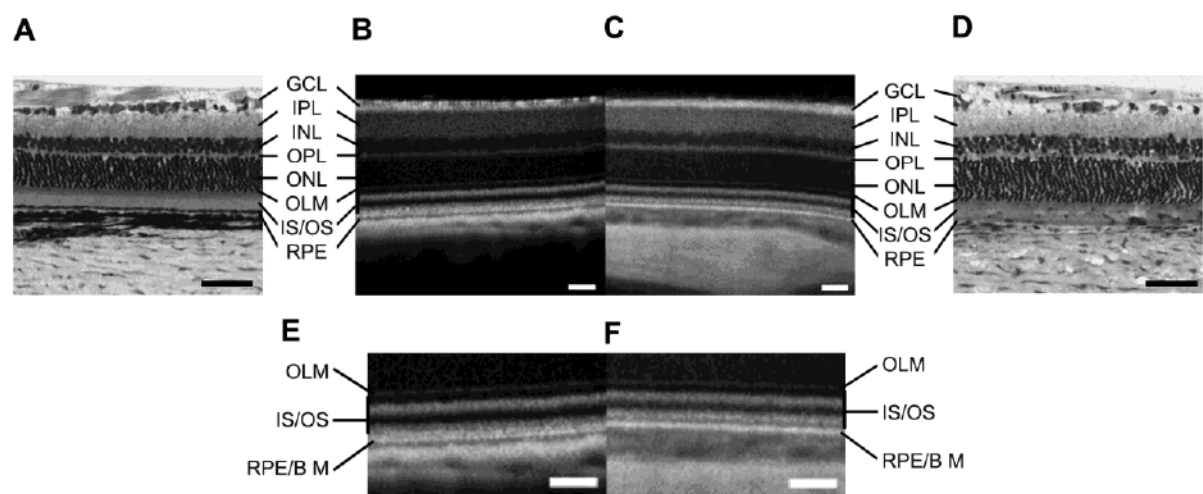


Fig. S2: Comparison of SD-OCT images and histological sections of pigmented and albino rat retina.

Histological sections of Long Evans pigmented rat retina (A) and Wistar albino rat retina (D). SD-OCT images of pigmented rat retina (B) and albino rat retina (C). Zoom on pigmented rat outer retina (E) and albino rat outer retina (F). GCL = Ganglion Cell Layer, IPL = Inner Plexiform Layer, INL = Inner Nuclear Layer, OPL = Outer Plexiform Layer, ONL = Outer Nuclear Layer, OLM = Outer Limiting Membrane, IS = Inner Segments, OS = Outer Segments, RPE = Retinal Pigmented Epithelium, Bruch M = Bruch Membrane. Scale bar = 50 μ m.

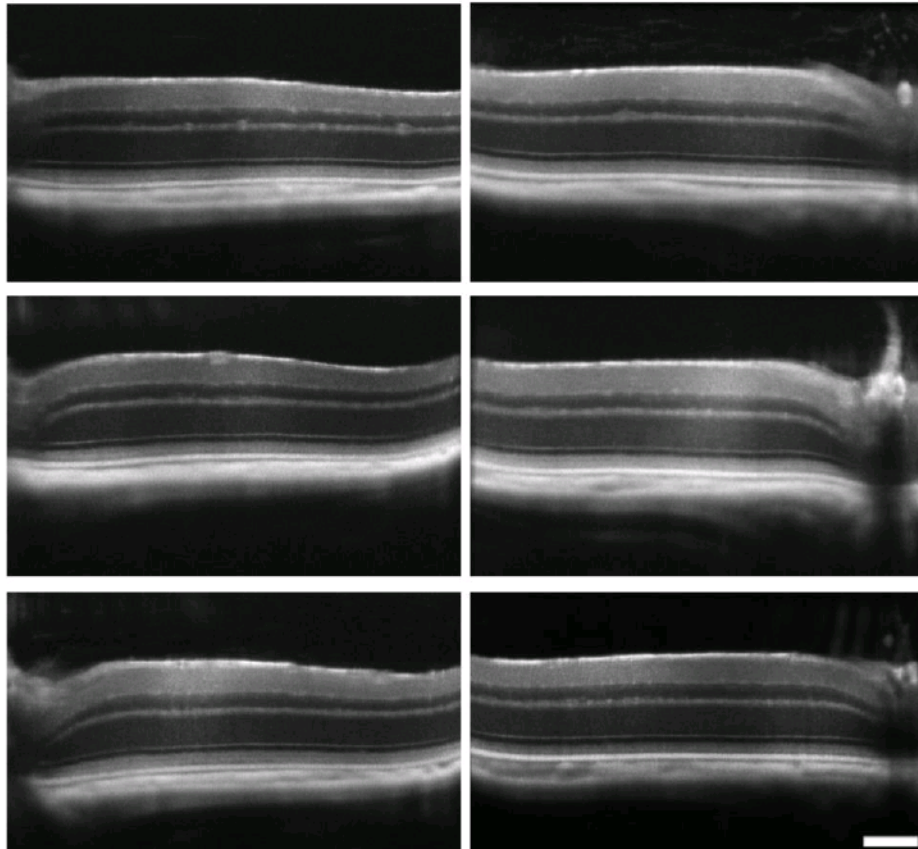


Fig. S3: Eyes of 3 animals at day 7 of light-challenge.

Right and left panels represent respectively right and left eyes of 3 C57BL/6J mice at day 7 after starting of light-challenge (i.e. 3 days after stopping continuous illumination). Scale bar = 50 μ m.

III. Complementary ongoing results.

(Materials and methods of this part are presented in Annex 2)

III.1. Development of new PTM *in vitro* and strategies to overcome PTM drawbacks.

III.1.a. A new PTM that repairs the fifth exon.

We have seen that among all strategies used to ameliorate the PTM efficiency, one can design the binding sequence of the PTM to hide the endogenous 3' acceptor splice site of the following exon. Even if it was not a success in our case for exon 1 (PTM 14) another group has demonstrated the efficiency of this strategy¹⁶⁵. Nevertheless, preventing *cis*-splicing could also induce exon skipping that could be at least as deleterious as mutations in the case of RHO. The only case in which this system is not litigious is its use on the acceptor splice site of the fifth exon. Indeed, exon 5 being the last one, cannot be targeted to induce exon skipping by masking acceptor site of intron 4. We thus designed a PTM (PTM15 – Figure 23A) that possesses a binding sequence including three complementary bases to the beginning of the fifth exon. We included a 3'UTR different from that of the *RHO* expressing construct, to differentiate *cis* from *trans*-splicing products (Figure 23B). After transient co-transfection in HEK293T cells of PTM15 and *RHO* constructs, we observed that PTM15 was able to induce *trans*-splicing. Nonetheless, we also obtained PCR products that came from *cis*-splicing events (Figure 23C). We now have to precisely estimate the *trans*-splicing rate by quantitative PCR to determine the real efficiency of the PTM15 and compare it to the previously characterized PTM.

III.1.b. Production of a truncated protein *in vitro* after expression of the PTM alone.

We speculated that the mutated rhodopsin protein would be less efficiently translated or more rapidly degraded in the cell. In this case it would in theory be possible to detect *trans*-splicing efficiency by quantification of the protein. To that aim, we analyzed by Western Blot (WB) protein samples from WT or mutated RHO-transfected HEK293T cells. Under the specific conditions used in these experiments (without heating the samples), WT RHO that came from WT mouse retina showed a main pool of proteins between 35 and 40 kDa (Figure 24B lane 1), corresponding to monomer forms of RHO (expected size = 39 kDa), while

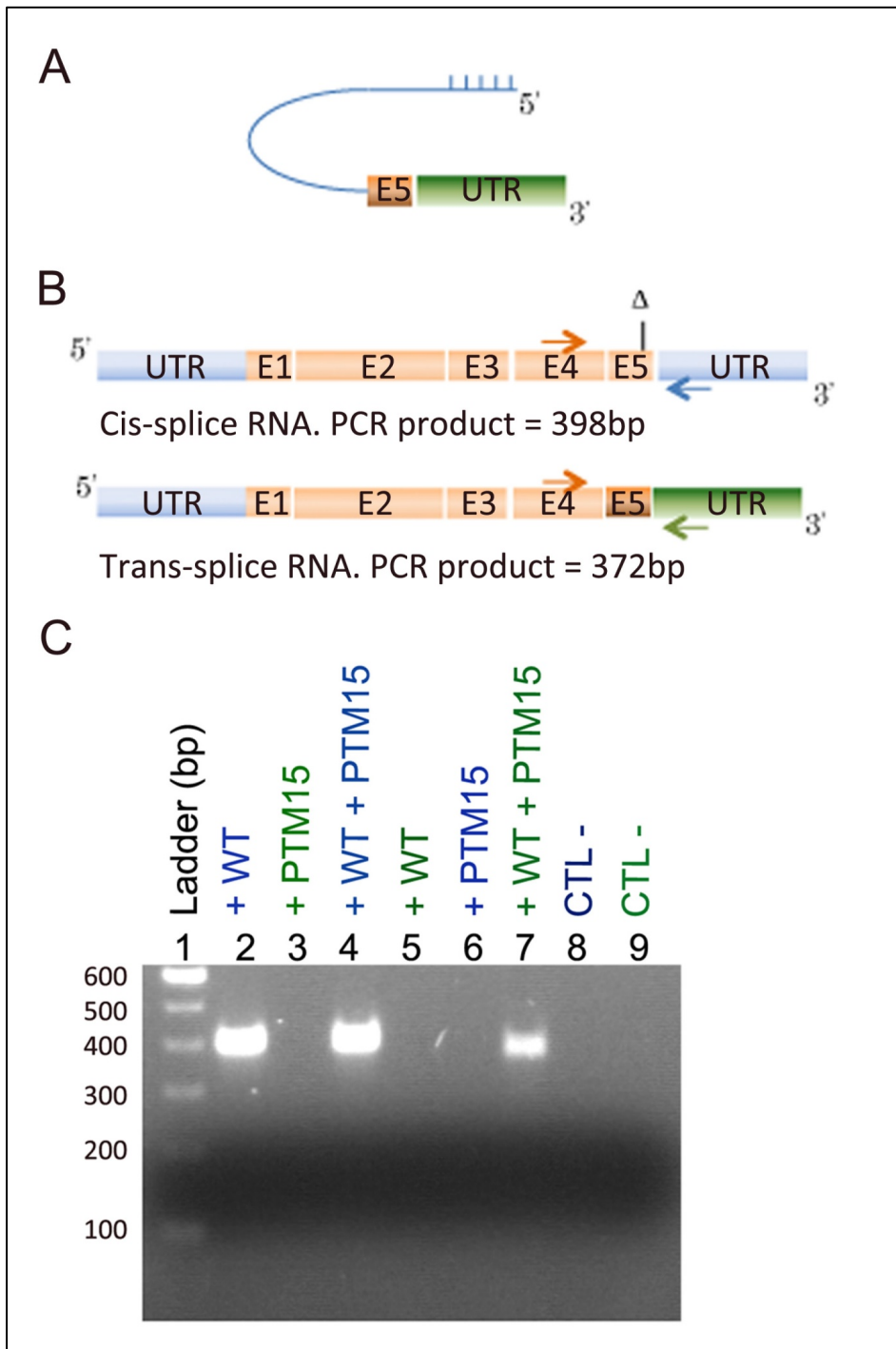


Figure 23: *Trans*-splicing efficiency of PTM 15.

A) The PTM 15 is composed, from 5' to 3', of a binding domain complementary to the end of the endogenous intron 4 and the beginning of exon 5 of rhodopsin, followed by an intronic sequence and the replacement sequence composed of exon 5 and 3'UTR. B) Localization of PCR primers (schematized by arrows) on cDNA obtained from *cis*-spliced and *trans*-spliced RNA. The blue primer is specific of *cis*-spliced UTR sequence while the green one is specific of *trans*-spliced UTR sequence. C) RT-PCR on RNA extracted from cells transfected by WT RHO construct alone (+WT), PTM15 construct alone (+PTM15) or both constructs (+WT +PTM15). The legend color given for each lane indicates the primers used for PCR amplification (described on B). Both *cis*-spliced and *trans*-spliced products result from the action of PTM15.

multimeric forms were also present. The same profile was obtained for samples transfected with mutated *RHO* (Figure 24A lanes 4 and 5 – Figure 24B lane 5) except for the P347L mutation that was not recognized by our antibody (Figure 24A lane 6), whereas transfected WT *RHO* formed insoluble aggregates that were visualized as smears (Figure 24A lane 3 – Figure 24B lane 8). To precisely quantify the rhodopsin content, WB leading to a single band at the expected molecular weight of the monomeric form would be needed. However, despite all our efforts, we were not able to set up such experimental conditions, most probably because, upon denaturation, rhodopsin forms large aggregates that remain in the upper part of the gel. However, these WB allowed us to observe the profile obtained for transfected cells including those with the PTM20 construct alone. Indeed, because the PTM is a RNA molecule that can potentially be translated, other groups have sometimes observed abnormal and unexpected proteins that came from PTM translation^{155,174}. Unfortunately, we also observed that transfection with PTM20 alone was responsible of the production of a protein of about 20 kDa (Figure 24B lane6). This means that without *RHO* expression, PTM20 was not inactive as expected, but was translated into a truncated RHO protein.

III.1.c. Strategies to prevent production of truncated protein.

Because a truncated RHO protein could be at least as harmful as mutation for PR, we tested two different strategies in order to avoid the production of this truncated protein from PTM20. Production of a protein means that PTM20 transcripts are stabilized before being translocated into the cytoplasm and translated. Stabilization of a mRNA involves the presence of a cap and a polyA tail at 5' and 3' extremities, respectively. The cap being added by proteins recruited by the carboxy-terminal domain of RNA polymerase II¹⁸⁰, we firstly imagined to mediate expression of PTM20 under the control of a polymerase III promoter (Figure 25A), to avoid the adding of a cap and thus to avoid stabilization of the PTM if it is not engaged in a *trans*-splicing reaction – the cap being brought by target mRNA in this case. We thus generated a construct with PTM20 (PTM27) or PTM0 (PTM28) for the negative control, under the expression of the U6 promoter. Unfortunately, after transient transfection of one of these constructs associated with *RHO* expression, the *trans*-splicing rate obtained at the RNA level was close to zero (Figure 25C). The use of a polymerase III promoter thus was not efficient to produce PTM20. This last point must now be assessed by specific PCR between exon 2 and 5 after cell transfection with PTM 20 construct alone.

The second strategy that we developed to avoid production of truncated protein was to prevent translation initiation. This one required an ATG initiation sequence, preferentially

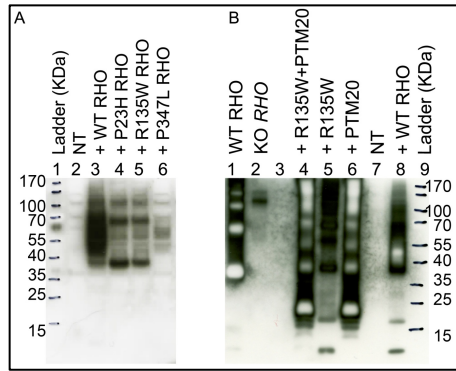


Figure 24: Characterization of RHO by western blot.

A) Western blot on proteins extracted from HEK293T cells after transfection of normal or mutated rhodopsin constructs. NT= Non-Transfected cells. B) Western blot on proteins extracted from transfected HEK293T cells (lanes 4 to 8) or mouse retina (lanes 1 and 2). WT RHO (lane 1)= C57Bl6J mouse retina, KO RHO= rhodopsin knockout mouse retina, NT= Non-Transfected cells. Quantification of RHO is not possible on western blot due to smear obtained with WT RHO in cells (lane 3 on A and lane 8 on B). Transfection of PTM20 alone induces truncated protein production (lane 6 on B).

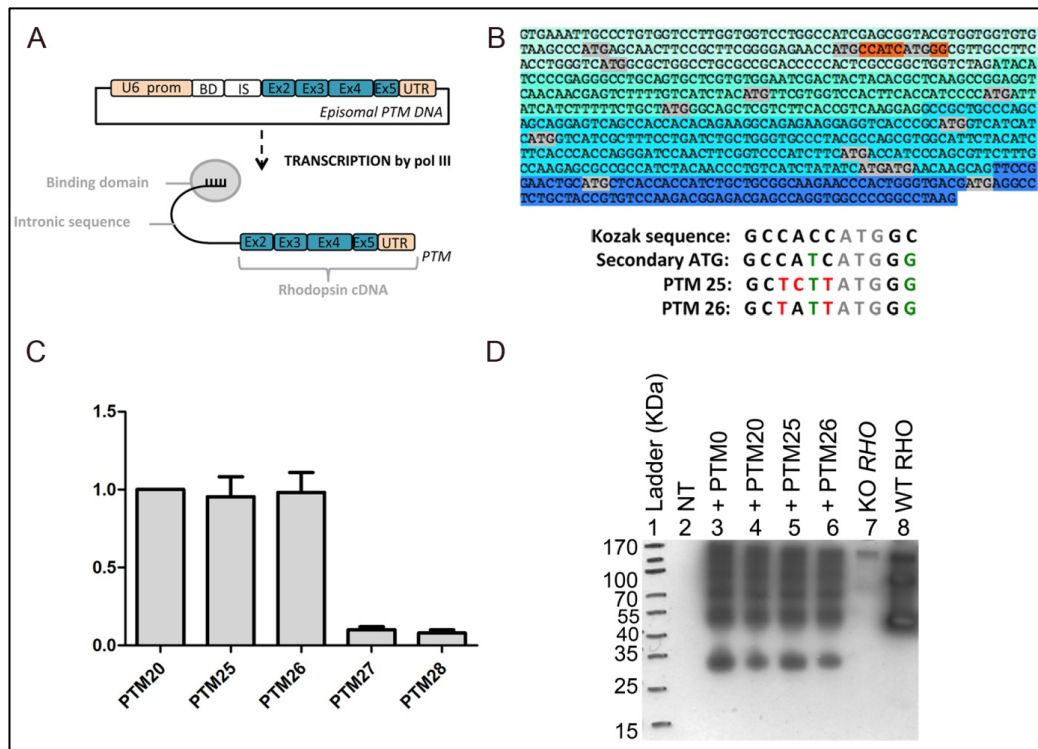


Figure 25: Strategies developed to avoid translation of the PTM alone.

A) Schematic representation of the transcription of PTM sequence by the polymerase III under the control of U6 promoter. B) Localization of secondary ATG (in grey) present in rhodopsin cDNA between exon 2 and exon 5. Exons are defined by different blue colors. The sequence closed to the KOZAK one surrounding the secondary ATG that presumably lead to translation initiation and synthesis of a partial protein product is highlighted in orange. C) Quantification at RNA level of *trans*-splicing rate obtained with PTM25, 26, 27 and 28 (respectively PTM20 and PTM0 expressed under the control of U6 promoter). after transient co-transfection of PTM and RHO constructs in HEK293T cells. Results are normalized with value obtained for PTM20. D) Western blot on proteins extracted from transfected HEK293T cells (lanes 2 to 6) or mouse retina (lanes 7 and 8). NT= Non-Transfected cells, KO RHO= rhodopsin knockout mouse retina, WT RHO (lane 8) = C57Bl6J mouse retina. PTM27 and 28 do not induce *trans*-splicing reaction (C) and PTM25 and 26 also lead to truncated protein production (D).

included within a KOZAK sequence²⁴⁷. The lack of exon 1 in PTM20 implied that translation was initiated on a secondary ATG. We localized 14 ATG present between the beginning of exon2 and the end of exon5, including 11 in frame (Figure 25B), meaning that they could induce production of a protein that conserved the C-terminal of RHO and was thus detectable by our RHO antibody, as previously described. Among them, 4 ATG could induce synthesis of a protein of more than 15 kDa, and only one presented a surrounding sequence that shared 9 bases with the 11 base KOZAK consensus sequence (only 5 or 6 bases for the three others). We thus modified this sequence by site-directed mutagenesis, introducing 2 silent mutations (PTM26) plus a third that induced a substitution from isoleucine to leucine to constitute PTM25 (Figure 25B). After transient co-transfection of one of these constructs associated with RHO, we observed a *trans*-splicing rate equivalent to that obtained with PTM20 at the RNA level (Figure 25C). Nevertheless, analysis of protein production from these molecules clearly gave the same profile as PTM20. Indeed, we observed by WB a protein of around 20 kDa after transfection of PTM25 and PTM26 construct each alone. This strategy is thus inefficient to prevent truncated protein production from PTM.

III.1.d. Analysis of PTM translation alone *in vivo*.

Since the PTM induced synthesis of a truncated protein *in vitro*, we decided to test if it was also true *in vivo*. We subretinally co-injected P21 *RHO* knockout mice with AAV2/8 *bRho* (bovin rhodopsin promoter)-PTM0 or PTM20 and AAV2/8 *bRho*-GFP in a 5:1 ratio. The use of this mouse model allowed elimination of endogenous RHO, and thus if rhodopsin protein was detected, it could come only from the translation of the PTM. Unexpectedly, we did not observe any truncated protein from PTM in transduced retina (Figure 26A), even though the transduction seemed to occur correctly as measured by detection of GFP in three of four transduced retina (Figure 26A), which corresponded to GFP intensities observed on eye fundus (Figure 26B). Because we injected 5 times more AAV-PTM than AAV-GFP, and knowing that both constructs shared the same promoter and the same vector, we were easily confident that PTM was expressed in GFP-positive eyes. We could thus imagine that truncated protein production observed *in vitro* did not occur *in vivo* because target cells (from HEK293T to rod PR) and/or vectors (from plasmid to AAV) differed.

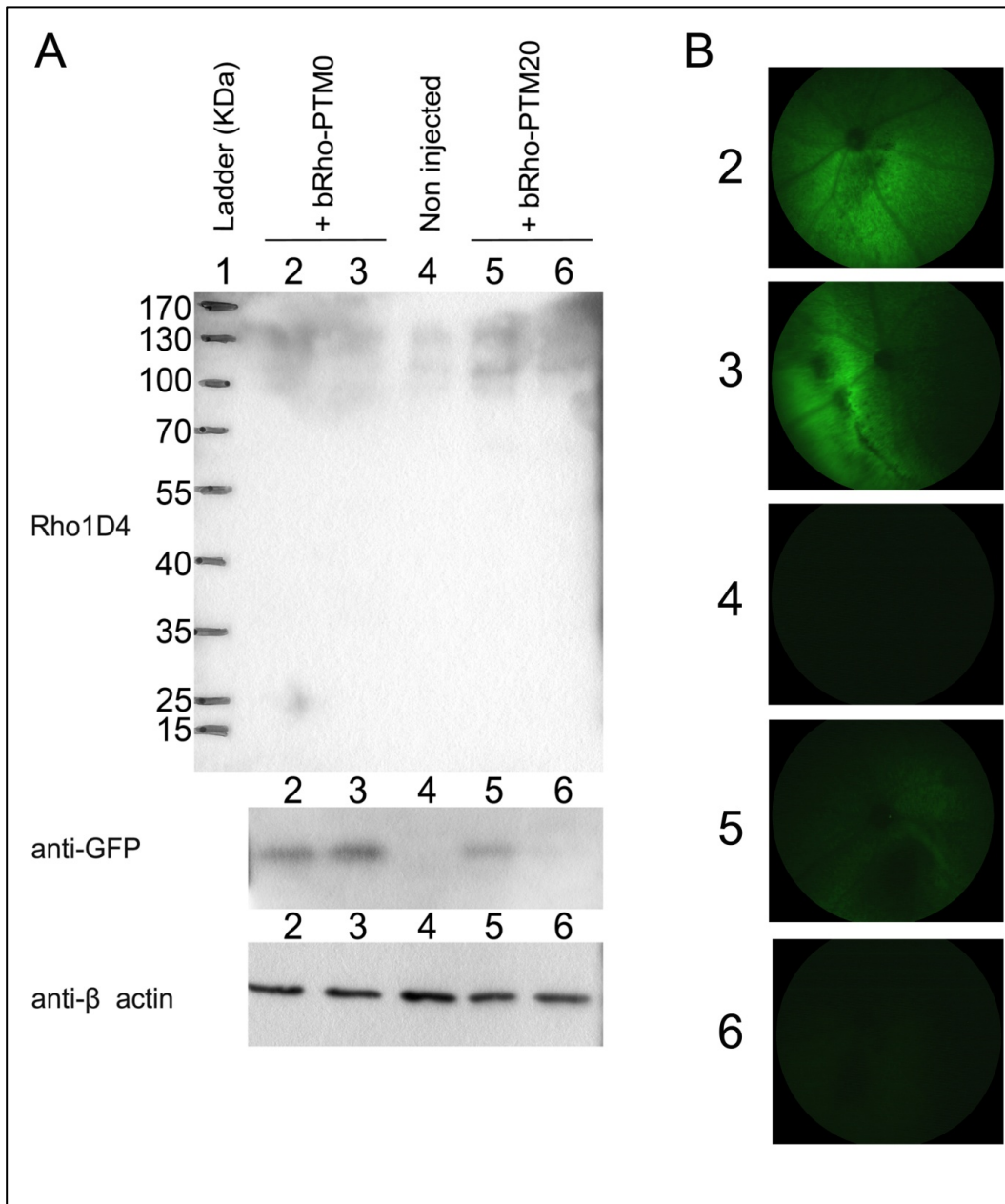


Figure 26: Subretinal co-injection of AAV2/8 bRho-PTM0 or PTM20 and AAV2/8 bRho-GFP in KO RHO mice to study the translation of PTM alone.

A) Western blot of proteins extracted from KO RHO mouse retina, one week after co-transduction with AAV2/8 bRho-GFP and AAV2/8 bRho-PTM0 (lanes 2 and 3) or PTM20 (lanes 5 and 6) in a 1:7 ratio. “Non injected” correspond to proteins extracted from non-injected RHO KO mouse retina. The upper panel corresponds to the RHO detection, the middle one to the GFP detection and the lower one to the β-actin detection, as a loading control. B) Eye fundus of transduced retina to detect GFP expression before proteins extraction used in western blot analyses (A). The 5 images were obtained using the same settings of the camera parameters. Numbers on the left of each image correspond to lane numbers on western blot illustration. No truncated protein is produced *in vivo* from the PTM20 alone.

III.2. Study of the therapeutic effects of *trans*-splicing in a humanized mouse model.

III.2.a. The humanized $Rho^{+/-}$ P347S RHO^+ mouse model.

The choice of our animal model was dictated by the necessity of a rhodopsin-induced RP model, which carried at least one mutated human *RHO* cDNA copy. To be closest to human patients, which are most of the time heterozygous, we generated a $Rho^{+/-}$ P347S RHO^+ mouse model, by crossing two already well-described mouse models: $Rho^{-/57,248}$ and P347S $RHO^{+/+66}$. Follow-up of the $Rho^{+/-}$ P347S RHO^+ mouse retina (F1 generation) by SD-OCT showed a dramatic degeneration of the whole retina compared to WT at P60 certainly mainly due to that of ONL (Figure 27B) and almost absent PR segments (Figure 27A). The humanized $Rho^{+/-}$ P347S RHO^+ mouse retina thus serves as a model of severe RP induced by a *RHO* mutation, characterized by rapid PR degeneration.

III.2.b. Choice of parameters that regulate PTM expression *in vivo*.

PTM expression can be modulated by four factors: delivery method, quantity of viral vector (i.e. volume of injection and titer of viral solution), choice of viral vector and type of promoter. We decided to subretinally inject AAV2/8 based on previous studies showing that this delivery route and serotype led to strong expression in PR²⁰³. We tested two titers of viral solution, 1.5×10^{11} and 10^{10} vg/eye, and two promoters, b*Rho* and CMV. Results obtained showed that both promoters allowed efficient PR targeting at both concentrations of viral particles (Figure 28). Nevertheless, we observed that even if PR were in all cases the cells expressing the transgene the most, Müller glial and bipolar cells at least expressed also GFP at both concentrations under the CMV promoter, and only at the highest one and in a few injected retina under the b*Rho* promoter. It is important to note that the state of the retina may influence these results, as for example the quasi-total PR degeneration in the third panel of Figure 28. Interestingly, we demonstrated that AAV2/8 b*Rho*-GFP subretinally injected at 10^{10} vg/eye generated a GFP expression profile specific to PR, at least in retinas that still presented a PR layer (Figure 28 4th panel).

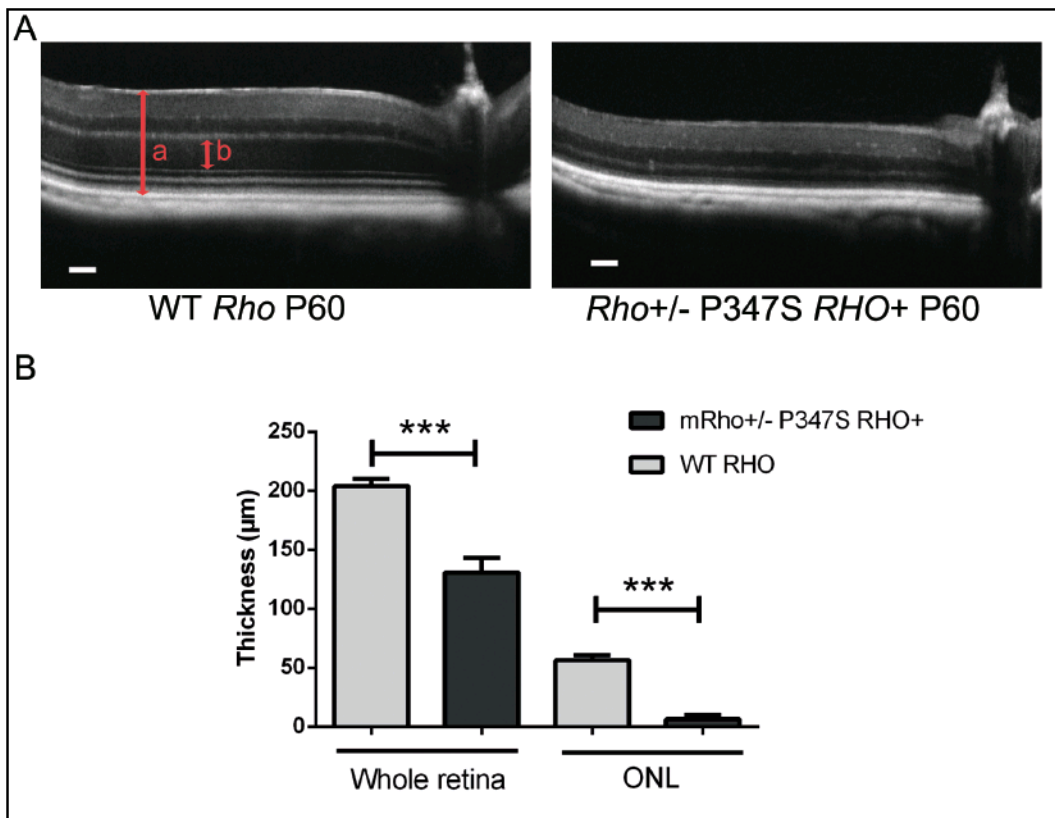


Figure 27: Characterization of *Rho*^{+/-} P347S *RHO*⁺ mouse model by SD-OCT.

A) SD-OCT images of a C57Bl6J WT mouse retina (left) and a *Rho*^{+/-} P347S *RHO*⁺ mouse retina (right), both at P60. a= thickness of the whole retina; b= thickness of the ONL (outer nuclear layer) Scale bar= 50µm. B) Comparison of whole retina and ONL thicknesses, in WT mouse retina and *Rho*^{+/-} P347S *RHO*⁺ mouse retina. Statistical analysis=Mann-Whitney test, n=8.

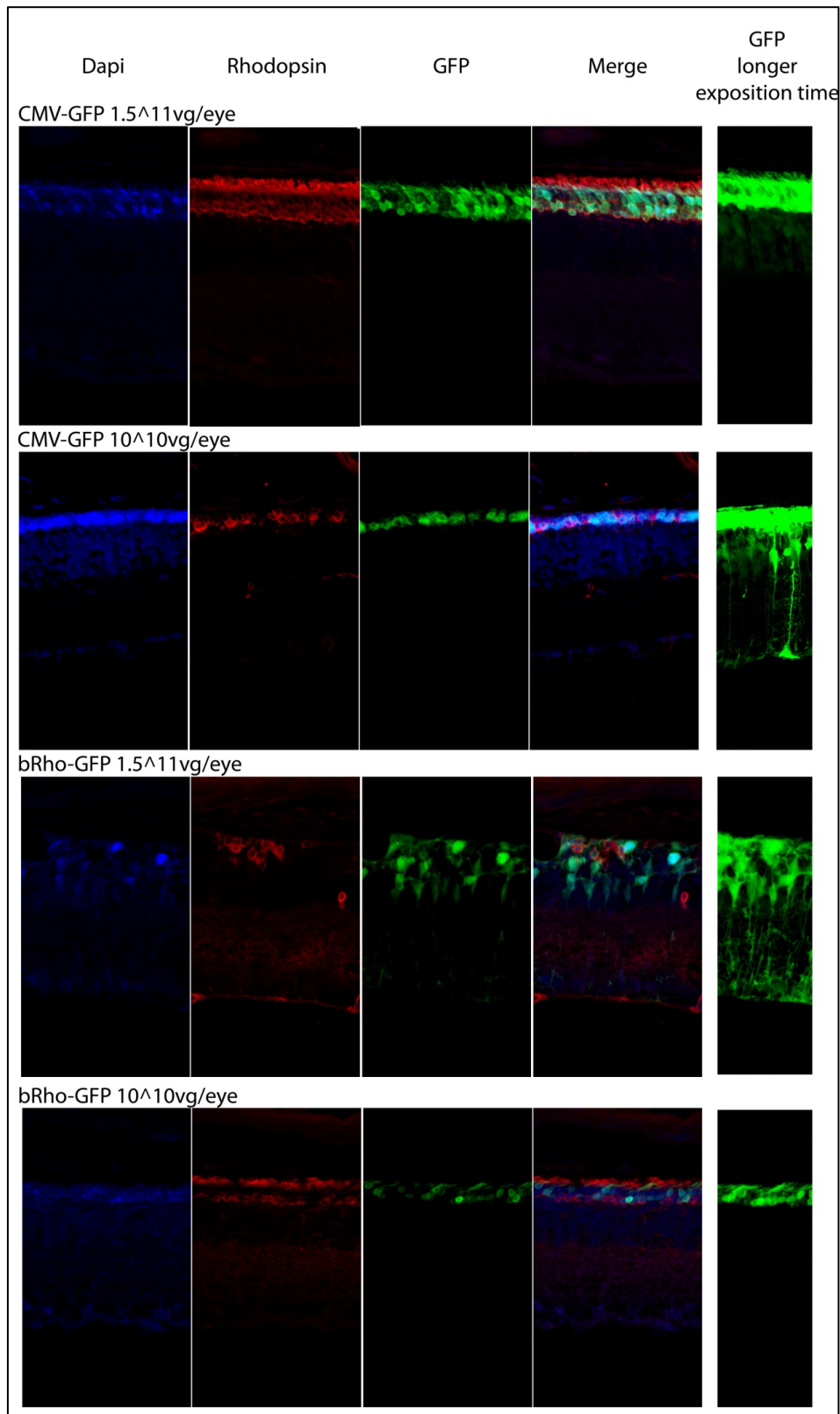


Figure 28: Comparison of bRho and CMV promoters, and test of two viral vector titers *in vivo*. Analysis by confocal microscopy of histological sections of *Rho*^{+/-} P347S *RHO*⁺ mouse retina subretinally injected by AAV2/8 *bRho*-GFP (lower panels) or AAV2/8 CMV-GFP (upper panels). Two titers of each AAV preparation have been tested and are mentioned on the top left corner of each panel. Sections have been labeled with DAPI (first column) and specific rhodopsin antibody (second column). The expression of GFP (without immunolabeling to intensify GFP detection) is also shown on the third column under low exposition time to avoid saturation, and on the fifth column after overexposition to visualize cells that express few quantities of GFP. The subretinal injection of 10¹⁰vg/eye of AAV2/8 *bRho*-GFP allows obtaining a specific expression in photoreceptors.

III.2.c. Effect of AAV2/8 bRho-PTM20 injection in *Rho*^{+/-} P347S *RHO*⁺ mice.

To study the effect of *trans*-splicing induced by PTM transduction *in vivo*, we co-injected a medium dose (8×10^{10} vg/eye) of AAV2/8 bRho-PTM0 or PTM20 and AAV2/8 bRho-GFP in a 1:7 ratio, in P23 to P30 *Rho*^{+/-} P347S *RHO*⁺ mice. One week later, quantification of *trans*-splicing events at the RNA level showed significant differences between GFP or PTM0 expression (values included in background) versus PTM20 expression, meaning that *trans*-splicing occurred *in vivo* (Figure 29 B). Moreover, we observed that the *trans*-splicing rate correlated with GFP expression observed on the eye fundus (Figure 29A). Nevertheless, the follow-up by SD-OCT of a second series of experiments in these mice from P30 to P60 showed that *trans*-splicing did not reduce or slow down PR degeneration compared to mice injected with PTM0 (data not shown). We concluded that maybe the *trans*-splicing rate was not enough to observe a therapeutic effect in the severe model of RP, or that AAV administration at P23 was already too late to prevent PR degeneration. We thus undertook the same injection at P3 to P5. Even if results sometimes allowed us to obtain pan-retinal expression of the transgene (Figure 30A), eyes were often damaged, with loss of lens transparency or abnormal pigmentation on eye fundus (Figure 30A). SD-OCT also revealed abnormalities in retinal layer structure and retinal detachment that did not spontaneously reverse (Figure 30B). We concluded that subretinal injections on P3 to P5 seemed to generate too many damages to follow potential benefits of a therapeutic strategy in the case of our model.

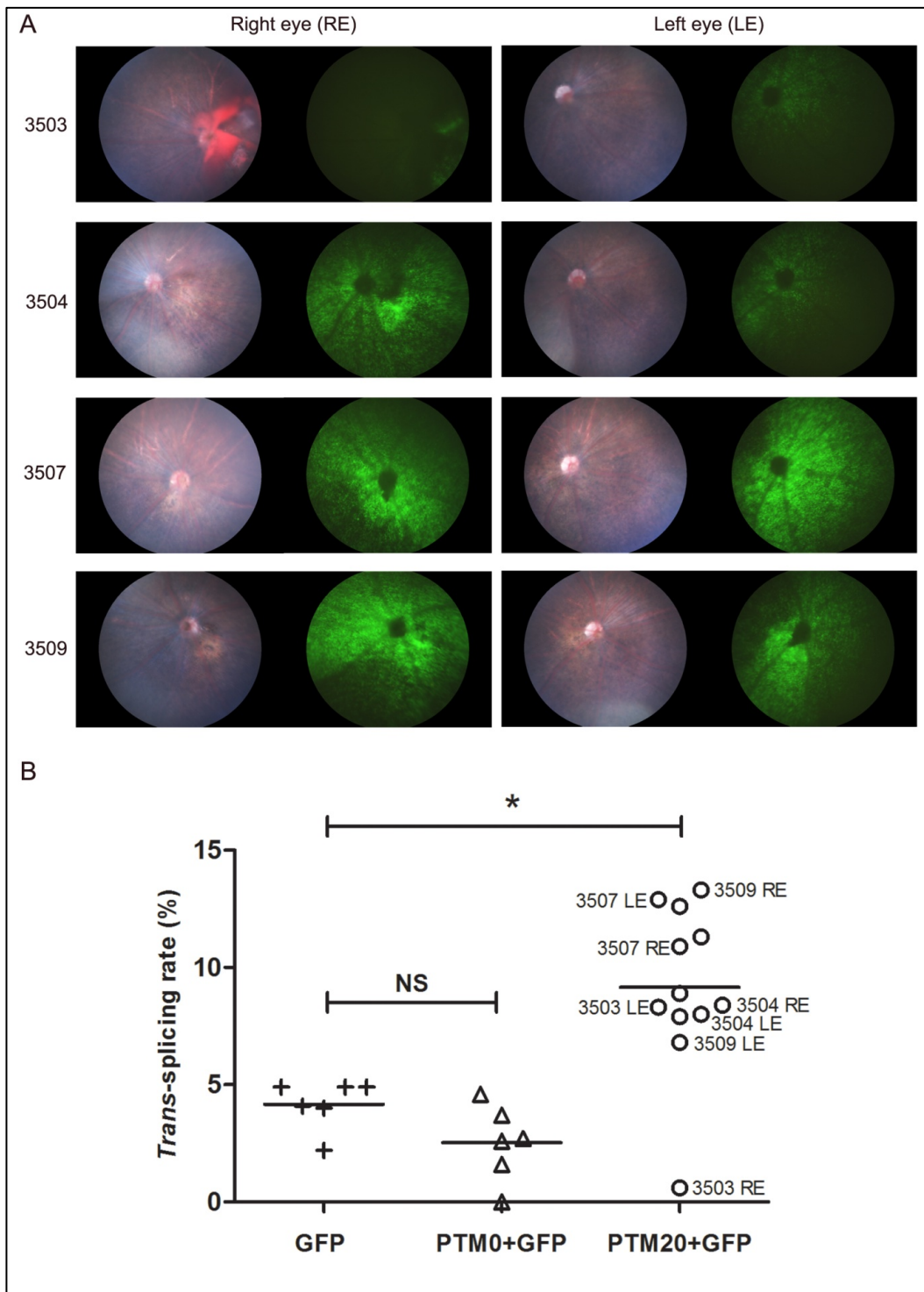


Figure 29: *Trans*-splicing efficiency determined *in vivo* after injection of AAV2/8 b*Rho*-PTM20 in *Rho*^{+/-} P347S *RHO*⁺ mice at P23.

A) Eye fundus of transduced retina with AAV2/8 b*Rho*-GFP and AAV2/8 b*Rho*-PTM20 in a 1:7 ratio. One week after subretinal injection, a color fundus (left picture) and a green fluorescence fundus (GFP detection, right picture) were performed. Numbers on the left of each panel correspond to mice identification numbers and are reported in B. B) Quantification at RNA level of *trans*-splicing rate on whole retina transduced by AAV2/8 b*Rho*-GFP alone (GFP) or co-transduced with AAV2/8 b*Rho*-PTM0 (PTM0+GFP) or AAV2/8 b*Rho*-PTM20 (PTM20+GFP) in a 1:7 ratio. Statistical analysis: Dunn's test. PTM20 induces *trans*-splicing events *in vivo*.

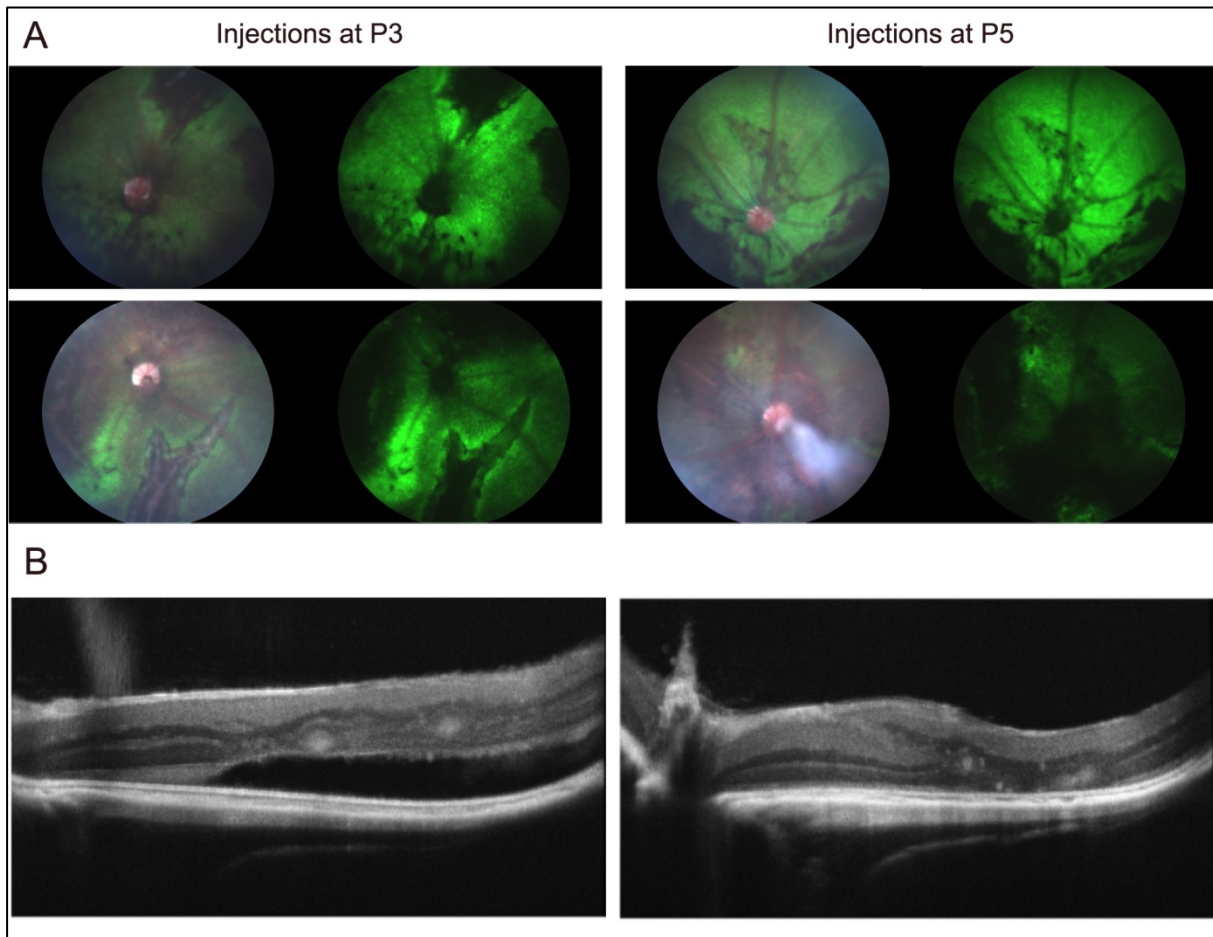


Figure 30: Subretinal injections at P3 to P5 in $Rho^{+/-}$ P347S RHO^{+} mice.

A) Eye fundus of transduced retina with AAV2/8 *bRho*-GFP. One month after subretinal injection, a color fundus (left picture) and a green fluorescence fundus (GFP detection, right picture) were performed. B) Observation of retina layers by SD-OCT one month after subretinal injection of AAV2/8 *bRho*-GFP in neonates. Retinas present some persistent detachment (left) or aberrant organization of layers (right).

DISCUSSION AND PERSPECTIVES

I. The PTM sequence: the key to efficient SMaRT technology.

As demonstrated in my PhD project and most SMaRT technology studies, the PTM sequence completely influences the *trans*-splicing efficiency. First of all, the size and the localization of the binding domain are crucial to promote *trans*-splicing. We have shown that a PTM can be totally inefficient (PTM2, 3, 11) or *trans*-splice $\frac{1}{4}$ of all rhodopsin RNA (PTM1) only by modifying its binding domain. This could be explained by several hypotheses that suggest the *trans*-splicing rate is most certainly influenced by combinatorial actions, including: (i) the size of the binding sequence, which determines its specificity and thus improves the binding probability if the sequence is highly specific (even if this is not the only parameter, regarding the fact that our PTM have all the same size and induce different *trans*-splicing rates) (ii) the accessibility of the PTM binding sequence and of the complementary sequence on the target pre-mRNA, which have to be available, i.e. not involved in stable secondary structures, (iii) the localization of the binding domain, which can more or less induce the proximity of the donor splice site and the acceptor one of both pre-mRNA molecules, or hide the endogenous acceptor splice site. Concerning this last strategy, it is important to keep in mind that targeting the endogenous acceptor splice site could also induce exon skipping or intron retention, thus modifying the final mRNA sequence. Moreover, while some studies have shown a real interest in the use of this strategy¹⁶⁵, others¹⁵⁵ including ours, demonstrated that benefits are not systematic. Risks of targeting the endogenous acceptor splice site must be considered.

Other modifications can be introduced into the PTM, such as addition of an intronic sequence, endogenous or artificial, into the replacement sequence^{28,162}. In our hands it was a real success, improving the *trans*-splicing rate from 25% to 40%. Nevertheless we also observed that the localization and the sequence of the intron seriously impacted *trans*-splicing rate. Indeed, while the restoration of the endogenous intron 3 into the PTM sequence or the addition of an artificial intron between exon 2 and 3 increased *trans*-splicing efficiency, the same artificial intron introduced in the middle of exon 3 decreased the *trans*-splicing rate. This demonstrates that the sequence of the intron is not sufficient to induce alone the splicing event. As described in the introduction (part III.1.c), the splicing mechanism is regulated by a combination of factors that promote or inhibit spliceosome recruitment, depending on specific sequences and their environment. We can thus imagine that located between two exons, the

intron helps the recruitment of splicing factors, while inserted into an exon, it participates in splicing repression for example by recruiting splicing factors that activate or repress splicing depending on their localization (see Introduction, part III.1.c). Finally, we conclude that in a general way, the addition of an intronic sequence between two exons of the PTM replacement sequence facilitates the *trans*-splicing reaction but not always with the same efficiency.

The last part of the PTM that can be modified is the artificial intronic sequence present between the binding domain and the replacement sequence. This one brings a functional branch point, a polypyrimidine tract and the 3' acceptor splice site, which are essential elements to generate the splice reaction in *trans*. It should also be possible to introduce specific sequences that recruit splicing factors (ISE for intronic splicing enhancer) but it is important to keep in mind that the secondary structure of the RNA is crucial at the 5' end of the PTM to keep the binding of the endogenous pre-mRNA as efficient as possible.

Unfortunately, concerning all these possibilities, there are currently no clear rules, and to date predictive tools are not potent enough to take into account all elements and predict the PTM efficiency with 100% confidence. In the current situation, the best way to select the most efficient PTM may be the use of screening systems, as developed by Koller *et al.*^{154,165}. Nevertheless, as discussed previously, the binding domain is not the only element that can dramatically influence the PTM efficiency, screening systems allowing testing of the effect that intronic sequence addition can have, for example, would also be required.

Another possibility is to favor PTM action by addition of a second RNA sequence, such as an ASO or a U7snRNA for example, which will inhibit *cis*-splicing or facilitate spliceosome recruitment. Nevertheless, even if they can be introduced into the same vector³⁴, this firstly implies the necessity to transport and generate transcripts of both molecules. Moreover, this also raises the question of the specificity of both sequences. The possible benefit should thus be precisely evaluated, compared to the risk.

II. How to achieve more *trans*-splicing than *cis*-splicing?

An important property of *trans*-splicing is that it does not repress the natural *cis*-splicing (except under particular conditions as described above), meaning that the quantity of synthesized proteins is unchanged, which is an advantage of this technology, particularly when targeting rhodopsin mutations. Nevertheless, to reach a production of WT protein

widely superior to that of mutated ones, the *trans*-splicing has to be the major splice event. To promote that, several issues have to be avoided:

- The coupling between transcription and splicing. Even if it is not essential for obtaining a splice event, splicing and transcription have been described to be relatively simultaneous (see Introduction, part II.1.c). This is due to the recruitment of elements for the splicing machinery by the carboxy-terminal domain of the polymerase II. A strategy to favor *trans*-splicing might be to slow down the transcription of rhodopsin pre-mRNA, or induce breaks in this step. However, it seems difficult to play on this ubiquitous mechanism by specifically acting on rhodopsin pre-mRNA, and a general modification on all pre-mRNA would be too dangerous for the cell. We can thus more easily imagine influencing the speed of action of PTM, by playing on its availability and its proximity with the target pre-mRNA as described below.

- The availability of the PTM is directly linked to its quantity. As shown by our experiments (see Results, part I), the ratio between the PTM and the target pre-mRNA modifies the *trans*-splicing rate. In physiological conditions, this means one must strive to express maximal PTM in the target cells.

- The last crucial point to increase *trans*-splicing efficiency is certainly to promote proximity between the PTM and the target pre-mRNA. Indeed, as for any tool that repairs RNA molecules, the first step is the recognition and the binding of the target pre-mRNA by the PTM. This implies that the PTM has to be localized near the transcription site of rhodopsin, to bind the RNA before *cis*-splicing occurs. By transfection or AAV transduction of the target cells, there is no control on the PTM transcription site, which can be anywhere in the nucleus. This certainly represents a major issue that reduces *trans*-splicing efficiency. To avoid losing PTM in the nucleus, we could imagine the future development of a viral vector that allows targeted integration. This last one would be useful to introduce the PTM sequence near its target gene, ensuring proximity between the two RNA.

In addition to these possibilities, we have to consider that we are not able to predict the minimal *trans*-splicing rate required to prevent rod degeneration. Indeed, as previously described (Introduction, part I.3.c), phenotype and severity of rhodopsin mutations are really heterogeneous, meaning that even if in several conditions a *trans*-splicing rate close to 100% could be achieved, in other cases a moderate *trans*-splicing rate may be enough to trigger a substantial therapeutic benefit.

III. The main drawbacks of PTM.

In my opinion, the two main drawbacks of SMaRT technology that could prevent its use in human therapeutic application relate to the PTM specificity, and its translation as a partial protein product.

- Concerning the first issue, we have not studied the non-specificity of our PTM in details. We have demonstrated that without a binding domain (PTM0), the *trans*-splicing rate was not significantly different from the background meaning that the binding domain allows specificity of the reaction as expected. Moreover, by PCR amplification with primers in exon 1 and 5, we obtained only one PCR product, corresponding to what was expected. This implies that there was no aberrant splicing of the rhodopsin pre-mRNA due to the presence of the PTM, as sometimes observed¹⁵⁶. We thus did not observe non-specific *trans*-splicing, but this result has to be confirmed further by RACE PCR or RNA sequencing, to validate the fact that the PTM does not interact with any other pre-mRNA in the cell.

- Regarding the translation of the PTM alone, we and others observed that this phenomenon is possible even if the PTM does not carry the major initiation ATG codon^{155,174}. This implies the production of a truncated protein, which lacks the N-terminus. If maybe it can be translated without consequences in some situations, we can easily imagine that in the case of rhodopsin, in which point mutations in its N-terminal domain lead to severe degeneration, the lack of this sequence could be really damaging. Moreover, it is not conceivable to create a therapeutic tool that could induce production of truncated proteins. To avoid this phenomenon, we tried to prevent the PTM translation by identifying a secondary ATG, able to initiate the translation mechanism. We localized the presence of a KOZAK sequence around one of the potential secondary initiation ATG codons, and mutated it to avoid the translation initiation. A KOZAK sequence is a consensus sequence present in eukaryotes, flanking the initiation ATG. However, the silent or missense (isoleucine to leucine) mutations that we have introduced did not prevent the synthesis of the truncated protein. Maybe the truncated protein was still produced because we did not target the correct initiation ATG, despite the fact that we targeted the secondary ATG, with the sequence the closest to the KOZAK one and which gave an ORF corresponding to the protein size observed on western blot. It is possible to directly mutate the ATG sequence to be sure that translation initiation is blocked, but as ATG is the only methionine-coding codon, it requires the utilization of a missense mutation. However, this alternative is not applicable to develop a

therapeutic tool because of consequences on both secondary and tertiary structures of the protein, and thus its interaction and function, which could be important.

Another possibility that we explored was to induce the transcription of the PTM under the control of a RNA polymerase III promoter. U6 is described as a strong and ubiquitous promoter, naturally used to control the transcription of non-coding small nuclear RNA by RNA polymerase III, what is diverted to produce shRNA. The idea behind using this promoter was to prevent the stability of PTM copies, which were not implicated in *trans*-splicing reaction, and their export to the cytoplasm by limiting their capping. Indeed, the cap is systematically added on the 5' extremity of each RNA transcribed by the RNA polymerase II, because capping enzymes are recruited by the C-terminal domain of the RNA polymerase II. By inducing the transcription of the PTM by the RNA polymerase III, capping of the RNA should be absent or reduced allowing the degradation of uncommitted PTM in subsequent *trans*-splicing reactions by exonucleases and/or reduce the cap-dependent translation initiation. Unfortunately, we did not succeed in obtaining an appropriate *trans*-splicing efficiency in these conditions. This can certainly be explained by the limited capacity of RNA polymerase III to transcribe long RNA, regarding the fact that it is naturally used to transcribe small RNA.

We can thus envision in the future the development of a system that following cleaving leads to the degradation of PTM specifically present in the cytoplasm, before the initiation of translation. Another possibility should be to induce the de-capping of PTM, but in a specific way, that seems to be difficult to achieve, knowing that the capping is a general mechanism of all RNA produced by RNA polymerase II.

Nonetheless, we surprisingly observed that this phenomenon of PTM translation alone did not occur *in vivo* in *Rho*^{-/-} mice. The subretinal co-injection of AAV2/8 b*Rho*-PTM 0 or 20 and AAV2/8 b*Rho*-GFP showed that the transduction and the transgene transcription were efficient in rods, thanks to the direct visualization of GFP *in vivo*, whereas no truncated protein was detected by western blot in these retina. We can speculate on several hypotheses to explain this difference, considering the points summarized in Table 5. First of all, this can be easily explained by the change from an *in vitro* system to *in vivo* one. A lot of studies have demonstrated that phenomenon observed *in vitro* can be difficult or even impossible to reproduce *in vivo*, only because experiments done on isolated cells cannot take into consideration all environmental and biological interactions that occur in an entire living organism. We can also imagine that the species can influence the translation: the PTM is mainly composed of human rhodopsin RNA, which can possess sequences that are not

	HEK 293T cells	<i>Rho</i>^{-/-} mouse model
System	in vitro	in vivo
Species	human	mouse
Cell introduction pathway	transient transfection	transduction
Vector	plasmid	AAV
Promoter	CMV	<i>bRho</i>

Table 5: Comparison of parameters used for the study of the PTM translation *in vitro* and *in vivo*.

recognized the same way in mouse cells compared to human. However, the probability of this hypothesis is quite low considering similarities between human and mouse rhodopsin exons. Another possibility could be that the PTM was expressed less following AAV2/8-mediated transduction of mouse rods with the bRho promoter, than following transient transfection of HEK293T cells with the CMV promoter. This could be due to the partial transduction of the retina, associated with the difference between CMV and *bRho* promoters, even if rhodopsin is highly expressed in rods. Despite the fact that we used GFP to provide an idea of transduction, transcription and translation efficiencies, we cannot estimate the quantity of PTM in retina samples compared to those of cell extracts. It is thus possible that a truncated protein was present *in vivo* after PTM transduction, but at a very low level. We can also imagine that the structure of the cell, which differs greatly between HEK293T and rods, can be implicated in the difference found between *in vivo* and *in vitro* results. Indeed, the particular localization of an RNA into the cytoplasm can induce its degradation²⁵. Neurons, and particularly rods, present an atypical organization that can require a specific localization of RNA to promote their translation. This localization being dependent of RNA-binding proteins and thus of the RNA sequence means PTM could be degraded into the cytoplasm while the entire rhodopsin RNA is not potentially explaining why the truncated protein was not observed in rods.

Generally eukaryotic cells possess a lot of RNA control systems that HEK293T cells could have lost regarding the fact that this cell line has been kept in cell culture for years. Indeed, considering that (i) more than 90% of the genes expressed in mammals are alternatively spliced and it has been estimated that almost half of them generate at least one form with a premature termination codon, (ii) and more than three-quarters of RNA pol II transcripts may be formed of noncoding RNA and be subject to rapid degradation²⁵, the eukaryotic cell has developed important RNA surveillance and degradation systems. A nuclear surveillance system checks newly synthesized RNA and transfers aberrant RNA (aberrantly processed, modified or misfolded) to the exosome that destroys them²⁴⁹, while nonsense-mediated decay, nonstop decay and no-go decay control the quality of translation in the cytoplasm²⁵⁰. All these systems are thus quite reassuring concerning the two main drawbacks of PTM described above. In case of PTM translation or off-target *trans*-splicing, we can hope that most of the time this will lead to generation of aberrant mRNA which can be detected by surveillance systems and degraded. Nevertheless, this will need to be assessed for each PTM design for which a clinical use is envisioned.

IV. Following-up potential beneficial effects in a humanized mouse model.

After the selection of the most efficient PTM *in vitro*, and the observation that no truncated protein seems to be produced from the PTM alone *in vivo*, we tried to observe and to quantify *trans*-splicing effect on rhodopsin mutations and rod degeneration *in vivo*. To that aim, we first of all worked on optical coherence tomography (OCT) to improve the output of our set-up (see Results, part 2). Indeed, because *retinitis pigmentosa* is a degenerative disease, we wanted to follow up the evolution of photoreceptors in presence of our PTM. Of course ERG gives functional information about the retina, and histology allows comparison of the cell state at the final time-point of the *in vivo* study, but OCT is one of the most powerful imaging tools to observe evolution of a given population of neurons in the same animal over time. We improved the image resolution by processing movies, and were able to undoubtedly identify outer retinal layers by comparing albino and pigmented animals, and by subretinal injections of oil. We used this technology with our improvements to follow up the rod degeneration in *Rho*^{-/-} mouse model already characterized by histology²⁵¹, and demonstrated that OCT can be used to obtain highly accurate values of outer retina layer thickness.

Next, we decided to test the PTM efficiency *in vivo* in mice bearing one wild type allele of mouse *Rho* and one mutant allele of human *RHO*, that we obtained in the first generation of a breeding between *Rho*^{-/-} knockout mice and P347S *RHO*^{+/+} transgenic mice. The subretinal injection of AAV2/8 bRho-PTM20 at P23 to P30 induced a *trans*-splicing rate of around 10% by quantification at the RNA level. This result is really encouraging and most likely significantly underestimated because it represents the *trans*-splicing rate of the entire retina, not only the transduced cells. Indeed, contrary to our experiments using cellular models, we did not specifically select PTM-expressing cells to estimate *trans*-splicing rate *in vivo*, meaning that *trans*-splicing was necessarily much higher in transduced cells.

The strain used carries a WT and a mutated rhodopsin allele, which allows recreation of a heterogeneous context, as usually found in rhodopsin-induced RP patients. Nonetheless, the WT rhodopsin copy is a mouse one, while the mutated copy is a human one. The fact is that when we quantified the *trans*-splicing rate at RNA level, we only analyzed *trans*-splicing events on the human pre-mRNA because primers used for PCR amplification were specific of the human sequence (Annex 1). Considering the high heterogeneity between mouse and human rhodopsin introns, the PTM reacts only with the human pre-mRNA. We thus

quantified *in vivo* the total *trans*-splicing events. In the context of two copies of the human rhodopsin alleles, we can thus imagine that the *trans*-splicing rate could be reduced from half. Nevertheless, we do not know exactly how many P347S *RHO*⁺ transgenes are present in these mice (several transgenes could be inserted in tandem), which implies that the number of mutated pre-mRNA could be equivalent to or even higher than a 2-human alleles system. Moreover, in my opinion the limiting factor of *trans*-splicing here is certainly not the quantity of PTM, but rather the speed of action. If this hypothesis is true, we should be able to obtain the same *trans*-splicing rate in patients that we observed in our animal model.

Because we do not know exactly what *trans*-splicing rate will be sufficient to prevent disease development, and it is certainly dependent on the implicated mutation, it is essential to study photoreceptor degeneration after PTM transduction, to conclude the potential benefits of *trans*-splicing. Unfortunately, the *trans*-splicing rate we observed *in vivo* was not sufficient to induce a phenotype rescue. Indeed, we observed no difference on OCT measurement one month after injection between mice treated with AAV-GFP alone or co-injected with AAV-PTM0 or 20. Several hypotheses can explain this result:

- The *trans*-splicing rate was too weak to generate enough repaired proteins to stop the photoreceptor degenerative process,
- The transduced cells were too few to obtain a visible effect *in vivo*,
- The *Rho*^{+/-} P347S *RHO*⁺ mouse model presents a degeneration too advanced at P23-P30 (the time of injection) to stop the degenerative process.

To address the third issue, we tried a subretinal injection at P3 to P5, and the consequences on the retina and the eye in general were dramatic, leading to reorganization of the retinal layers. Another possibility that we will develop in the future will be an intracardiac injection using pups (P3 to P5) with an AAV2/9 2YF bRho-PTM 20 (this serotype has already been described to efficiently target PR using this method²⁵²). By injecting 10% fluorescein in the heart of P3 to P4 mice, we have already clearly demonstrated the feasibility of the injection, and paved the way for AAV2/9 Y2F bRho-PTM20 injection (Figure 31). This strategy should allow targeting of the photoreceptors at an early stage, and in a pan retinal way.

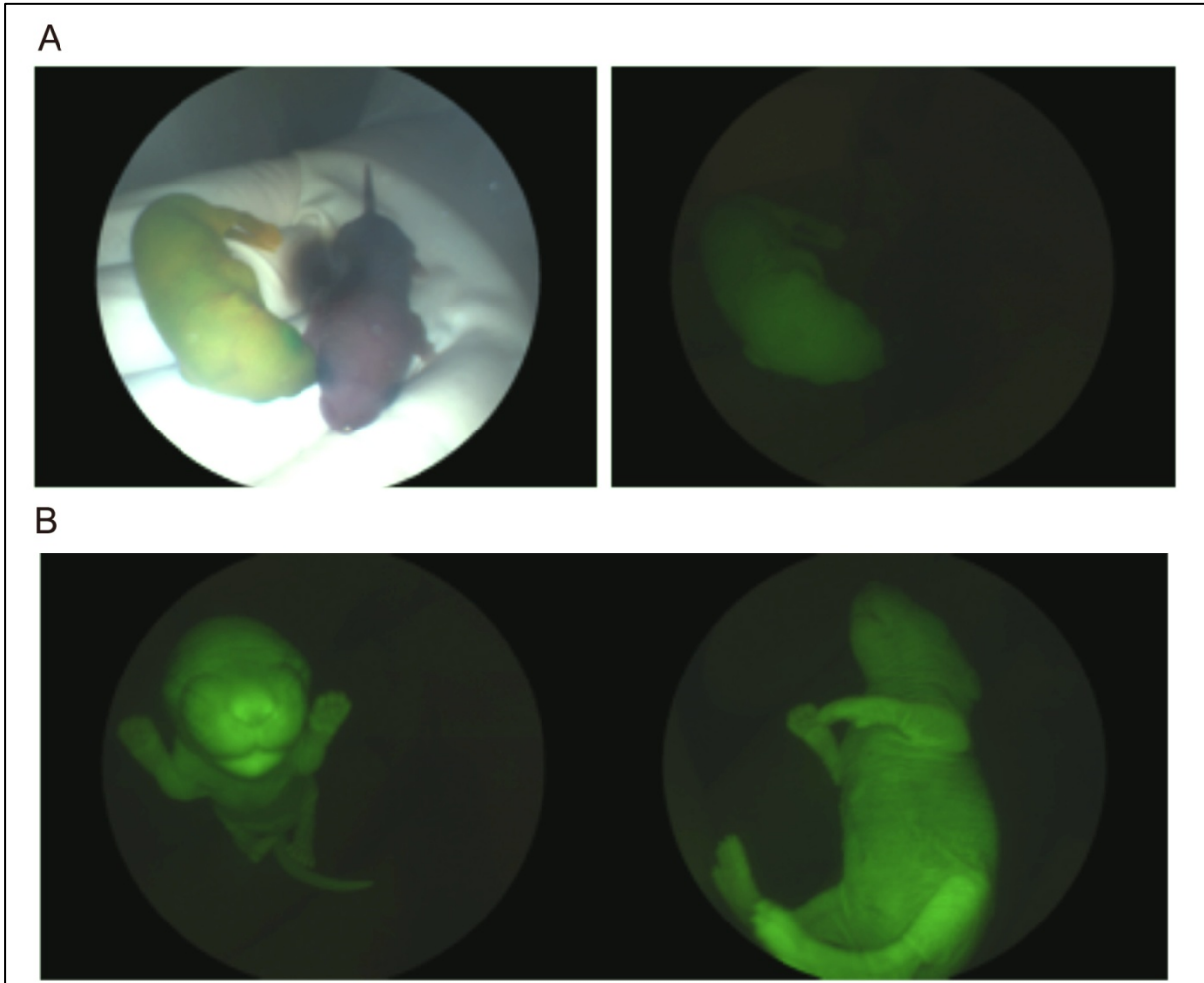


Figure 31: Intracardiac injections of fluorescein in C57Bl6J mice at P4.

A) 24 hours after intracardiac injection of fluorescein, one injected pup (on the left) and one non-injected pup (on the right) were exposed to white light (left panel) or GFP filter to visualize fluorescein (right panel) on microm III. B) Observation of fluorescein in one injected pup on microm III with GFP filter.

V. Envisaging a therapeutic application in humans.

My conclusion about our work on *trans*-splicing is that some questions about PTM specificity and translation still require exploration, but the results obtained in this study pave the way for a use of SMaRT technology to prevent *retinitis pigmentosa* due to mutated rhodopsin, for which there is still no treatment. Nevertheless, the proof of efficacy *in vivo* is still required before thinking about the next step.

The classical approach to each new therapeutic tool is to achieve the proof of concept in cell and/or small animal models, before confirming results in a study using bigger animals, like non-human primates. Since there is no relevant model for our study in larger species (with the whole human rhodopsin gene) this step would only be useful to implement biodistribution and toxicity tests.

Finally, considering that the 120 rhodopsin mutations are localized along all the protein sequence, and that P23H is one of the most prevalent particularly in American population, we can also imagine developing a 5' *trans*-splicing tool to repair all mutations present in exon 1. Indeed, it is possible to create a PTM that promotes *trans*-splicing with the endogenous rhodopsin pre-mRNA and replaces the exon 1 (as described in Figure 32). Nevertheless, only a limited number of 5' *trans*-splicing studies have been implemented to date^{28,152,167}, meaning that only limited data has been collected on this strategy. Development of strategies to improve efficiency and prevent PTM translation are now required, considering that this PTM will obviously possess the translation initiation ATG codon (but will be devoid of any polyadenylation signal).

VI. The future of therapeutic strategies to prevent mutant rhodopsin expression.

Among current strategies developed today to prevent the RP development due to the expression of a mutated RHO, we can easily imagine a great future for several strategies:

-the use of RNAi coupled to normal gene expression. The RNAi field has shown an explosive development these last decades in a lot of different disease contexts, evidence of the efficiency of this technology. The proof of principle of this strategy has already been obtained in the case of rhodopsin (see Introduction, part II.2.b), and will certainly provide an

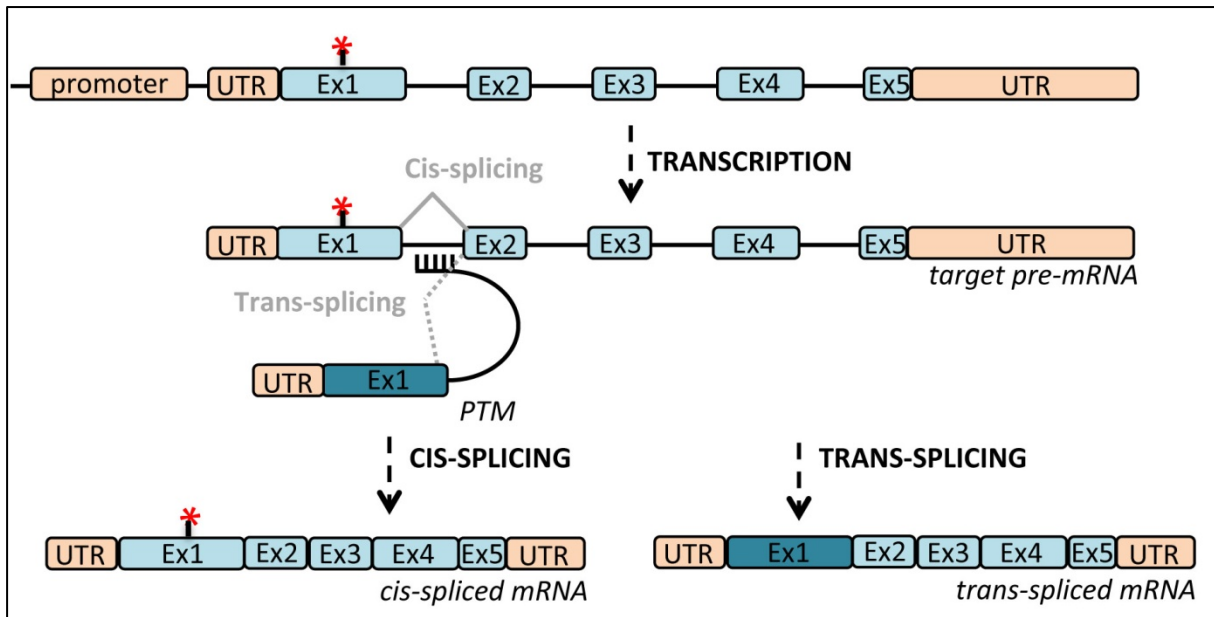


Figure 32: SMART technology for rhodopsin RNA with 5' *trans*-splicing approach.

The PTM is composed of the 5'UTR and the exon1 of rhodopsin RNA, followed by an intronic sequence and a binding domain that targets the intron 1 of endogenous rhodopsin pre-mRNA. In this case, the PTM construct is devoid of a polyadenylation signal. The *trans*-splicing reaction induced by the PTM allows generating a rhodopsin mRNA devoid of any mutation in exon1.

interesting therapeutic approach at least in the case of mutation-dependent systems, particularly for the P23H mutation. Nonetheless, potential off-target effects should be considered.

-an endonuclease combined to a homologous sequence. Regarding the numerous endonuclease based-systems that exist, the most hopeful in a general way and which will be certainly for rhodopsin, is the CRISPR system. Nevertheless, this strategy is mutation-dependent and thus requires the development of as many tools as there are mutations.

Even if these approaches can reach clinical trials for humans, the necessity of a normal rhodopsin expression level should be kept in mind and could be one of the major issues.

The fact that SMaRT technology respects the endogenous expression level, and that only two PTM would be sufficient to repair all rhodopsin mutations represent two essential advantages, which promise a great future for SMaRT technology even if the road ahead is still long.

VII. Considering gene therapies for retinal diseases over the next few decades.

Gene therapy for gene-replacement in retinal diseases has recently shown an important progression, with the pioneer study done on LCA, showing great beneficial effects on humans without notable side effects. This study brings proof that gene therapy can be safely applied to ocular diseases, and thus opens the door to gene therapy for all other monogenic retinal diseases. The gene-replacement strategy requires acting before the total degeneration of gene-expressing cells occurs, and implies development of a specific approach for each disease-causing gene. To increase the possibilities, gene therapies for neuroprotection and optogenetic approaches are currently progressing. These allow respectively (i) protection of remaining cells from the degenerative process to slow down the disease progression, and (ii) development in an unaffected cell type of properties lost in degenerative cells (Figure 33) as for example the possibility to integrate photons in bipolar or ganglion cells instead of PR. It is essential to combine these different approaches, to bring a therapeutic solution for each case of retinal disease, depending on the evolution step of the disease. All these strategies require nonetheless an efficient and safe vector and injection route. AAV vectors seem to be the most promising vector to target the retina. Moreover, the development of new AAV serotypes increasingly specific and efficient in targeting and transducing retinal cells opens the door to

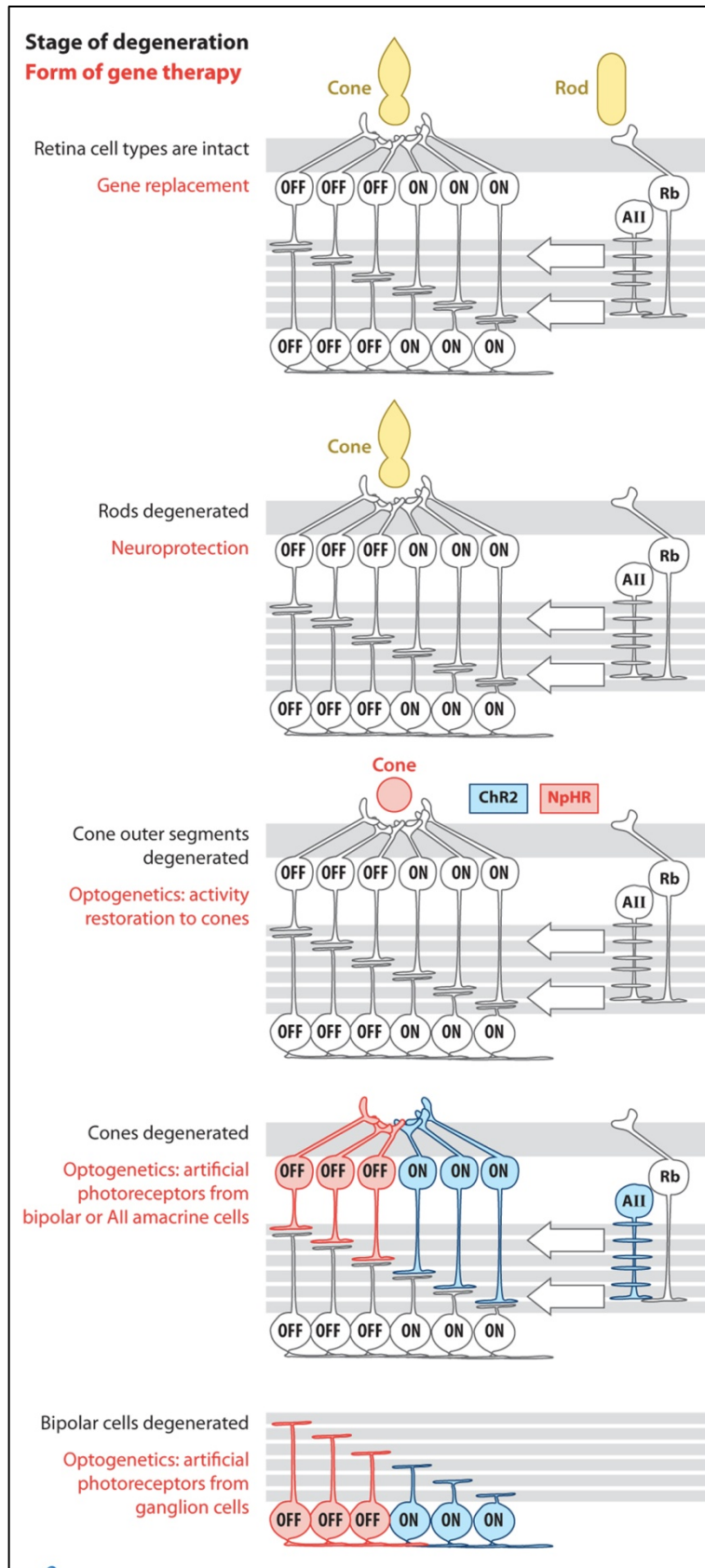


Figure 33: Stages of retinal degeneration and the forms of gene therapy that can be used in that stage.

Extracted from *Sahel and Roska, Annual review of Neuroscience, 2013.*

new clinical applications in eye diseases. In my opinion, the main issue in the application of gene therapy in humans is now certainly linked to the injection route of the viral vector. Subretinal injections generate a retinal detachment that often does not persist, but can induce some damage if it occurs on the fovea²⁵³. The generation of AAV vectors able to efficiently transduce retinal cells after intravitreal injection is currently an ongoing work and represents a new step to make safer retinal therapeutic approaches.

It seems clear that gene therapy will have a promising future in treatment of retinal diseases, considering the rapid progression in the last decades in terms of efficiency of targeting, transduction and safety. This strategy remains the only viable option that can act at the origin of the disease, by directly linking genotype and phenotype.

BIBLIOGRAPHY

- 1 Rieke F, Baylor DA. Single-photon detection by rod cells of the retina. *Rev Mod Phys* 1998; **70**: 1027–1036.
- 2 Nathans J, Hogness DS. Isolation and nucleotide sequence of the gene encoding human rhodopsin. *Proc Natl Acad Sci U S A* 1984; **81**: 4851–4855.
- 3 Palczewski K. G protein-coupled receptor rhodopsin. *Annu Rev Biochem* 2006; **75**: 743–767.
- 4 Mendes HF, van der Spuy J, Chapple JP, Cheetham ME. Mechanisms of cell death in rhodopsin retinitis pigmentosa: implications for therapy. *Trends Mol Med* 2005; **11**: 177–185.
- 5 Chan F, Hauswirth WW, Wensel TG, Wilson JH. Efficient mutagenesis of the rhodopsin gene in rod photoreceptor neurons in mice. *Nucleic Acids Res* 2011; **39**: 5955–5966.
- 6 Greenwald DL, Cashman SM, Kumar-Singh R. Engineered zinc finger nuclease-mediated homologous recombination of the human rhodopsin gene. *Invest Ophthalmol Vis Sci* 2010; **51**: 6374–6380.
- 7 Mussolino C, Sanges D, Marrocco E, Bonetti C, Di Vicino U, Marigo V *et al*. Zinc-finger-based transcriptional repression of rhodopsin in a model of dominant retinitis pigmentosa. *EMBO Mol Med* 2011; **3**: 118–128.
- 8 Chadderton N, Millington-Ward S, Palfi A, O'Reilly M, Tuohy G, Humphries MM *et al*. Improved Retinal Function in a Mouse Model of Dominant Retinitis Pigmentosa Following AAV-delivered Gene Therapy. *Mol Ther* 2009; **17**: 593–599.
- 9 Mao H, Gorbatyuk MS, Rossmiller B, Hauswirth WW, Lewin AS. Long-term rescue of retinal structure and function by rhodopsin RNA replacement with a single adeno-associated viral vector in P23H RHO transgenic mice. *Hum Gene Ther* 2012; **23**: 356–366.
- 10 Greenwald DL, Cashman SM, Kumar-Singh R. Mutation-independent rescue of a novel mouse model of Retinitis Pigmentosa. *Gene Ther* 2013; **20**: 425–434.
- 11 LaVail MM, Yasumura D, Matthes MT, Drenser KA, Flannery JG, Lewin AS *et al*. Ribozyme rescue of photoreceptor cells in P23H transgenic rats: long-term survival and late-stage therapy. *Proc Natl Acad Sci U S A* 2000; **97**: 11488–11493.
- 12 Gorbatyuk M, Justilien V, Liu J, Hauswirth WW, Lewin AS. Preservation of photoreceptor morphology and function in P23H rats using an allele independent ribozyme. *Exp Eye Res* 2007; **84**: 44–52.
- 13 LaVail MM, Yasumura D, Matthes MT, Lau-Villacorta C, Unoki K, Sung CH *et al*. Protection of mouse photoreceptors by survival factors in retinal degenerations. *Invest*

Ophthalmol Vis Sci 1998; **39**: 592–602.

14 Sieving PA, Caruso RC, Tao W, Coleman HR, Thompson DJS, Fullmer KR *et al*. Ciliary neurotrophic factor (CNTF) for human retinal degeneration: Phase I trial of CNTF delivered by encapsulated cell intraocular implants. *Proc Natl Acad Sci U S A* 2006; **103**: 3896–3901.

15 Pearson RA, Barber AC, Rizzi M, Hippert C, Xue T, West EL *et al*. Restoration of vision after transplantation of photoreceptors. *Nature* 2012; **485**: 99–103.

16 Barber AC, Hippert C, Duran Y, West EL, Bainbridge JWB, Warre-Cornish K *et al*. Repair of the degenerate retina by photoreceptor transplantation. *Proc Natl Acad Sci* 2013; **110**: 354–359.

17 Gonzalez-Cordero A, West EL, Pearson RA, Duran Y, Carvalho LS, Chu CJ *et al*. Photoreceptor precursors derived from three-dimensional embryonic stem cell cultures integrate and mature within adult degenerate retina. *Nat Biotechnol* 2013; **31**: 741–747.

18 Warre-Cornish K, Barber AC, Sowden JC, Ali RR, Pearson RA. Migration, Integration and Maturation of Photoreceptor Precursors Following Transplantation in the Mouse Retina. *Stem Cells Dev* 2013. doi:10.1089/scd.2013.0471.

19 Lagali PS, Balya D, Awatramani GB, Münch TA, Kim DS, Busskamp V *et al*. Light-activated channels targeted to ON bipolar cells restore visual function in retinal degeneration. *Nat Neurosci* 2008; **11**: 667–675.

20 Doroudchi MM, Greenberg KP, Liu J, Silka KA, Boyden ES, Lockridge JA *et al*. Virally delivered channelrhodopsin-2 safely and effectively restores visual function in multiple mouse models of blindness. *Mol Ther J Am Soc Gene Ther* 2011; **19**: 1220–1229.

21 Busskamp V, Duebel J, Balya D, Fradot M, Viney TJ, Siegert S *et al*. Genetic reactivation of cone photoreceptors restores visual responses in retinitis pigmentosa. *Science* 2010; **329**: 413–417.

22 Macé E, Caplette R, Marre O, Sengupta A, Chaffiol A, Barbe P *et al*. Targeting channelrhodopsin-2 to ON-bipolar cells with vitreally administered AAV restores ON and OFF visual responses in blind mice. *Mol Ther J Am Soc Gene Ther* 2014. doi:10.1038/mt.2014.154.

23 Da Cruz L, Coley BF, Dorn J, Merlini F, Filley E, Christopher P *et al*. The Argus II epiretinal prosthesis system allows letter and word reading and long-term function in patients with profound vision loss. *Br J Ophthalmol* 2013; **97**: 632–636.

24 Chuang AT, Margo CE, Greenberg PB. Retinal implants: a systematic review. *Br J Ophthalmol* 2014. doi:10.1136/bjophthalmol-2013-303708.

25 *Lewin's Genes XI*. Jones & Bartlett Publishers, 2014.

- 26 Valadkhan S, Jaladat Y. The spliceosomal proteome: at the heart of the largest cellular ribonucleoprotein machine. *Proteomics* 2010; **10**: 4128–4141.
- 27 Puttaraju M, Jamison SF, Mansfield SG, Garcia-Blanco MA, Mitchell LG. Spliceosome-mediated RNA trans-splicing as a tool for gene therapy. *Nat Biotechnol* 1999; **17**: 246–252.
- 28 Mansfield SG, Clark RH, Puttaraju M, Kole J, Cohn JA, Mitchell LG *et al.* 5' exon replacement and repair by spliceosome-mediated RNA trans-splicing. *RNA N Y N* 2003; **9**: 1290–1297.
- 29 Mansfield SG, Kole J, Puttaraju M, Yang CC, Garcia-Blanco MA, Cohn JA *et al.* Repair of CFTR mRNA by spliceosome-mediated RNA trans-splicing. *Gene Ther* 2000; **7**: 1885–1895.
- 30 Liu X, Jiang Q, Mansfield SG, Puttaraju M, Zhang Y, Zhou W *et al.* Partial correction of endogenous DeltaF508 CFTR in human cystic fibrosis airway epithelia by spliceosome-mediated RNA trans-splicing. *Nat Biotechnol* 2002; **20**: 47–52.
- 31 Liu X, Luo M, Zhang LN, Yan Z, Zak R, Ding W *et al.* Spliceosome-mediated RNA trans-splicing with recombinant adeno-associated virus partially restores cystic fibrosis transmembrane conductance regulator function to polarized human cystic fibrosis airway epithelial cells. *Hum Gene Ther* 2005; **16**: 1116–1123.
- 32 Chao H, Mansfield SG, Bartel RC, Hiriyan S, Mitchell LG, Garcia-Blanco MA *et al.* Phenotype correction of hemophilia A mice by spliceosome-mediated RNA trans-splicing. *Nat Med* 2003; **9**: 1015–1019.
- 33 Shababi M, Lorson CL. Optimization of SMN trans-splicing through the analysis of SMN introns. *J Mol Neurosci MN* 2012; **46**: 459–469.
- 34 Coady TH, Lorson CL. Trans-splicing-mediated improvement in a severe mouse model of spinal muscular atrophy. *J Neurosci Off J Soc Neurosci* 2010; **30**: 126–130.
- 35 Coady TH, Baughan TD, Shababi M, Passini MA, Lorson CL. Development of a single vector system that enhances trans-splicing of SMN2 transcripts. *PloS One* 2008; **3**: e3468.
- 36 Coady TH, Shababi M, Tullis GE, Lorson CL. Restoration of SMN function: delivery of a trans-splicing RNA re-directs SMN2 pre-mRNA splicing. *Mol Ther J Am Soc Gene Ther* 2007; **15**: 1471–1478.
- 37 Tahara M, Pergolizzi RG, Kobayashi H, Krause A, Luettich K, Lesser ML *et al.* Trans-splicing repair of CD40 ligand deficiency results in naturally regulated correction of a mouse model of hyper-IgM X-linked immunodeficiency. *Nat Med* 2004; **10**: 835–841.
- 38 Sung C-H, Chuang J-Z. The cell biology of vision. *J Cell Biol* 2010; **190**: 953–963.

- 39 Panda-Jonas S, Jonas JB, Jakobczyk M, Schneider U. Retinal photoreceptor count, retinal surface area, and optic disc size in normal human eyes. *Ophthalmology* 1994; **101**: 519–523.
- 40 Young RW, Bok D. Participation of the retinal pigment epithelium in the rod outer segment renewal process. *J Cell Biol* 1969; **42**: 392–403.
- 41 Farrar GJ, Kenna PF, Humphries P. On the genetics of retinitis pigmentosa and on mutation-independent approaches to therapeutic intervention. *EMBO J* 2002; **21**: 857–864.
- 42 Milam AH, Li ZY, Fariss RN. Histopathology of the human retina in retinitis pigmentosa. *Prog Retin Eye Res* 1998; **17**: 175–205.
- 43 Fahim AT, Daiger SP, Weleber RG. Retinitis Pigmentosa Overview. In: Pagon RA, Adam MP, Bird TD, Dolan CR, Fong C-T, Smith RJ *et al.* (eds). *GeneReviews*(®). University of Washington, Seattle: Seattle (WA), 1993<http://www.ncbi.nlm.nih.gov/books/NBK1417/> (accessed 16 Apr2014).
- 44 Hartong DT, Berson EL, Dryja TP. Retinitis pigmentosa. *Lancet* 2006; **368**: 1795–1809.
- 45 Petit C. Usher syndrome: from genetics to pathogenesis. *Annu Rev Genomics Hum Genet* 2001; **2**: 271–297.
- 46 Laurence JZ, Moon RC. Four cases of ‘retinitis pigmentosa’ occurring in the same family, and accompanied by general imperfections of development. 1866. *Obes Res* 1995; **3**: 400–403.
- 47 Sheffield VC, Nishimura D, Stone EM. The molecular genetics of Bardet–Biedl syndrome. *Curr Opin Genet Dev* 2001; **11**: 317–321.
- 48 Wierzbicki AS, Lloyd MD, Schofield CJ, Feher MD, Gibberd FB. Refsum’s disease: a peroxisomal disorder affecting phytanic acid α -oxidation. *J Neurochem* 2002; **80**: 727–735.
- 49 Jones JW, Ways P. Abnormalities of High Density Lipoproteins in Abetalipoproteinemia*. *J Clin Invest* 1967; **46**: 1151–1161.
- 50 Ouahchi K, Arita M, Kayden H, Hentati F, Ben Hamida M, Sokol R *et al.* Ataxia with isolated vitamin E deficiency is caused by mutations in the alpha-tocopherol transfer protein. *Nat Genet* 1995; **9**: 141–145.
- 51 McWilliam P, Farrar GJ, Kenna P, Bradley DG, Humphries MM, Sharp EM *et al.* Autosomal dominant retinitis pigmentosa (ADRP): localization of an ADRP gene to the long arm of chromosome 3. *Genomics* 1989; **5**: 619–622.
- 52 Hargrave PA, McDowell JH. Rhodopsin and phototransduction: a model system

- for G protein-linked receptors. *FASEB J Off Publ Fed Am Soc Exp Biol* 1992; **6**: 2323–2331.
- 53 Ripps H, Weale RA. Rhodopsin Regeneration in Man. *Nature* 1969; **222**: 775–777.
- 54 Palczewski K. Chemistry and biology of vision. *J Biol Chem* 2012; **287**: 1612–1619.
- 55 Sung CH, Makino C, Baylor D, Nathans J. A rhodopsin gene mutation responsible for autosomal dominant retinitis pigmentosa results in a protein that is defective in localization to the photoreceptor outer segment. *J Neurosci Off J Soc Neurosci* 1994; **14**: 5818–5833.
- 56 Audo I, Manes G, Mohand-Saïd S, Friedrich A, Lancelot M-E, Antonio A *et al*. Spectrum of rhodopsin mutations in French autosomal dominant rod-cone dystrophy patients. *Invest Ophthalmol Vis Sci* 2010; **51**: 3687–3700.
- 57 Lem J, Krasnoperova NV, Calvert PD, Kosaras B, Cameron DA, Nicolò M *et al*. Morphological, physiological, and biochemical changes in rhodopsin knockout mice. *Proc Natl Acad Sci U S A* 1999; **96**: 736–741.
- 58 Sung CH, Schneider BG, Agarwal N, Papermaster DS, Nathans J. Functional heterogeneity of mutant rhodopsins responsible for autosomal dominant retinitis pigmentosa. *Proc Natl Acad Sci U S A* 1991; **88**: 8840–8844.
- 59 Sung CH, Davenport CM, Nathans J. Rhodopsin mutations responsible for autosomal dominant retinitis pigmentosa. Clustering of functional classes along the polypeptide chain. *J Biol Chem* 1993; **268**: 26645–26649.
- 60 Kunte MM, Choudhury S, Manheim JF, Shinde VM, Miura M, Chiodo VA *et al*. ER stress is involved in T17M rhodopsin-induced retinal degeneration. *Invest Ophthalmol Vis Sci* 2012; **53**: 3792–3800.
- 61 Gorbatyuk MS, Knox T, LaVail MM, Gorbatyuk OS, Noorwez SM, Hauswirth WW *et al*. Restoration of visual function in P23H rhodopsin transgenic rats by gene delivery of BiP/Grp78. *Proc Natl Acad Sci U S A* 2010; **107**: 5961–5966.
- 62 Sakami S, Maeda T, Bereta G, Okano K, Golczak M, Sumaroka A *et al*. Probing mechanisms of photoreceptor degeneration in a new mouse model of the common form of autosomal dominant retinitis pigmentosa due to P23H opsin mutations. *J Biol Chem* 2011; **286**: 10551–10567.
- 63 Olsson JE, Gordon JW, Pawlyk BS, Roof D, Hayes A, Molday RS *et al*. Transgenic mice with a rhodopsin mutation (Pro23His): A mouse model of autosomal dominant retinitis pigmentosa. *Neuron* 1992; **9**: 815–830.
- 64 Saliba RS, Munro PMG, Luthert PJ, Cheetham ME. The cellular fate of mutant rhodopsin: quality control, degradation and aggresome formation. *J Cell Sci* 2002; **115**:

2907–2918.

65 Chen Y-F, Wang I-J, Lin LLK, Chen M-S. Examining rhodopsin retention in endoplasmic reticulum and intracellular localization in vitro and in vivo by using truncated rhodopsin fragments. *J Cell Biochem* 2011; **112**: 520–530.

66 Li T, Snyder WK, Olsson JE, Dryja TP. Transgenic mice carrying the dominant rhodopsin mutation P347S: evidence for defective vectorial transport of rhodopsin to the outer segments. *Proc Natl Acad Sci U S A* 1996; **93**: 14176–14181.

67 Chuang J-Z, Vega C, Jun W, Sung C-H. Structural and functional impairment of endocytic pathways by retinitis pigmentosa mutant rhodopsin-arrestin complexes. *J Clin Invest* 2004; **114**: 131–140.

68 Li T, Franson WK, Gordon JW, Berson EL, Dryja TP. Constitutive activation of phototransduction by K296E opsin is not a cause of photoreceptor degeneration. *Proc Natl Acad Sci U S A* 1995; **92**: 3551–3555.

69 Lem J, Fain GL. Constitutive opsin signaling: night blindness or retinal degeneration? *Trends Mol Med* 2004; **10**: 150–157.

70 Humphries MM, Rancourt D, Farrar GJ, Kenna P, Hazel M, Bush RA *et al.* Retinopathy induced in mice by targeted disruption of the rhodopsin gene. *Nat Genet* 1997; **15**: 216–219.

71 Dykens JA, Carroll AK, Wiley S, Covey DF, Cai ZY, Zhao L *et al.* Photoreceptor preservation in the S334ter model of retinitis pigmentosa by a novel estradiol analog. *Biochem Pharmacol* 2004; **68**: 1971–1984.

72 Barone I, Novelli E, Piano I, Gargini C, Strettoi E. Environmental enrichment extends photoreceptor survival and visual function in a mouse model of retinitis pigmentosa. *PLoS One* 2012; **7**: e50726.

73 Emerich DF, Thanos CG. NT-501: an ophthalmic implant of polymer-encapsulated ciliary neurotrophic factor-producing cells. *Curr Opin Mol Ther* 2008; **10**: 506–515.

74 Berson EL, Rosner B, Sandberg MA, Hayes KC, Nicholson BW, Weigel-DiFranco C *et al.* A randomized trial of vitamin A and vitamin E supplementation for retinitis pigmentosa. *Arch Ophthalmol* 1993; **111**: 761–772.

75 Feskanich D, Singh V, Willett WC, Colditz GA. Vitamin A intake and hip fractures among postmenopausal women. *JAMA J Am Med Assoc* 2002; **287**: 47–54.

76 Michaëlsson K, Lithell H, Vessby B, Melhus H. Serum retinol levels and the risk of fracture. *N Engl J Med* 2003; **348**: 287–294.

77 Lammer EJ, Chen DT, Hoar RM, Agnish ND, Benke PJ, Braun JT *et al.* Retinoic acid embryopathy. *N Engl J Med* 1985; **313**: 837–841.

- 78 Hoffman DR, Locke KG, Wheaton DH, Fish GE, Spencer R, Birch DG. A randomized, placebo-controlled clinical trial of docosahexaenoic acid supplementation for X-linked retinitis pigmentosa. *Am J Ophthalmol* 2004; **137**: 704–718.
- 79 Bahrami H, Melia M, Dagnelie G. Lutein supplementation in retinitis pigmentosa: PC-based vision assessment in a randomized double-masked placebo-controlled clinical trial [NCT00029289]. *BMC Ophthalmol* 2006; **6**: 23.
- 80 Kamao H, Mandai M, Okamoto S, Sakai N, Suga A, Sugita S *et al*. Characterization of human induced pluripotent stem cell-derived retinal pigment epithelium cell sheets aiming for clinical application. *Stem Cell Rep* 2014; **2**: 205–218.
- 81 Léveillard T, Fridlich R, Clérin E, Aït-Ali N, Millet-Puel G, Jaillard C *et al*. Therapeutic strategy for handling inherited retinal degenerations in a gene-independent manner using rod-derived cone viability factors. *C R Biol* 2014; **337**: 207–213.
- 82 Yang Y, Mohand-Said S, Danan A, Simonutti M, Fontaine V, Clerin E *et al*. Functional cone rescue by RdCVF protein in a dominant model of retinitis pigmentosa. *Mol Ther J Am Soc Gene Ther* 2009; **17**: 787–795.
- 83 Mao H, James T Jr, Schwein A, Shabashvili AE, Hauswirth WW, Gorbatyuk MS *et al*. AAV delivery of wild-type rhodopsin preserves retinal function in a mouse model of autosomal dominant retinitis pigmentosa. *Hum Gene Ther* 2011; **22**: 567–575.
- 84 Griciuc A, Aron L, Piccoli G, Ueffing M. Clearance of Rhodopsin(P23H) aggregates requires the ERAD effector VCP. *Biochim Biophys Acta* 2010; **1803**: 424–434.
- 85 Gorbatyuk MS, Knox T, LaVail MM, Gorbatyuk OS, Noorwez SM, Hauswirth WW *et al*. Restoration of visual function in P23H rhodopsin transgenic rats by gene delivery of BiP/Grp78. *Proc Natl Acad Sci U S A* 2010; **107**: 5961–5966.
- 86 Noorwez SM, Ostrov DA, McDowell JH, Krebs MP, Kaushal S. A high-throughput screening method for small-molecule pharmacologic chaperones of misfolded rhodopsin. *Invest Ophthalmol Vis Sci* 2008; **49**: 3224–3230.
- 87 Mendes HF, Cheetham ME. Pharmacological manipulation of gain-of-function and dominant-negative mechanisms in rhodopsin retinitis pigmentosa. *Hum Mol Genet* 2008; **17**: 3043–3054.
- 88 Keeney S, Neale MJ. Initiation of meiotic recombination by formation of DNA double-strand breaks: mechanism and regulation. *Biochem Soc Trans* 2006; **34**: 523–525.
- 89 White RR, Sung P, Vestal CG, Benedetto G, Cornelio N, Richardson C. Double-strand break repair by interchromosomal recombination: an in vivo repair mechanism utilized by multiple somatic tissues in mammals. *PLoS One* 2013; **8**: e84379.

- 90 Pardo B, Gómez-González B, Aguilera A. DNA repair in mammalian cells: DNA double-strand break repair: how to fix a broken relationship. *Cell Mol Life Sci CMLS* 2009; **66**: 1039–1056.
- 91 Smithies O, Gregg RG, Boggs SS, Koralewski MA, Kucherlapati RS. Insertion of DNA sequences into the human chromosomal beta-globin locus by homologous recombination. *Nature* 1985; **317**: 230–234.
- 92 Doetschman T, Gregg RG, Maeda N, Hooper ML, Melton DW, Thompson S *et al*. Targetted correction of a mutant HPRT gene in mouse embryonic stem cells. *Nature* 1987; **330**: 576–578.
- 93 Rouet P, Smih F, Jasin M. Introduction of double-strand breaks into the genome of mouse cells by expression of a rare-cutting endonuclease. *Mol Cell Biol* 1994; **14**: 8096.
- 94 Choulika A, Perrin A, Dujon B, Nicolas JF. Induction of homologous recombination in mammalian chromosomes by using the I-SceI system of *Saccharomyces cerevisiae*. *Mol Cell Biol* 1995; **15**: 1968.
- 95 Silva G, Poirot L, Galetto R, Smith J, Montoya G, Duchateau P *et al*. Meganucleases and other tools for targeted genome engineering: perspectives and challenges for gene therapy. *Curr Gene Ther* 2011; **11**: 11–27.
- 96 Epinat J-C, Arnould S, Chames P, Rochaix P, Desfontaines D, Puzin C *et al*. A novel engineered meganuclease induces homologous recombination in yeast and mammalian cells. *Nucleic Acids Res* 2003; **31**: 2952–2962.
- 97 Gaj T, Gersbach CA, Barbas CF 3rd. ZFN, TALEN, and CRISPR/Cas-based methods for genome engineering. *Trends Biotechnol* 2013; **31**: 397–405.
- 98 Mojica FJM, Díez-Villaseñor C, García-Martínez J, Soria E. Intervening sequences of regularly spaced prokaryotic repeats derive from foreign genetic elements. *J Mol Evol* 2005; **60**: 174–182.
- 99 Wilkinson R, Wiedenheft B. A CRISPR method for genome engineering. *F1000Prime Rep* 2014; **6**. doi:10.12703/P6-3.
- 100 Mali P, Yang L, Esvelt KM, Aach J, Guell M, DiCarlo JE *et al*. RNA-Guided Human Genome Engineering via Cas9. *Science* 2013; **339**: 823–826.
- 101 Cong L, Ran FA, Cox D, Lin S, Barretto R, Habib N *et al*. Multiplex Genome Engineering Using CRISPR/Cas Systems. *Science* 2013; **339**: 819–823.
- 102 Mercer AC, Gaj T, Fuller RP, Barbas CF. Chimeric TALE recombinases with programmable DNA sequence specificity. *Nucleic Acids Res* 2012; **40**: 11163–11172.
- 103 Gaj T, Mercer AC, Sirk SJ, Smith HL, Barbas CF. A comprehensive approach to zinc-finger recombinase customization enables genomic targeting in human cells. *Nucleic*

Acids Res 2013; **41**: 3937–3946.

104 Sera T. Zinc-finger-based artificial transcription factors and their applications. *Adv Drug Deliv Rev* 2009; **61**: 513–526.

105 Beru N, Smith D, Goldwasser E. Evidence suggesting negative regulation of the erythropoietin gene by ribonucleoprotein. *J Biol Chem* 1990; **265**: 14100–14104.

106 Mol JN, van der Krol AR, van Tunen AJ, van Blokland R, de Lange P, Stuitje AR. Regulation of plant gene expression by antisense RNA. *FEBS Lett* 1990; **268**: 427–430.

107 Fire A, Xu S, Montgomery MK, Kostas SA, Driver SE, Mello CC. Potent and specific genetic interference by double-stranded RNA in *Caenorhabditis elegans*. *Nature* 1998; **391**: 806–811.

108 Bei Y, Pressman S, Carthew R. SnapShot: Small RNA-Mediated Epigenetic Modifications. *Cell* 2007; **130**: 756.e1–756.e2.

109 McManus MT, Sharp PA. Gene silencing in mammals by small interfering RNAs. *Nat Rev Genet* 2002; **3**: 737–747.

110 Großhans H, Filipowicz W. Molecular biology: The expanding world of small RNAs. *Nature* 2008; **451**: 414–416.

111 Eulalio A, Huntzinger E, Izaurralde E. Getting to the Root of miRNA-Mediated Gene Silencing. *Cell* 2008; **132**: 9–14.

112 Fellmann C, Lowe SW. Stable RNA interference rules for silencing. *Nat Cell Biol* 2014; **16**: 10–18.

113 Boudreau RL, Martins I, Davidson BL. Artificial microRNAs as siRNA shuttles: improved safety as compared to shRNAs in vitro and in vivo. *Mol Ther J Am Soc Gene Ther* 2009; **17**: 169–175.

114 Grimm D, Streetz KL, Jopling CL, Storm TA, Pandey K, Davis CR *et al*. Fatality in mice due to oversaturation of cellular microRNA/short hairpin RNA pathways. *Nature* 2006; **441**: 537–541.

115 Bassik MC, Lebbink RJ, Churchman LS, Ingolia NT, Patena W, LeProust EM *et al*. Rapid creation and quantitative monitoring of high coverage shRNA libraries. *Nat Methods* 2009; **6**: 443–445.

116 Li L, Lin X, Khvorova A, Fesik SW, Shen Y. Defining the optimal parameters for hairpin-based knockdown constructs. *RNA N Y N* 2007; **13**: 1765–1774.

117 Fellmann C, Zuber J, McJunkin K, Chang K, Malone CD, Dickins RA *et al*. Functional identification of optimized RNAi triggers using a massively parallel sensor assay. *Mol Cell* 2011; **41**: 733–746.

- 118 Kiang A-S, Palfi A, Ader M, Kenna PF, Millington-Ward S, Clark G *et al.* Toward a gene therapy for dominant disease: validation of an RNA interference-based mutation-independent approach. *Mol Ther J Am Soc Gene Ther* 2005; **12**: 555–561.
- 119 O'Reilly M, Palfi A, Chadderton N, Millington-Ward S, Ader M, Cronin T *et al.* RNA interference-mediated suppression and replacement of human rhodopsin in vivo. *Am J Hum Genet* 2007; **81**: 127–135.
- 120 Tessitore A, Parisi F, Denti MA, Allocca M, Di Vicino U, Domenici L *et al.* Preferential silencing of a common dominant rhodopsin mutation does not inhibit retinal degeneration in a transgenic model. *Mol Ther J Am Soc Gene Ther* 2006; **14**: 692–699.
- 121 Millington-Ward S, Chadderton N, O'Reilly M, Palfi A, Goldmann T, Kilty C *et al.* Suppression and replacement gene therapy for autosomal dominant disease in a murine model of dominant retinitis pigmentosa. *Mol Ther J Am Soc Gene Ther* 2011; **19**: 642–649.
- 122 Perriman RJ, Gerlach WL. Manipulating gene expression by ribozyme technology. *Curr Opin Biotechnol* 1990; **1**: 86–91.
- 123 Birikh KR, Heaton PA, Eckstein F. The Structure, Function and Application of the Hammerhead Ribozyme. *Eur J Biochem* 1997; **245**: 1–16.
- 124 Lilley DMJ. Folding and catalysis by the hairpin ribozyme. *FEBS Lett* 1999; **452**: 26–30.
- 125 Hauswirth WW, Lewin AS. Ribozyme uses in retinal gene therapy. *Prog Retin Eye Res* 2000; **19**: 689–710.
- 126 Drenser KA, Timmers AM, Hauswirth WW, Lewin AS. Ribozyme-targeted destruction of RNA associated with autosomal-dominant retinitis pigmentosa. *Invest Ophthalmol Vis Sci* 1998; **39**: 681–689.
- 127 Shimayama T, Nishikawa S, Taira K. Generality of the NUX rule: kinetic analysis of the results of systematic mutations in the trinucleotide at the cleavage site of hammerhead ribozymes. *Biochemistry (Mosc)* 1995; **34**: 3649–3654.
- 128 Lewin AS, Drenser KA, Hauswirth WW, Nishikawa S, Yasumura D, Flannery JG *et al.* Ribozyme rescue of photoreceptor cells in a transgenic rat model of autosomal dominant retinitis pigmentosa. *Nat Med* 1998; **4**: 967–971.
- 129 O'Neill B, Millington-Ward S, O'Reilly M, Tuohy G, Kiang AS, Kenna PF *et al.* Ribozyme-based therapeutic approaches for autosomal dominant retinitis pigmentosa. *Invest Ophthalmol Vis Sci* 2000; **41**: 2863–2869.
- 130 Sullivan JM, Pietras KM, Shin BJ, Misasi JN. Hammerhead ribozymes designed to

cleave all human rod opsin mRNAs which cause autosomal dominant retinitis pigmentosa. *Mol Vis* 2002; **8**: 102–113.

131 Gorbatyuk MS, Pang JJ, Thomas J Jr, Hauswirth WW, Lewin AS. Knockdown of wild-type mouse rhodopsin using an AAV vectored ribozyme as part of an RNA replacement approach. *Mol Vis* 2005; **11**: 648–656.

132 Tonegawa S, Maxam AM, Tizard R, Bernard O, Gilbert W. Sequence of a mouse germ-line gene for a variable region of an immunoglobulin light chain. *Proc Natl Acad Sci U S A* 1978; **75**: 1485–1489.

133 Berget SM, Moore C, Sharp PA. Spliced segments at the 5' terminus of adenovirus 2 late mRNA. *Proc Natl Acad Sci U S A* 1977; **74**: 3171–3175.

134 Chow LT, Gelinas RE, Broker TR, Roberts RJ. An amazing sequence arrangement at the 5' ends of adenovirus 2 messenger RNA. *Cell* 1977; **12**: 1–8.

135 Breathnach R, Mandel JL, Chambon P. Ovalbumin gene is split in chicken DNA. *Nature* 1977; **270**: 314–319.

136 Mandel JL, Breathnach R, Gerlinger P, Le Meur M, Gannon F, Chambon P. Organization of coding and intervening sequences in the chicken ovalbumin split gene. *Cell* 1978; **14**: 641–653.

137 Wahl MC, Will CL, Lührmann R. The spliceosome: design principles of a dynamic RNP machine. *Cell* 2009; **136**: 701–718.

138 Pan Q, Shai O, Lee LJ, Frey BJ, Blencowe BJ. Deep surveying of alternative splicing complexity in the human transcriptome by high-throughput sequencing. *Nat Genet* 2008; **40**: 1413–1415.

139 Wang ET, Sandberg R, Luo S, Khrebtkova I, Zhang L, Mayr C *et al.* Alternative isoform regulation in human tissue transcriptomes. *Nature* 2008; **456**: 470–476.

140 Garcia-Blanco MA, Baraniak AP, Lasda EL. Alternative splicing in disease and therapy. *Nat Biotechnol* 2004; **22**: 535–546.

141 Kornblihtt AR, de la Mata M, Fededa JP, Munoz MJ, Nogues G. Multiple links between transcription and splicing. *RNA N Y N* 2004; **10**: 1489–1498.

142 Sullenger BA, Cech TR. Ribozyme-mediated repair of defective mRNA by targeted, trans-splicing. *Nature* 1994; **371**: 619–622.

143 Murphy WJ, Watkins KP, Agabian N. Identification of a novel Y branch structure as an intermediate in trypanosome mRNA processing: evidence for trans splicing. *Cell* 1986; **47**: 517–525.

144 Sutton RE, Boothroyd JC. Evidence for trans splicing in trypanosomes. *Cell* 1986;

47: 527–535.

145 Caudevilla C, Serra D, Miliar A, Codony C, Asins G, Bach M *et al.* Natural trans-splicing in carnitine octanoyltransferase pre-mRNAs in rat liver. *Proc Natl Acad Sci U S A* 1998; **95**: 12185–12190.

146 Finta C, Zaphiropoulos PG. Intergenic mRNA molecules resulting from trans-splicing. *J Biol Chem* 2002; **277**: 5882–5890.

147 Wu C-S, Yu C-Y, Chuang C-Y, Hsiao M, Kao C-F, Kuo H-C *et al.* Integrative transcriptome sequencing identifies trans-splicing events with important roles in human embryonic stem cell pluripotency. *Genome Res* 2014; **24**: 25–36.

148 Flouriot G, Brand H, Seraphin B, Gannon F. Natural trans-spliced mRNAs are generated from the human estrogen receptor-alpha (hER alpha) gene. *J Biol Chem* 2002; **277**: 26244–26251.

149 Takahara T, Kanazu SI, Yanagisawa S, Akanuma H. Heterogeneous Sp1 mRNAs in human HepG2 cells include a product of homotypic trans-splicing. *J Biol Chem* 2000; **275**: 38067–38072.

150 Li BL, Li XL, Duan ZJ, Lee O, Lin S, Ma ZM *et al.* Human acyl-CoA:cholesterol acyltransferase-1 (ACAT-1) gene organization and evidence that the 4.3-kilobase ACAT-1 mRNA is produced from two different chromosomes. *J Biol Chem* 1999; **274**: 11060–11071.

151 Romani A, Guerra E, Trerotola M, Alberti S. Detection and analysis of spliced chimeric mRNAs in sequence databanks. *Nucleic Acids Res* 2003; **31**: e17.

152 Rindt H, Yen P-F, Thebeau CN, Peterson TS, Weisman GA, Lorson CL. Replacement of huntingtin exon 1 by trans-splicing. *Cell Mol Life Sci CMLS* 2012; **69**: 4191–4204.

153 Wally V, Klausegger A, Koller U, Lochmüller H, Krause S, Wiche G *et al.* 5' trans-splicing repair of the PLEC1 gene. *J Invest Dermatol* 2008; **128**: 568–574.

154 Koller U, Wally V, Mitchell LG, Klausegger A, Murauer EM, Mayr E *et al.* A novel screening system improves genetic correction by internal exon replacement. *Nucleic Acids Res* 2011; **39**: e108.

155 Monjaret F, Bourg N, Suel L, Roudaut C, Le Roy F, Richard I *et al.* Cis-splicing and translation of the pre-trans-splicing molecule combine with efficiency in spliceosome-mediated RNA trans-splicing. *Mol Ther J Am Soc Gene Ther* 2014; **22**: 1176–1187.

156 Kikumori T, Cote GJ, Gagel RF. Promiscuity of pre-mRNA spliceosome-mediated trans splicing: a problem for gene therapy? *Hum Gene Ther* 2001; **12**: 1429–1441.

157 Rodriguez-Martin T, Garcia-Blanco MA, Mansfield SG, Grover AC, Hutton M, Yu Q *et al.* Reprogramming of tau alternative splicing by spliceosome-mediated RNA trans-

- splicing: implications for tauopathies. *Proc Natl Acad Sci U S A* 2005; **102**: 15659–15664.
- 158 Rodriguez-Martin T, Anthony K, Garcia-Blanco MA, Mansfield SG, Anderton BH, Gallo J-M. Correction of tau mis-splicing caused by FTDP-17 MAPT mutations by spliceosome-mediated RNA trans-splicing. *Hum Mol Genet* 2009; **18**: 3266–3273.
- 159 Kierlin-Duncan MN, Sullenger BA. Using 5'-PTMs to repair mutant beta-globin transcripts. *RNA N Y N* 2007; **13**: 1317–1327.
- 160 Zayed H, Xia L, Yerich A, Yant SR, Kay MA, Puttaraju M *et al*. Correction of DNA protein kinase deficiency by spliceosome-mediated RNA trans-splicing and sleeping beauty transposon delivery. *Mol Ther J Am Soc Gene Ther* 2007; **15**: 1273–1279.
- 161 Chen HY, Kathirvel P, Yee WC, Lai PS. Correction of dystrophin myotonia type 1 pre-mRNA transcripts by artificial trans-splicing. *Gene Ther* 2009; **16**: 211–217.
- 162 Lorain S, Peccate C, Le Hir M, Griffith G, Philippi S, Precigout G *et al*. Dystrophin rescue by trans-splicing: a strategy for DMD genotypes not eligible for exon skipping approaches. *Nucleic Acids Res* 2013; **41**: 8391–8402.
- 163 Lorain S, Peccate C, Le Hir M, Garcia L. Exon exchange approach to repair Duchenne dystrophin transcripts. *PloS One* 2010; **5**: e10894.
- 164 Wally V, Brunner M, Lettner T, Wagner M, Koller U, Trost A *et al*. K14 mRNA reprogramming for dominant epidermolysis bullosa simplex. *Hum Mol Genet* 2010; **19**: 4715–4725.
- 165 Murauer EM, Koller U, Hainzl S, Wally V, Bauer JW. A reporter-based screen to identify potent 3' trans-splicing molecules for endogenous RNA repair. *Hum Gene Ther Methods* 2013; **24**: 19–27.
- 166 Murauer EM, Gache Y, Gratz IK, Klausegger A, Muss W, Gruber C *et al*. Functional correction of type VII collagen expression in dystrophic epidermolysis bullosa. *J Invest Dermatol* 2011; **131**: 74–83.
- 167 Sachot S. *Étude du trans-épissage comme outil de thérapie génique dans le modèle canin de la mucopolysaccharidose de type VII*. Nantes, 2009 <http://www.theses.fr/2009NANT31VS> (accessed 13 Mar 2014).
- 168 Wang J, Mansfield SG, Cote CA, Jiang PD, Weng K, Amar MJA *et al*. Trans-splicing into highly abundant albumin transcripts for production of therapeutic proteins in vivo. *Mol Ther J Am Soc Gene Ther* 2009; **17**: 343–351.
- 169 Gruber C, Koller U, Murauer EM, Hainzl S, Hüttner C, Kocher T *et al*. The design and optimization of RNA trans-splicing molecules for skin cancer therapy. *Mol Oncol* 2013; **7**: 1056–1068.
- 170 Nakayama K, Pergolizzi RG, Crystal RG. Gene transfer-mediated pre-mRNA

segmental trans-splicing as a strategy to deliver intracellular toxins for cancer therapy. *Cancer Res* 2005; **65**: 254–263.

171 Patrick M, Puttaraju M, DiPasquale J, Quintero J, Yang Y, Garcia-Blanco MA *et al.* 293. Optimizing the Efficacy of Spliceosome-Mediated RNA Trans-Splicing (SMaRT™) for Suicide Gene Therapy of Cervical Cancer. *Mol Ther* 2005; **11**: S115–S115.

172 Walls ZF, Puttaraju M, Temple GF, Gambhir SS. A generalizable strategy for imaging pre-mRNA levels in living subjects using spliceosome-mediated RNA trans-splicing. *J Nucl Med Off Publ Soc Nucl Med* 2008; **49**: 1146–1154.

173 Bhaumik S, Walls Z, Puttaraju M, Mitchell LG, Gambhir SS. Molecular imaging of gene expression in living subjects by spliceosome-mediated RNA trans-splicing. *Proc Natl Acad Sci U S A* 2004; **101**: 8693–8698.

174 Puttaraju M, DiPasquale J, Baker CC, Mitchell LG, Garcia-Blanco MA. Messenger RNA repair and restoration of protein function by spliceosome-mediated RNA trans-splicing. *Mol Ther J Am Soc Gene Ther* 2001; **4**: 105–114.

175 Takahara T, Tasic B, Maniatis T, Akanuma H, Yanagisawa S. Delay in synthesis of the 3' splice site promotes trans-splicing of the preceding 5' splice site. *Mol Cell* 2005; **18**: 245–251.

176 Wang Y, Ma M, Xiao X, Wang Z. Intronic splicing enhancers, cognate splicing factors and context-dependent regulation rules. *Nat Struct Mol Biol* 2012; **19**: 1044–1052.

177 Goyenvalle A, Wright J, Babbs A, Wilkins V, Garcia L, Davies KE. Engineering multiple U7snRNA constructs to induce single and multiexon-skipping for Duchenne muscular dystrophy. *Mol Ther J Am Soc Gene Ther* 2012; **20**: 1212–1221.

178 Goyenvalle A, Vulin A, Fougereousse F, Leturcq F, Kaplan J-C, Garcia L *et al.* Rescue of dystrophic muscle through U7 snRNA-mediated exon skipping. *Science* 2004; **306**: 1796–1799.

179 Wagner E, Lykke-Andersen J. mRNA surveillance: the perfect persist. *J Cell Sci* 2002; **115**: 3033–3038.

180 McCracken S, Fong N, Rosonina E, Yankulov K, Brothers G, Siderovski D *et al.* 5'-Capping enzymes are targeted to pre-mRNA by binding to the phosphorylated carboxy-terminal domain of RNA polymerase II. *Genes Dev* 1997; **11**: 3306–3318.

181 Taylor AW, Kaplan HJ. Ocular immune privilege in the year 2010: ocular immune privilege and uveitis. *Ocul Immunol Inflamm* 2010; **18**: 488–492.

182 Cavazzana-Calvo M, Hacein-Bey S, de Saint Basile G, Gross F, Yvon E, Nusbaum P *et al.* Gene therapy of human severe combined immunodeficiency (SCID)-X1 disease.

Science 2000; **288**: 669–672.

183 Aiuti A, Slavin S, Aker M, Ficara F, Deola S, Mortellaro A *et al.* Correction of ADA-SCID by stem cell gene therapy combined with nonmyeloablative conditioning. *Science* 2002; **296**: 2410–2413.

184 Hacein-Bey-Abina S, Kalle CV, Schmidt M, McCormack MP, Wulffraat N, Leboulch P *et al.* LMO2-Associated Clonal T Cell Proliferation in Two Patients after Gene Therapy for SCID-X1. *Science* 2003; **302**: 415–419.

185 Durand S, Cimorelli A. The inside out of lentiviral vectors. *Viruses* 2011; **3**: 132–159.

186 Yáñez-Muñoz RJ, Balagán KS, MacNeil A, Howe SJ, Schmidt M, Smith AJ *et al.* Effective gene therapy with nonintegrating lentiviral vectors. *Nat Med* 2006; **12**: 348–353.

187 Bemelmans A-P, Bonnel S, Houhou L, Dufour N, Nandrot E, Helmlinger D *et al.* Retinal cell type expression specificity of HIV-1-derived gene transfer vectors upon subretinal injection in the adult rat: influence of pseudotyping and promoter. *J Gene Med* 2005; **7**: 1367–1374.

188 Auricchio A, Kobinger G, Anand V, Hildinger M, O'Connor E, Maguire AM *et al.* Exchange of surface proteins impacts on viral vector cellular specificity and transduction characteristics: the retina as a model. *Hum Mol Genet* 2001; **10**: 3075–3081.

189 Bainbridge JW, Stephens C, Parsley K, Demaison C, Halfyard A, Thrasher AJ *et al.* In vivo gene transfer to the mouse eye using an HIV-based lentiviral vector; efficient long-term transduction of corneal endothelium and retinal pigment epithelium. *Gene Ther* 2001; **8**: 1665–1668.

190 Kostic C, Chiodini F, Salmon P, Wiznerowicz M, Deglon N, Hornfeld D *et al.* Activity analysis of housekeeping promoters using self-inactivating lentiviral vector delivery into the mouse retina. *Gene Ther* 2003; **10**: 818–821.

191 Cronin J, Zhang X-Y, Reiser J. Altering the tropism of lentiviral vectors through pseudotyping. *Curr Gene Ther* 2005; **5**: 387–398.

192 McConnell MJ, Imperiale MJ. Biology of Adenovirus and Its Use as a Vector for Gene Therapy. *Hum Gene Ther* 2004; **15**: 1022–1033.

193 Kreppel F, Luther TT, Semkova I, Schraermeyer U, Kochanek S. Long-term transgene expression in the RPE after gene transfer with a high-capacity adenoviral vector. *Invest Ophthalmol Vis Sci* 2002; **43**: 1965–1970.

194 Wu L, Lam S, Cao H, Guan R, Duan R, van der Kooy D *et al.* Subretinal gene delivery using helper-dependent adenoviral vectors. *Cell Biosci* 2011; **1**: 15.

- 195 ATCHISON RW, CASTO BC, HAMMON WM. ADENOVIRUS-ASSOCIATED DEFECTIVE VIRUS PARTICLES. *Science* 1965; **149**: 754–756.
- 196 Warrington KH Jr, Herzog RW. Treatment of human disease by adeno-associated viral gene transfer. *Hum Genet* 2006; **119**: 571–603.
- 197 Alexander JJ, Hauswirth WW. Adeno-associated viral vectors and the retina. *Adv Exp Med Biol* 2008; **613**: 121–128.
- 198 Koerber JT, Maheshri N, Kaspar BK, Schaffer DV. Construction of diverse adeno-associated viral libraries for directed evolution of enhanced gene delivery vehicles. *Nat Protoc* 2006; **1**: 701–706.
- 199 Bennett J, Duan D, Engelhardt JF, Maguire AM. Real-time, noninvasive in vivo assessment of adeno-associated virus-mediated retinal transduction. *Invest Ophthalmol Vis Sci* 1997; **38**: 2857–2863.
- 200 Ali RR, Reichel MB, Thrasher AJ, Levinsky RJ, Kinnon C, Kanuga N *et al*. Gene Transfer into the Mouse Retina Mediated by an Adeno-Associated Viral Vector. *Hum Mol Genet* 1996; **5**: 591–594.
- 201 Flannery JG, Zolotukhin S, Vaquero MI, LaVail MM, Muzyczka N, Hauswirth WW. Efficient photoreceptor-targeted gene expression in vivo by recombinant adeno-associated virus. *Proc Natl Acad Sci U S A* 1997; **94**: 6916–6921.
- 202 Stieger K, Cronin T, Bennett J, Rolling F. Adeno-associated virus mediated gene therapy for retinal degenerative diseases. *Methods Mol Biol Clifton NJ* 2011; **807**: 179–218.
- 203 Allocca M, Mussolino C, Garcia-Hoyos M, Sanges D, Iodice C, Petrillo M *et al*. Novel Adeno-Associated Virus Serotypes Efficiently Transduce Murine Photoreceptors. *J Virol* 2007; **81**: 11372–11380.
- 204 Mussolino C, della Corte M, Rossi S, Viola F, Di Vicino U, Marrocco E *et al*. AAV-mediated photoreceptor transduction of the pig cone-enriched retina. *Gene Ther* 2011; **18**: 637–645.
- 205 Stieger K, Colle M-A, Dubreil L, Mendes-Madeira A, Weber M, Le Meur G *et al*. Subretinal delivery of recombinant AAV serotype 8 vector in dogs results in gene transfer to neurons in the brain. *Mol Ther J Am Soc Gene Ther* 2008; **16**: 916–923.
- 206 Vandenberghe LH, Bell P, Maguire AM, Cearley CN, Xiao R, Calcedo R *et al*. Dosage thresholds for AAV2 and AAV8 photoreceptor gene therapy in monkey. *Sci Transl Med* 2011; **3**: 88ra54.
- 207 Natkunarajah M, Trittibach P, McIntosh J, Duran Y, Barker SE, Smith AJ *et al*. Assessment of ocular transduction using single-stranded and self-complementary

- recombinant adeno-associated virus serotype 2/8. *Gene Ther* 2008; **15**: 463–467.
- 208 Reich SJ, Auricchio A, Hildinger M, Glover E, Maguire AM, Wilson JM *et al*. Efficient trans-splicing in the retina expands the utility of adeno-associated virus as a vector for gene therapy. *Hum Gene Ther* 2003; **14**: 37–44.
- 209 Song Y, Lou HH, Boyer JL, Limberis MP, Vandenberghe LH, Hackett NR *et al*. Functional cystic fibrosis transmembrane conductance regulator expression in cystic fibrosis airway epithelial cells by AAV6.2-mediated segmental trans-splicing. *Hum Gene Ther* 2009; **20**: 267–281.
- 210 Den Hollander AI, Roepman R, Koenekoop RK, Cremers FPM. Leber congenital amaurosis: genes, proteins and disease mechanisms. *Prog Retin Eye Res* 2008; **27**: 391–419.
- 211 Falk MJ, Zhang Q, Nakamaru-Ogiso E, Kannabiran C, Fonseca-Kelly Z, Chakarova C *et al*. NMNAT1 mutations cause Leber congenital amaurosis. *Nat Genet* 2012; **44**: 1040–1045.
- 212 Acland GM, Aguirre GD, Ray J, Zhang Q, Aleman TS, Cideciyan AV *et al*. Gene therapy restores vision in a canine model of childhood blindness. *Nat Genet* 2001; **28**: 92–95.
- 213 Acland GM, Aguirre GD, Bennett J, Aleman TS, Cideciyan AV, Bennicelli J *et al*. Long-term restoration of rod and cone vision by single dose rAAV-mediated gene transfer to the retina in a canine model of childhood blindness. *Mol Ther J Am Soc Gene Ther* 2005; **12**: 1072–1082.
- 214 Boye SE, Boye SL, Lewin AS, Hauswirth WW. A Comprehensive Review of Retinal Gene Therapy. *Mol Ther* 2013; **21**: 509–519.
- 215 Bainbridge JWB, Smith AJ, Barker SS, Robbie S, Henderson R, Balaggan K *et al*. Effect of gene therapy on visual function in Leber’s congenital amaurosis. *N Engl J Med* 2008; **358**: 2231–2239.
- 216 Hauswirth WW, Aleman TS, Kaushal S, Cideciyan AV, Schwartz SB, Wang L *et al*. Treatment of leber congenital amaurosis due to RPE65 mutations by ocular subretinal injection of adeno-associated virus gene vector: short-term results of a phase I trial. *Hum Gene Ther* 2008; **19**: 979–990.
- 217 Maguire AM, Simonelli F, Pierce EA, Pugh EN Jr, Mingozzi F, Bennicelli J *et al*. Safety and efficacy of gene transfer for Leber’s congenital amaurosis. *N Engl J Med* 2008; **358**: 2240–2248.
- 218 Cideciyan AV, Hauswirth WW, Aleman TS, Kaushal S, Schwartz SB, Boye SL *et al*. Human RPE65 gene therapy for Leber congenital amaurosis: persistence of early visual improvements and safety at 1 year. *Hum Gene Ther* 2009; **20**: 999–1004.

- 219 Cideciyan AV, Hauswirth WW, Aleman TS, Kaushal S, Schwartz SB, Boye SL *et al*. Vision 1 year after gene therapy for Leber's congenital amaurosis. *N Engl J Med* 2009; **361**: 725–727.
- 220 Simonelli F, Maguire AM, Testa F, Pierce EA, Mingozzi F, Bennicelli JL *et al*. Gene therapy for Leber's congenital amaurosis is safe and effective through 1.5 years after vector administration. *Mol Ther J Am Soc Gene Ther* 2010; **18**: 643–650.
- 221 Maguire AM, High KA, Auricchio A, Wright JF, Pierce EA, Testa F *et al*. Age-dependent effects of RPE65 gene therapy for Leber's congenital amaurosis: a phase 1 dose-escalation trial. *Lancet* 2009; **374**: 1597–1605.
- 222 Tan E, Ding X-Q, Saadi A, Agarwal N, Naash MI, Al-Ubaidi MR. Expression of Cone-Photoreceptor-Specific Antigens in a Cell Line Derived from Retinal Tumors in Transgenic Mice. *Invest Ophthalmol Vis Sci* 2004; **45**: 764–768.
- 223 Polo AD, Farber DB. Rod photoreceptor-specific gene expression in human retinoblastoma cells. *Proc Natl Acad Sci* 1995; **92**: 4016–4020.
- 224 Laabich A, Vissvesvaran GP, Lieu KL, Murata K, McGinn TE, Manmoto CC *et al*. Protective Effect of Crocin against Blue Light- and White Light-Mediated Photoreceptor Cell Death in Bovine and Primate Retinal Primary Cell Culture. *Invest Ophthalmol Vis Sci* 2006; **47**: 3156–3163.
- 225 Traverso V, Kinkl N, Grimm L, Sahel J, Hicks D. Basic Fibroblast and Epidermal Growth Factors Stimulate Survival in Adult Porcine Photoreceptor Cell Cultures. *Invest Ophthalmol Vis Sci* 2003; **44**: 4550–4558.
- 226 Reidel B, Orisme W, Goldmann T, Smith WC, Wolfrum U. Photoreceptor vitality in organotypic cultures of mature vertebrate retinas validated by light-dependent molecular movements. *Vision Res* 2006; **46**: 4464–4471.
- 227 Lamba DA, Karl MO, Ware CB, Reh TA. Efficient generation of retinal progenitor cells from human embryonic stem cells. *Proc Natl Acad Sci* 2006; **103**: 12769–12774.
- 228 Zhou L, Wang W, Liu Y, Fernandez de Castro J, Ezashi T, Telugu BPVL *et al*. Differentiation of induced pluripotent stem cells of swine into rod photoreceptors and their integration into the retina. *Stem Cells Dayt Ohio* 2011; **29**: 972–980.
- 229 Lamba DA, McUsic A, Hirata RK, Wang P-R, Russell D, Reh TA. Generation, purification and transplantation of photoreceptors derived from human induced pluripotent stem cells. *PloS One* 2010; **5**: e8763.
- 230 Illing ME, Rajan RS, Bence NF, Kopito RR. A rhodopsin mutant linked to autosomal dominant retinitis pigmentosa is prone to aggregate and interacts with the ubiquitin proteasome system. *J Biol Chem* 2002; **277**: 34150–34160.

- 231 Lin JH, Li H, Yasumura D, Cohen HR, Zhang C, Panning B *et al.* IRE1 signaling affects cell fate during the unfolded protein response. *Science* 2007; **318**: 944–949.
- 232 Chiang W-C, Messah C, Lin JH. IRE1 directs proteasomal and lysosomal degradation of misfolded rhodopsin. *Mol Biol Cell* 2012; **23**: 758–770.
- 233 Chiang W-C, Hiramatsu N, Messah C, Kroeger H, Lin JH. Selective activation of ATF6 and PERK endoplasmic reticulum stress signaling pathways prevent mutant rhodopsin accumulation. *Invest Ophthalmol Vis Sci* 2012; **53**: 7159–7166.
- 234 Opefi CA, South K, Reynolds CA, Smith SO, Reeves PJ. Retinitis pigmentosa mutants provide insight into the role of the N-terminal cap in rhodopsin folding, structure, and function. *J Biol Chem* 2013; **288**: 33912–33926.
- 235 Kijas JW, Cideciyan AV, Aleman TS, Pianta MJ, Pearce-Kelling SE, Miller BJ *et al.* Naturally occurring rhodopsin mutation in the dog causes retinal dysfunction and degeneration mimicking human dominant retinitis pigmentosa. *Proc Natl Acad Sci U S A* 2002; **99**: 6328–6333.
- 236 Iakhine R, Chorna-Ornan I, Zars T, Elia N, Cheng Y, Selinger Z *et al.* Novel dominant rhodopsin mutation triggers two mechanisms of retinal degeneration and photoreceptor desensitization. *J Neurosci Off J Soc Neurosci* 2004; **24**: 2516–2526.
- 237 Galy A, Roux MJ, Sahel JA, Lévillard T, Giangrande A. Rhodopsin maturation defects induce photoreceptor death by apoptosis: a fly model for RhodopsinPro23His human retinitis pigmentosa. *Hum Mol Genet* 2005; **14**: 2547–2557.
- 238 Nakao T, Tsujikawa M, Notomi S, Ikeda Y, Nishida K. The role of mislocalized phototransduction in photoreceptor cell death of retinitis pigmentosa. *PloS One* 2012; **7**: e32472.
- 239 Green ES, Menz MD, LaVail MM, Flannery JG. Characterization of rhodopsin mis-sorting and constitutive activation in a transgenic rat model of retinitis pigmentosa. *Invest Ophthalmol Vis Sci* 2000; **41**: 1546–1553.
- 240 Jones BW, Kondo M, Terasaki H, Watt CB, Rapp K, Anderson J *et al.* Retinal remodeling in the Tg P347L rabbit, a large-eye model of retinal degeneration. *J Comp Neurol* 2011; **519**: 2713–2733.
- 241 Petters RM, Alexander CA, Wells KD, Collins EB, Sommer JR, Blanton MR *et al.* Genetically engineered large animal model for studying cone photoreceptor survival and degeneration in retinitis pigmentosa. *Nat Biotechnol* 1997; **15**: 965–970.
- 242 Ross JW, Fernandez de Castro JP, Zhao J, Samuel M, Walters E, Rios C *et al.* Generation of an inbred miniature pig model of retinitis pigmentosa. *Invest Ophthalmol Vis Sci* 2012; **53**: 501–507.

- 243 Sancho-Pelluz J, Tosi J, Hsu C-W, Lee F, Wolpert K, Tabacaru MR *et al.* Mice with a D190N mutation in the gene encoding rhodopsin: a model for human autosomal-dominant retinitis pigmentosa. *Mol Med Camb Mass* 2012; **18**: 549–555.
- 244 Zhang N, Kolesnikov AV, Jastrzebska B, Mustafi D, Sawada O, Maeda T *et al.* Autosomal recessive retinitis pigmentosa E150K opsin mice exhibit photoreceptor disorganization. *J Clin Invest* 2013; **123**: 121–137.
- 245 Naash MI, Hollyfield JG, al-Ubaidi MR, Baehr W. Simulation of human autosomal dominant retinitis pigmentosa in transgenic mice expressing a mutated murine opsin gene. *Proc Natl Acad Sci U S A* 1993; **90**: 5499–5503.
- 246 Swaroop A, Kim D, Forrest D. Transcriptional regulation of photoreceptor development and homeostasis in the mammalian retina. *Nat Rev Neurosci* 2010; **11**: 563–576.
- 247 Kozak M. At least six nucleotides preceding the AUG initiator codon enhance translation in mammalian cells. *J Mol Biol* 1987; **196**: 947–950.
- 248 Berger A, Cavallero S, Dominguez E, Barbe P, Simonutti M, Sahel J-A *et al.* Spectral-Domain Optical Coherence Tomography of the Rodent Eye: Highlighting Layers of the Outer Retina Using Signal Averaging and Comparison with Histology. *PLoS ONE* 2014; **9**: e96494.
- 249 Houseley J, LaCava J, Tollervey D. RNA-quality control by the exosome. *Nat Rev Mol Cell Biol* 2006; **7**: 529–539.
- 250 Isken O, Maquat LE. Quality control of eukaryotic mRNA: safeguarding cells from abnormal mRNA function. *Genes Dev* 2007; **21**: 1833–1856.
- 251 Lem J, Krasnoperova NV, Calvert PD, Kosaras B, Cameron DA, Nicolò M *et al.* Morphological, physiological, and biochemical changes in rhodopsin knockout mice. *Proc Natl Acad Sci U S A* 1999; **96**: 736–741.
- 252 Dalkara D, Byrne LC, Lee T, Hoffmann NV, Schaffer DV, Flannery JG. Enhanced gene delivery to the neonatal retina through systemic administration of tyrosine-mutated AAV9. *Gene Ther* 2012; **19**: 176–181.
- 253 Jacobson SG, Cideciyan AV, Ratnakaram R, Heon E, Schwartz SB, Roman AJ *et al.* Gene therapy for leber congenital amaurosis caused by RPE65 mutations: safety and efficacy in 15 children and adults followed up to 3 years. *Arch Ophthalmol* 2012; **130**: 9–24.

ANNEXES

Annex 1: mouse versus human sequences of rhodopsin mRNA and proteins.

Human rhodopsin Mouse rhodopsin Differences Specific primers

- Comparison of mRNA sequences:

```

1>ATGAAATGGACAGAAAGGCCCTAACTTCTACGTGCCCTTCTCCAATGCG--ACGGGTGTGGTACGACGCCCTTCGAGTACCCACAGTACTACCTGGTGA>98
1>ATGAAATGGACAGAAAGGCCCTAACTTCTACGTGCCCTTCTCCAATGCG--ACGGGTGTGGTACGACGCCCTTCGAGTACCCACAGTACTACCTGGTGA>98

99>GCCATGGCAGTTCTCCATGCTGGCCGCTACATGTTTCTGCTGATCGTGCTGGGCTTCCCATCAACTTCTCAGCGTCTACGTCCAGTCCAGCACAAG>198
99>GCCATGGCAGTTCTCCATGCTGGCCGCTACATGTTTCTGCTGATCGTGCTGGGCTTCCCATCAACTTCTCAGCGTCTACGTCCAGTCCAGCACAAG>198

199>AAGCTGCBACGCTCTCAACTACATCTCTGCTCAACCTAGCCGTTGGCTGACCTCTTCATGGTCTAGGTGGCTTCACCAGCACCCCTCTACACCTCTCTGC>298
199>AAGCTGCBACGCTCTCAACTACATCTCTGCTCAACCTAGCCGTTGGCTGACCTCTTCATGGTCTAGGTGGCTTCACCAGCACCCCTCTACACCTCTCTGC>298

299>ATGGATACTTCTGCTTTCGGGCCACAGGATGCAATTTGGAGGGCTTCTTTGCCACCCTGGCGGTGAAATGCCCCTGTGGTCTTGGTGGTCTGGCCAT>398
299>ATGGATACTTCTGCTTTCGGGCCACAGGATGCAATTTGGAGGGCTTCTTTGCCACCCTGGCGGTGAAATGCCCCTGTGGTCTTGGTGGTCTGGCCAT>398

399>CGAGCGGTACGTGGTGGTGTGAAGCCATGAGCAACTTCCGCTTCGGGGAGAACCATGCCATCATGGGCGTTCCTTACCTGGGTTCATGGCGTGGCC>498
399>CGAGCGGTACGTGGTGGTGTGAAGCCATGAGCAACTTCCGCTTCGGGGAGAACCATGCCATCATGGGCGTTCCTTACCTGGGTTCATGGCGTGGCC>498

499>TGCCTGACCCCACTCGCCGGCTGGTCCAGGTACATCCCGAGGGCTGACGTCTCTGTGGAATCGACTACTACAGCTCAAGCCGAGGTCAACA>598
499>TGCCTGACCCCACTCGCCGGCTGGTCCAGGTACATCCCGAGGGCTGACGTCTCTGTGGAATCGACTACTACAGCTCAAGCCGAGGTCAACA>598

599>ACGAGTCTTTTGTACATACATGTTCTGGTCCACTTCACCATCCCATGATATCATCTTTTCTGCTATGGGCGCTCGTCTTCCACCGTCAAGGAGGC>698
599>ACGAGTCTTTTGTACATACATGTTCTGGTCCACTTCACCATCCCATGATATCATCTTTTCTGCTATGGGCGCTCGTCTTCCACCGTCAAGGAGGC>698

699>CGCTGCCAGCAGCAGGAGTCAGCCACCACAGAAAGGACAGAAAGGAGTACCCGATGGTTCATCATATGGTTCATCTCTTCTGATCTGCTGGG>796
699>CGCTGCCAGCAGCAGGAGTCAGCCACCACAGAAAGGACAGAAAGGAGTACCCGATGGTTCATCATATGGTTCATCTCTTCTGATCTGCTGGG>796

797>TGCCTGACCCCACTCGCCGGCTGGTCCAGGTACATCCCGAGGGCTGACGTCTCTGTGGAATCGACTACTACAGCTCAAGCCGAGGTCAACA>895
797>TGCCTGACCCCACTCGCCGGCTGGTCCAGGTACATCCCGAGGGCTGACGTCTCTGTGGAATCGACTACTACAGCTCAAGCCGAGGTCAACA>895

896>CCATCTACAACCCGTGTCATCTATCATGATGAACAAGCAGTTCCGGAAGTGCATGCTCAACCAC--CATCTGCTGGCGGAAGAACCCACTGGGTGACGATG>994
896>CCATCTACAACCCGTGTCATCTATCATGATGAACAAGCAGTTCCGGAAGTGCATGCTCAACCAC--CATCTGCTGGCGGAAGAACCCACTGGGTGACGATG>994

995>A-G--GCCTCTGCTACCG-TGTCCAAGACGGAGACAGCCAGGTGGCCCGCCTAA>1047
992>ACACGCCTCTGCACCGCTTCCAAGACGGAGACAGCCAGGTGGCTCCGCTCAAA>1047

```

- Comparison of protein sequences:

```

MNGTEGPNFYVFPFSNATGVVRSPEFYQYYLAEPWQFSMLAAYMFLILVGFPINFLTYVTVQHKKLRPLNYILLNAVADLFMVLG
MNGTEGPNFYVFPFSNATGVVRSPEFYQYYLAEPWQFSMLAAYMFLILVGFPINFLTYVTVQHKKLRPLNYILLNAVADLFMVLG

GFTSTLYTSLHGYFVFGPTGCLNLEGGFATLGGEIALWLSVLVAIERVVVCKPMSNFRFGENHAIMGVAFTWVVMALACAAPPLAGWSRYI
GFTSTLYTSLHGYFVFGPTGCLNLEGGFATLGGEIALWLSVLVAIERVVVCKPMSNFRFGENHAIMGVAFTWVVMALACAAPPLAGWSRYI

PEGLQCSGIDYITLKPEVNNESFVIYMFVVFHTIPMIIFFCYQQLVFTVKEAAAQQQESATTQKAEKEVTRMVIIMVIAFLICWVVPYAS
PEGLQCSGIDYITLKPEVNNESFVIYMFVVFHTIPMIIFFCYQQLVFTVKEAAAQQQESATTQKAEKEVTRMVIIMVIAFLICWVVPYAS

VAFYIFTHQGSNFGPIFMTIPAFFAKSAAIYNPVIYIMMNK QFRNCMLTTCGKNPLGDDEASATVSKTETSQVAPA*
VAFYIFTHQGSNFGPIFMTIPAFFAKSSAIYNPVIYIMMNK QFRNCMLTTCGKNPLGDDEASATVSKTETSQVAPA*

```

Annex 2: Supplemental materials and methods.

Quantification of PTM15 *trans*-splicing

PCR primers used to quantify the *trans*-splicing efficiency of PTM15: forward=5'-aagagcggcccatctacaa-3'; reverse *cis*-splicing=5'-acaagaagctgggtcggcg-3'; reverse *trans*-splicing=5'-tctgataggcagcctgcact-3'.

Western blot

HEK293T cells and retinal protein extracts were obtained from dissociation in a buffer containing: 50mM HEPES, pH 7.4; 150mM NaCl; 10% glycérol; 1,5 mM MgCl₂; 1% Triton X-100. The total protein concentration was measured using a Biorad protein assay, and 10 µg of total protein was used to detect individual proteins. Samples were not subject to heat denaturation. The detection of proteins was performed using the following antibodies: anti-rhodopsin (MAB5356 Millipore 1:2000), anti-GFP (A11122 Molecular probes 1:2000), anti-actin (A5060 sigma) and anti-mouse IgG or anti-rabbit IgG, HRP-linked antibodies.

AAV vector production

AAV vectors express GFP or PTM under the control of the bovine rhodopsin (*brho*) promoter. Self-complementary genome-containing plasmids were constructed by deleting the D sequence and the terminal resolution site from one of the inverted terminal repeats. Briefly, AAV2 vectors were generated by packaging AAV2-based recombinant single-stranded (ss) or self-complementary (sc) genomes into the AAV9 or AAV2 capsids. Virions were produced by transfecting HEK293 cells with (i) the adenovirus helper plasmid (pXX6-80), (ii) the AAV packaging plasmid encoding the rep2 and the cap2 or the cap9 genes, and (iii) the AAV2 shuttle plasmid containing the gene encoding GFP or PTM in a ss or sc genome. Recombinant vectors (rAAV) were purified by ultracentrifugation on a discontinuous iodixaniol density gradient followed by dialysis against the formulation buffer of the vector stocks, namely phosphate-buffered saline containing 0.5 mM MgCl₂ and 1.25 mM KCl (PBS-MK; five buffer changes, 3 hours per round of dialysis). Physical particles were quantified by real-time PCR. Vector titers are expressed as viral genomes per milliliter (vg/ml).

Animals

C57BL/6JRj mice were purchased from Janvier SA (Le Genest-Saint-Isle, France). *Rho*^{-/-} knockout mice were provided by Dr Janis Lem (Tufts University, Boston, MA, USA) and P347S *RHO*^{+/+} were provided by Dr Peter Humphries (Trinity College Dublin, Ireland). We used the first generation of a breeding between *Rho*^{-/-} knockout mice and P347S *RHO*^{+/+} transgenic mice to obtain *Rho*^{+/-} P347S *RHO*⁺ mice. Mice were maintained at the Institut de la Vision animal facility under pathogen-free

conditions. All animals were housed in a 12h/12h light/dark cycle with food and water available *ad libitum*.

Subretinal injection

Animals were anesthetized by intraperitoneal injection of ketamine (50 mg/kg, Virbac) and xylazine (10 mg/kg, Bayer HealthCare), and their pupils were dilated with tropicamide (Mydriaticum®, Théa) and phenylephrin (Néosynéphrine®, Europhtha). Subretinal injections were performed with a 33-gauge blunt needle mounted on a 10 µl syringe (Hamilton, USA). Briefly, a hole was created through the sclera/choroid/retina layers using the sharp tip of a 30-gauge needle, and the blunt needle of the Hamilton syringe was then gently inserted into the vitreous cavity through this hole. The needle was pushed further into the vitreous cavity until going through the retina to the opposite side of its entry site into the eye. After injection, the needle was left in place for an additional 10 seconds to prevent leakage of the injected fluid. A successful subretinal injection was checked by visualization of a subretinal bleb. An anti-inflammatory and antibacterial ointment (Sterdex®, Novartis) was then applied locally.

Intracardiac injection

Pups were immobilized to localize the heart. A volume of 10 µL of fluorescein 10% was rapidly injected directly into the heart using a 0.3mL insulin syringe (Myjector®, Terumo®). After injection, pups were allowed to recover for several minutes on a 37°C heating pad before being returned to their cages.

OCT measures

Pupils were dilated with tropicamide (Mydriaticum®, Théa, France) and phenylephrin (Néosynéphrine®, Europhtha, France). Animals were then anesthetized by inhalation of Isoflurane (Axience, France) and placed in the front of the SD-OCT imaging device (Bioptigen 840nm HHP; Bioptigen, North Carolina, USA). Eyes were kept moisturized with 9‰ NaCl during the whole procedure. Image acquisitions were performed using the following parameters: Rectangular scan/ 1000 A-scan per B-scan/ 100B-scan 1 frame or 4B-scans 16 frames. Acquired images were saved as .avi files and processed with Fiji software (available at <http://fiji.sc/Fiji>). Firstly, image artifacts due to breathing movements were eliminated by using the StackReg Plugin. Then, using "Z project" function set to "Sum Slices", each movie was converted into a single image by compiling a Z-projection of all images of the movie. Thus, the final image resulted from the maximum projection of sixteen or one hundred images sampled every micron, which means 16 or 100 microns retinal width depending on the selected parameter. This manipulation eliminates most of the noise observed on individual images, which helped to show very clearly the reflectance

differences present at the level of the outer retina. Retinal layers thicknesses were manually measured on this maximum projection image in an axis perpendicular to the individual layers and about 500 μ m from the optic nerve using Fiji software.

Micron III imaging

Pupils were dilated with tropicamide (Mydriaticum®, Théa, France) and phenylephrin (Néosynephrine®, Europhta, France). Animals were then anesthetized by inhalation of Isoflurane (Axience, France) and Fundus photographs were taken with the Micron III retinal imaging microscope from Phoenix Research Laboratories (Phoenix, AZ). Eyes were kept moisturized with Lubrithal gel (Dechra, England) during the whole procedure.

SUMMARY

Gene therapy for autosomal dominant *retinitis pigmentosa*: repair of rhodopsin mRNA by SMaRT technology

Retinitis pigmentosa are hereditary retinal dystrophies involving degeneration of photoreceptors leading to blindness and for which there is currently no treatment. The most frequent cause of the disease is a point mutation in the rhodopsin gene, responsible for approximately 30% of autosomal dominant forms. In this case, a therapeutic intervention that restores the expression level of the normal protein is not sufficient because the mutant protein causes a gain of function or dominant negative effect, deleterious for photoreceptors. A change in rhodopsin expression level induces also damages to the retina. Therapeutic strategy should thus both suppress mutant protein expression and restore expression of the normal one to physiologic level.

My PhD project was to develop a therapeutic tool, based on SMaRT (Spliceosome Mediated RNA *Trans*-splicing) technology to repair rhodopsin (RHO) pre-mRNA. This required introducing by gene transfer into the target cell an exogenous RNA, called PTM for Pre-mRNA *Trans*-splicing Molecule. This one was able to specifically bind the RHO pre-mRNA and promote a splice reaction in *trans*, leading to the replacement of the mutated exon of this pre-mRNA by a normal one.

Firstly, we engineered 14 PTM targeting different sequences of the first intron of RHO pre-mRNA. These PTM should thus be able to repair any mutation in exons 2, 3, 4 and 5. After transient co-transfection of HEK293T cells with a PTM-encoding plasmid and a wild type (WT) or mutant RHO-encoding plasmid, we quantified the *trans*-splicing rate at RNA level. The maximum *trans*-splicing efficiency was about 25%. We improved this score to 40% by adding an intron into the replacement sequence of the PTM.

In a second step, we created WT or mutated (P23H/R135W/P347L) RHO stable expression cell lines by lentiviral transduction. These ones presented RHO localization at the plasma membrane (WT/P347L RHO) or retained into the cell (P23H/R135W RHO) depending on the mutation. After transfection of these cell lines with a plasmid expressing the most efficient RHO-PTM, we determined with the ImageStreamX Mark II Imaging Flow Cytometer that *trans*-splicing was efficient enough to partially restore localization to the plasma membrane of repaired RHO.

In parallel, we used *mRho*^{+/-} *RHO* P347S⁺ mice, a humanized heterozygous mouse model, to test *trans*-splicing efficiency *in vivo*. Firstly, we implemented a processing of SD-OCT (spectral domain-optical coherence tomography) images that allowed precisely quantifying retinal degeneration in mice. Using this technology, we determined that our humanized mouse model of rhodopsin mutation was indeed subject to a very rapid degeneration of the photoreceptors. After subretinal injection of AAV2/8 bRho-PTM20, we finally demonstrated that *trans*-splicing occurred *in vivo*, and could repair RHO pre-mRNA, but that improvements are still required to observe a phenotypic rescue of photoreceptors degeneration *in vivo*.